Rockefeller University
Digital Commons @ RU

Student Theses and Dissertations

2012

Chemical Reporters for Investigating Lipidated Proteins at the Host-Pathogen Interface

Guillaume Charron

Follow this and additional works at: http://digitalcommons.rockefeller.edu/student_theses_and_dissertations

 Part of the Life Sciences Commons

Recommended Citation

Charron, Guillaume, "Chemical Reporters for Investigating Lipidated Proteins at the Host-Pathogen Interface" (2012). *Student Theses and Dissertations.* Paper 158.

This Thesis is brought to you for free and open access by Digital Commons @ RU. It has been accepted for inclusion in Student Theses and Dissertations by an authorized administrator of Digital Commons @ RU. For more information, please contact mcsweej@mail.rockefeller.edu.

CHEMICAL REPORTERS FOR INVESTIGATING LIPIDATED PROTEINS AT THE HOST-PATHOGEN INTERFACE

A Thesis Presented to the Faculty of

The Rockefeller University

in Partial Fulfillment of the Requirements for

the degree of Doctor of Philosophy

by

Guillaume Charron

June 2012

© Copyright by Guillaume Charron 2012

CHEMICAL REPORTERS FOR INVESTIGATING LIPIDATED PROTEINS AT THE HOST-PATHOGEN INTERFACE

Guillaume Charron, Ph.D.

The Rockefeller University 2012

Lipidation of proteins regulates many cellular processes such as signaling transduction and membrane sorting by modulating protein localization and protein-protein interactions. As such, defects in protein lipidation can render host cells more susceptible to microbial infection and are also associated with a variety of human diseases ranging from cancer to neurological disorders. Moreover, viral and bacterial pathogens can exploit and modulate the host lipidation machinery to enhance infection. Robust biochemical methods for characterizing lipidated proteins are therefore important for understanding fundamental physiology and disease mechanisms. In this thesis, I report the development of alkyne-lipid chemical reporters that afford more sensitive detection and proteomic analysis of fatty-acylated and prenylated proteins using bioorthogonal ligation methods. Alkynyl-fatty acids of 14 and 18 carbons afforded enhanced detection of *N*-myristoylated and *S*-palmitoylated proteins, respectively, while alkynyl-farnesol allowed more robust analysis of *S*-prenylated proteins. These new lipid chemical reporters enabled the discovery of bacterial virulence factors that are lipid-modified by host enzymes during infection as well as lipidated host proteins (IFITM3 and ZAP) involved in cellular resistance to viruses. My thesis work highlights the utility of alkyne lipid reporters for biochemical analysis of lipidated proteins at the host-pathogen interface that will hopefully help other biological studies.

ACKNOWLEDGMENTS

I wish to express my gratitude to all those who have supported me throughout my time at The Rockefeller University, as mentors, teachers, collaborators, colleagues and companions. In particular, I thank

First and foremost, my advisor and mentor Dr Howard Hang. I am grateful for his guidance throughout the years and his rigorous efforts to train me into becoming an accomplished scientist. He offered me invaluable insights into how to approach scientific problems, properly design experiments to address the questions, appropriately interpret the results, and efficiently report our findings in acclaimed peer-reviewed journals. Since I was the second graduate student to join his laboratory, he also offered me the opportunity to have a glance at the rewards and difficulties in setting-up a laboratory and starting an independent scientist career. All of these will guide me positively throughout my own personal profession.

Dr Tarun Kapoor, who as the chair of my thesis committee dutifully followed my progress over the course of my studies and helped me keep a clear picture of my own goals. His care and criticism were always appreciated.

Dr Hening Lin, for his excellent course that introduced and fascinated me with the intricacies of protein post-translational modifications. This certainly influenced me to later on join Dr Hang's research group and I thank him for this and for being a member of my thesis committee.

Dr Stephen Goff, the external member of my thesis committee, who showed immediate interest in my research. I am honored to have as an examiner the scientist who discovered ZAP, a protein that I studied in this thesis.

Dr Margaret Macdonald and Dr Melody Li, for their enthusiasm in the collaboration on the ZAP project. Working with them was stimulating and appreciated, and I thank them for taking the time to train me for the experiments with viruses.

Dr Haiteng Deng and the staff of The Rockefeller Proteomics Resource Center for streamlining the mass spectrometry analysis.

Members of the Hang research group for sharing advice and reagents, and for stimulating conversations. I would like to especially thank: Dr Jacob Yount, Dr John Wilson and Dr Mingzi Zhang for their availability and prevalence in my initial training in biological methods; Dr Kelvin Tsou, Dr Yu-Ying Yang and Dr Anuradha Raghavan for their interest in organic chemistry discussions; and all other lab members for the great interdisciplinary atmosphere of the laboratory.

The Weill Cornell / Rockefeller / Sloan-Kettering Tri-Institutional Training Program in Chemical Biology for funding and giving me the opportunity to study abroad.

My family and friends, whose support and encouragements have been invaluable.

TABLE OF CONTENTS

LIST OF FIGURES

LIST OF TABLES

CHAPTER I. Introduction

Post-translational lipidation of proteins is an important mechanism to regulate protein trafficking and activity in eukaryotes[1]. Targeting of proteins to membranes by lipidation plays key roles in many physiological processes and when not regulated properly can lead to cancer[2] and neurological disorders[3]. Dissecting the precise roles of protein lipidation in physiology and disease is a major challenge, but recent advances in chemical biology have now afforded new chemical reporters of protein lipidation that have improved the detection and analysis of lipidated proteins[4-6]. In this thesis, I report the development of alkynyl-lipids as improved chemical reporters of protein fatty-acylation[7] and prenylation[8], and their application towards the characterization of lipid-mediated host-pathogen interactions[8-12].

1.1 Membrane targeting of lipidated proteins

Eukaryotic cell membranes are composed of a vast assortment of amphipathic lipids, which consist of a hydrophobic and a hydrophilic portion. The hydrophobic moieties are entropically driven by water to self-associate, while the hydrophilic moieties interact with aqueous environments and with each other, which is the physical basis for the spontaneous formation of membrane bilayers[13]. Membranes thus allow for the segregation of the cell's content from its external environment (plasma membrane) and the further compartmentalization of the content of discrete intracellular organelles (endoplasmic reticulum (ER), Golgi apparatus, endocytic vacuoles, etc.) where specific chemical reactions are isolated for increased biochemical efficiency and restricted dissemination of reaction products[13].

Recent advances in mass spectrometry have revealed the existence of >1,000 different lipid species in eukaryotic cells arising from the variations in headgroups and aliphatic chains[14]. In cells, membrane lipids can adopt various fluid and solid phases depending on their structure and environment. These phases have specific properties that determine the spatial arrangement and motional freedom of membrane lipids and proteins, and will therefore affect membrane functionality[15]. The adopted phase depends on lipid structure: long, saturated hydrocarbon chains (as found in sphingolipids) tend to adopt solid-like phases due to their efficient packing; while *cis*-unsaturated hydrocarbon chains (most phosphatidylcholine (PtdCho) molecules have one) tend to be enriched in liquid phases where *cis*-unsaturations impose a conformational constraint preventing optimal alignment of lipid chains. When combined with sphingolipids, cholesterol has the remarkable ability of forming a liquid-ordered phase that has the high order of a solid but the high translational motility of a liquid[16]. Moreover, PtdCho plus cholesterol can adopt two coexisting fluid phases: liquid-ordered and liquid-disordered[17]. The coexistence of two fluid phases with different physical characteristics within a single membrane plane creates energetically unfavorable phase boundaries where some membrane proteins cluster to decrease the line energy (tension) between domains[18].

Diverse lipid compositions of each organelle membranes are maintained through specific localized lipid metabolism and lipid transport, allowing distinct membrane biophysical properties and protein associations. For example, the ER membrane composition (60 mol% PtdCho, 25 mol% phosphatidylethanolamine (PE) and 10 mol% phosphatitylinositol (PI)) results in loose lipid packing while the plasma membrane

composition (25 mol% PI, 15 mol% PE, 30-40 mol% cholesterol, 10 mol% sphingolipids and 5 mol% phosphatidylserine) allows for the formation of ordered cholesterol-rich lipid-protein microdomains which can be stabilized to function in membrane trafficking and signaling[19]. Protein association to specific membranes is dictated by various hydrophobic domains and/or lipid modifications. These lipid modifications include glycophosphatidylinositol (GPI) anchors, cysteine fatty-acylation, N-terminal myristoylation, and C-terminal isoprenylation (Figure 1). Evidence suggests that modification by long saturated lipids (GPI anchors and palmitoylation) recruits both peripheral and transmembrane proteins to ordered lipid domains, while short, unsaturated and/or branched hydrocarbon chain modifications (such as myristoylation and isoprenylation) prevent such association[20].

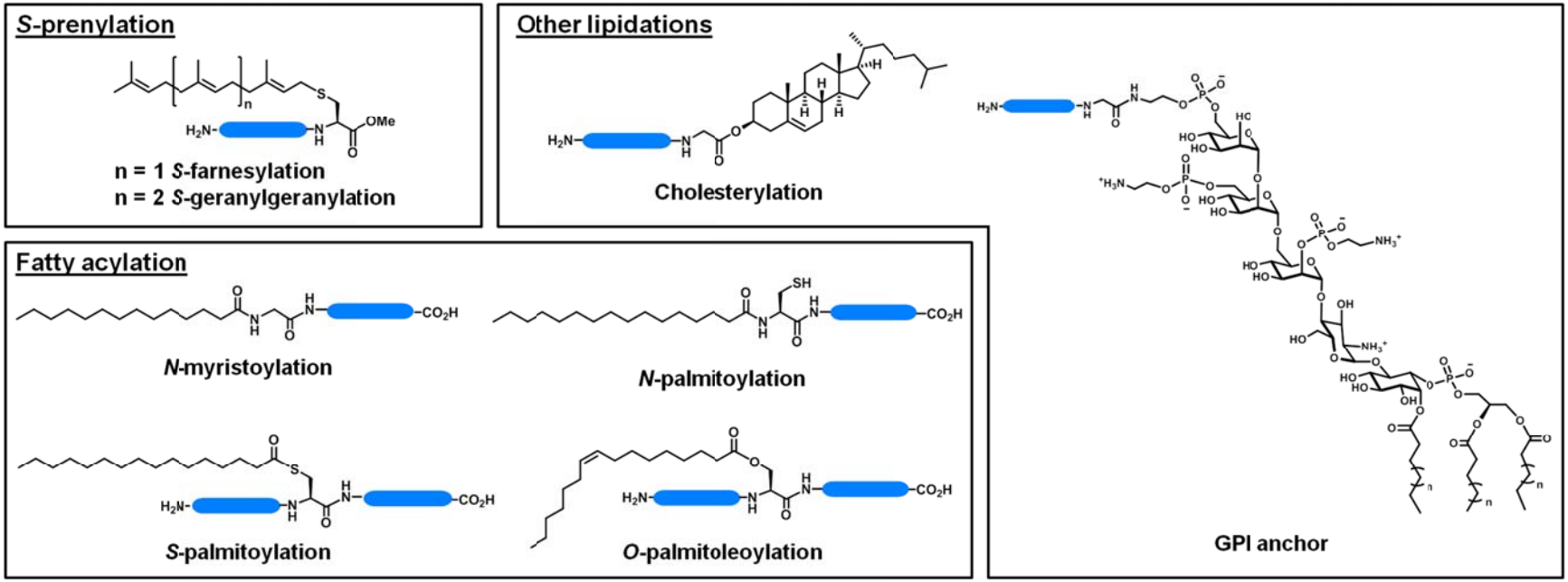

Figure 1: Survey of protein lipidation in eukaryotes. N-, S-and O-prefixes describe the linkage of the lipid attachment to proteins.

1.2 Protein fatty-acylation in eukaryotes

Fatty-acylated proteins are synthesized by discrete families of acyltransferases that utilize fatty acid–CoA substrates to yield cytoplasmic proteins that are *N*-myristoylated[21] or *S*-palmitoylated[22] as well as secreted proteins that can be *S*-, *N*-, or *O*-acylated[23-24] (Figure 1). *N*-Myristoyltransferases (NMTs, 2 in mammals, 1 in yeast) catalyze the transfer of myristic acid to N-terminal glycine residues of proteins bearing the GXXXS/T consensus sequence (Figure 2a)[21]. Alternatively the DHHC–protein acyltransferases (DHHC–PATs, ~23 in mammals, 7 in budding yeast) install palmitic acid onto cysteine residues of proteins (Figure 2b)[22]. In comparison to *N*-myristoylation, DHHC-PAT-mediated *S*-palmitoylation has no defined amino acid consensus sequence and *S*-palmitoylation sites are often modified with a heterogeneous composition of fatty acids. Moreover, *S*-palmitoylation is reversible, modulated by cellular stimulation and regulated by yet uncharacterized lipases[22], which suggests the *S*-acylation cycle may be particularly important for regulating dynamic processes in cells. Indeed, *S*-palmitoylation of *N*-myristoylated or *S*-prenylated proteins is typically required for stable membrane targeting of many proteins[1]. While many fatty-acylated proteins have been identified and are associated with various cellular pathways, their specific functions and mechanisms of regulation in physiology and disease remain to be explored.

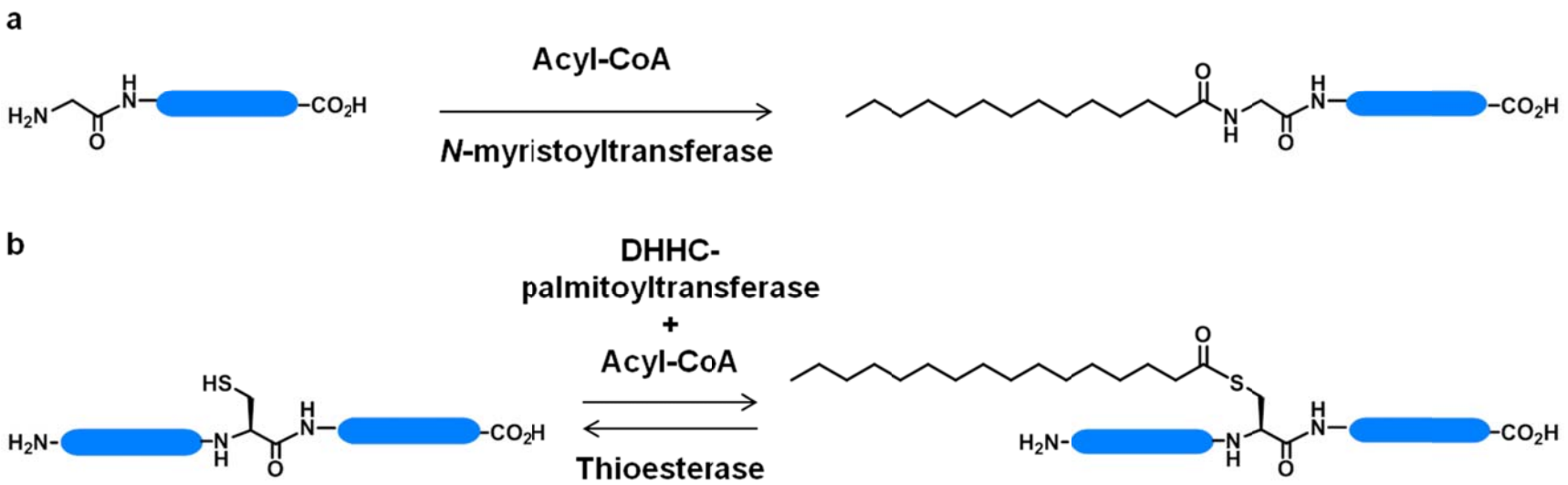

Figure 2: Protein fatty-acylation. (**a**) *N*-myristoylation. (**b**) DHHC-mediated *S*-palmitoylation.

1.3 Protein prenylation in eukaryotes

Protein prenylation encompasses *S*-farnesylation and *S*-geranylgeranylation (Figure 1), which are catalyzed by farnesyltransferase (FTase) and geranylgeranyltransferase I and II (GGTase I and GGTase II), respectively[25]. FTase and GGTase I transfer farnesyl pyrophosphate and geranylgeranyl pyrophosphate, respectively, onto the C-terminus of proteins that contain a C-terminal CaaX motif, where C is the modified cysteine, 'a' are often aliphatic amino acids and X represents an amino acid that determines specificity for the prenyltransferase. For example, X is frequently Met, Gln, or Ser for FTase, and Leu or Phe for GGTase I, whereas some CaaX motif proteins are substrates for both prenyltransferases. Following *S*-prenylation, the endopeptidase Ras converting enzyme 1 (RCE1) cleaves the tripeptide (aaX) to reveal a C-terminal cysteine that is subsequently methylated by isoprenylcysteine carboxyl methyltransferase (ICMT) (Figure 3a). In contrast, GGTase II (also called RabGGTase), a structurally and functionally different prenyltransferase, dually *S*-geranylgeranylates the family of Rab proteins at their C-terminal cysteine residues (Figure 3b). RabGGTase substrate specificity is not dictated by a consensus sequence but by Rab escort proteins (REPs) that bind Rab proteins and target them for enzymatic modification[25]. The largest group of *S*-prenylated proteins is the Ras superfamily of GTPases that encompasses the Ras, Rho/Rac and Rab subfamilies of proteins, which play critical regulatory roles in a variety of cellular processes, from cellular signaling to immune system functions[26].

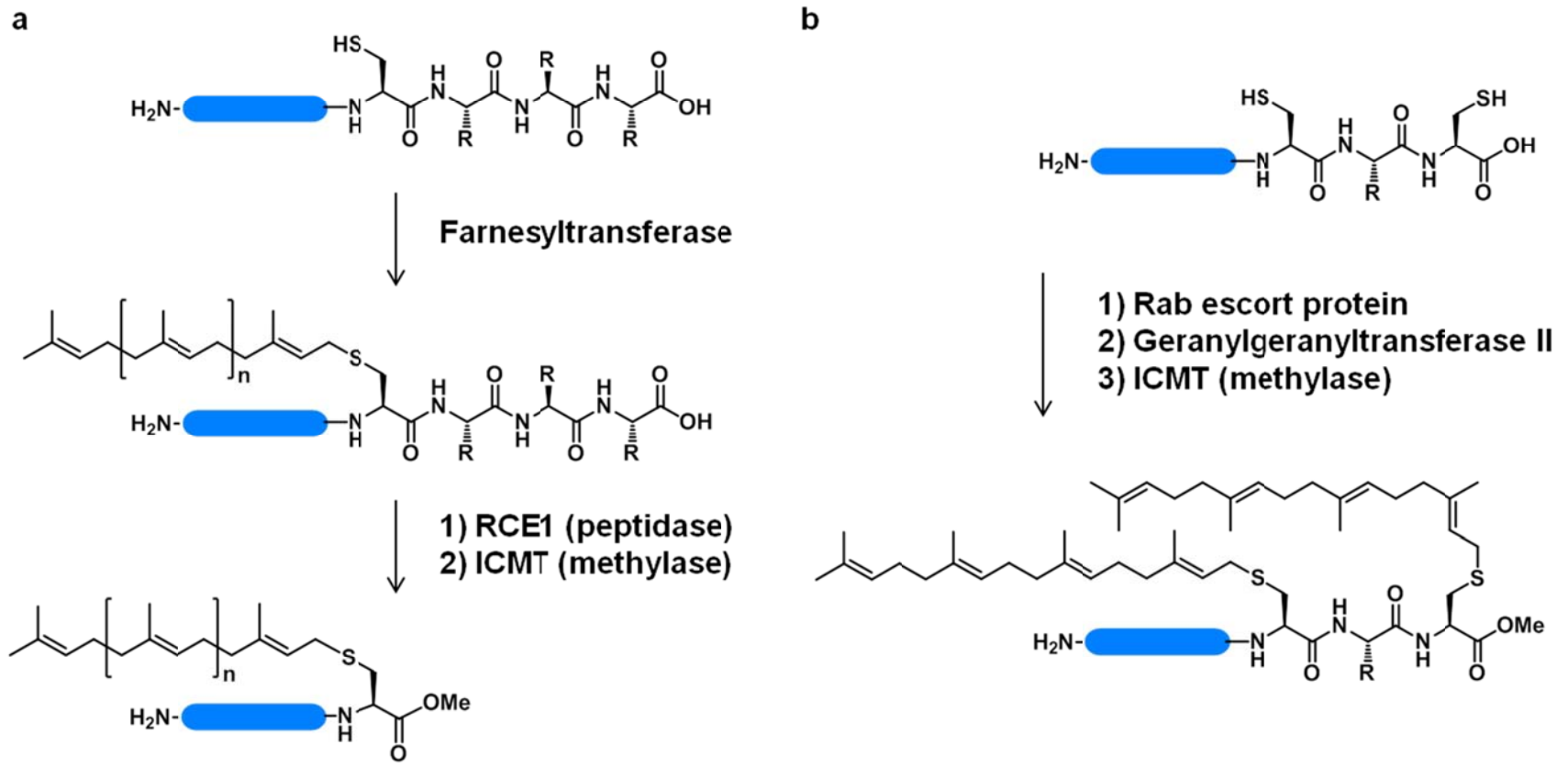

Figure 3: Protein prenylation. (**a**) *S*-prenylation of CaaX proteins followed by cleavage of aaX tripeptide by Ras converting enzyme 1 (RCE1) and methylation by isoprenylcysteine carboxyl methyltransferase (ICMT). n = 1: *S*-farnesylation, n = 2: *S*-geranylgeranylation. (**b**) Dual *S*-geranylgeranylation of Rab proteins.

1.4 Protein lipidation in host-pathogen interactions

Viral and bacterial pathogens evolved an array of mechanisms to subvert and exploit host immune systems for effective infection and replication[27]. Viruses gain entry into cells by exploiting specific lipid receptors to bind host cells and induce changes in membrane properties, which results in endocytosis and intracellular transport of viruses to their site of replication[28]. Several of these viral proteins exploit the host post-translational machinery to gain lipid anchors that regulate their function, membrane association and localization in the cell (Table 1). For example, HIV-1 Gag protein multimerization[29], influenza virus M2 protein lipid raft targeting[30], and large hepatitis delta antigen viral assembly[31] require myristoylation, palmitoylation and farnesylation, respectively.

Intracellular bacterial pathogens secrete effector proteins into host cells which co-opt host signaling pathways[32], subvert membrane transport pathways[33] and remodel host cellular membranes[34] to facilitate entry and evade lysosomal degradation. Several of these bacterial effectors also make use of the host protein lipidation machinery to regulate their localization and function in the cell (Table 2). For example, myristoylation-dependent targeting to the host plasma membrane of Avr proteins from *Pseudomonas syringae* enhances their virulence function[35]. Palmitoylation and prenylation of *Salmonella typhimurium* SifA[36], and prenylation of *Legionella pneumophila*[37-38] effectors is required to target them to the bacteria-containing vacuoles and promote infection. Pathogens thus utilize host-specific protein post-translational lipidation to access the subcellular compartments where they function.

Table 1: Survey of lipidated viral proteins.

Protein Name	Viruses	Modification	Site of lipidation	Sequence
Nef	Lentiviruses (HIV, SIV)	*N*-myristoylation	2	MGGKWS-
Gag	Retroviruses, Poxviruses	*N*-myristoylation	2	MGQIFS-
Large surface antigen	Hepatitis B virus	*N*-myristoylation	2	MGQNLS-
v-Src	Rous sarcoma virus	*N*-myristoylation	2	MGSSKS-
B5	Vaccinia virus	*S*-palmitoylation	301,303	-VCSCD-
M2	Influenza virus	*S*-palmitoylation	50	-FKCIY-
CM2	Influenza C virus	*S*-palmitoylation	324	-RWCGD-
MIR2	Kaposi's sarcoma-associated herpes virus	*S*-palmitoylation	146	-GICRV-
Large delta antigen	Hepatitis delta virus	*S*-farnesylation	211	-CRPQ
Us2	Pseudorabies virus	*S*-prenylation	253	-CTIS

Table 2: Survey of lipidated bacterial effectors.

Protein Name	Bacteria	Modification	Site of lipidation	Sequence
AvrRpm1	*Pseudomonas syringae*	*N*-myristoylation	2	MGCVSS-
AvrB	*Pseudomonas syringae*	*N*-myristoylation	2	MGCVSS-
AvrPto	*Pseudomonas syringae*	*N*-myristoylation	2	MGNICV-
AvrPphB	*Pseudomonas syringae*	*N*-myristoylation	63	-KGCASS-
AvrPphB	*Pseudomonas syringae*	*S*-palmitoylation	64	-KGCASS-
SifA	*Salmonella typhimurium*	*S*-palmitoylation	331	-CLCCFL
SifA	*Salmonella typhimurium*	*S*-geranylgeranylation	333	-CLCCFL
AnkB	*Legionella pneumophila*	*S*-farnesylation	169	-CVLC

Protein lipidation also regulates innate or adaptive immunity in plant and animals. For example, specific recognition of *Pseudomonas syringae* effector proteins AvrPto and AvrPtoB in tomato plants by Pto kinase and subsequent induction of defense responses is mediated by Pto myristoylation[39]. In mammalian cells, the initiation and propagation of T cell signaling requires the organization of receptors and signaling proteins such as CD4 and CD8 co-receptors, Src-family kinases, and the adaptor protein LAT, which are localized to lipid rafts due to their palmitoylation[40]. Prenylation of the Ras superfamily of GTPases is required for receptor-mediated activation, cell migration and membrane transport in mammalian cells through the Ras, Rho and Rab proteins, respectively[26]. Robust detection of lipidated proteins is challenging and improved detection methods would allow for further characterization of protein lipidation in host-pathogen interactions.

1.5 Chemical reporters for studying protein lipidation in cells

Protein lipidation in cells has historically been visualized by metabolic labeling with radioactive (^{3}H, ^{14}C) lipids followed by autoradiography of labeled proteins[41]. While effective, radioactivity often requires long exposure times and is hazardous[41-42]. The development of bioorthogonal labeling reactions (Figure 4a,b) and chemical reporters (azide-modified lipids, Figure 4c)[43] has provided improved methods for the detection of protein lipidation in cells (Figure 4d). For example, an azide-derivative of farnesol (az-FOH, Figure 4c) can be utilized by mammalian cells, installed onto prenylated proteins and readily visualized by streptavidin blot after reaction with phosphine–biotin reagents via the Staudinger ligation[44] (Figure 4a). Likewise, azido-fatty acids (az-12 and az-15, Figure 4c) can be metabolically incorporated onto *N*-myristoylated or *S*-palmitoylated proteins depending on their chain length and readily visualized after bioorthogonal labeling with secondary detection tags[45] (Figure 4d). Shorter fatty acid chemical reporter (az-12) preferentially labels *N*-myristoylated proteins, while longer chain analog (az-15) selectively targets *S*-palmitoylation[45-47] (Figure 4c). It should be noted that protein fatty-acylation in cells is heterogeneous, as some *S*-palmitoylated proteins are labeled with shorter and longer chain fatty acids. These fatty acid chemical reporters can also be utilized to detect the lipidation of secreted proteins such as Wnts[48].

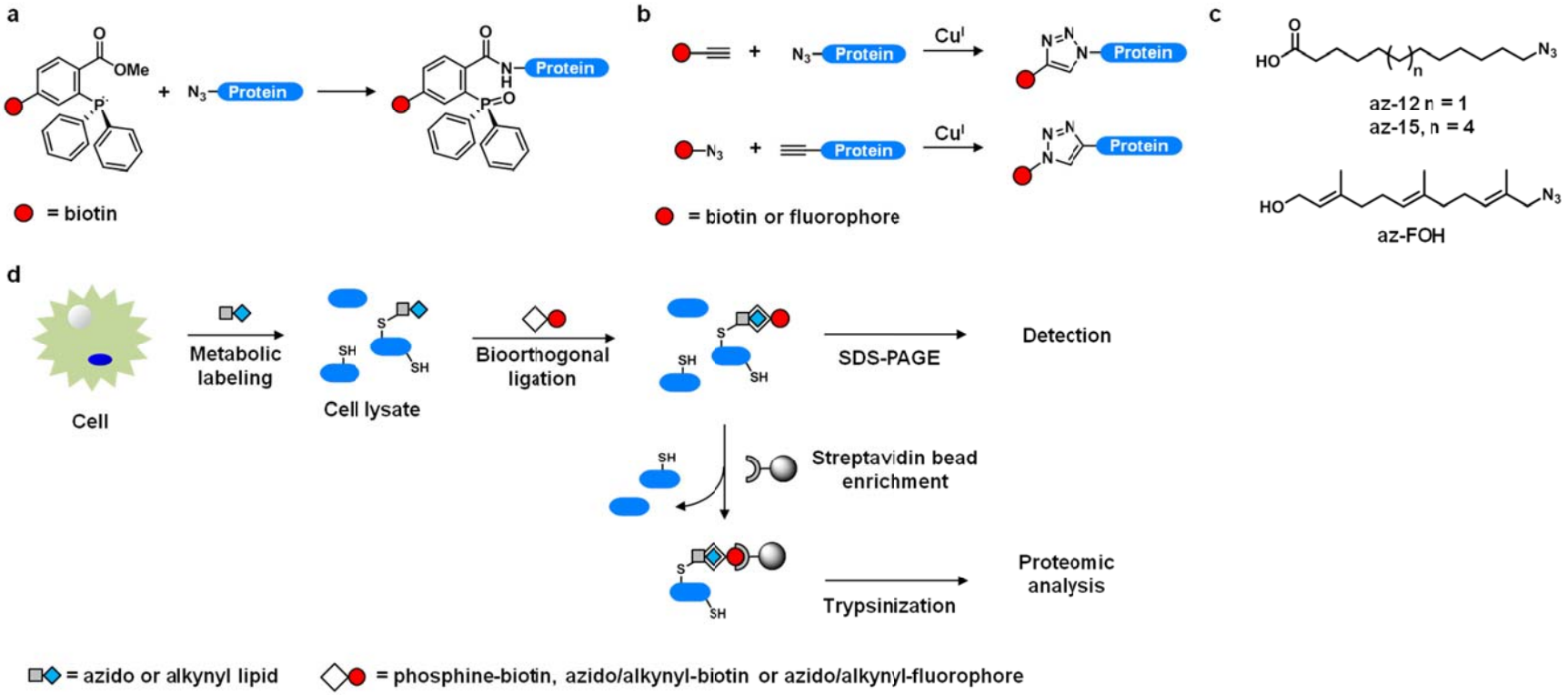

Figure 4: Lipidated proteins analysis using bioorthogonal ligation reactions. (**a**) Staudinger ligation. (**b**) Copper-catalyzed azide/alkyne cycloaddition (CuAAC). (**c**) Panel of azido-lipid analogs for protein lipidation studies. (**e**) Metabolic labeling of prenylated or fatty-acylated proteins in cells with azido chemical reporters followed by bioorthogonal labeling with a fluorophore for in-gel fluorescence detection or with biotin for affinity enrichment followed by subsequent proteomic analysis.

Azido-lipids/phosphine-biotin provides a convenient means to visualize prenylated and fatty-acylated proteins; however, immunoblotting methods are not ideal for analyzing quantitative changes in protein lipidation necessary for investigating dynamics or regulatory mechanisms. Advances in bioorthogonal labeling methods employing the copper-catalyzed azide/alkyne cycloaddition[49-51] (CuAAC, Figure 4b) suggested an opportunity to improve the analysis of lipidated proteins with chemical reporters. As with the Staudinger ligation, background labeling does occur in the CuAAC reaction when the alkyne reagent is present in excess, but significantly lower levels of non-specific reaction occur when the azide partner is employed in high concentration[52]. Thus, for the analysis of lipidated proteins, it would be advantageous to use lipid analogs that incorporate alkyne functional groups so that subsequent labeling could be performed with the more selective azide-containing reagent present in excess. In this thesis, I report the robust fluorescent detection of fatty-acylated and prenylated proteins with alkynyl-lipid chemical reporters that enable rapid biochemical analysis as well as proteomics of protein lipidation in mammalian cells.

CHAPTER II. Chemical reporters of protein fatty-acylation

I synthesized a series of alkynyl-fatty acids of different lengths as potential chemical reporters as well as a panel of biotinylated (alk-biotin, az-biotin) and fluorescent (alk-rho, az-rho) detection tags to explore the detection of fatty-acylated proteins with CuAAC (Figure 5).

2.1 Alkynyl-fatty acids synthesis

To generate gram quantities of alkynyl-fatty acids, I envisioned using the alkyne zipper reaction[53] to isomerize the internal alkyne of an acetylenic alcohol into a terminal alkyne followed by oxidation of the alcohol to the carboxylic acid (Figure 5a). Selective C-alkylation of dilithiated propargyl alcohol with different lengths of alkyl halides in liquid ammonia using lithium amide as the base afforded internal alkynyl alcohols (**1**, **2**, **3**) in good yields (93-97%, Figure 5a). Isomerization of the internal alkyne to the terminal position was accomplished via lithium wire and potassium *tert*-butoxide in 1,2-diaminopropane (70-78%, Figure 5a). Finally, the desired alkynyl-fatty acids (**alk-12**, **alk-14** and **alk-16**) were obtained after Jones oxidation (68-70%, Figure 5a).

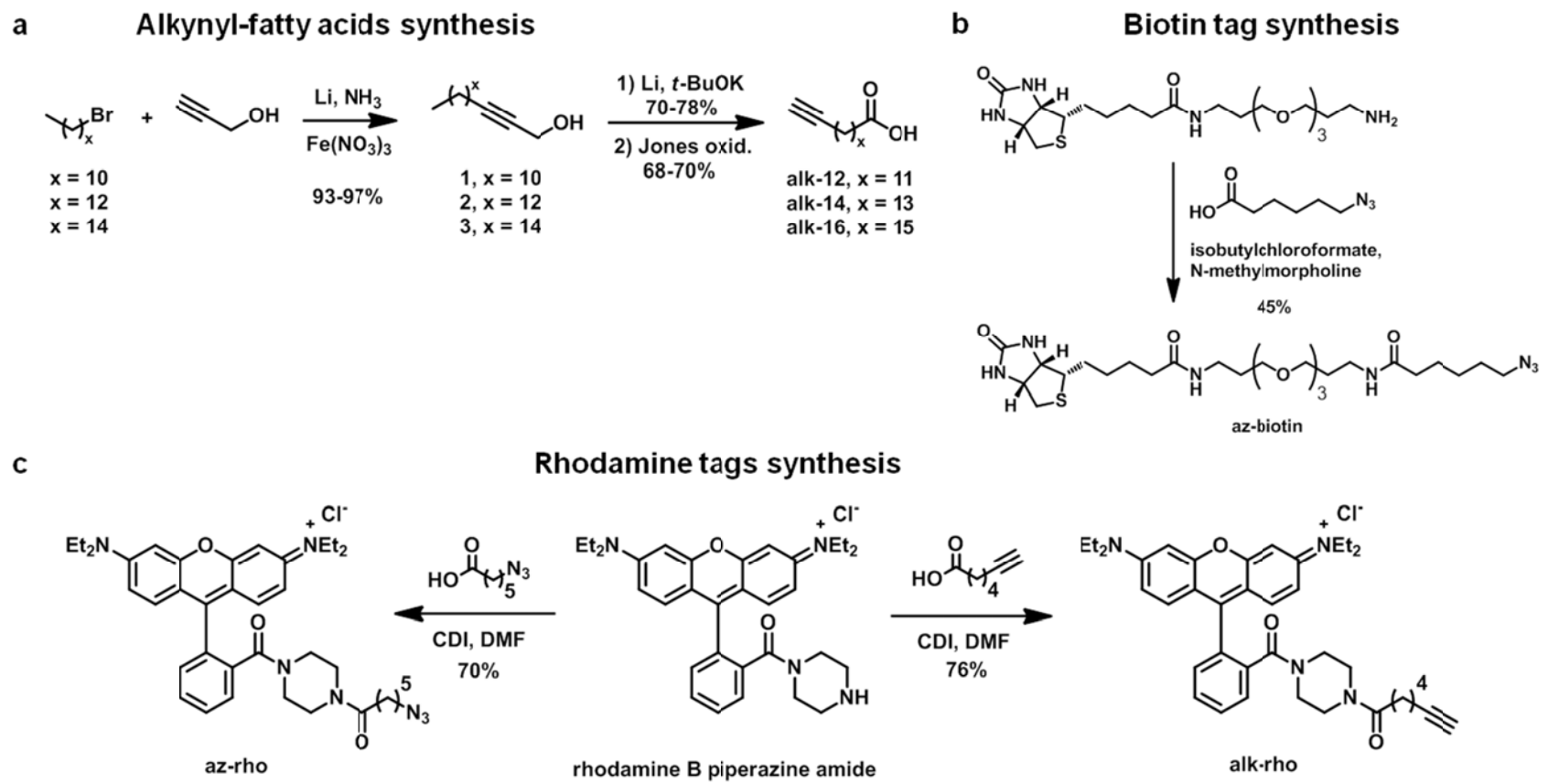

Figure 5: Synthesis of alkynyl-fatty acids and secondary detection tags. (**a**) Alkynyl-fatty acids synthesis. (**b**) Azido-biotin detection tag synthesis. (**c**) Rhodamine detection tags synthesis.

Secondary reaction tags for CuAAC were also synthesized. Azido-biotin (**az-biotin**) tag was obtained by coupling pegylated biotin[54] with 6-azidohexanoic acid chloroformate (45%, Figure 5b). The synthesis of fluorescent azide/alkyne tags was based on the efficient functionalization of Rhodamine B to the rhodamine-piperazine amide derivative[55]. Multigram quantities of these water-soluble fluorophores can be prepared from inexpensive precursors and purified without the use of chromatography. Rhodamine-piperazine amide was then acylated via carbonyldiimidazole transacylation with either 6-heptynoic acid to generate alkynyl-rhodamine (**alk-rho**, 76%, Figure 5c) or 6-azidohexanoic acid to yield azido-rhodamine (**az-rho**, 70%, Figure 5c).

2.2 Alkynyl-fatty acids characterization

2.2.1 Comparative analysis of bioorthogonal labeling methods

Comparative analysis of the Staudinger ligation and CuAAC reaction with azido-fatty acid-labeled cell lysates and biotinylated detection probes (phos-biotin and alk-biotin, respectively) revealed significantly improved detection of fatty-acylated proteins by streptavidin blotting with CuAAC (Figure 6a). We then investigated whether the orientation of alkyne and azide functional groups would influence the overall sensitivity of fatty-acylated protein analysis using CuAAC. Cells were metabolically labeled with azide- or alkynyl-analogues of myristic acid (az-12, alk-12) or palmitic acid (az-15, alk-14, alk-16) and assayed for the specific detection of fatty-acylated proteins in cell lysates using biotin (alk-biotin, az-biotin) or fluorescence (alk-rho, az-rho) detection tags and streptavidin blotting (Figure 6b) or in-gel fluorescence scanning (Figure 7a), respectively. Profiles of fatty-acylated proteins visualized by in-gel fluorescence scanning revealed substantially more proteins compared to streptavidin blotting, particularly with the

palmitic acid analogues (az-15, alk-14 and alk-16). Like their azide counterparts, the alkynyl-fatty acids (alk-12, alk-14 and alk-16) functioned as efficient chemical reporters of protein fatty-acylation and exhibited chain length-dependent protein labeling (Figure 7a). The similar profiles of fatty-acylated proteins visualized by azido- or alkynyl-fatty acid metabolic labeling and CuAAC in-gel fluorescence analysis reinforce the concept that the small azide and alkyne chemical reporters afford efficient tools to visualize protein fatty-acylation in cells (Figure 7a). Comparative analysis of fatty-acylated proteins visualized by in-gel fluorescence scanning demonstrated that alkynyl-fatty acid chemical reporters, in combination with the azido-rhodamine (az-rho) detection tag, improve the sensitivity of bioorthogonal labeling compared to the reverse CuAAC orientation owing to lower background signal (Figure 6b,7a). These observations are consistent with other studies using alkyne- or azide-functionalized chemical probes[52, 56].

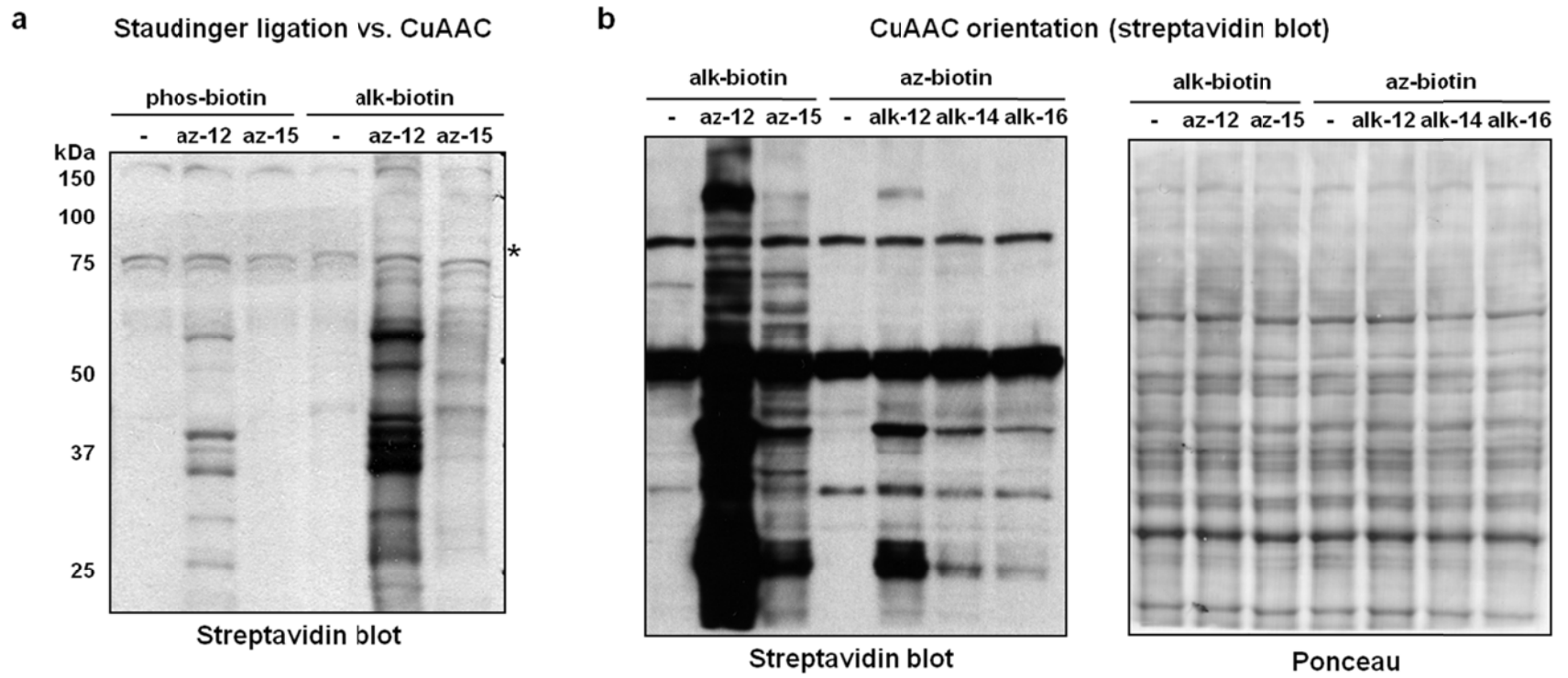

Figure 6: Biochemical analysis of chemical reporters for protein fatty-acylation in mammalian cells. (**a**) Staudinger ligation versus CuAAC. (*) Indicates comparable levels of endogenously biotinylated proteins. (**b**) Alkyne/azide orientation comparative analysis of protein fatty-acylation with CuAAC by streptavidin blot. Comparable levels of protein loading were demonstrated by Ponceau staining of the membrane. Experiments were performed with cell lysates from Jurkat T cells metabolically labeled with DMSO (-), 20 μM azido- or alkynyl-fatty acids (az-12, az-15, alk-12, alk-14 or alk-16).

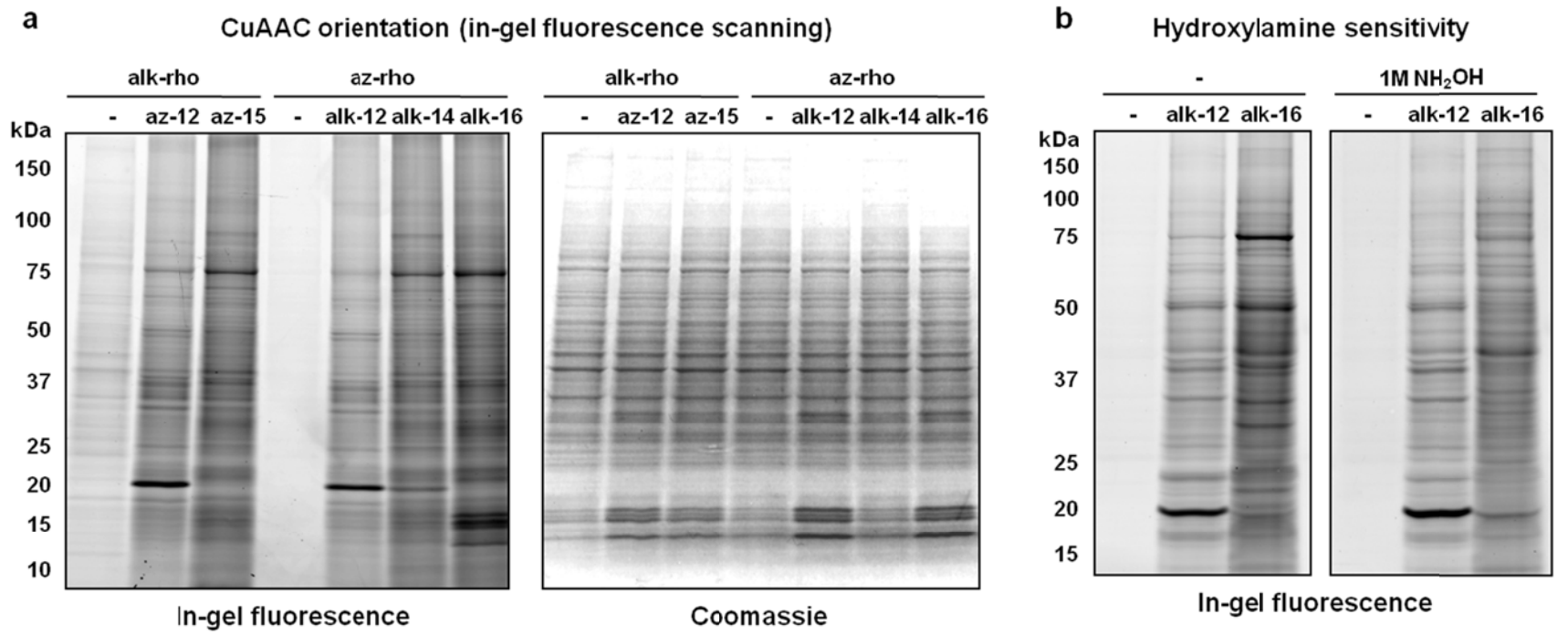

Figure 7: Biochemical analysis of chemical reporters for protein fatty-acylation in mammalian cells. (**a**) Alkyne/azide orientation comparative analysis of protein fatty-acylation with CuAAC by in-gel fluorescence scanning. Comparable levels of protein loading were demonstrated by Coomassie staining of the gel. (**d**) Hydroxylamine sensitivity of proteins in Jurkat cell lysates labeled with alkynyl-fatty acids. Experiments were performed with cell lysates from Jurkat T cells metabolically labeled with DMSO (-), 20 μM azido- or alkynyl-fatty acids (az-12, az-15, alk-12, alk-14 or alk-16).

2.2.2 Specificity and generality of fatty-acylated protein labeling with chemical reporters

Having established robust fluorescence detection of proteins metabolically labeled with alkynyl-fatty acid chemical reporters, we determined their kinetics and specificity of labeling fatty-acylated proteins in cells. Time- and dose-dependent analyses of metabolic labeling with the alkynyl-fatty acids revealed that CuAAC and in-gel fluorescence imaging protocol required shorter labeling time (minutes) and lower concentrations of fatty acid chemical reporters to robustly detect fatty-acylated proteins compared to streptavidin blotting[22] (Figure 8a,b). Competition of alkynyl-fatty acid protein labeling (alk-12, alk-14 and alk-16) with naturally occurring fatty acids revealed that alk-12 protein labeling is preferentially blocked by myristic acid, whereas alk-14 and alk-16 protein labeling is most effectively reduced by palmitic acid (Figure 9a,b). Inhibition of protein synthesis with cycloheximide (CHX) abrogated the metabolic labeling of several prominent polypeptides by alk-12 (Figure 10a). Most proteins targeted by alk-12, alk-14 and alk-16 were resistant to CHX treatment, however, suggesting fatty-acylation of these protein substrates occurs posttranslationally. Coincubation of the alkynyl-fatty acids with 2-hydroxymyristic acid (HMA), a reported *N*-myristoylation inhibitor[57], selectively blocked alk-12 protein labeling compared to alk-14 and alk-16 (Figure 10b). In contrast, addition of 2-bromopalmitic acid (2BP), a nonspecific *S*-palmitoylation inhibitor[58], at concentrations that did not induce cell death reduced protein labeling with alk-12, alk-14 and alk-16 (Figure 10c). To differentiate between *N*-myristoylated and *S*-acylated proteins, az-rho-modified alkynyl-fatty acid-labeled cell lysates were subjected to in-gel treatment with hydroxylamine (NH_2OH)[59], which preferentially cleaves thioesters at

neutral pH. The fluorescent signals of alkynyl-fatty acid-labeled proteins were reduced after in-gel exposure to NH_2OH; however, the CHX-sensitive proteins labeled by alk-12 were resistant to NH_2OH cleavage (Figure 7b). These experiments suggest that alk-12 cotranslationally targets *N*-myristoylated proteins (CHX-sensitive and NH_2OH-resistant) as well as *S*-acylated proteins (CHX-resistant and NH_2OH-sensitive), whereas alk-16 preferentially labels *S*-acylated proteins in cell lysates. Protein labeling with alk-14 appears to represent a combination of alk-12 and alk-16 labeling, which is consistent with previous metabolic labeling experiments using az-14, an azido-fatty acid analogue bearing 14-carbons[45].

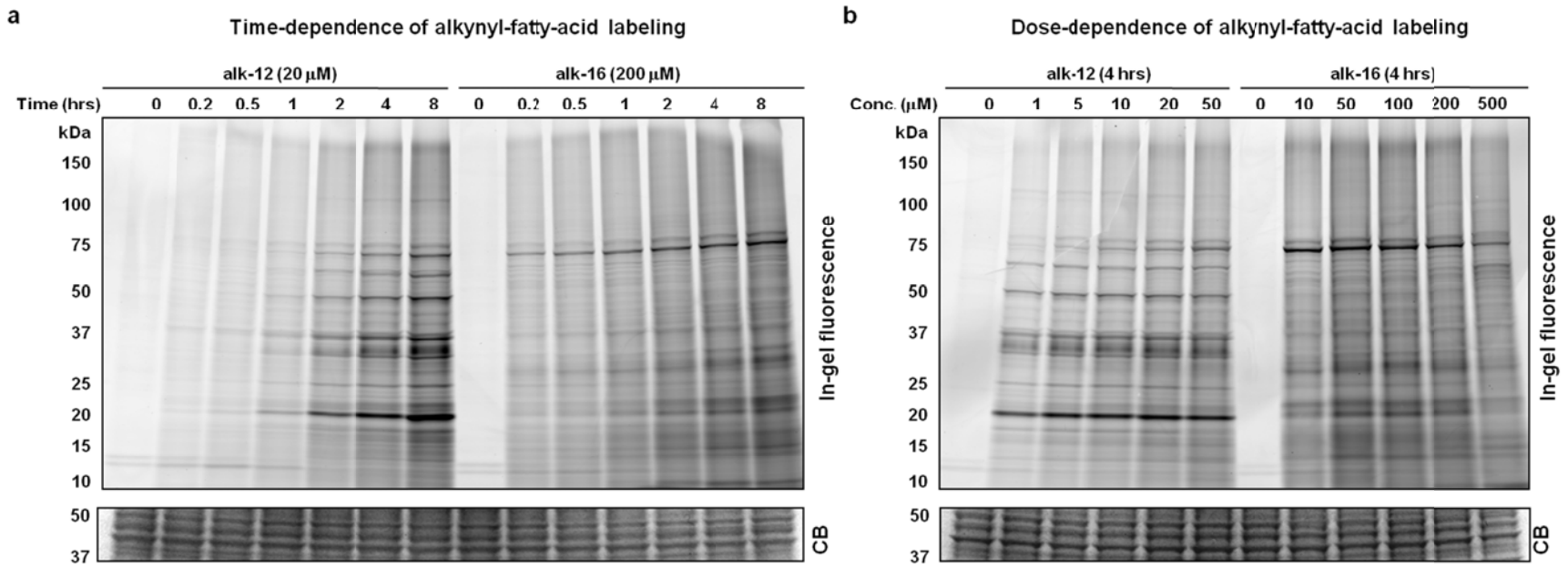

Figure 8: Specificity of alkynyl-fatty acids labeling in cells. (**a**) Labeling of Jurkat cells with alk-12 (20 μM) and alk-16 (200 μM) over time (hours). (**b**) Labeling of Jurkat cells with alk-12 and alk-16 at different concentrations (μM) over 4 hours. Upper panels, in-gel fluorescence. Lower panels, comparable levels of protein loading was demonstrated by Coomassie staining of the gel.

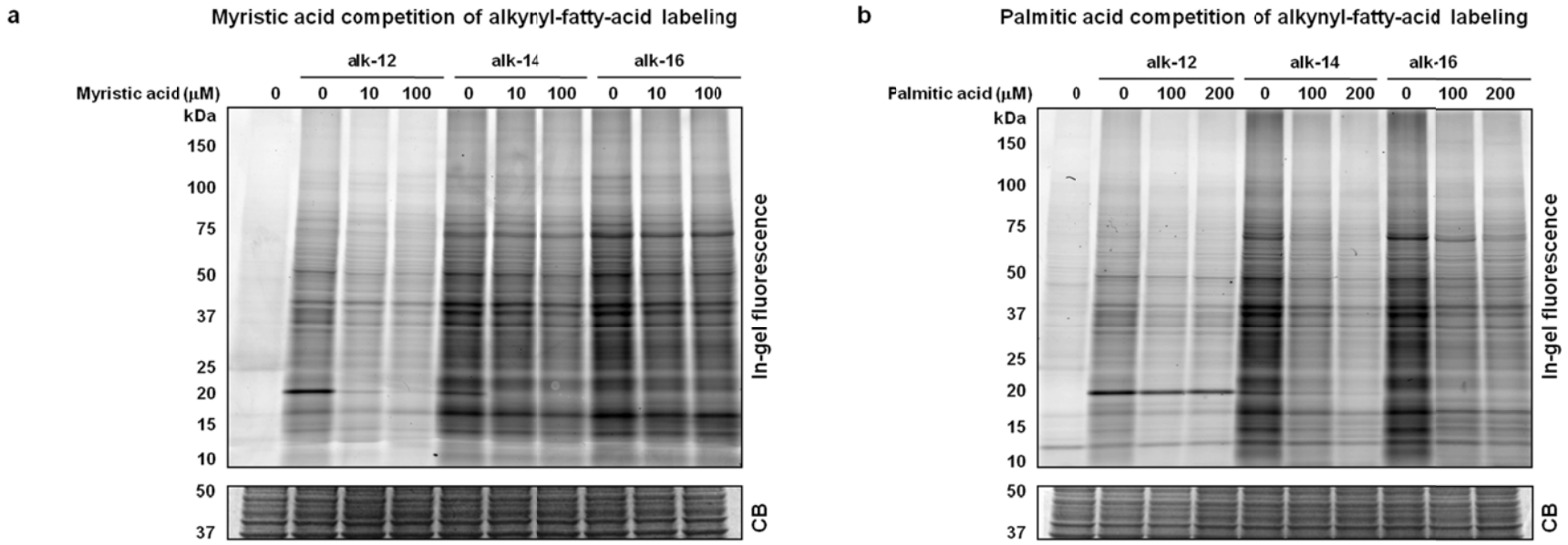

Figure 9: Specificity of alkynyl-fatty acids labeling in cells. (**a**) Competition of alk-12, alk-14 and alk-16 (10 μM) labeling in Jurkat cells with different concentrations of myristic acid. (**b**) Same as in **a**, but with different concentrations of palmitic acid. Upper panels, in-gel fluorescence. Lower panels, comparable levels of protein loading was demonstrated by Coomassie staining of the gel.

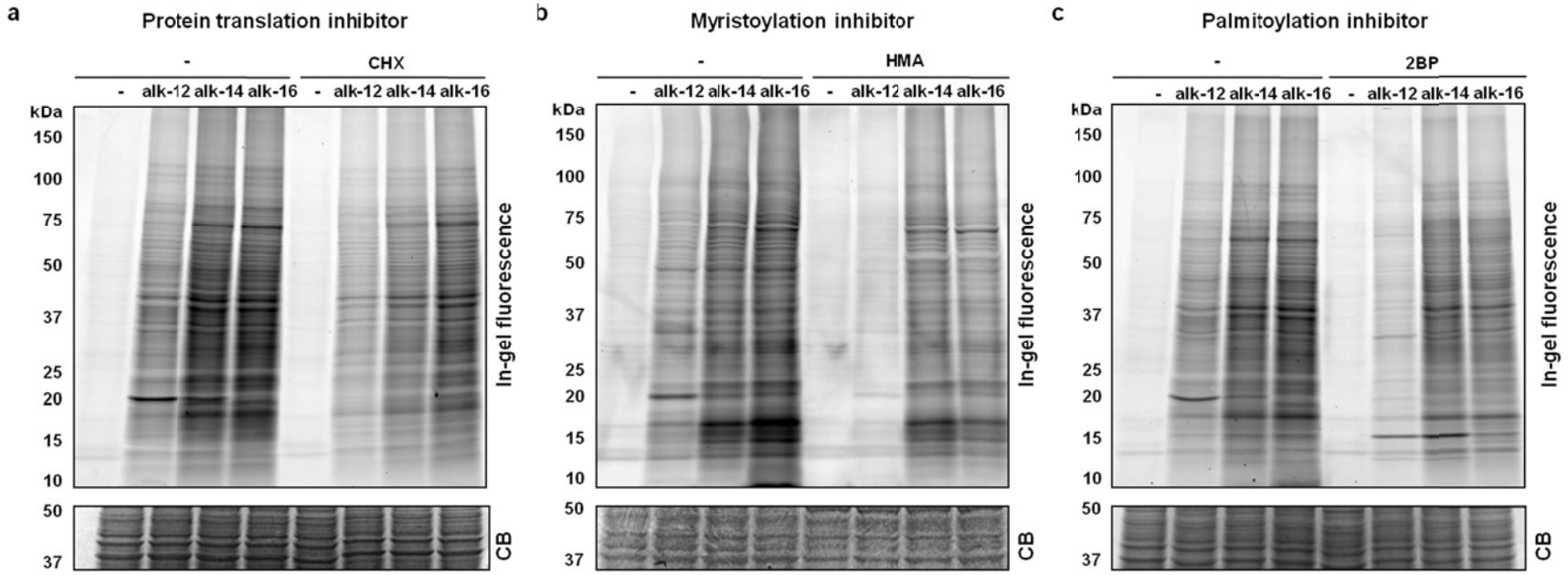

Figure 10: Specificity of alkynyl-fatty acids labeling in cells. (**a**) Inhibition of alk-12, alk-14 and alk-16 (20 μM) labeling in Jurkat cells with cycloheximide (CHX) (10 μM). (**b**) Same as in **a**, but with 2-hydroxymyristic acid (HMA) (1 mM). (**c**) Same as in **a**, but with 2-bromopalmitate (2BP) (50 μM). Upper panels, in-gel fluorescence. Lower panels, comparable levels of protein loading was demonstrated by Coomassie staining of the gel.

We further evaluated the efficiency and specificity of our chemical reporters in the detection of different classes of fatty-acylated proteins: *N*-myristoylated and *S*-palmitoylated – Lck[60] and Fyn[61], *S*-palmitoylated only - Linker for Activation of T Cells (LAT)[62], and *S*-palmitoylated and *S*-prenylated – Ras[63] (Figure 11a). For these studies, Jurkat cells were metabolically labeled with azido- (az-12, az-15) or alkynyl- (alk-12, alk-16) fatty acids. Proteins of interest were immunoprecipitated from cell lysates, subjected to CuAAC with biotinylated (alk-biotin, az-biotin) or fluorescent (alk-rho, az-rho) detection tags prior to visualization by streptavidin blot (Figure 11b) or in-gel fluorescence scanning (Figure 11c), respectively. As with cell lysates, in-gel fluorescence detection of the immunopurified fatty-acylated proteins (Lck, LAT and Ras) was markedly improved compared to streptavidin blotting and alkynyl-fatty acids/azido-rhodamine afforded the optimal signal-to-noise for fluorescent detection (Figure 11b,c). For example, *S*-acylation of LAT was observed with myristic acid analogues (az-12, alk-12) and nearly undetectable using palmitic acid analogues (az-15, alk-16) by streptavidin blotting (Figure 11b, top panels), but was robustly visualized by in-gel fluorescence scanning (Figure 11c, top panels). Similar observations were obtained with Lck and Ras (Figure 11b,c, middle and bottom panels). Although it is unclear why the detection of *S*-acylated proteins is more efficient with myristic acid analogues (az-12, alk-12) compared to palmitic acid analogues (az-15, alk-16) by streptavidin blotting, direct in-gel fluorescence detection affords more consistent, reproducible and specific visualization of fatty-acylated proteins that avoids any variability associated with immunoblotting of hydrophobic lipidated proteins (Figure 11b,c).

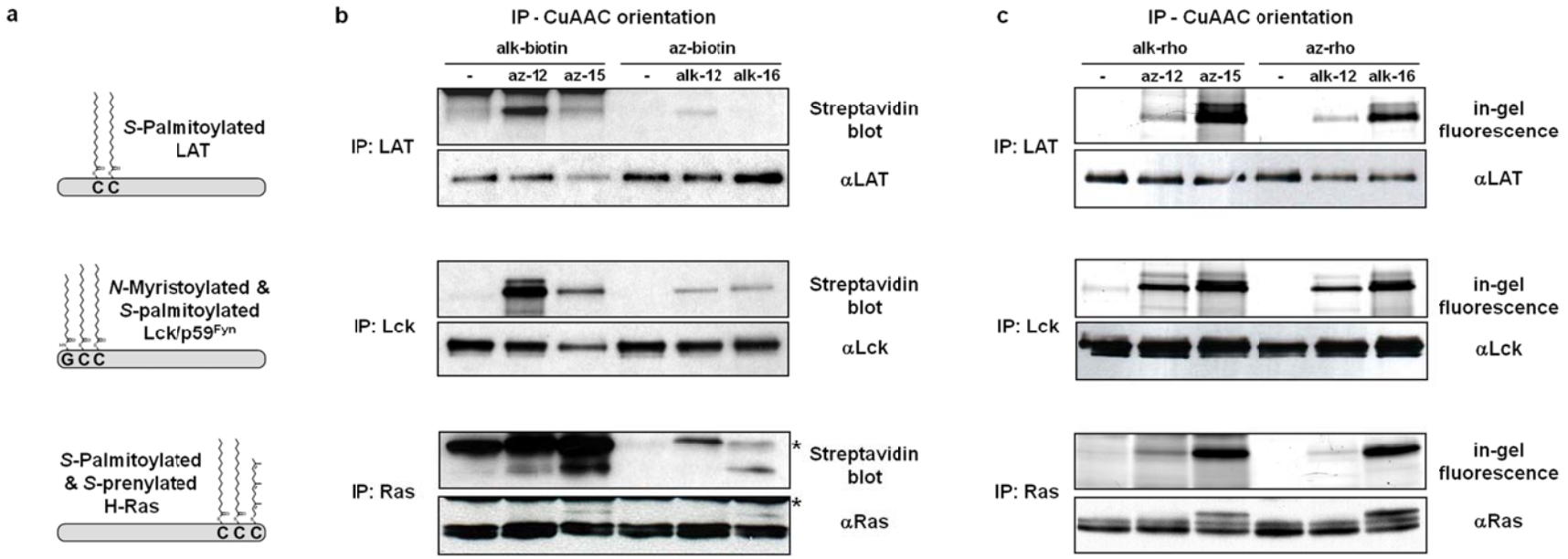

Figure 11: Robust visualization of fatty-acylated proteins after immunoprecipitation. (**a**) Schematic representation of lipidation sites for LAT (*S*-palmitoyl-Cys26, *S*-palmitoyl-Cys29), Lck (*N*-myristoyl-Gly2, *S*-palmitoyl-Cys3, *S*-palmitoyl-Cys5), H-Ras (*S*-palmitoyl-Cys181, *S*-palmitoyl-Cys184, *S*-prenyl-Cys186) and Fyn (*N*-myristoyl-Gly2, *S*-palmitoyl-Cys3, *S*-palmitoyl-Cys6), examples of different classes of fatty-acylated proteins. (**b**) Comparative analysis of CuAAC orientation with Lck, LAT and Ras by streptavidin blotting. (*) Indicates nonspecific cross-reactivity of streptavidin or anti-mouse secondary antibody with light-chain of anti-Ras antibody. (**c**) Comparative analysis of CuAAC orientation with Lck, LAT and Ras by in-gel fluorescence scanning. Upper panels, in-gel fluorescence. Lower panels, comparable levels of protein loading was demonstrated by blotting for the corresponding protein.

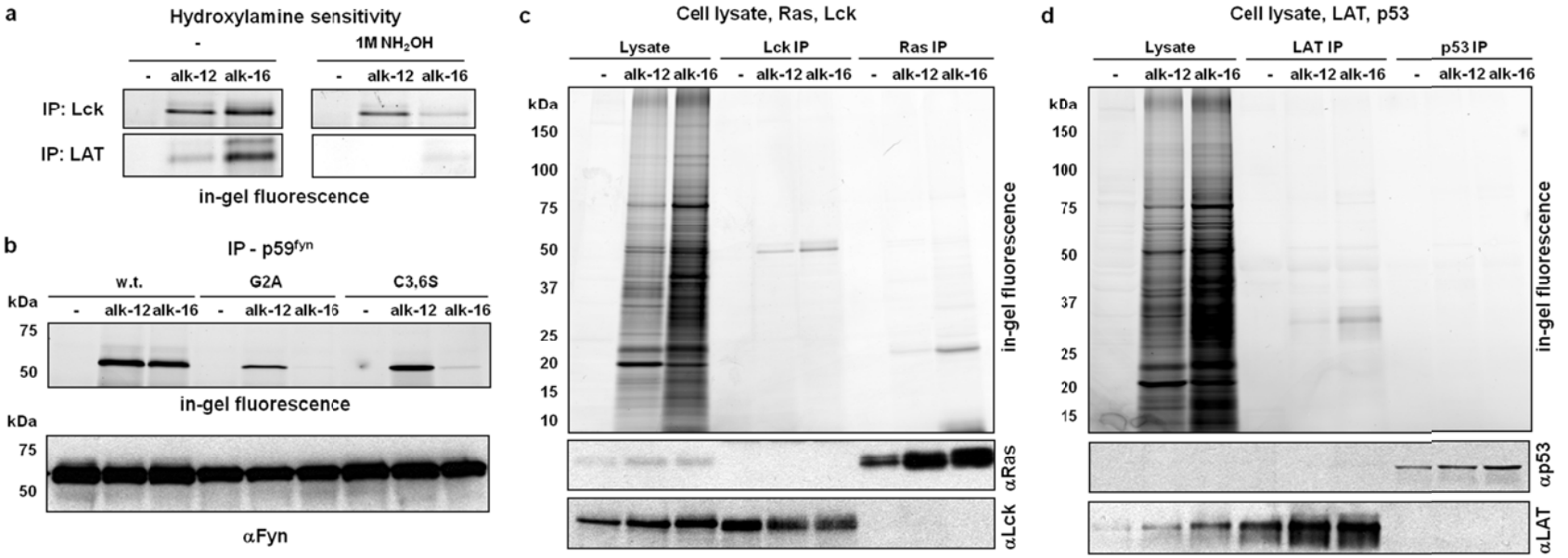

Figure 12: Robust visualization of fatty-acylated proteins after immunoprecipitation. (**a**) Hydroxylamine sensitivity of alkynyl-fatty acid Lck and LAT labeling. Experiments were performed with cell lysates from Jurkat T cells metabolically labeled with DMSO (-), 20 μM azido- or alkynyl-fatty acids (az-12, az-15, alk-12, or alk-16). (**b**) Comparative analysis of acylation state of wild-type, G2A mutant and C3,6S mutant Fyn. HeLa cells were metabolically labeled with DMSO (-) or alkynyl-fatty acids (20 μM alk-12 or alk-16). Comparable protein load was demonstrated by blotting for the corresponding proteins. (**c**) Immunoprecipitation of Ras and Lck from Jurkat cell lysates labeled with alk-12 or alk-16 (20 μM). (**d**) Immunoprecipitation of LAT and p53 from Jurkat cell lysates labeled with alk-12 or alk-16 (20 μM). Upper panels, in-gel fluorescence. Lower panels, comparable levels of protein loading was demonstrated by blotting for the corresponding protein.

Fatty acid chemical reporters combined with fluorescence detection enables specific detection of *N*-myristoylated and *S*-palmitoylated proteins. Fatty-acylation of Lck, a *N*-myristoylated and *S*-palmitoylated protein, was readily observed with myristic acid (az-12 and alk-12) and palmitic acid (az-15, alk-16) chemical reporters, whereas LAT and Ras, *S*-palmitoylated proteins without N-terminal Gly residues, were more prominently labeled with palmitic acid chemical reporters (az-15, alk-16) (Figure 11c). The low levels of LAT and Ras labeling with az-12 and alk-12 is consistent with our experiments with cell lysates (Figure 7c,d), which further demonstrates that myristic acid analogues can be incorporated onto *S*-acylated proteins, albeit less efficiently than longer chain fatty acids. These observations are not unexpected, as *S*-acylation is known to involve a heterogeneous composition of fatty acids[64]. In-gel NH_2OH treatment of alkynyl-fatty acid labeled Lck and LAT reduced the fluorescent signal derived from alk-16 on both proteins, but did not alter the alk-12 labeling of Lck (Figure 12a). We also analyzed the specificity of our fatty acid chemical reporters with wild-type and mutant constructs of p59 Fyn[61], a well-characterized *N*-myristoylated and *S*-palmitoylated Src-family kinase, by overexpression in HeLa cells, metabolic labeling and immunoprecipitation (Figure 12b). Fatty-acylation of wild-type Fyn is readily detected with alk-12 and alk-16 labeling, whereas the *N*-myristoylation G2A mutant exhibited significantly reduced alk-12 labeling and was undetectable with alk-16 (Figure 12b). The dual *S*-palmitoylation-deficient C3,6S mutant Fyn was efficiently labeled with alk-12 and not with alk-16 (Figure 12b). These results are quantitatively identical to previously described experiments using radiolabeled fatty acids, which also demonstrated residual labeling of G2A mutant Fyn with a ^{125}I-myristic acid analog and no labeling with ^{125}I-

palmitic acid analogue[61, 65]. Our experiments therefore also support the model that *N*-myristoylation precedes *S*-palmitoylation and highlight the possibility of fatty-acylation at N-terminal alanine residues. In contrast to LAT, Lck, Ras and Fyn, no alkynyl-fatty acid labeling was observed for p53, a prominent acetylated protein for which fatty-acylation has not been reported[66], when analyzed in parallel with LAT, Lck and Ras (Figure 12c,d). Collectively, our experiments with cell lysates and specific proteins demonstrate that alk-12 and alk-14 label *N*-myristoylated and *S*-acylated proteins, whereas longer-chain fatty acid chemical reporters such as alk-16 preferentially target *S*-acylated proteins.

The generality of our method was evaluated by labeling different mammalian cell types (HeLa, 3T3, DC2.4, Jurkat and primary splenocytes) with alkynyl-fatty acids (alk-12 or alk-16). This comparative analysis revealed remarkably diverse profiles of fatty-acylated proteins amongst different cell types (Figure 13a,b). While some fatty-acylated polypeptide bands are common among the different cell types, distinct *N*-myristoylation and *S*-palmitoylation patterns are readily apparent. Indeed, the complete repertoire of fatty-acylated proteins varies dramatically between epithelial cell lines (HeLa and NIH 3T3 fibroblasts), a monocyte-derived cell line (DC2.4), T cells (Jurkat) and splenocytes (Figure 13a,b). These experiments highlight the utility of our fatty acid chemical reporters and improved detection conditions, which demonstrate unique profiles of fatty-acylated proteins in discrete cell types and primary tissues that undoubtedly contribute to specific cellular properties.

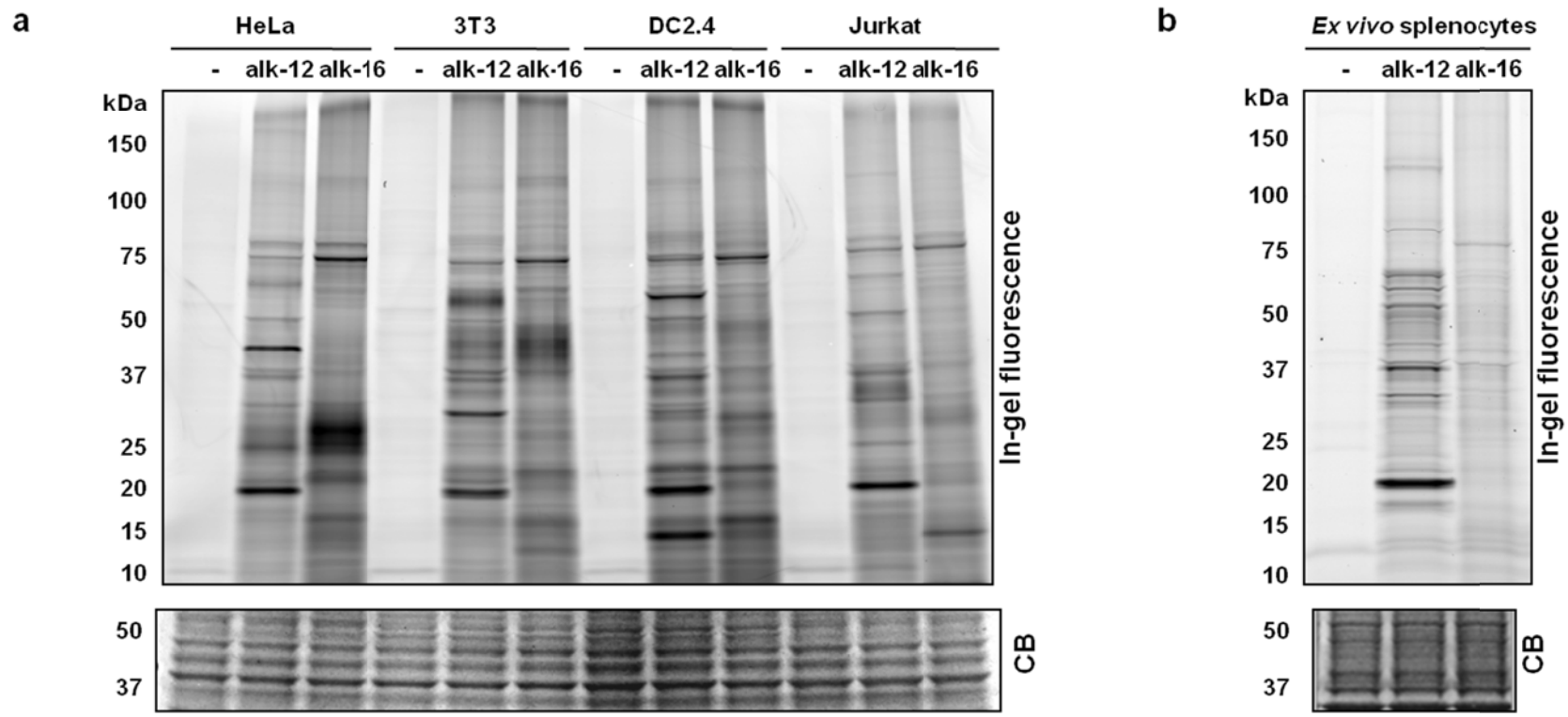

Figure 13: Profile of fatty-acylated proteomes in different cell lines and mouse tissues. Fatty-acylated proteins from (**a**) mammalian cell lines (HeLa, 3T3, DC2.4 or Jurkat T cells) or (**b**) splenocytes metabolically labeled with DMSO (-) or alkynyl-fatty acids (20 μM alk-12 or 200 μM alk-16). Comparable levels of protein loading were demonstrated by Coomassie staining of the gels.

The visualization of fatty-acylated proteins from living animals would afford new opportunities to address protein lipidation in physiology and disease. To explore the utility of our fatty acid chemical reporters *in vivo*, mice were intraperitoneally injected with alkynyl-fatty acids (alk-12 or alk-16) and analyzed for protein fatty-acylation in various tissues. Following one hour of metabolic labeling with our alkynyl-fatty acids *in vivo*, protein fatty-acylation could be visualized in cell lysates prepared from splenocyte, liver and kidney (Figure 14a). In particular, *in vivo* labeling with alk-12 afforded a discrete profile of fatty-acylated proteins from splenocytes similar to *ex vivo* labeling (Figure 13b,14a). While the profile of *S*-palmitoylated proteins with alk-16 was not as prevalent as *ex vivo* labeling experiments, specific fatty-acylated proteins are clearly detected from tissues (Figure 14a). The analysis of protein fatty-acylation profiles at different times after *in vivo* administration in splenocyte and liver lysates revealed that the labeling of fatty-acylated proteins decreases over time (Figure 14b). These experiments suggest that protein fatty-acylation is quite dynamic *in vivo*. Nonetheless, these *in vivo* labeling experiments demonstrate that alkynyl-fatty acid chemical reporters can function in living animals and enable the specific detection of fatty-acylated proteins in primary tissues. It should also be noted that our fatty acid chemical reporters were well tolerated by the mice, as no overt toxicity was observed following *in vivo* administration, even after several days.

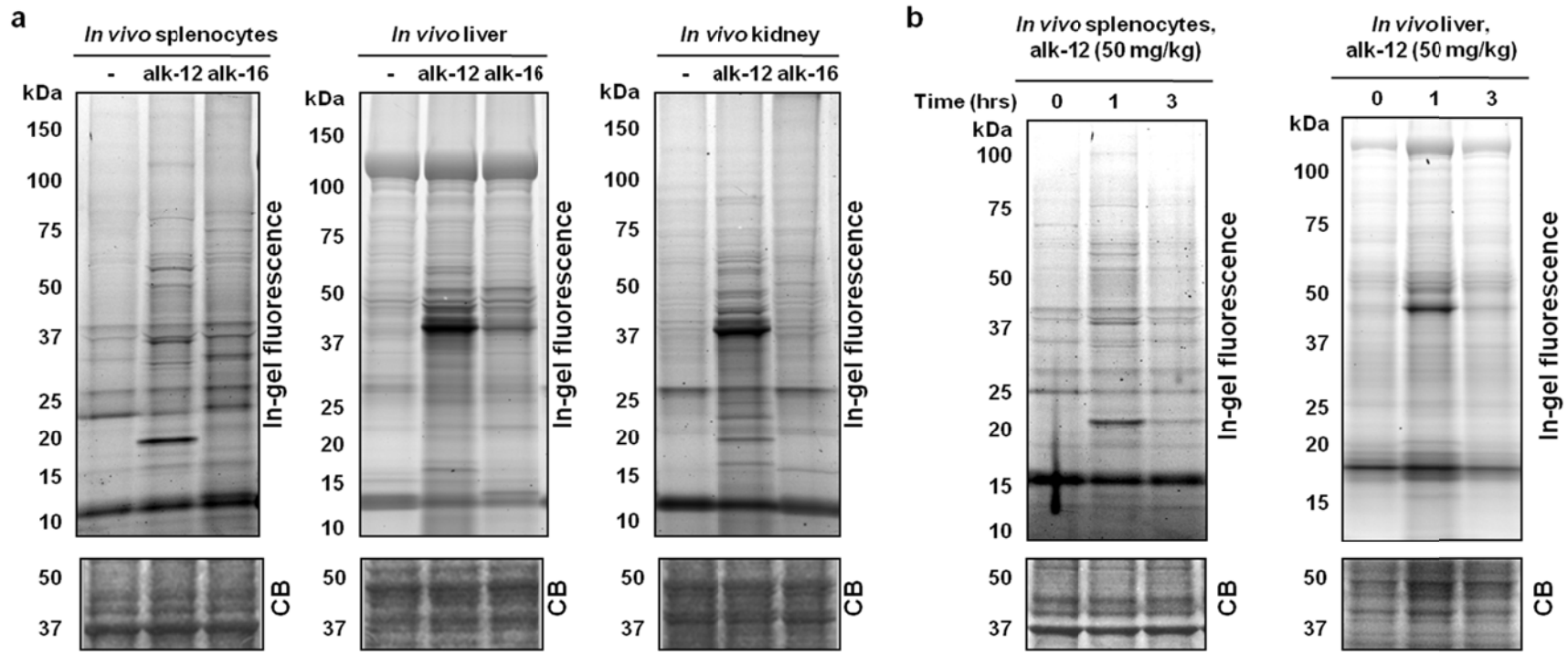

Figure 14: Profile of fatty-acylated proteomes in mouse tissues. (**a**) Fatty-acylated proteins from splenocytes, liver and kidney after intraperitoneal administration of alk-12 (250 mg/kg) or alk-16 (250 mg/kg) to mice. (**b**) Time-course of fatty-acylated proteins from splenocytes and liver after intraperitoneal administration of alk-12 (50 mg/kg) to mice. Comparable levels of protein loading were demonstrated by Coomassie staining of the gels.

2.3 Application of fatty acid chemical reporters

The utility of alkynyl-fatty acids for the detection and analysis of fatty-acylated proteins in cells was demonstrated through several collaborations. The large-scale proteomic analysis of mammalian proteins targeted by alkynyl-fatty acid chemical reporters in total cell lysates from fully solubilized Jurkat T cells identified known fatty-acylated proteins and many new candidates, including nuclear proteins and in particular histone H3 variants[67]. This collaboration with Dr John Wilson revealed that histones H3.1, H3.2, and H3.3 are modified with fatty acid chemical reporters and identified the conserved cysteine 110 as a new site of *S*-acylation on histone H3.2. This newly discovered modification of histone H3 could have implications for nuclear organization and chromatin regulation. Proteomic studies with Dr Jacob Yount also identified over 150 lipid-modified proteins with diverse cellular functions, including innate immunity, by large-scale profiling of palmitoylated proteins with alkynyl-fatty acid alk-16 in a dendritic cell line[10]. The study revealed that *S*-palmitoylation of interferon-induced transmembrane protein 3 (IFITM3) on membrane-proximal cysteines controls its clustering in membrane compartments and its antiviral activity against influenza virus. The sites of *S*-palmitoylation are highly conserved among the IFITM family of proteins in vertebrates, which suggests that *S*-palmitoylation of these immune effectors may be an ancient post-translational modification that is crucial for host resistance to viral infections.

Metabolic labeling of bacteria with fatty acid chemical reporters by Kavita Rangan allowed rapid profiling of largely uncharacterized bacterial lipoproteins[9]. We identified many candidate lipoproteins in *Escherichia coli* and detected a novel fatty-

acylation modification on YjgF. Dr Stuart Hicks in the Galan Laboratory at Yale School of Medicine also showed that *S*-palmitoylation of a conserved cysteine residue within the N-terminal domains of *Salmonella typhimurium* secreted effectors SspH2 and SseI localizes them to the plasma membrane of host cells and that effector protein lipidation is critical for effector function[12].

Using these fatty acid reporters, Dr Mingzi Zhang and Dr Lun Kelvin Tsou described a tandem labeling and detection method to simultaneously monitor dynamic *S*-palmitoylation and protein turnover[68]. By combining *S*-acylation (alk-16) and cotranslational (az-12) fatty acid chemical reporters with orthogonal azide/alkyne fluorophores, dual pulse-chase analysis of Lck revealed accelerated palmitate cycling upon T-cell activation. Pharmacological perturbation of Lck palmitate turnover suggests yet uncharacterized serine hydrolases contribute to dynamic *S*-acylation in cells. Dr Stuart Hicks in Machamer Laboratory (Johns Hopkins University) also observed differential dynamics of palmitoylation sites in a G protein-coupled receptor (GPCR), the cytoplasmic tail of β_1-adrenergic receptor[69]. Palmitoylation at the proximal site, a consensus for GPCRs, is remarkably stable, while palmitoylation at the distal site is rapidly turned over. These sites are modified in different cellular compartments, and the distal palmitoylation site contributes to efficient internalization of the receptor following agonist stimulation. Our results have important implications for function and regulation of the clinically important β_1-adrenergic receptor.

The proteomic analysis of fatty-acylated proteins using alkynyl-fatty acid chemical reporters has revealed a greater diversity of lipid-modified proteins in mammalian and bacterial cells than previously appreciated and identified novel post-

translational fatty-acylation of proteins. Detection of *S*-palmitoylation of IFITM3, YjgF, SspH2, SseI and β_1-adrenergic receptor are important for elucidating their mechanism of action and for the design of therapeutics. Furthermore, tandem imaging method using fatty-acid chemical reporters allows the investigation of dynamic palmitoylation-dependent regulation of protein function. The sensitivity and efficiency of alkynyl-fatty acid chemical reporter and CuAAC ligation should facilitate the functional characterization of cellular factors and drugs that modulate protein *S*-acylation in the future.

CHAPTER III. Chemical reporters of protein prenylation

3.1 Alkynyl-isoprenoids synthesis

We designed alkynyl-isoprenol chemical reporters based on farnesol, since corresponding chemical reporters are substrates of FTase and GGTase-I *in vitro*[70]. We utilized a synthetic scheme that would allow access to a diverse panel of alkynyl-farnesol derivatives (**alk-FOH**, **alk-FOH-2** and **alk-FOH-3**), as well as an azide analog (**az-FOH**) for comparison purposes, from a common intermediate (Figure 15). After THP protection, commercially available farnesol can be selectively oxidized at the terminal allylic position[71] to give functionalized farnesol derivative **4**. Allylic alcohol **4** was then alkylated with propargyl bromide to obtain protected alkynyl-farnesol **5**, and then deprotected in acidic ethanol yielding **alk-FOH**, a precursor to previously reported alkynyl-farnesol diphosphate that can be incorporated onto peptide substrates by both FTase and GGTase-I *in vitro*[70]. Corey-Kim like halogenation[72] of allylic alcohol **4** enabled access to allylic bromide intermediate **6**. CuI/K_2CO_3 mediated coupling with TMS-acetylene afforded enyne **7**, which was subsequently deprotected in two steps to yield **alk-FOH-2**. Alternatively, allyl bromide **6** was alkylated with lithiated TMS-1-propyne to give enyne **8**, which after deprotection afforded **alk-FOH-3** that is one methylene unit longer than **alk-FOH-2**. **Az-FOH** was also obtained in a similar manner by displacement of the bromide **6** with sodium azide to obtain **9**, followed by THP deprotection (Figure 15).

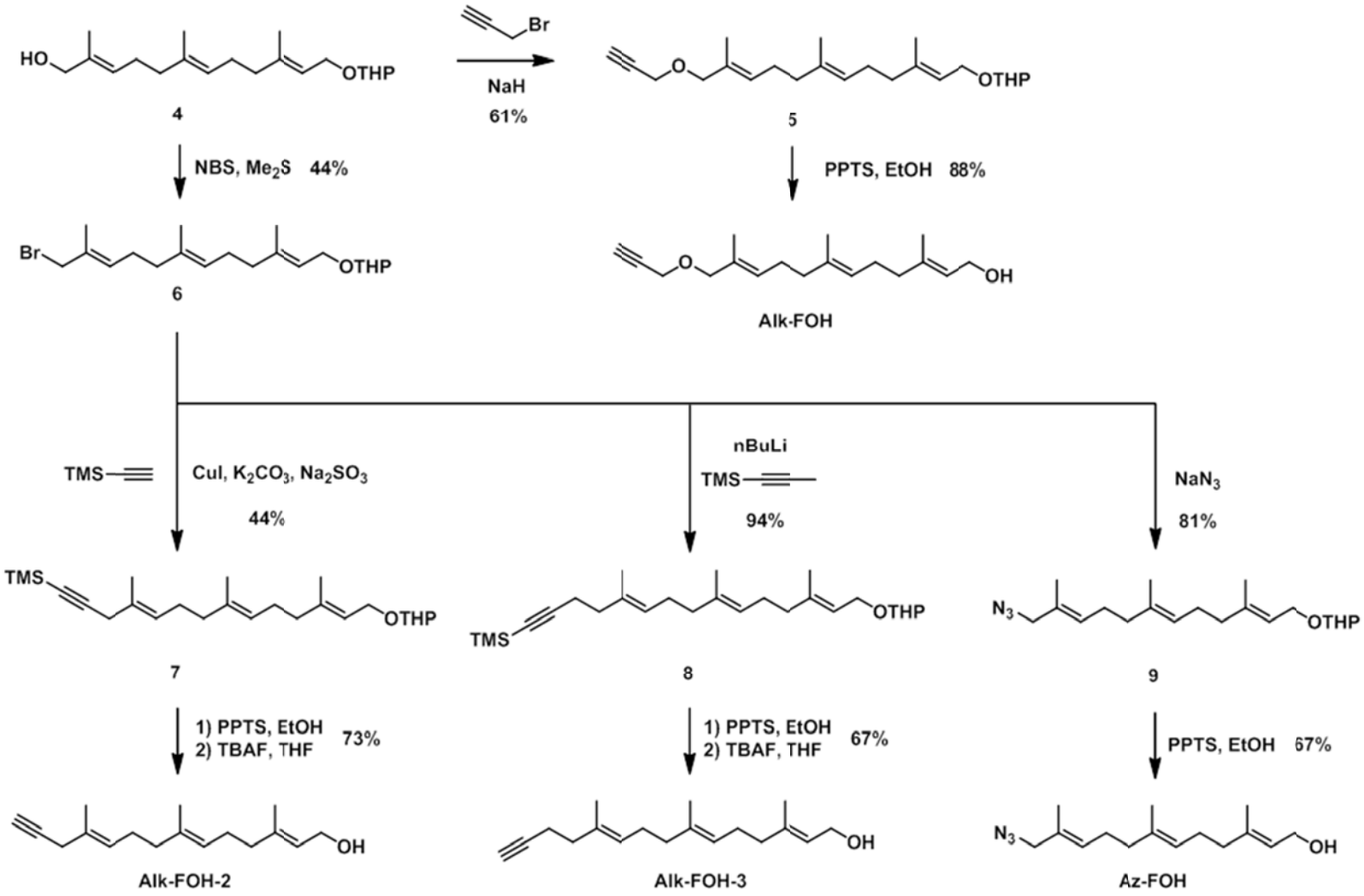

Figure 15: Synthesis of prenylation reporters.

3.2 Alkynyl-isoprenoids characterization

3.2.1 Comparative analysis of bioorthogonal labeling methods

With all three alkynyl-farnesol reporters in hand, we assayed whether these compounds would be metabolically incorporated into mammalian cells and installed onto endogenous target proteins. Jurkat T cells were incubated with alk-FOH, alk-FOH-2, alk-FOH-3 or az-FOH at 50 μM for 4 hrs, lysed and conjugated to azido-rhodamine[7] (in the case of alk-FOHs) or alk-rhodamine[7] (for az-FOH) via CuAAC, separated by SDS-PAGE and analyzed by in-gel fluorescence scanning (Figure 16a). The banding pattern of proteins with the alk-FOH probes was similar to az-FOH labeling, suggesting that all three alk-FOHs were incorporated onto farnesylated proteins. Labeling was stronger with alk-FOH and alk-FOH-3 with markedly stronger signal in the 20-25 kDa molecular weight region known to comprise small GTPases. We also determined the effect of HMG-CoA reductase inhibitors (lovastatin) on the incorporation efficiency and detection sensitivity in comparison to az-FOH. Robust signal over the background was obtained without HMG-CoA reductase inhibitors using alkynyl-FOHs, whereas only few specific bands could be detected with previously reported az-FOH[73]. Optimal concentration for alk-FOH was 50 μM, as judged by labeling of Jurkat cell lysates (Figure 16b). Addition of alk-FOH at 100 μM resulted in cellular toxicity that was not observed at lower concentrations (data not shown).

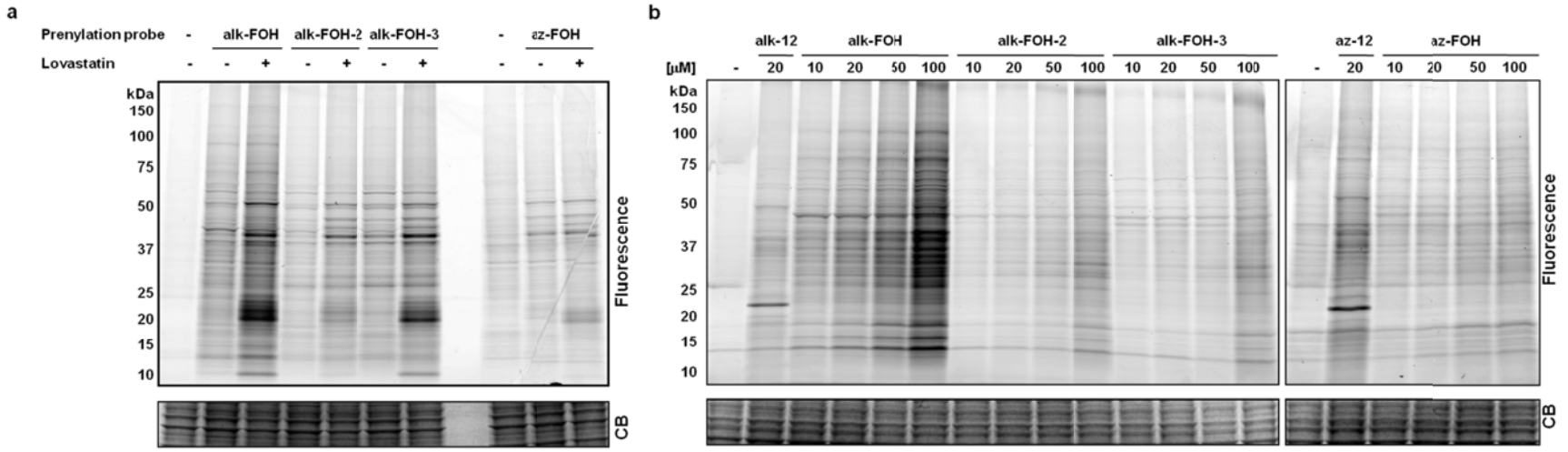

Figure 16: Comparative analysis of prenylation reporters. Cell lysates labeled with alkynyl-isoprenols (alk-FOH, alk-FOH-2 and alk-FOH-3) or azido-isoprenol (az-FOH) were conjugated via CuAAC to azido-rhodamine (az-rho) or alkynyl-rhodamine (alk-rho), respectively. Lysates (20 μg) were separated by SDS-PAGE and scanned for fluorescence (top panels) or stained with Coomassie blue as a loading control (lower panels). (**a**) Jurkat cells were treated or not with 20 μM lovastatin for 24 hours before supplementing the media with prenylation reporters (50 μM, 4 hours). (**b**) Dose-dependent metabolic labeling with prenylation reporters. Jurkat cells were treated with different concentrations of prenylation reporters for 4 hours. Protein *N*-myristoylation reporters alk-12 and az-12 were used as positive controls to compare labeling intensity with protein *S*-prenylation reporters.

3.2.2 Specificity and generality of prenylated protein labeling with chemical reporters

To determine whether the alkynyl-farnesol reporters indeed targeted *S*-prenylated proteins, we evaluated the labeling of known farnesylated protein (H-Ras) and two different classes of geranylgeranylated proteins (RhoA and Rab7). All three reporters successfully visualized Ras farnesylation upon lovastatin treatment (Figure 17a). Nonetheless, alk-FOH and alk-FOH-3 afforded better detection of Ras farnesylation than alk-FOH-2 and az-FOH, even at endogenous levels (without lovastatin pre-treatment, Figure 17a). We focused on alk-FOH, as this chemical reporter can be readily synthesized and stable compared to other alkynyl-farnesol reporters. Alk-FOH was then assayed with a known substrate protein of each prenyltransferase in HeLa cells transiently expressing Ras for FTase, RhoA for GGTase-I and Rab7 for GGTase-II. All three proteins were labeled by alk-FOH (Figure 17b). Furthermore, selective depletion of the Ras signal was observed when incubating the cells with a FTase inhibitor (FTI-277, 10 μM), and selective diminution of the RhoA signal was observed with a GGTase-I inhibitor (GGTI-2133, 10 μM) while the signal was unaffected in the case of Rab7 (Figure 17b). This demonstrates that alk-FOH can be incorporated as a substrate for all three prenyltransferases in cells and hence a useful tool to detect protein *S*-prenylation. Alk-FOH was also incorporated by a variety of other cell types (fibroblasts: HeLa, 3T3; leukocytes: Jurkat, DC2.4 and RAW264.7) demonstrating the generality of this chemical reporter (Figure 17c). Each cell line exhibited a different banding pattern, highlighting the heterogeneity of *S*-prenylated proteins among unique cell types.

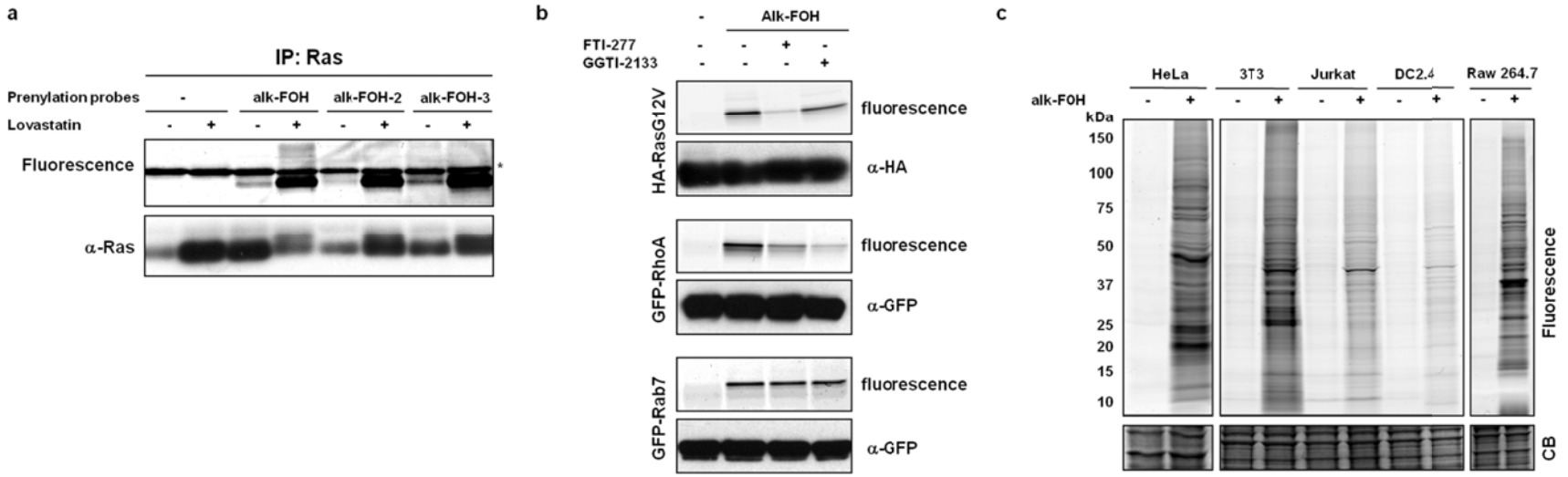

Figure 17: Fluorescent visualization of protein *S*-prenylation on known prenylated proteins and in different cell types. (**a**) Jurkat cells were treated or not with 20 μM lovastatin for 24 hours before supplementing the media with prenylation reporters (50 μM, 4 hours). Immunopurified Ras labeled with alkynyl-isoprenols (alk-FOH, alk-FOH-2 and alk-FOH-3) was conjugated via CuAAC to azido-rhodamine (az-rho), followed by separation by SDS-PAGE and fluorescence detection (top panel) or immunoblotting as a loading control (lower panel). (**b**) HeLa cells transiently expressing HA-RasG12V, GFP-RhoA or GFP-Rab7 were treated or not with 10 μM FTI-277 or GGTI-2133 for 1 hour before supplementing the media with prenylation reporter alk-FOH (50 μM, 4 hours). Immunopurified proteins labeled with alk-FOH were conjugated via CuAAC to azido-rhodamine (az-rho), followed by separation by SDS-PAGE and fluorescence detection (top panels) or immunoblotting as a loading control (lower panels). (**c**) Profiling of protein *S*-prenylation in different cell types. HeLa, 3T3, Jurkat, DC2.4 or RAW264.7 cells were treated with 10 μM lovastatin for 12 hours before supplementing the media with alk-FOH (20 μM, 1 hour). Cell lysates were conjugated via CuAAC to azido-rhodamine (az-rho). Lysates (20 μg) were separated by SDS-PAGE and scanned for fluorescence (top panel) or stained with Coomassie blue as a loading control (lower panel).

3.2.3 Detection of prenylated bacterial effector

Having demonstrated the efficient detection of *S*-prenylated proteins in mammalian cells with alk-FOH, I evaluated *S*-prenylation of *Salmonella* type III secretion system effector SifA[8]. The bacterial protein effector SifA is translocated into the host cytoplasm after bacterial infection and localizes to membranes of the *Salmonella*-containing vacuoles (SCVs)[74]. SifA induces the formation of tubular membrane extensions of the SCV termed *Salmonella*-induced filaments (Sifs)[74], which are necessary for maintaining the integrity of the SCV and *Salmonella* virulence[75]. The C-terminal motif of SifA (^{331}CLCCFL^{336}) contains an unusual prenylation motif that can be interpreted either as a CaaX motif and/or a Rab protein motif (CCXX) and *S. typhimurium* lacking this SifA C-terminal hexapeptide exhibited a significant defect in bacterial replication[76]. Although the *S*-prenylation prediction suite (PrePS)[77] does not recognize SifA as a substrate for any prenyltransferase, SifA was labeled specifically at cysteine 333 by [^{3}H]mevalonic acid in rabbit reticulocyte lysate *in vitro*[36]. These data suggest that SifA is *S*-prenylated by the host cell machinery for recruitment to the SCV membrane[36, 76], although SifA *S*-prenylation could not be detected by [^{3}H]mevalonic acid labeling in cells. The precise roles of SifA *S*-palmitoylation and *S*-prenylation during *Salmonella* infection are unclear, as single point mutations of putative lipidation sites do not recapitulate the defect in *Salmonella* replication observed with the SifA mutant lacking the entire C-terminal hexapeptide[36, 76].

To provide more insight into SifA *S*-prenylation in cells, N-terminally HA-tagged SifA (HA-SifA) was transiently expressed in HeLa cells and metabolically labeled with alk-FOH. HA-SifA was then immunopurified, reacted with az-rho via CuAAC and

analyzed by in-gel fluorescence scanning. Alk-FOH afforded robust visualization of SifA prenylation in cells for the first time (Figure 18a). As opposed to previous *in vitro* radioactive labeling studies[36], we observed residual cellular HA-SifA prenylation (~40%) in the presence of GGTase-I inhibitors (GGTI-298 or GGTI-2133, 10 μM). Furthermore, inhibition of FTase (with FTI-277, 10 μM) or dual inhibition of FTase and GGTase-I in cells retained residual SifA prenylation (~20% and ~50%, respectively) (Figure 18a), suggesting that SifA is a substrate for more than GGTase-I. Single mutations of SifA C-terminal cysteines to serines (HA-SifA^{C333S}, HA-SifA^{C334S}) each retained about 30% of prenylation compared to wild-type, while dual mutations (HA-SifA^{C333,334S}) or triple cysteine mutations (HA-SifA^{C331,333,334S}) were not prenylated by alk-FOH in cells (Figure 18b), suggesting that SifA is dually prenylated at cysteines 333 and 334. These results are in contrast with SifA *in vitro* radioactive labeling studies, where a single mutation (HA-SifA^{C333S}) was sufficient to deplete SifA prenylation[36].

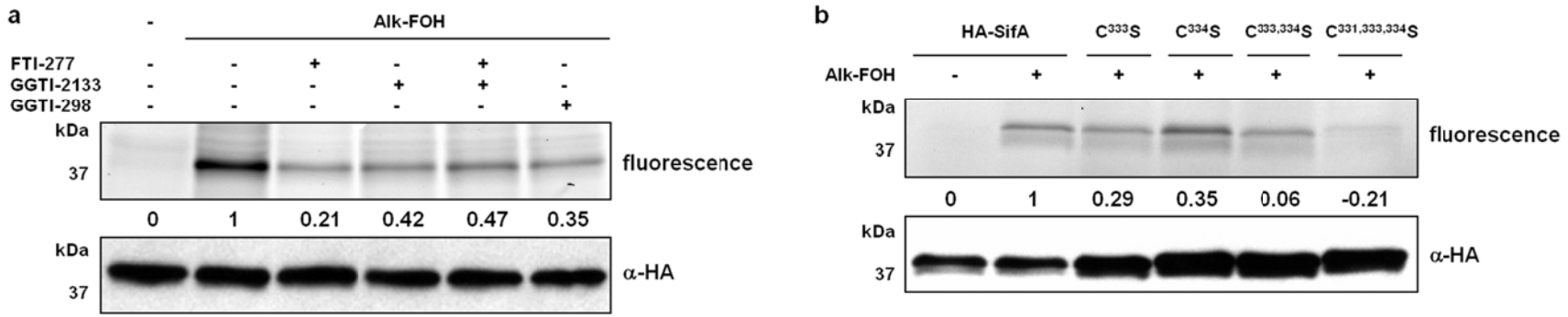

Figure 18: Detection of prenylation of *Salmonella* SifA bacterial effectors prenylation. (**a**) HeLa cells transiently expressing HA-SifA were treated with either 10 μM FTI-277, GGTI-298, GGTI-2133 or 10 μM of both FTI-277 and GGTI-2133, or with DMSO as a solvent control, for 1 h before supplementing the media with prenylation reporter alk-FOH (50 μM, 4 h). (**b**) HeLa cells transiently expressing HA-SifA, HA-SifA^{C333S}, HA-SifA^{C334S}, HA-SifA^{C333,334S}, or HA-SifA^{C331,333,334S} were treated with prenylation reporter alk-FOH (50 μM, 4 h). Immunopurified proteins labeled with alk-FOH were conjugated via CuAAC to azido-rhodamine (az-rho), followed by separation by SDS-PAGE and fluorescence detection or immunoblotting as a loading control. Fluorescence was quantified by mean fluorescence intensity adjusted for loading and normalized for background (0) and strongest signal (1).

Collaboration with the Roy laboratory (Yale School of Medicine) also enabled the identification of prenylated *Legionella pneumophila* effector proteins[11]. Upon phagocytosis, *Legionella* delays endocytic maturation of the vacuole in which it resides[78-79] and promotes the recruitment and fusion of early secretory vesicles to the vacuolar membrane[80-82]. Successful establishment of a vacuole that supports bacterial replication is mediated by the collective action of bacterial effector proteins[83-85] that are translocated into the host cytosol by *Legionella* via a specialized type IV secretion system called Dot/Icm[86-87]. The translocated effectors subvert different host processes to conduct vacuole remodeling[88]. Although the functions of most of the over 200 *Legionella* effectors identified so far remain largely unknown, many of the bacterial effectors have been found to modulate host functions at the cytosolic face of host membrane compartments[89-91]. Many of these effectors are incorporated into the pathogen-containing vacuolar membrane by unknown mechanisms and recent genomic analyses of *Legionella* revealed effectors bearing a C-terminal CaaX motif[11, 38], suggesting protein prenylation may target effectors to membrane compartments.

To further define the mechanisms used for membrane localization of *Legionella* effector proteins, we have been investigating the role protein prenylation by host enzymes might play in this process. Individual polypeptides from the proteomes of *L. pneumophila* strain *Philadelphia*, strain *Paris*, strain *Lens*, and strain *Corby* were analyzed for the presence of a cysteine residue at the fourth position from the C terminus and analyzed using the prenylation prediction program PrePS[77] to identify proteins having an appropriate CaaX motif. Ten *Legionella* proteins containing high confidence putative CaaX motif were identified and they lacked homology outside of the CaaX

motif, suggesting that these proteins encode different functions (Figure 19a). They were translocated into the cytosol of eukaryotic cells by the Dot/Icm system, and they associated to membranes in a CaaX-dependent manner. Alk-FOH labeled 293T cells expressing GFP-fusions of *Legionella* CaaX effectors, immunoprecipitation and CuAAC fluorescent tagging revealed incorporation of alk-FOH, and demonstrated that these proteins are prenylated at the Cys residue of the CaaX motif unlike their CS mutants (Figure 19b). To distinguish which prenyltransferases mediate lipidation of the individual proteins, the activity of FTase or GGTase I was perturbed using different pharmacological inhibitors. Lpg2144, Lpl2806, and Lpl2477 were found to be FTase substrates, whereas Lpg0254, Lpg1976, Lpg2375, Lpg2525, Lpl1863, and Lpg2541 were substrates recognized by both FTase and GGTase I (Figure 19b). Lpp1863 failed to incorporate alk-FOH, suggesting that Lpp1863 contains a non-functional CaaX motif. These data provide biochemical evidence that *Legionella* effectors are lipidated and specific substrates of the eukaryotic prenylation machinery. We demonstrated that subversion of the eukaryotic prenylation machinery is a mechanism that is used for the targeting of bacterial effectors to host membrane-bound compartments.

Figure 19 (next page): Detection of prenylation of *Legionella* bacterial effectors prenylation. (**a**) Putative domains encoded within *Legionella* CaaX effectors. ANK, ankyrin repeat domain; RCC1, regulator of chromosome condensation domain. (**b**) HeLa cells transiently expressing *Legionella* effector-GFP fusion proteins and isogenic CS mutants in the presence/absence of FTI-227 (10 μM) or GGTI-2133 (10 μM) for 1 hour before supplementing the media with prenylation reporter alk-FOH (50 μM, 4 hours). Immunopurified proteins labeled with alk-FOH were conjugated via CuAAC to azido-rhodamine (az-rho), followed by separation by SDS-PAGE and fluorescence detection or immunoblotting as a loading control. Fluorescence was quantified by mean fluorescence intensity adjusted for loading and normalized for background (0) and strongest signal (1).

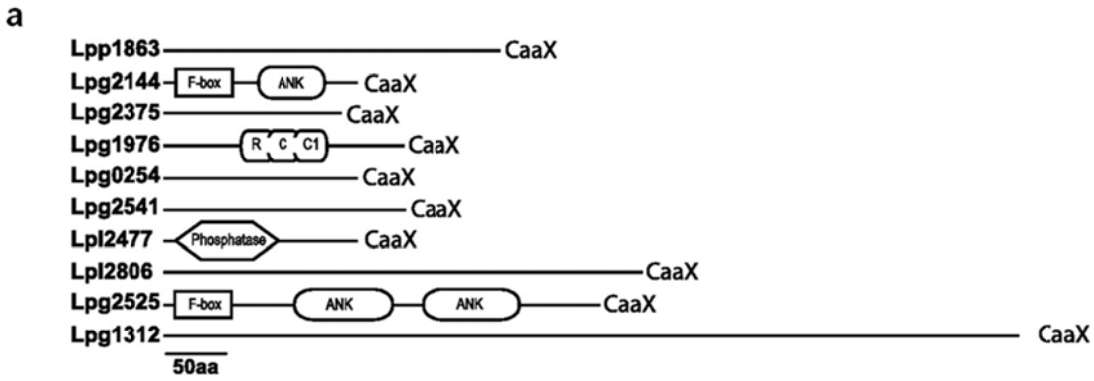
a
Lpp1863
CaaX
Lpg2144
F-box
ANK
CaaX
Lpg2375
CaaX
Lpg1976
R
C
C1
CaaX
Lpg0254
CaaX
Lpg2541
CaaX
Lpl2477
Phosphatase
CaaX
Lpl2806
CaaX
Lpg2525
F-box
ANK
ANK
CaaX
Lpg1312
CaaX
50aa

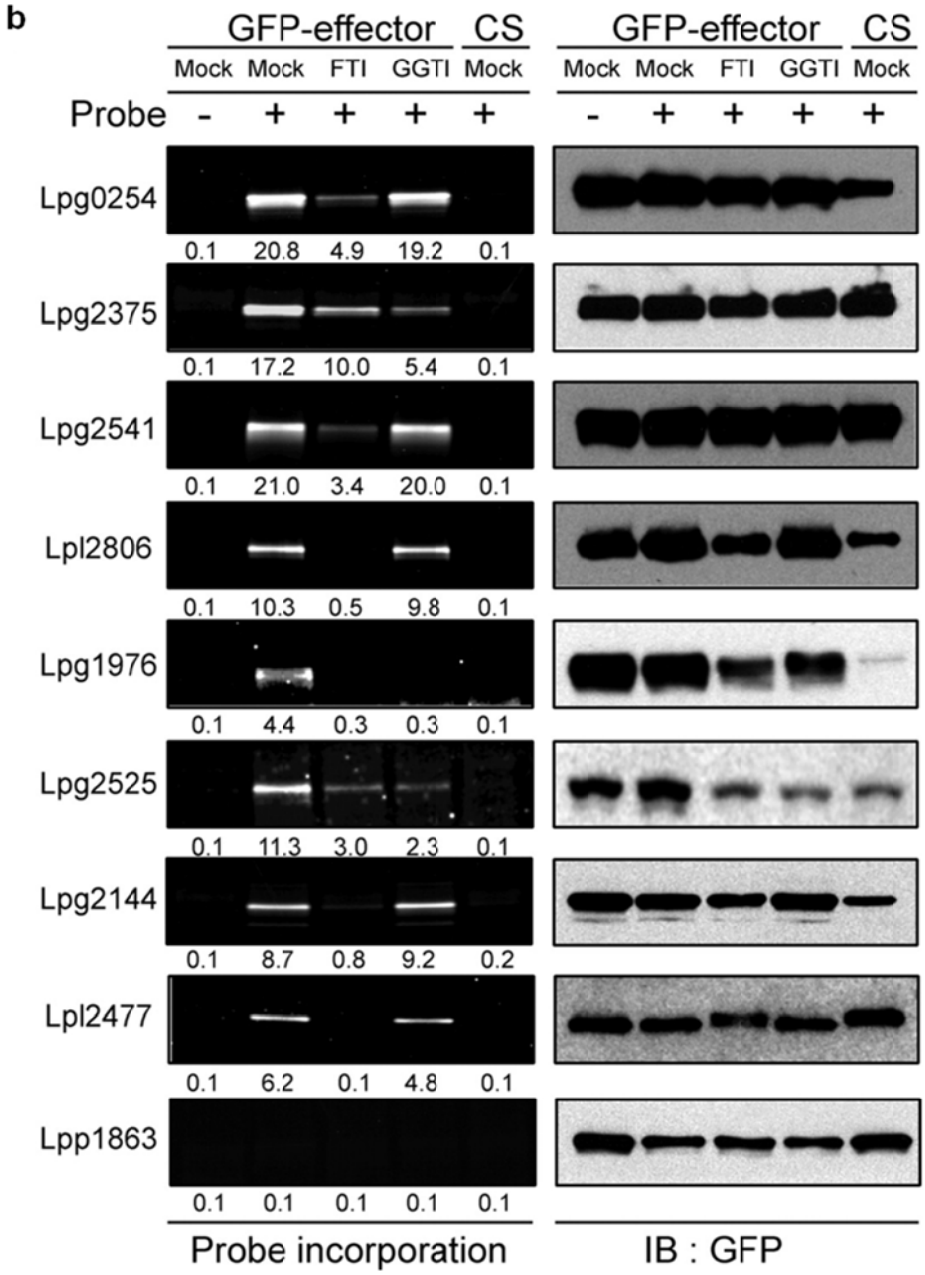
b
GFP-effector
CS
GFP-effector
CS
Mock Mock FTI GGTI Mock
Mock Mock FTI GGTI Mock
Probe - + + + + - + + + +
Lpg0254
0.1 20.8 4.9 19.2 0.1
Lpg2375
0.1 17.2 10.0 5.4 0.1
Lpg2541
0.1 21.0 3.4 20.0 0.1
Lpl2806
0.1 10.3 0.5 9.8 0.1
Lpg1976
0.1 4.4 0.3 0.3 0.1
Lpg2525
0.1 11.3 3.0 2.3 0.1
Lpg2144
0.1 8.7 0.8 9.2 0.2
Lpl2477
0.1 6.2 0.1 4.8 0.1
Lpp1863
0.1 0.1 0.1 0.1 0.1
Probe incorporation
IB : GFP

3.3 Proteomic identification of prenylated proteins

Although bioinformatics predict hundreds of prenylated proteins in eukaryotes based on CaaX or C(X)C motifs of known substrates[77], only a small fraction has been characterized biochemically and experimentally validated. The application of azido- or biotin-isoprenoid chemical reporters have enabled the enrichment and identification of farnesylated[44] or geranylgeranylated protein subsets[73, 92], but the general proteomic coverage of prenylated proteins has been limited. Having demonstrated that alkynyl-farnesol (alk-FOH) enables more efficient labeling and detection of prenylated proteins in mammalian cells compared to their azide-counterparts using CuAAC[8, 93], I envisioned the application of this lipid chemical reporter for the enrichment and identification of prenylated proteins using improved bioorthogonal proteomic methods. We recently developed an azide-biotin tag for CuAAC that incorporates an azobenzene moiety that can be selectively cleaved by reduction with sodium dithionite, allowing selective elution of streptavidin bound proteins under conditions compatible with mass spectrometry analysis[94-95].

3.3.1 Synthesis of cleavable linker azido-azo-biotin for proteomic analysis

Tyramine (**10**) was converted to the azido-phenol (**11**) via diazo-transfer from triflyl azide[96] in good yield (Figure 20). The azobenzene (**12**) was then readily accessible through diazotization of 4-aminobenzoic acid and reaction with azido-phenol (**11**). Subsequent coupling of the corresponding *N*-hydroxysuccinimide-ester (**13**) with pegylated-biotin-amine (from Figure 5b) afforded az-azo-biotin (Figure 20).

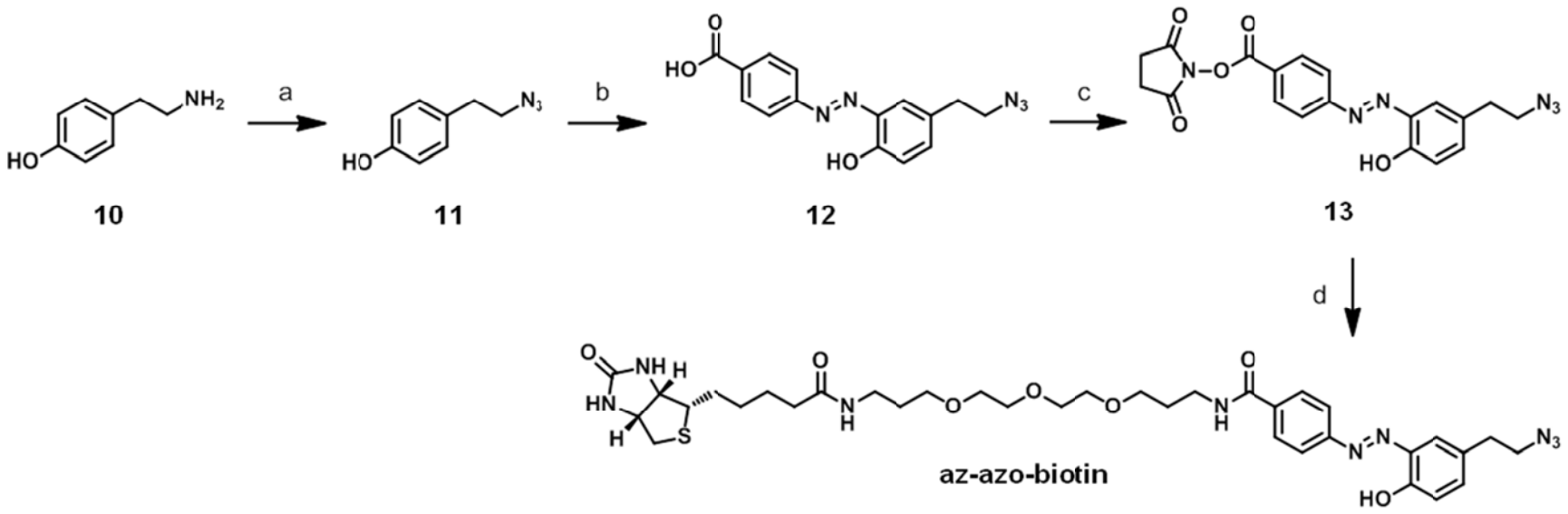

Figure 20: Synthesis of azido-azo-biotin. (**a**) TfN_3, $ZnCl_2$, TEA, CH_3CN, H_2O, 96% yield. (**b**) i. $NaNO_2$, 6M HCl, 4-aminobenzoic acid. ii. Et_3N, THF, 45~55% yield over two steps. (**c**) DCC, *N*-hydroxysuccinimide, THF, 79%. (**d**) Biotin-PEG-NH_2, DMF, 80% yield.

3.3.2 Proteomic analysis of prenylated proteins in RAW264.7 macrophages

To identify lipid-modified proteins involved in immune responses to microbial infections, we performed a large-scale profiling of prenylated proteins in the mouse macrophage line RAW264.7[97] using the isoprenoid chemical reporter alkynyl-farnesol (alk-FOH)[8] and CuAAC. Alk-FOH targets the substrates of all three prenyltransferases in cells: CaaX *S*-farnesylated and *S*-geranylgeranylated proteins, as well as C(X)C RabGTPases[8]. In-gel fluorescence profiling of RAW264.7 cell lysates reacted with an azide-functionalized fluorophore, azido-rhodamine (az-rho)[7], demonstrated that a diverse repertoire of proteins are metabolically labeled by alk-FOH (Figure 21a). Cell lysates were then reacted with a cleavable affinity tag (az-azo-biotin)[94] for enrichment of alk-FOH labeled proteins with streptavidin beads, selective elution and gel-based proteomic identification by mass spectrometry. Coomassie blue staining of proteins retrieved with streptavidin beads and sodium dithionite ($Na_2S_2O_4$) elution demonstrates the specificity of alk-FOH and CuAAC labeling methods (Figure 21b). Proteins identified in three independent experimental runs were compiled and categorized into high- and medium-confidence lists on the basis of the total number of assigned spectra and the fold-increase above control samples that were not labeled with alk-FOH. For this analysis, we selectively identified 114 proteins by alk-FOH labeling as compared to control samples, with 52 and 62 proteins assigned to high- and medium-confidence lists, respectively (Figure 21c, Tables 3 and 4). Of the high-confidence list, 35 percent (23 + 12) of hits bear a carboxyl-terminal CaaX or C(X)C motif, respectively (Table 3). Of these putative prenylated proteins, 61 percent of high- and medium-confidence hits have been reported in previous labeling and enrichment studies with biotin, azide or alkyne

chemical reporters in other cell types (Tables 3 and 4). These proteins include K-Ras, Cdc42, Lamin-B1, DnaJA2, Rap2C and Rab proteins (Figure 21c, Tables 3 and 4). In addition, RhoA, Ptp4A, Ykt6, Rac2, Brox and RhoG, which have predicted prenylation sites, were recovered in our alk-FOH proteomic dataset (Figure 21c, Tables 3 and 4). In comparison with previous proteomic studies that targeted subsets of *S*-prenylated proteins[44, 73, 92-93], our proteomic analysis of alk-FOH labeled proteins recovered both farnesylated and geranylgeranylated proteins as well as many other candidate isoprenoid-modified proteins (Tables 3 and 4). Notably, we identified the long-isoform of zinc-finger antiviral protein (ZAPL) as a high-confidence hit, which was not previously annotated as a prenylated protein.

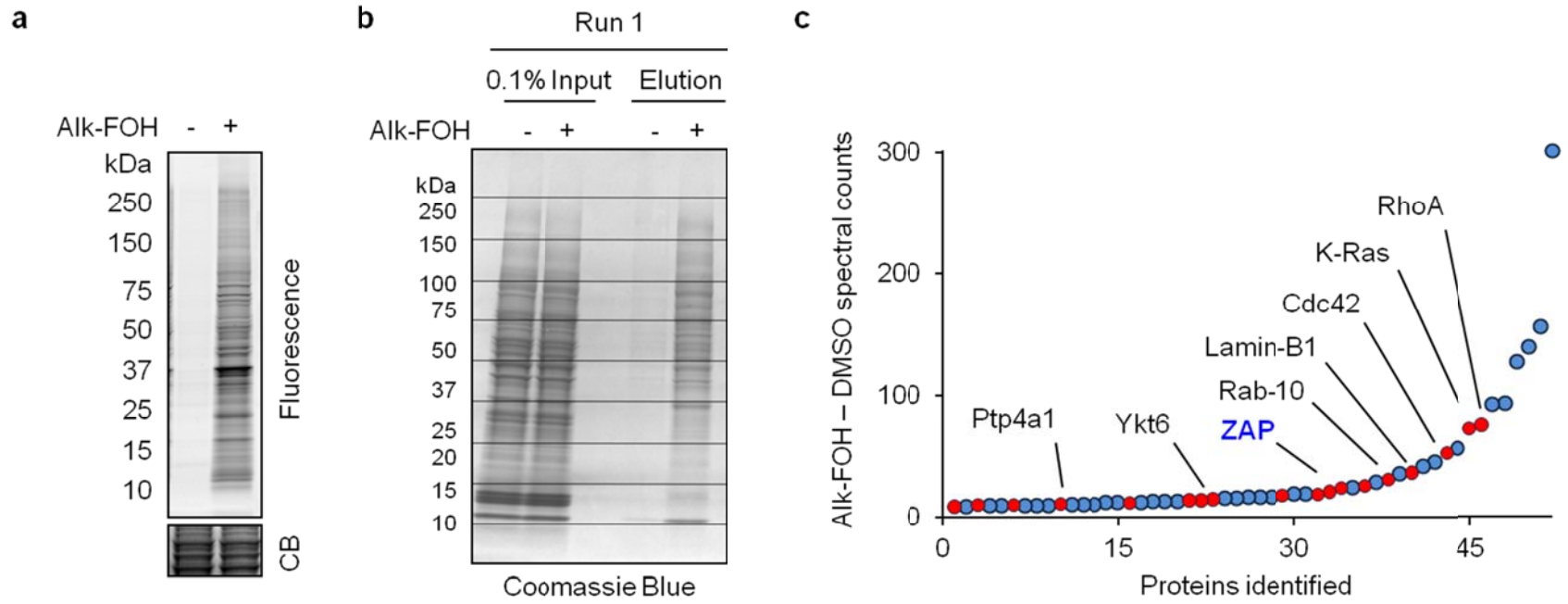

Figure 21: Visualization and identification of prenylated proteins in RAW264.7 macrophages. (**a**,**b**,**c**) RAW264.7 macrophages pretreated for 12 h with 10 μM lovastatin then incubated for 12 h with 50 μM alk-FOH or DMSO as a control. In **a**, cell lysates were reacted with az-rho by CuAAC, and proteins were separated by SDS-PAGE for visualization by fluorescence gel scanning. Coomassie blue (CB) staining demonstrates comparable loading. In **b** and **c**, lysates from lovastatin-treated cells were reacted with az-azo-biotin by CuAAC for enrichment of alk-FOH labeled proteins with streptavidin beads and identification by mass spectrometry. In **c**, for each high-confidence identified protein, the difference of assigned peptide spectral counts from the alk-FOH and DMSO samples was plotted. Proteins with a carboxyl-terminal CaaX or C(X)C motif are shown in red. Several known prenylated proteins are labeled in black and ZAP, the highest ranked protein not known to be prenylated, is labeled in bold blue.

Table 3 (next page): Proteins selectively identified with high confidence in alk-FOH samples by mass spectrometry. Data was categorized as high confidence if the sum of assigned spectra was at least 10 fold greater for alk-FOH samples than the sum of DMSO samples (column labeled α), or if the sum of assigned spectra was at least 10 if no spectra was assigned in DMSO samples (column labeled Δ). Data was compared to other chemical reporter based prenylome proteomics data sets from the Zhao[44], Tamanoi[73], Alexandrov[92] and Distefano[93] groups. Proteins bearing a C-terminal CaaX or C(X)C motif were shaded green, and the motif sequence was displayed, along with the prenyltransferase preference for the substrate according to UniProtKB database and PrePS prenylation prediction. CaaX proteins were shaded red if they had not been previously reported as prenylated in UniProtKB.

Table 3: Proteins selectively identified with high confidence in alk-FOH samples by mass spectrometry.

				lovastatin +																
				1		2		3		SUM		Other groups				CaaX/Rab	Swiss-prot	PrePS prediction		
#	Gene	Description	Accession #	-	+	-	+	-	+	Δ	α	Alexandrov	Distefano	Zhao	Tamanoi	motif	annotation	FTase	GGTase-I	GGTase-II
1	Pfkp	Isoform 1 of 6-phosphofructokinase type C	IPI00124444	0	52	0	48	15	217	302	21									
2	Aldh9a1	4-trimethylaminobutyraldehyde dehydrogenase	IPI00124372	0	18	0	26	0	113	157	-									
3	Atp2a2	Isoform SERCA2B of Sarcoplasmic/endoplasmic reticulum calcium ATPase 2	IPI00338964	0	46	0	41	4	57	140	36									
4	Acaa1a	3-ketoacyl-CoA thiolase A, peroxisomal	IPI00121833	0	24	0	34	9	79	128	15									
5	Vdac2	Voltage-dependent anion-selective channel protein 2	IPI00122547	1	17	2	17	4	67	94	14									
6	Hsd17b4	Peroxisomal multifunctional enzyme type 2	IPI00331628	0	11	0	13	0	69	93	-									
7	Rhoa	Transforming protein RhoA	IPI00315100	0	24	1	14	2	41	76	26					CLIL	GGTase-I	++	+++	
8	Kras	Isoform 2B of GTPase KRas	IPI00134941	0	10	0	8	0	55	73	-			X		CVIM	FTase	+++	+++	
9	Slc25a5	ADP/ATP translocase 2	IPI00127841	0	6	1	7	7	52	57	8									
10	Cdc42	Isoform 2 of Cell division control protein 42 homolog	IPI00113849	0	3	0	1	0	49	53	-			X		CVLL	GGTase-I	++	+++	
11	Ptges2	prostaglandin E synthase 2	IPI00947625	0	18	0	17	0	11	46	-									
12	Hmox2	Heme oxygenase 2	IPI00309322	0	13	0	12	0	17	42	-									
13	Lmnb1	Lamin-B1	IPI00230394	1	21	0	17	0	0	37	38		X	X		CAIM	FTase	+++	+++	
14	Eprs	Bifunctional aminoacyl-tRNA synthetase	IPI00339916 (+1)	1	11	0	12	1	15	36	19									
15	Rab10	Ras-related protein Rab-10	IPI00130118	0	4	1	5	0	23	31	32	X				SKCC	GGTase-II			+++
16	Hsd17b12	Isoform 1 of Estradiol 17-beta-dehydrogenase 12	IPI00119219	0	0	0	2	2	29	29	16									
17	Dnaja2	DnaJ homolog subfamily A member 2	IPI00136251	0	7	0	5	1	15	26	27			X		CAHQ	FTase			
18	Mybbp1a	Myb-binding protein 1A	IPI00331361	2	13	0	14	0	0	25	14									
19	Rap2c	Ras-related protein Rap-2c	IPI00466588	0	6	0	2	0	16	24	-			X	X	CVVQ	GGTase-I	++		
20	Rab31	ras-related protein Rab-31	IPI00222632	0	5	0	3	0	13	21	-	X				RRCC	GGTase-II			+++
21	Zc3hav1	Zinc finger CCCH-type antiviral protein 1	IPI00136572	0	3	0	6	0	10	19	-					CIIS		+		
22	Soat1	Sterol O-acyltransferase 1	IPI00278153 (+1)	0	2	0	3	0	14	19	-									
23	Pfkl	6-phosphofructokinase, liver type	IPI00387312	0	3	0	0	2	18	19	11									
24	Ptp4a2	Protein tyrosine phosphatase type IVA 2	IPI00116529	0	2	0	2	0	14	18	-					CCVQ	FTase	+		
25	Pcbp1	Poly(rC)-binding protein 1	IPI00128904	0	3	0	7	1	8	17	18									
26	Tmem38b	Trimeric intracellular cation channel type B	IPI00119084	0	9	0	5	0	3	17	-									
27	Rtn3	Isoform 1 of Reticulon-3	IPI00470981 (+2)	0	7	0	6	2	6	17	10									
28	Cyb5b	Cytochrome b5 type B	IPI00315794	0	5	1	5	0	7	16	17									
29	Atp5h	ATP synthase subunit d, mitochondrial	IPI00230507 (+1)	0	8	1	9	1	1	16	9									
30	Ykt6	Synaptobrevin homolog YKT6	IPI00453771	0	5	0	1	0	9	15	-					CAIM	FTase	++	+++	
31	Rab1	Ras-related protein Rab-1A	IPI00114560 (+1)	0	6	0	4	0	4	14	-	X			X	GGCC	GGTase-II			+++
32	Rab18	Ras-related protein Rab-18	IPI00116770	0	2	0	2	0	10	14	-	X			X	CSVL	GGTase-I	+	++	+++
33	Mtch2	Mitochondrial carrier homolog 2	IPI00132039	0	1	0	2	1	11	13	14									
34	Reep5	receptor expression-enhancing protein 5	IPI00315463	0	3	0	5	0	5	13	-									
35	Prdx6	Peroxiredoxin-6	IPI00555059 (+1)	0	6	0	3	0	4	13	-									
36	Slc25a3	Phosphate carrier protein, mitochondrial	IPI00124771 (+1)	0	0	0	2	1	11	12	13									
37	Rab-7	Ras-related protein Rab-7a	IPI00408892	0	4	0	2	1	7	12	13	X	X		X	SCSC	GGTase-II			+++
38	Fads2	Fatty acid desaturase 2	IPI00129362	0	2	0	4	0	6	12	-									
39	Hmha1	Isoform 1 of Minor histocompatibility protein HA-1	IPI00830876	0	4	0	5	0	3	12	-									
40	Slc3a2	4F2 cell-surface antigen heavy chain	IPI00114641 (+1)	0	2	0	1	1	9	11	12									
41	Eif4g1	eukaryotic translation initiation factor 4, gamma 1	IPI00858249	0	4	0	4	0	3	11	-									
42	Fxyd5	FXYD domain-containing ion transport regulator 5	IPI00129933	0	3	0	2	0	6	11	-									
43	Ptp4a1	Protein tyrosine phosphatase type IVA 1	IPI00133490	0	3	0	0	0	8	11	-					CCIQ	FTase	+++		
44	Vdac3	Voltage-dependent anion-selective channel protein 3	IPI00122548	0	0	0	1	1	10	10	11									
45	Fcer1g	High affinity immunoglobulin epsilon receptor subunit gamma	IPI00119293	1	0	0	1	0	10	10	11									
46	Tmed10	Isoform 1 of Transmembrane emp24 domain-containing protein 10	IPI00466570	0	4	0	3	1	4	10	11									
47	Nrp2	neuropilin-2 isoform 3 precursor	IPI00755777	0	0	0	0	0	10	10	-					CCSEA				
48	mt-Co2	Cytochrome c oxidase subunit 2	IPI00131176	0	2	0	3	0	5	10	-									
49	Serbp1	Isoform 1 of Plasminogen activator inhibitor 1 RNA-binding protein	IPI00471475 (+3)	0	4	0	6	0	0	10	-									
50	Rab5c	Ras-related protein Rab-5C	IPI00224518 (+1)	0	3	0	5	0	2	10	-	X			X	CCSN	GGTase-II			+++
51	Numa1	nuclear mitotic apparatus protein 1	IPI00263048	1	6	0	4	0	0	9	10									
52	Rab1b	Ras-related protein Rab-1B	IPI00133706	0	5	1	3	0	2	9	10	X	X			GGCC	GGTase-II			+++

Table 4 (next 2 pages): Proteins selectively identified with medium confidence in alk-FOH samples. Same as Table 3 except data was medium confidence if the sum of assigned spectra was at least 8 fold greater for alk-FOH samples than DMSO samples or if the sum was at least 4 if no spectra assigned in DMSO samples.

Table 4: Proteins selectively identified with medium confidence in alk-FOH samples by mass spectrometry.

				lovastatin +																	
				1		2		3		SUM		Other groups				CaaX/Rab	Swiss-prot	PrePS prediction			
#	Gene	Description	Accession #	-	+	-	+	-	+	Δ	α	Alexandrov	Distefano	Zhao	Tamanoi	motif	annotation	FTase	GGTase-I	GGTase-II	
53	Nceh1	Neutral cholesterol ester hydrolase 1	IPI00403586	0	0	0	2	0	7	9	-										
54	Sf3b2	splicing factor 3b, subunit 2	IPI00349401	0	6	0	3	0	0	9	-										
55	Tmpo	Isoform Beta of Lamina-associated polypeptide 2, isoforms beta/delta/epsilon/gamma	IPI00320399 (+3)	0	4	0	5	0	0	9	-										
56	Spcs2	Signal peptidase complex subunit 2	IPI00228236	0	4	0	3	0	2	9	-										
57	Hsdl1	Inactive hydroxysteroid dehydrogenase-like protein 1	IPI00225301	0	1	0	1	0	7	9	-										
58	Tmem173	Isoform 1 of Transmembrane protein 173	IPI00674006 (+1)	0	2	0	2	1	5	8	9										
59	Nup155	Nuclear pore complex protein Nup155	IPI00453821 (+1)	0	1	0	5	1	3	8	9										
60	Lass2	LAG1 longevity assurance homolog 2	IPI00126253	0	0	0	1	1	8	8	9										
61	Rac2	Ras-related C3 botulinum toxin substrate 2	IPI00137618	0	4	0	1	0	3	8	-					CSLL	GGTase-I	+	++		
62	Ermp1	Isoform 1 of Endoplasmic reticulum metallopeptidase 1	IPI00407222	0	0	0	0	0	8	8	-										
63	Ipo5	Isoform 1 of Importin-5	IPI00626994	0	1	0	0	1	7	7	8										
64	Arf1	ADP-ribosylation factor 1	IPI00221613 (+1)	0	4	0	0	1	4	7	8										
65	Fmnl1	Isoform 1 of Formin-like protein 1	IPI00123377	0	1	0	2	1	5	7	8										
66	Cse1l	Exportin-2	IPI00112414	1	2	0	1	0	5	7	8										
67	Rab2a	Ras-related protein Rab-2A	IPI00137227	0	3	0	1	1	4	7	8	X		X		X	GGCC	GGTase-II			+++
68	Pdcd11	Protein RRP5 homolog	IPI00551454	0	3	0	4	0	0	7	-										
69	Lrrc59	Leucine-rich repeat-containing protein 59	IPI00123281	0	2	0	1	0	4	7	-										
70	Txndc12	Thioredoxin domain-containing protein 12	IPI00133110	0	1	0	2	0	4	7	-										
71	Hmox1	Heme oxygenase 1	IPI00131577	0	0	0	1	0	6	7	-										
72	Rbm8a	Isoform 2 of RNA-binding protein 8A	IPI00109860	0	4	0	3	0	0	7	-										
73	Atl3	Isoform 1 of Atlastin-3	IPI00458393 (+1)	0	1	0	2	0	3	6	-										
74	Bax	Apoptosis regulator BAX	IPI00120684 (+1)	0	1	0	0	0	5	6	-										
75	Vat1	Synaptic vesicle membrane protein VAT-1 homolog	IPI00126072	0	0	0	0	0	6	6	-										
76	U2surp	U2 snRNP-associated SURP motif-containing protein 1	IPI00467507	0	2	0	4	0	0	6	-										
77	Cd44	CD44 antigen isoform c precursor	IPI00223769 (+21)	0	0	0	0	0	6	6	-										
78	Stom	Erythrocyte band 7 integral membrane protein	IPI00323748	0	1	0	2	0	3	6	-										
79	Arl1	ADP-ribosylation factor-like protein 1	IPI00278498	0	1	0	1	0	4	6	-										
80	Adpgk	Isoform 1 of ADP-dependent glucokinase	IPI00132529 (+1)	0	0	0	0	0	6	6	-										
81	Tap1	Antigen peptide transporter 1	IPI00129803	0	2	0	2	0	1	5	-										
82	Rab14	Ras-related protein Rab-14	IPI00126042	0	0	0	0	0	5	5	-	X			X	GCGC	GGTase-II				+++
83	Tor1aip1	Lamina-associated polypeptide 1B	IPI00762273	0	2	0	2	0	1	5	-										
84	Ugt1a7c	UDP-glucuronosyltransferase 1-7C	IPI00417181	0	0	0	2	0	3	5	-										
85	Got1	Aspartate aminotransferase, cytoplasmic	IPI00230204 (+1)	0	0	0	1	0	4	5	-										
86	Tomm40	Mitochondrial import receptor subunit TOM40 homolog	IPI00474157	0	0	0	2	0	3	5	-										
87	Slc7a5	Large neutral amino acids transporter small subunit 1	IPI00129395	0	2	0	2	0	1	5	-										
88	Prdx3	Thioredoxin-dependent peroxide reductase, mitochondrial	IPI00116192	0	2	0	0	0	3	5	-										
89	Sec23b	Protein transport protein Sec23B	IPI00317604	0	1	0	1	0	3	5	-										
90	Ifitm3	Interferon-induced transmembrane protein 3	IPI00133243	0	0	0	0	0	5	5	-										
91	Pmpca	Mitochondrial-processing peptidase subunit alpha	IPI00120199	0	1	0	2	0	2	5	-										
92	Brox	Isoform 1 of BRO1 domain-containing protein BROX	IPI00453679	0	0	0	0	0	5	5	-					CSVS	FTase	++			
93	Dctn1	Isoform 1 of Dynactin subunit 1	IPI00115663 (+1)	0	1	0	1	0	2	4	-										
94	Mars	Methionyl-tRNA synthetase, cytoplasmic	IPI00461469 (+1)	0	1	0	2	0	1	4	-										
95	Rps3a	40S ribosomal protein S3a	IPI00331345 (+2)	0	0	0	3	0	1	4	-										
96	Apex1	DNA-(apurinic or apyrimidinic site) lyase	IPI00224152	0	0	0	3	0	1	4	-										
97	Acsl1	Long-chain-fatty-acid--CoA ligase 1	IPI00112549 (+2)	0	2	0	2	0	0	4	-										
98	Nup160	Isoform 1 of Nuclear pore complex protein Nup160	IPI00129535	0	2	0	1	0	1	4	-										
99	Eftud2	116 kDa U5 small nuclear ribonucleoprotein component isoform b	IPI00649950	0	1	0	3	0	0	4	-										
100	Nomo1	Nodal modulator 1	IPI00222429	0	3	0	1	0	0	4	-										
101	Eif3a	Eukaryotic translation initiation factor 3 subunit A	IPI00129276 (+1)	0	1	0	0	0	3	4	-										
102	Nesprin-3	Isoform 1 of Nesprin-3	IPI00457960	0	0	0	0	0	4	4	-										
103	Mthfd1	C-1-tetrahydrofolate synthase, cytoplasmic	IPI00953783	0	2	0	2	0	0	4	-										
104	Cpsf1	Cleavage and polyadenylation specificity factor subunit 1	IPI00110363	0	1	0	3	0	0	4	-										

105	Pebp1	Phosphatidylethanolamine-binding protein 1	IPI00137730	0	1	0	1	0	2	4	-										
106	Ndufa5	NADH dehydrogenase [ubiquinone] 1 alpha subcomplex subunit 5	IPI00331332	0	0	0	4	0	0	4	-										
107	Rpl21	60S ribosomal protein L21	IPI00315548 (+3)	0	2	0	0	0	2	4	-										
108	Sf3a1	Splicing factor 3A subunit 1	IPI00408796	0	3	0	1	0	0	4	-										
109	Abhd12	Monoacylglycerol lipase ABHD12	IPI00165731	0	0	0	0	0	4	4	-										
110	Gnaq	Guanine nucleotide-binding protein G(q) subunit alpha	IPI00228618	0	0	0	1	0	3	4	-										
111	Psmb5	Proteasome subunit beta type-5	IPI00317902	0	2	0	2	0	0	4	-										
112	Rhog	Rho-related GTP-binding protein RhoG	IPI00116558	0	0	0	2	0	2	4	-					CILL	GGTase-I	+	++		
113	Slc38a2	Sodium-coupled neutral amino acid transporter 2	IPI00453817	0	0	0	0	0	4	4	-										
114	Pgrmc2	Membrane-associated progesterone receptor component 2	IPI00351206	0	1	0	0	0	3	4	-										

3.4 *S*-farnesylation is crucial for membrane targeting and antiviral activity of zinc-finger antiviral protein long-isoform (ZAPL)

ZAP was originally identified in a rat cDNA overexpression screen for host factors that could significantly impair replication of Moloney murine leukemia virus (MuLV) as an N-terminal protein fused to the Zeocin resistance marker[98]. This original ZAP construct consisting of the first 254 amino acids of rat ZAP (rNZAP) fused to the marker (Figure 22a), inhibited the replication of various alphaviruses[99], filoviruses[100] and retroviruses[98, 101], but did not affect host susceptibility to other viruses such as vesicular stomatitis virus, poliovirus, yellow fever virus and herpes simplex virus type 1[99]. Additional experiments suggested that rNZAP did not interfere with MuLV entry, viral DNA synthesis and integration, and viral RNA production in the nucleus, but decreased the level of posttranscriptional viral mRNA in the cytoplasm[98]. Similarly, rNZAP inhibited Sindbis virus (SINV) replication by blocking post-entry steps of translation and amplification of incoming viral RNA[99]. rNZAP is predominantly localized in the cytoplasm at steady state, but shuttles between the cytoplasm and the nucleus in a CRM1-dependent manner[102]. rNZAP is also proposed to bind cytoplasmic viral mRNA through its second and fourth CCCH-type zinc-fingers[100, 103], although recent structural studies suggest a role for all 4 zinc-fingers in forming an RNA binding groove[104]. ZAP recruits p72 DEAD-box[105] and DHX30 DEXH-box[106] RNA helicases, and the RNA processing exosome[107] for optimal depletion of viral mRNA. While early ZAP studies were conducted with rNZAP, the analysis of full-length rat ZAP (rZAP), which bears an additional WWE domain predicted to mediate specific protein-protein interactions in ubiquitin and ADP-ribose conjugation

systems[108] (Figure 22a), suggests similar antiviral activity against MuLV[98]. Recent reports have suggested that human ZAP (hZAP) recruits both the 3' and 5' mRNA degradation machinery since it binds adenylase poly(A)-specific ribonuclease to remove the poly(A) tail and the decapping complex Dcp1a/Dcp2 to remove the cap structure[101].

There are two ZAP isoforms arising from alternative splicing: ZAP-long (ZAPL) and ZAP-short (ZAPS). Both have the same amino acid sequence but ZAPS lacks the carboxyl-terminal poly(ADP-ribose) polymerase (PARP)-like domain present in ZAPL (Figure 22a)[109]. Even though the PARP-like domain of ZAPL is predicted to be inactive, ZAPL/S isoforms have been annotated as PARP-13.1/2 respectively. Human ZAPL exhibits stronger antiviral activity than hZAPS against MuLV expression and Semliki forest virus infection[109], while both isoforms prevent HIV-1 infection[101]. The ZAP isoforms are relatively broadly expressed in human tissues[109], but the mRNA expression of hZAPS is markedly increased by IFNα treatment[110]. hZAPS is also more active than hZAPL in enhancing RIG-I-dependent signaling in response to 5'-triphosphate-modified RNA, suggesting regulation of ZAP activity can enhance or even amplify IFN responses[110]. In addition, ZAPS and ZAPL are both polyADP-ribosylated and been implicated in stablization of mRNA during cellular stress[111]. Interestingly, ZAPS polyADP-ribosylation is selectively elevated during cellular stress compared to ZAPL[111]. These results highlight a potential duality in the regulation and functions of ZAP isoforms. The role of *S*-prenylation on ZAPL (PARP-13.1/zc3hav1) localization and antiviral function has not been investigated. Here we show *S*-prenylation enhances the membrane targeting and antiviral activity of ZAPL.

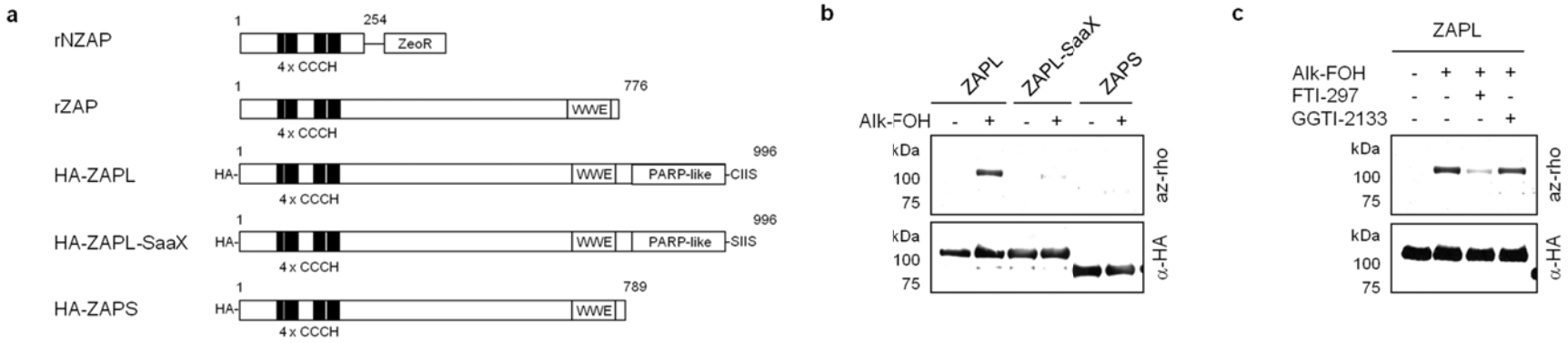

Figure 22: ZAP is *S*-farnesylated of Cys993. (**a**) Schematic representation of protein domains of rNZAP, rZAP and mouse HA-tagged ZAP constructs. (**b,c**) 293T cells were transfected with pCMV-HA-ZAPL, pCMV-HA-ZAPL-SaaX or pCMV-HA-ZAPS (shown in **a**) and labeled with 50 μM alk-FOH for 4 h. Cell lysates were subjected to anti-HA immunoprecipitation, reacted with az-rho by CuAAC, separated by SDS-PAGE and visualized by fluorescence gel scanning. Comparable protein loading was confirmed by anti-HA western blotting. In **c**, cells were pretreated for 1 h with 10 μM prenyltransferase inhibitors (FTI-297, farnesyltransferase inhibitor; GGTI-2133, geranylgeranyltransferase-I inhibitor) as indicated prior to alk-FOH labeling.

3.4.1 Long-isoform of ZAP is *S*-farnesylated

S-Prenylation of ZAP was investigated further to validate our alk-FOH proteomic data and explore the impact of this lipid modification on ZAP subcellular localization and antiviral activity. ZAP amino acid sequence analysis indicates that ZAPL, but not ZAPS, bears a carboxyl-terminal CaaX motif for protein prenylation (Figure 22a). Alk-FOH labeling of HEK293T and HeLa cells transfected with plasmids expressing hemagglutinin epitope (HA)-tagged mouse ZAP (HA-ZAP) followed by anti-HA immunoprecipitation, and CuAAC with az-rho and in-gel fluorescence scanning indicated that ZAPL, but not ZAPS, is indeed prenylated (Figure 22b,23a). Since protein *S*-prenylation is sometimes followed by protein *S*-palmitoylation to increase membrane affinity[1], we also labeled HA-ZAPL-expressing HeLa cells with alk-16, a chemical reporter of palmitoylation[7], but palmitoylation of ZAPL was not detected (Figure 23a). We then evaluated whether ZAPL is prenylated at cysteine (Cys) residue 993 of the CaaX motif. Alk-FOH labeling of HEK293T and HeLa cells transfected with a plasmid bearing a Cys-to-serine (Ser) mutation in HA-ZAPL, termed HA-ZAPL-SaaX (Figure 22a), showed a significant reduction in the level of ZAPL prenylation (Figure 22b,23b). To assess whether ZAPL is farnesylated or geranygeranylated, HEK293T and HeLa cells expressing HA-ZAPL were treated with farnesyltransferase or geranylgeranyltransferase-I inhibitors (FTI-297 or GGTI-2133, respectively) before alk-FOH labeling. While GGTI-treated cells had the same fluorescence level as non-treated cells, FTI-treated cells showed a marked decrease, suggesting the long-isoform of ZAP (ZAPL) is *S*-farnesylated at Cys993 (Figure 22c,23c).

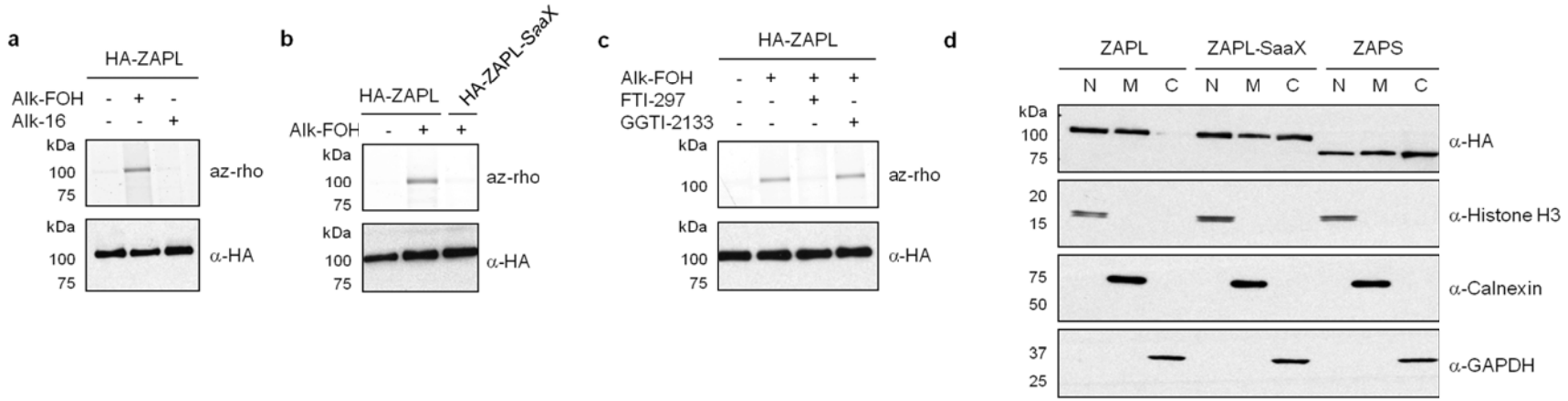

Figure 23: *S*-farnesylation of Cys993 excludes murine ZAPL from the cytosol. (**a-c**) HeLa cells were transfected with pCMV-HA-ZAPL or pCMV-HA-ZAPL-SaaX (shown in Figure 22a) and labeled with 50 μM alk-FOH for 4 h. Cell lysates were subjected to anti-HA immunoprecipitation, reacted with az-rho by CuAAC, separated by SDS-PAGE and visualized by fluorescence gel scanning. Comparable protein loading was confirmed by anti-HA western blotting. In **c**, cells were pretreated for 1 h with 10 μM prenyltransferase inhibitors (FTI-297, farnesyltransferase inhibitor; GGTI-2133, geranylgeranyltransferase-I inhibitor) as indicated prior to alk-FOH labeling. (**d**) MEF cells transfected with pCMV-HA-ZAPL, pCMV-HA-ZAPL-SaaX or pCMV-HA-ZAPS (shown in Figure 22a) were detergent fractionated in nuclear (N), membrane (M) and cytosolic (C) fractions, and their purity was assessed by anti-histone H3, anti-calnexin and anti-GAPDH western blotting, respectively. Cellular localization of HA-ZAP was assessed by anti-HA western blotting.

3.4.2 *S*-farnesylation controls membrane targeting and cellular localization of ZAPL

We next investigated if *S*-farnesylation of ZAPL affected membrane partitioning and cellular localization. For these studies mouse embryonic fibroblasts (MEFs) were transfected with HA-ZAPL, HA-ZAPL-SaaX, or HA-ZAPS and fractionated into cytoplasmic, membrane and nuclear fractions. Each fraction was analyzed for ZAP distribution by anti-HA immunoblot along with histone H3, calnexin and GAPDH as controls for nuclear, membrane and cytoplasmic fractions, respectively (Figure 23d). While ZAPS was found in nuclear, membrane and cytosolic fractions, ZAPL was markedly depleted from the cytosol (Figure 23d). This was attributed to *S*-farnesylation, as ZAPL-SaaX was redistributed to the cytosol similar to ZAPS (Figure 23d). MEFs transfected with the HA-ZAP constructs were also analyzed by immunofluorescence using confocal microscopy. While ZAPL exhibited punctate clusters, ZAPL-SaaX showed a more diffuse staining, similar to ZAPS (Figure 24a). Cotransfection of plasmids expressing HA-ZAP and cellular markers indicated that ZAPL localizes to lysosomes (LAMP1-GFP) and late endosomes (GFP-Rab7), but not early endosomes (GFP-Rab5) (Figure 24b). This localization was not observed with ZAPL-SaaX or ZAPS (Figure 25-27). *S*-farnesylation is thus required for targeting ZAPL to late endosomal and lysosomal compartments.

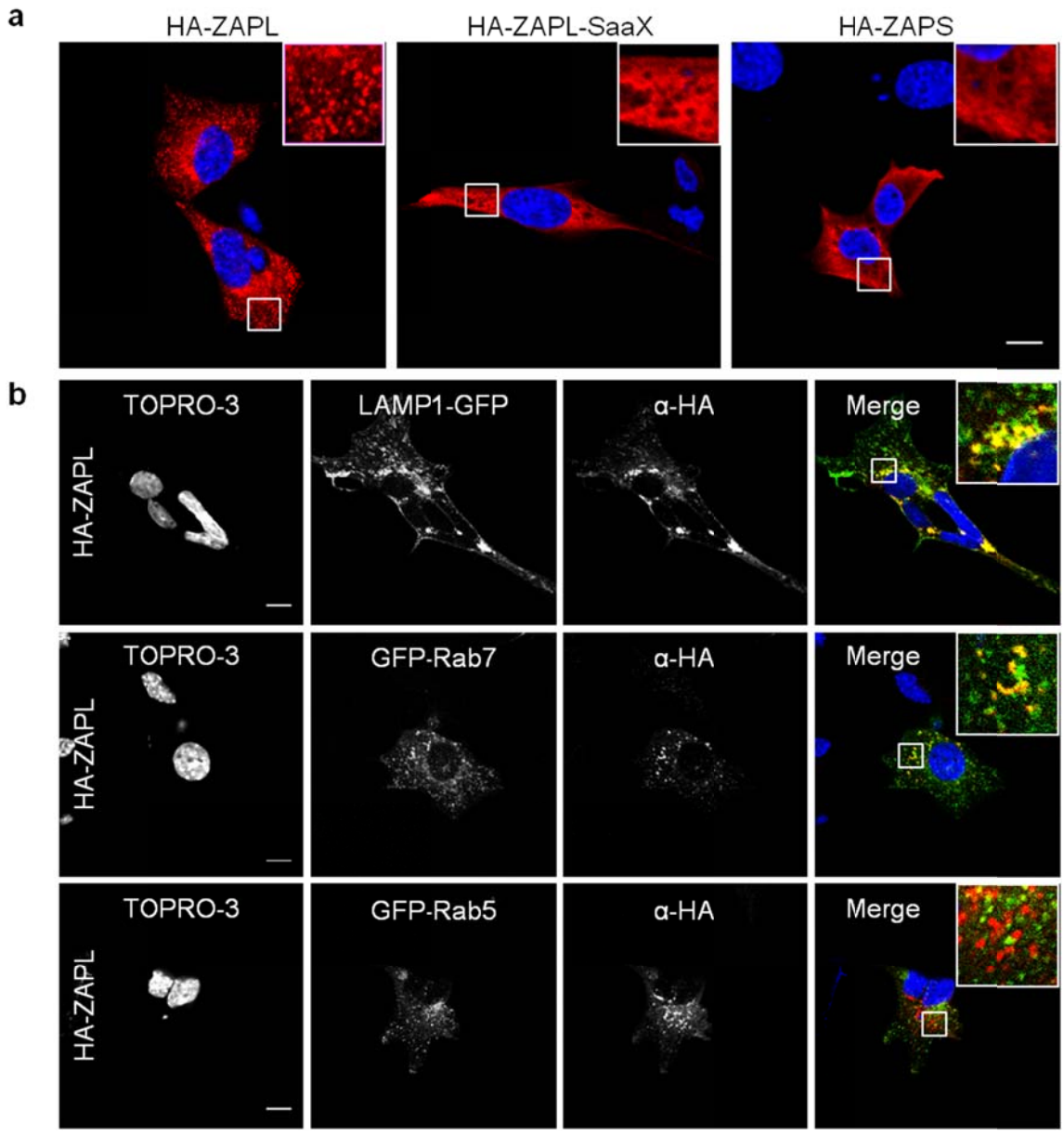

Figure 24: *S*-Farnesylation-dependent clustering of ZAPL to endo/lysosomes. (**a**) MEF cells grown on coverslips were transfected with pCMV-HA-ZAPL, pCMV-HA-ZAPL-SaaX or pCMV-HA-ZAPS and stained with anti-HA (red) and TOPRO-3 (blue). Insets are enlargements of the white-squared regions. Scale bar represents 10 μm. (**b**) MEFs were also co-transfected with pCMV-HA-ZAPL and plasmids expressing cellular markers LAMP1-GFP, GFP-Rab7 or GFP-Rab5 (green) as indicated.

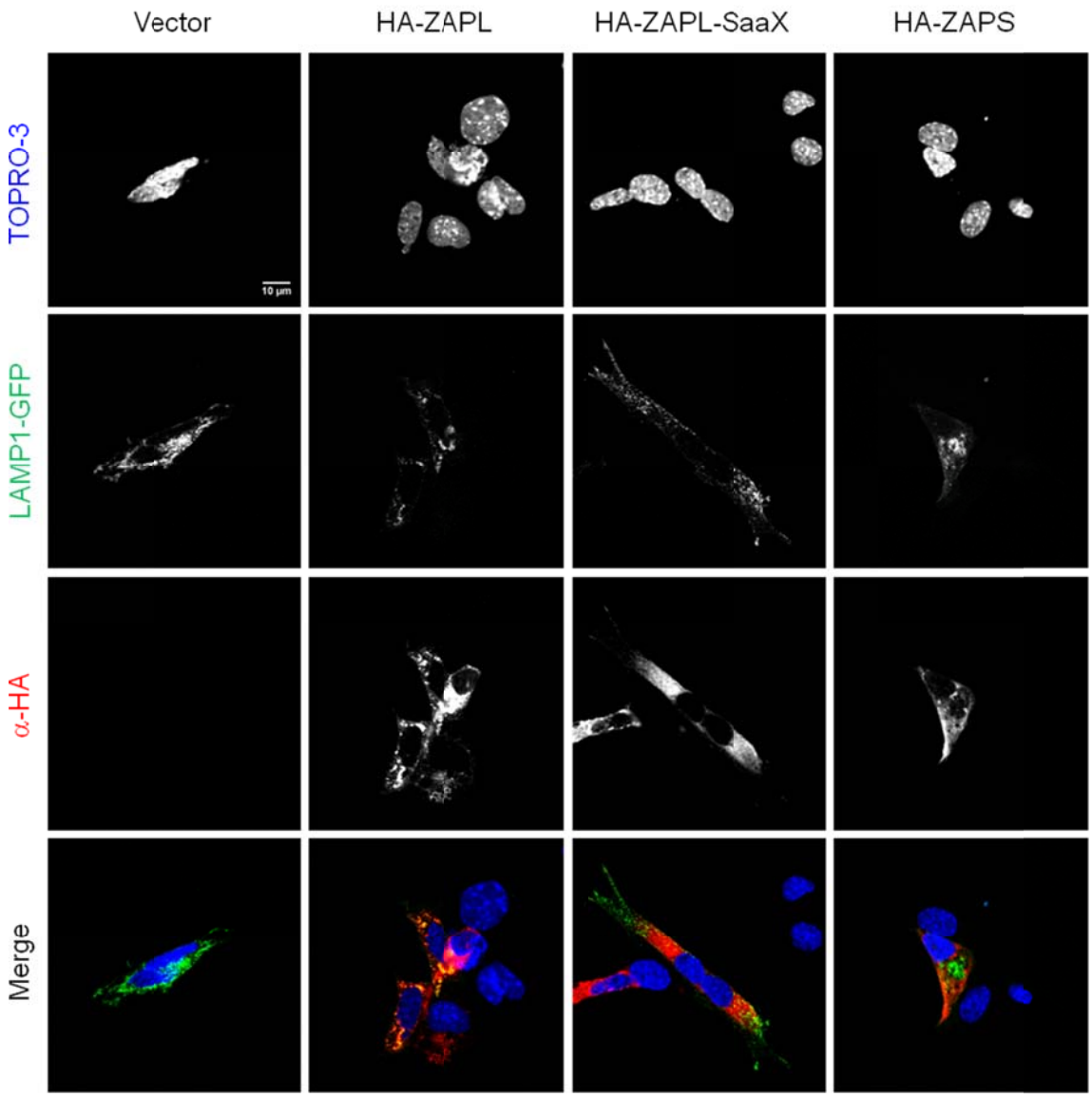

Figure 25: *S*-Farnesylation-dependent clustering of ZAPL with lysosomes. MEFs grown on coverslips were cotransfected with plasmids expressing lysosome cellular marker LAMP1-GFP (green) and pCMV-HA (vector), pCMV-HA-ZAPL, pCMV-HA-ZAPL-SaaX or pCMV-HA-ZAPS (shown in Figure 22a) and stained with anti-HA (red) and TOPRO-3 (blue). Scale bar represents 10 μm.

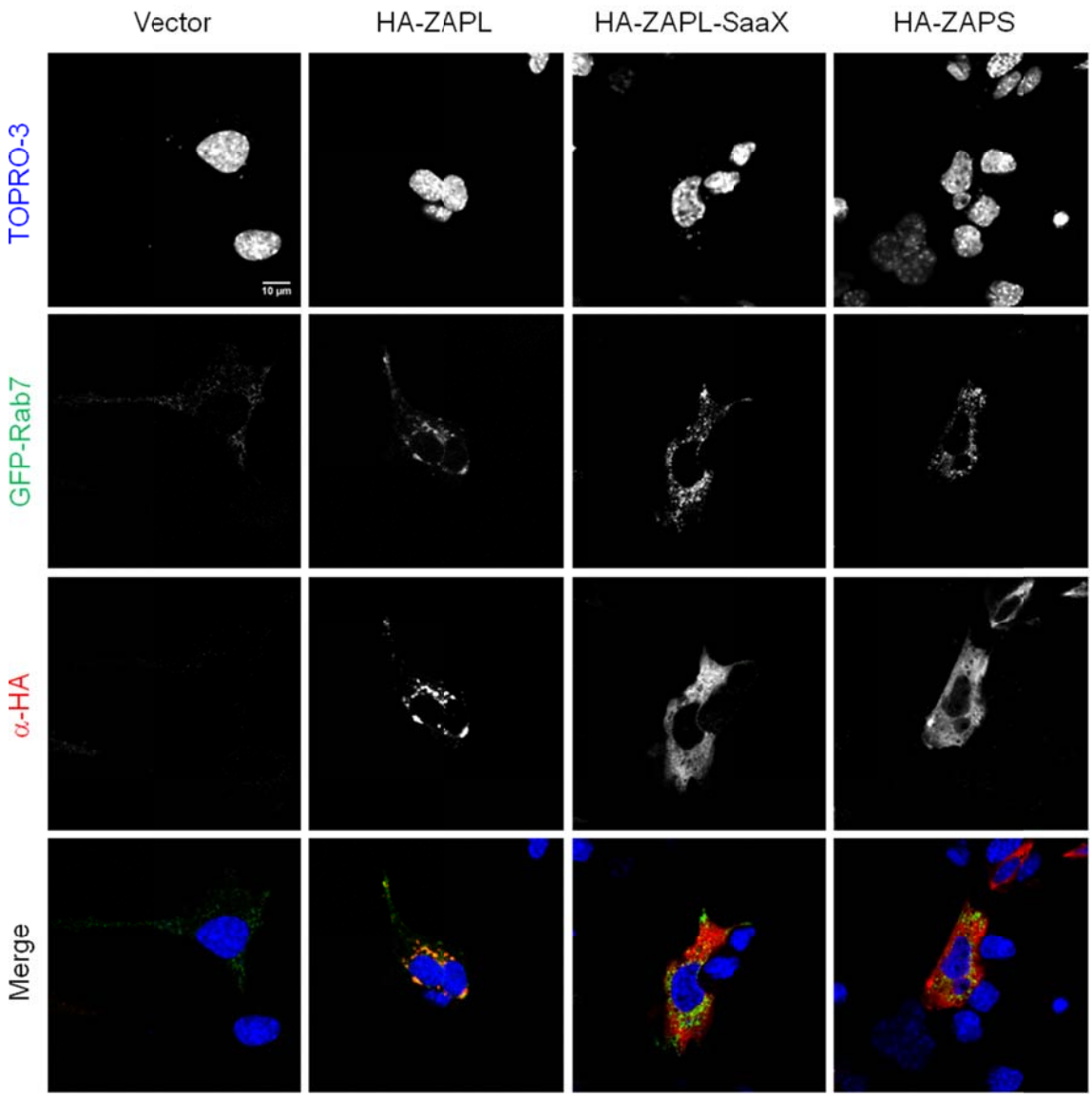

Figure 26: *S*-Farnesylation-dependent clustering of ZAPL with late endosomes. MEFs grown on coverslips were cotransfected with plasmids expressing late endosome cellular marker GFP-Rab7 (green) and pCMV-HA (vector), pCMV-HA-ZAPL, pCMV-HA-ZAPL-SaaX or pCMV-HA-ZAPS (shown in Figure 22a) and stained with anti-HA (red) and TOPRO-3 (blue). Scale bar represents 10 μm.

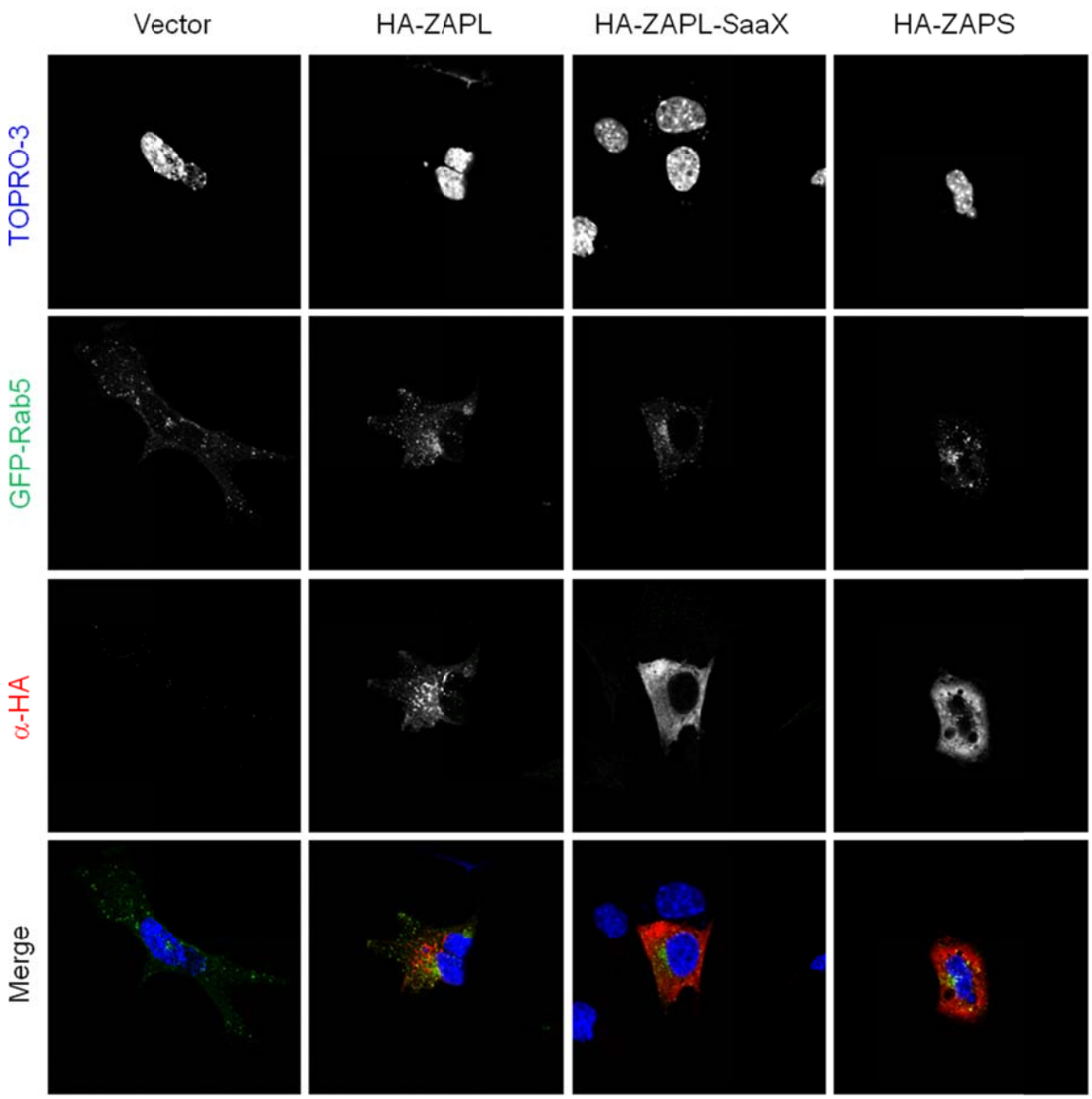

Figure 27: *S*-Farnesylation does not cluster ZAPL with early endosomes. MEFs grown on coverslips were cotransfected with plasmids expressing early endosome cellular marker GFP-Rab5 (green) and pCMV-HA (vector), pCMV-HA-ZAPL, pCMV-HA-ZAPL-SaaX or pCMV-HA-ZAPS (shown in Figure 22a) and stained with anti-HA (red) and TOPRO-3 (blue). Scale bar represents 10 μm.

3.4.3 *S*-farnesylation regulates ZAPL antiviral activity

We then determined whether isoform-specific *S*-farnesylation was crucial for ZAPL antiviral activity using Sindbis virus (SINV) as a prototypic alphavirus for these infection assays (in collaboration with the laboratory of Dr Margaret MacDonald, The Rockefeller University). Since murine ZAP mRNA level is upregulated by type I IFN[112] and ZAP exhibits homotypic interactions[113], we utilized Stat1-deficient (Stat1-/-) MEFs that are defective in IFN signaling[114] to mitigate the effects of IFN-induced endogenous ZAP. Stat1-/- MEFs transfected with HA-ZAP constructs were thus infected with a SINV encoding enhanced green fluorescent protein (TE/5'2J/GFP)[115] at a multiplicity of infection (MOI) of ~50 for 24 hours before immunostaining and flow cytometric analysis of the HA tag (ZAP) and EGFP (virus) expression. This allowed direct comparison of virus infection in transfected and non-transfected cells in the same sample by gating on the cells with high and low HA staining, respectively. Transfected Stat1-/- MEFs with low HA staining were infected at comparable levels (26-28%) to vector control samples (32%) (Figure 28a, lower quadrants; Figure 28b, grey). In addition, transfected cells expressed similar levels of different HA-ZAP proteins, as determined by the percentage of cells with high HA staining and the mean fluorescence intensity (MFI) of those cells (Figure 28a, upper quadrants). Only 5% of HA-ZAPL expressing Stat1-/- MEFs were infected while cells expressing the non-farnesylated HA-ZAPL-SaaX and HA-ZAPS proteins had higher levels of infected cells (14-15%; student *t*-test: $P = 0.00016$ and 0.00003, respectively) (Figure 28b, black). ZAPL inhibited SINV to a significantly greater extent than ZAPS (Figure 28c), with ZAPS demonstrating only 65% of the antiviral activity of ZAPL. This is consistent with previous ZAP studies with

MuLV[109]. This increased antiviral activity is mostly attributed to ZAPL *S*-farnesylation, since HA-ZAPL-SaaX expression resulted in infected cell levels similar to HA-ZAPS (Figure 28b,c). The *S*-farnesylation-dependent antiviral activity of ZAPL was also observed at a lower MOI (Figure 29a,b) and in HEK293T cells (Figure 29c-f). These results demonstrate *S*-farnesylation significantly enhances the antiviral activity of ZAPL.

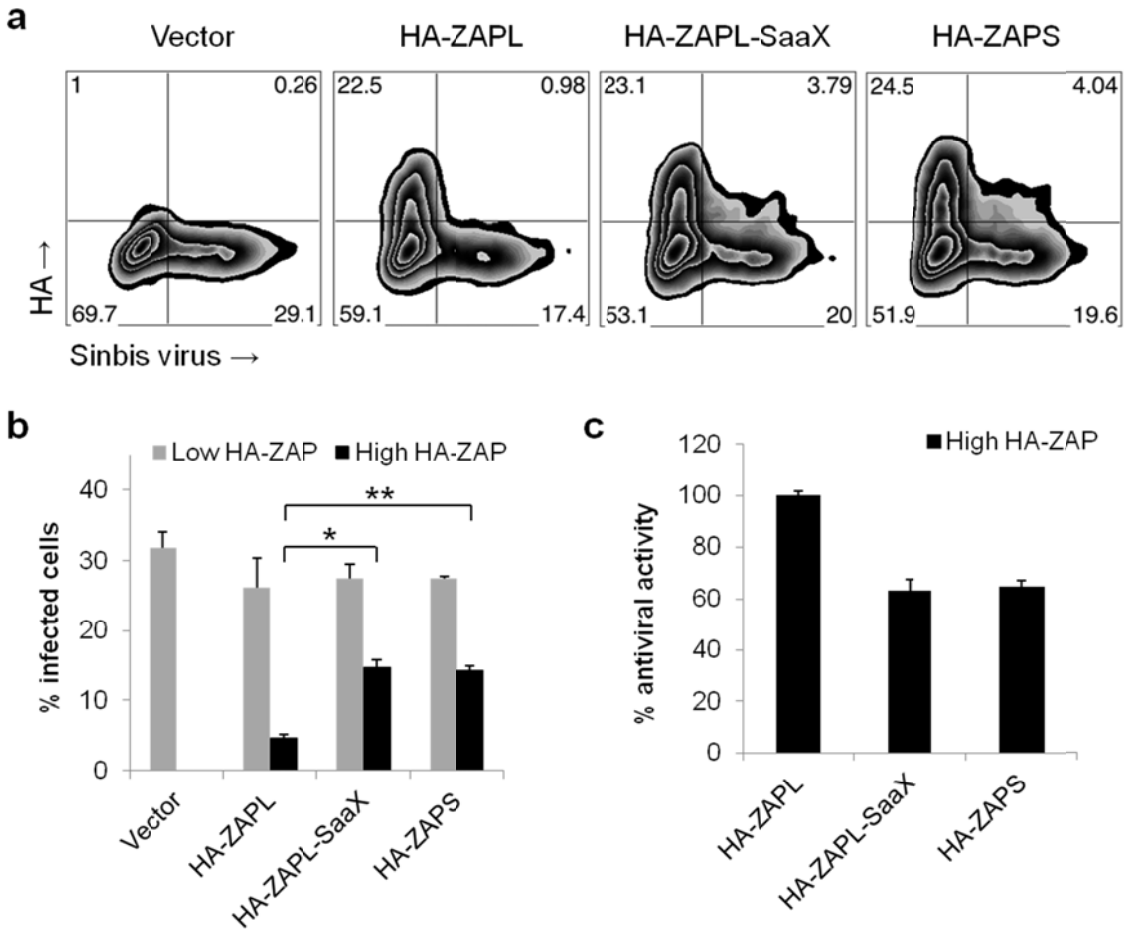

Figure 28: Antiviral activity of ZAPL is regulated by *S*-farnesylation. Stat1 -/- MEF cells were transfected with pCMV-HA (vector), pCMV-HA-ZAPL, pCMV-HA-ZAPL-SaaX or pCMV-HA-ZAPS (shown in Figure 22a) and infected with Sindbis virus encoding the enhanced green fluorescent protein (EGFP) from a duplicated subgenomic promoter (TE/5′2J/GFP) with multiplicity of infection (MOI) of ~50 for 24 h. Virus replication and ZAP protein levels were examined by flow cytometry using GFP fluorescence and anti-HA staining, respectively. After gating (shown in **a**), non-transfected and transfected cells expressing ZAP from the same culture were analyzed for the percentage of these cells that were infected (shown in **b**). **P* = 0.00016, ***P* = 0.00003 by Student's *t*-test; error represents s.d., *n* = 3. (**c**) Percentages in **b** were normalized such that the difference in infection rates for vector control and HA-ZAPL transfected cells was set at 100% antiviral activity.

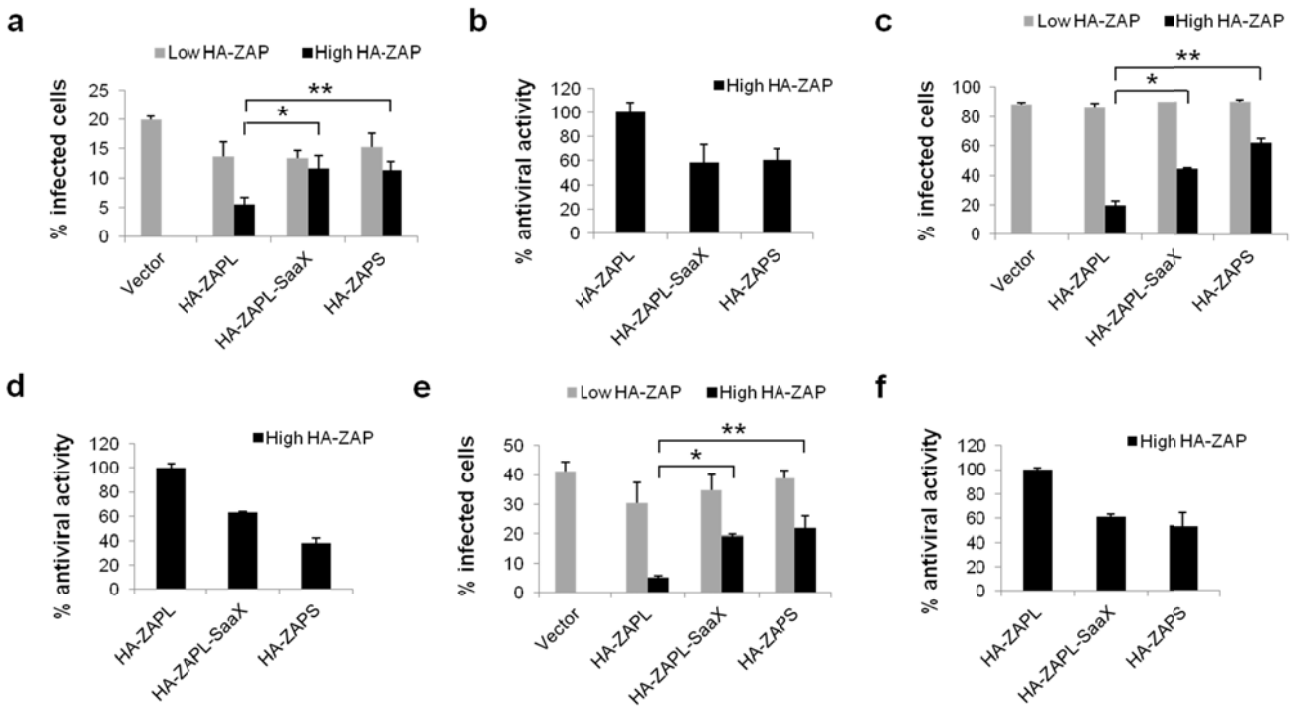

Figure 29: Antiviral activity of ZAPL is regulated by *S*-farnesylation. Stat1 -/- MEF (**a**, **b**) or HEK293T (**c**, **d**, **e**, **f**) cells were transfected with pCMV-HA (vector), pCMV-HA-ZAPL, pCMV-HA-ZAPL-SaaX or pCMV-HA-ZAPS (shown in Fig. 22a) and infected for 24 h with Sindbis virus encoding the enhanced green fluorescent protein (EGFP) from a duplicated subgenomic promoter (TE/5′2J/GFP) with the following multiplicity of infection (MOI): (**a**, **b**) ~15, (**c**, **d**) ~50, (**e**, **f**) ~15. Virus replication and ZAP protein levels were examined by flow cytometry using GFP fluorescence and anti-HA staining, respectively. After gating, non-transfected and transfected cells expressing ZAP from the same culture were analyzed for the percentage of these cells that were infected (shown in **a**, **c**, **e**). In **b**, **d** and **f**, percentages in **a**, **c** and **e**, respectively, were normalized such that the difference in infection rates for vector control and HA-ZAPL transfected cells was set at 100% antiviral activity. In **a** **P* = 0.013, ***P* = 0.005; in **c** **P* = 0.00007, ***P* = 0.00005; in **e** **P* = 0.00001, ***P* = 0.0024 by Student's *t*-test; error represents s.d., *n* = 3.

CHAPTER IV. Discussion

4.1 Improvements in detection of lipidated proteins

The installation of lipids onto proteins is a fundamental posttranslational modification that controls a wide variety of biological pathways but has been challenging to study. To address the limitations in the visualization of lipidated proteins, we have synthesized fatty acid and isoprenoid chemical reporters that allow rapid metabolic labeling of cells and robust fluorescence detection of lipidated proteins using bioorthogonal labeling methods. A comparative analysis of lipidated chemical reporters and bioorthogonal labeling methods revealed that alkynyl-fatty acids or alkynyl-farnesol in combination with azide-functionalized fluorophores afford the most sensitive method for the visualization of fatty-acylated and prenylated proteins, respectively, after CuAAC and in-gel fluorescence scanning. The in-gel fluorescence detection of lipidated proteins circumvents the need to transfer proteins onto membranes for immunoblotting, which can be problematic for hydrophobic polypeptides, and thus provides a more direct and quantitative means to analyze lipidated proteins. The sensitivity of this chemical approach enables robust detection of lipidated proteins within minutes after gel-electrophoresis compared to days or weeks with radioactive analogs, such that fatty-acylated and prenylated proteins expressed at endogenous levels can be readily visualized. The advances described here present significant improvements in the detection of protein lipidation compared to previously reported methods, which allowed the visualization of fatty-acylated proteins from primary tissues after metabolic labeling of living animals for the first time. Our approach also enabled the detection of *Salmonella* bacterial effector SifA, SspH2 and SseI palmitoylation and of *Legionella*

bacterial effectors prenylation in cells for the first time. Proteomic analysis of lipidated proteins was also improved such that we were able to enrich and identify new candidate lipidated proteins such as antiviral IFITM3 and ZAP. Our alkynyl-lipid chemical reporters therefore present new opportunities to dissect the functions of protein fatty-acylation and prenylation in physiology and disease.

4.2 Current limitations of lipid chemical reporters

As demonstrated by our proteomics experiments, alkynyl-lipid chemical reporters label enzymes associated with lipid synthesis and metabolism in addition to lipidated proteins. To evaluate the effect of degradation of chemical reporters of protein fatty acylation, we have recently synthesized 15-hexadecynyloxyacetic acid (HDYOA), a reporter that was designed to be resistant to β-oxidation based upon the molecular mechanism of fatty-acid metabolism, and we evaluated whether HDYOA could differentially target fatty-acylated proteins compared to metabolic enzymes[116]. HDYOA was able to label known candidate *S*-palmitoylated proteins similarly to ODYA. Accordingly, bioorthogonal proteomic analysis demonstrated that 70% of proteins labeled with alk-16 were also labeled with HDYOA. However, the proteins observed differentially in our proteomic studies suggested that a portion of alk-16 protein labeling is a result of β-oxidation. In contrast, downstream enzymes involved in β-oxidation of fatty acids were not targeted by HDYOA. Since HDYOA can label *S*-palmitoylated proteins and is not utilized by downstream β-oxidation pathways, this fatty acid chemical reporter may be particularly useful for bioorthogonal proteomic studies in cell types metabolically skewed toward fatty acid breakdown. This approach could also be applied to prevent the degradation of other chemical reporters.

4.3 Analysis of SifA prenylation in cells

The differences in SifA prenylation between our results and previous studies may be due to cellular labeling with alk-FOH compared to *in vitro* labeling with [^{3}H]mevalonic acid. The improved fluorescence detection with alk-FOH in cells may reveal low levels of *S*-prenylation not visualized by [^{3}H]mevalonic acid *in vitro*. Prenylation analyses of proteins bearing the unusual double cysteine CCXX C-terminal motif similar to SifA have been described. Geranylgeranyl modification of Rab5A (CCSN) is catalyzed by an enzyme in brain cytosol but not by purified GGTase I[117]. Similarly, Rab5A prenylation with GGTase II/REP-1 and [^{3}H]GGPP followed by mass spectrometry analysis demonstrated that Rab5A is geranylgeranylated on both cysteines by GGTase II[118]. However, the CCXX motif is not always a marker for GGTase II substrates: *in vitro* translational analyses by radioactive labeling in rabbit reticulocyte lysate demonstrated that both Ral-A (CCIL) and Ral-B (CCLL) are geranylgeranylated exclusively at the cysteine in the fourth position from the carboxyl terminus and [^{3}H]GGPP incorporation onto RalA/B could be blocked with GGTase I inhibitors[119-120]. Alternatively, Wrch-1, a Rho family GTPase bearing a CCFV C-terminal motif and a brain-specific isoform of Cdc42 with a CCIF motif were not to be prenylated, but instead *S*-fatty acylated[121-122]. CCXX can therefore be a motif for prenylation and *S*-palmitoylation. Nonetheless, our analyses of SifA prenylation with inhibitors of prenyltransferases and cysteine mutants suggest that SifA may be heterogeneously prenylated in host cells and single cysteine mutations do not completely abolish *S*-prenylation. While our cellular alk-FOH labeling of SifA differ from *in vitro* [^{3}H]mevalonic acid labeling studies, the robust and heterogeneous SifA prenylation from

our alk-FOH cellular labeling is consistent with residual membrane partitioning of these SifA mutants as well as their activity during *Salmonella* infection[36].

4.4 Analysis of isoform-specific farnesylation of ZAPL

Prenylation provides an essential membrane targeting mechanism that controls the functions of many proteins in eukaryotic biology. The direct biochemical analysis of these lipidated proteins can therefore reveal important activities in cellular membranes not readily apparent by monitoring protein expression alone. The application of an alkyne-farnesol reporter and improved bioorthogonal proteomics described here has enabled large-scale proteomic analysis of known prenylated proteins such as small GTPases as well as unannotated substrates like ZAPL. Our discovery and characterization of ZAPL lipidation demonstrates that *S*-farnesylation enhances the endolysosomal membrane targeting and inhibitory activity of this antiviral protein against SINV.

How ZAPL *S*-farnesylation promotes clustering to endosomes and lysosomes remains to be addressed. Prenylated proteins are constitutively excluded from detergent-resistant domains[123], which are lipid-ordered domains rich in cholesterol content. Although synthesis of cholesterol occurs in the ER, cholesterol is actively transported to the plasma membrane (PM) through the secretory pathway such that the PM is the cellular membrane with the highest cholesterol content[124]. While the ER and Golgi apparatus are continuously depleted of cholesterol from its transport to the PM, early endosomes have a cholesterol content similar to the PM as they bud off, and gradually decrease in cholesterol content as they mature to late endosomes and lysosomes[125]. By analogy, *S*-farnesylation-dependent clustering of ZAPL to endolysosomes could be

attributed to the increasing depletion of cholesterol in the endocytic pathway, and thus promote the localization of ZAPL at the site of entry of alphaviruses viral RNA. How ZAPL reaches endolysosomal membranes also remains unanswered. Is ZAPL passively diffusing from the cytosol to membranes or is it transported through the secretory pathway? These questions remain to be answered.

As ZAP is thought to inhibit SINV infection after virus entry but before amplification of newly synthesized plus strand genomic RNA[99], membrane targeting may place ZAPL near sites of membrane fusion to immediately target incoming viral RNA. Early SINV replication has now been observed in plasma membrane-associated cytopathic vacuoles (CV), which can then be transported into the cytosol in association with endosome-like vesicular organelles at a later stage of infection[126]. The *S*-farnesylated and membrane-associated ZAPL may therefore also interfere with assembly and replication of SINV as well as other viruses[98, 100-101], which have likewise been reported to assemble on cellular membranes[127]. Lipidation and membrane-association of ZAPL likely also contributes the differential activity of this long-isoform compared to ZAPS, which does not interfere with MuLV entry, viral DNA synthesis and integration, and viral RNA production in the nucleus, but decreased posttranscriptional viral mRNA in the cytoplasm[98] and is more active in enhancing RIG-I-dependent sensing of viral RNA[110]. These results suggest that *S*-farnesylated ZAPL exhibits a unique antiviral activity on cellular membranes, which may be important for the development of new antiviral strategies. Finally, these studies highlight how bioorthogonal proteomics of protein *S*-prenylation can reveal new insights into host-pathogen interactions that should be useful for exploring other biological pathways and human diseases.

CHAPTER V. Experimental methods

5.1 Plasmids construction

The human HA-Ras^{G12V} construct was a gift from Prof. Marilyn Resh (Memorial Sloan-Kettering Cancer Center), GFP-RhoA (plasmid 12965) and GFP-Rab7 (plasmid 12605) constructs were acquired from Addgene. ZAP-L was cloned from an interferon induced mouse dendritic cell (DC 2.4) cDNA library by PCR using sense primer ZAPL-SP: 5'-GGCC**GTCGAC**CATGACGGATCCCGAGGTATTC-3' and antisense primer ZAPL-AP: 5'-GGCC**GCGGCCGC**CTAACTAATTATGCATCCTT-3'. The sense primer introduces a SalI site (bolded) immediately upstream from the coding sequence as well as a nucleotide for in frame expression and the antisense primer introduces a NotI site (bolded) immediately downstream from the coding sequence to facilitate its cloning into the pCMV-HA mammalian expression vector (Clontech), yielding N-terminal HA-tagged ZAPL fusion (pCMV-HA-ZAPL). Mutagenesis was performed using the Stratagene Quikchange Multi Site-Directed Mutagenesis Kit on pCMV-HA-ZAPL template. Primers used for mutations are as follows: pCMV-HA-ZAPS: 5'-CTGGGGCATCACTGGCTGCTACTCTGGACCTCTTCTCTTCTG-3', pCMV-HA-ZAPL-SaaX: 5'-GAGAAAGAGAAAGGATCTATAATTAGTTAGGCG-3'.

5.2 Cell culture, transfections and metabolic labeling

Jurkat cells were cultured in RPMI medium 1640, while all other cells were cultured in DMEM, both supplemented with 10% fetal bovine serum (FBS), 100 U/mL penicillin and 100 μg/mL streptomycin. Cells were maintained in a humidified 37 °C incubator with 5% CO_2. HEK293T cells were transfected using X-tremeGENE 9 DNA

Transfection Reagent (Roche) while HeLa cells and MEFs were transfected using Lipofectamine 2000 (Invitrogen). Cells were treated with lipid reporters using the same volume of DMSO in the negative controls. For coincubation with inhibitors, cells were pretreated for 1 hour with the inhibitors prior to lipid reporter addition. Cells were then harvested, washed twice with ice-cold PBS and pelleted at 1000*g* for 5 min. Cells were directly lysed or flash frozen in liquid nitrogen and stored at -80 °C prior to lysis. Cell fractionation was performed with Qproteome Cell Compartment Kit (Qiagen, 37502) following manufacturer procedure.

Spleens were harvested from 6 week-old female C57/BL6 mice. Splenocytes were prepared by manual disruption of spleens using forceps. Red blood cells were eliminated using ACK lysis buffer. Splenocytes were pelleted and resuspended in either alk-12 or alk-16 (20 μM, 50 mM stock solution in DMSO) in RPMI medium 1640 supplemented with 2% FBS, 100 U/mL penicillin, and 100 μg/mL streptomycin using one spleen per labeling condition. The same volume of DMSO was used as a negative control. After 4-6 hours of labeling at 37 °C, the cells were pelleted at 1,000 g for 5 minutes, washed once with ice-cold PBS, and directly lysed.

5.2.1 Alkynyl-fatty acid *in vivo* labeling in mice

PBS containing 10% fatty acid free BSA (Sigma) was added to alk-12 and alk-16 (25 mg/mL), followed by brief sonication, warming to 37 °C, and IP injection of 200 μL into 6 week-old female C57/BL6 mice for 1 hour. Livers and kidney were harvested and incubated with Liberase 3 Blendzyme (Roche) at 37 °C for 30 min and homogenized prior to filtration with 0.4 μm cell strainers. Splenocytes were prepared by manual

disruption of spleens using forceps. Liver, kidney and splenocyte preparations were subjected to red blood cell lysis using ACK lysis buffer. Cells were pelleted at 1,000 g for 5 minutes, washed once with ice-cold PBS, and directly lysed.

5.3 Immunoprecipitation

Cell pellets obtained from 3 confluent wells of a 6-well plate were lysed with 150 μL of ice-cold Brij lysis buffer (1% Brij 97, 50 mM triethanolamine pH 7.4, 150 mM NaCl, 5× EDTA-free Roche protease inhibitor cocktail, 10 mM PMSF). Cell lysates were collected after centrifuging at 1000*g* for 5 min at 4 °C to remove cell debris. Protein concentration was determined by the BCA assay (Pierce). Proteins of interest were immunoprecipitated from 400 μg protein cell lysates in 250 μL ice-cold Brij lysis buffer using one of the following antibodies: mouse anti-Lck ($p56^{lck}$) monoclonal (Clone 3A5, Thermo Scientific), rabbit anti-LAT polyclonal (Upstate), rabbit anti-Fyn polyclonal (Upstate), anti-GFP rabbit pAb (ab290, Abcam) and 25 μL of packed protein A-agarose beads (Roche) per sample, or 15 μL of packed anti-v-H-ras (Ab-1) rat mAb (Y13-259) agarose conjugate (Calbiochem) or 25 μL of packed anti-HA (HA-7) mouse mAb agarose conjugate (Sigma). Upon incubation at 4 °C for 2 hours with a nutating mixer (Labnet), the beads were washed (3 x 1 mL) with ice-cold modified RIPA lysis buffer (1% Triton X-100, 1% sodium deoxycholate, 0.1% SDS, 50 mM triethanolamine pH 7.4, 150 mM NaCl).

5.4 Bioorthogonal ligation

5.4.1 Staudinger ligation

Cell lysates (50 μg) in 46.5 μL modified RIPA lysis buffer were reacted with 1 μL phosphine-biotin[128] (200 μM, 10 mM stock solution in DMSO) and 2.5 μL DTT (5 mM, 100 mM stock solution in deionized water) for a total reaction of volume of 50 μL for 1 hr at room temperature. DTT prevents non-specific oxidation of phosphine-biotin, which can increase levels of background labeling. The reactions were terminated by the addition of -20 °C methanol (1 mL) and placed at -20 °C for at least 1 hr, centrifuged at 18,000 g for 10 min at 0 °C to precipitate proteins. The supernatant from the samples were discarded. The protein pellets were allowed to air dry for 10 min, resuspended in 35 μL of resuspension buffer (4% SDS, 50 mM triethanolamine pH 7.4, 150 mM NaCl), diluted with 12.5 μL 4X reducing SDS-loading buffer (40% glycerol, 200 mM Tris-HCl pH 6.8, 8% SDS, 0.4% bromophenol blue) and 2.5 μL 2-mercaptoethanol, heated for 5 min at 95 ºC and ~20 μg of protein was loaded per gel lane for separation by SDS-PAGE (10% or 4-20% Bio-Rad Criterion Tris-HCl gel).

5.4.2 Cu^{I}-catalyzed azide-alkyne cycloaddition (CuAAC)

For immunoprecipitations, the purified protein bound to beads was suspended in 50 μL of ice-cold PBS, to which was added 3 μL freshly premixed CuAAC reaction cocktail [azido-rhodamine (100 μM, 10 mM stock solution in DMSO), tris(2-carboxyethyl)phosphine hydrochloride (TCEP) (1 mM, 50 mM freshly prepared stock solution in deionized water), tris[(1-benzyl-1*H*-1,2,3-triazol-4-yl)methyl]amine (TBTA) (100 μM, 10 mM stock solution in DMSO) and $CuSO_4 \cdot 5H_2O$ (1 mM, 50 mM freshly

prepared stock solution in deionized water)] for 1 h at 4 °C on a nutating mixer. The beads were washed (3 x 1 mL) with ice-cold modified RIPA lysis buffer, resuspended in 40 μL loading buffer [27.5 μL (4% SDS, 50 mM triethanolamine pH 7.4, 150 mM NaCl), 10 μL 4× SDS-loading buffer (40% glycerol, 200 mM Tris-HCl pH 6.8, 8% SDS, 0.4% bromophenol blue) and 2.5 μL 0.5 M Bond-Breaker TCEP Solution (Thermo Scientific)], heated for 5 min at 95 °C, and 20 μL of the supernatant was loaded on 2 separate SDS-PAGE gels (4−20% Bio-Rad Criterion Tris-HCl gel), one for fluorescence detection and the other for immunoblotting.

For cell lysates, 50 μg proteins were conjugated in 47 μl SDS-buffer (4% SDS, 50 mM triethanolamine pH 7.4, 150 mM NaCl) with 3 μL freshly premixed CuAAC reaction cocktail (same as above) for 1 hour at room temperature. Proteins were precipitated by adding ice-cold methanol (1 mL), placing at -80 °C overnight, centrifuging at 18000*g* for 10 min at 4 °C and discarding the supernatant. The protein pellets were allowed to air-dry, resuspended in 50 μL loading buffer (same as above), heated for 5 min at 95 °C, and 20 μg of protein was loaded on 2 separate SDS-PAGE gels.

5.5 Hydroxylamine cleavage of *S*-acylated proteins

After the proteins were separated by SDS-PAGE, the gel was soaked in 40% MeOH, 10% acetic acid, shaking overnight at room temperature, washed with deionized water (2 x 5 minutes) and scanned for the pre-hydroxylamine treatment fluorescence. The gel was then soaked in PBS, shaking 1 hour at room temperature, followed by soaking in 1 M NH_2OH (pH = 7.4), shaking 8 hours at room temperature, washing with

deionized water (2 x 5 minutes), and soaking in 40% MeOH, 10% acetic acid, shaking overnight at room temperature. The gel was finally washed with deionized water (2 x 5 minutes) and scanned for the post-hydroxylamine treatment fluorescence.

5.6 In-gel fluorescence imaging

After SDS-PAGE separation, the gel was soaked in destaining solution (40% MeOH, 10% acetic acid, 50% H_2O) overnight at 4 °C on an orbital shaker, rehydrated with deionized water and visualized scanning the gel on an Amersham Biosciences Typhoon 9400 variable mode imager (excitation 532 nm, 580 nm filter, 30 nm band-pass).

5.7 Immunoblotting

Proteins separated by SDS-PAGE were transferred (50 mM Tris, 50 mM glycine, 0.1% SDS, 10% MeOH in deionized water, Bio-Rad Trans-Blot Semi-Dry Cell, 20 V, 45 min) onto a nitrocellulose membrane (0.45 μm, Bio-Rad) which was subsequently blocked (10% non-fat dried milk, 2% BSA and 0.1% Tween-20 in PBS) overnight at 4 °C on an orbital shaker. The membrane was washed thrice with PBST (0.1% Tween-20 in PBS), and incubated with one of the following primary antibodies: mouse anti-Lck (p56lck) monoclonal (Clone 3A5, Thermo Scientific), mouse anti-LAT monoclonal (2E9, Upstate), mouse anti-Fyn monoclonal (S1, Chemicon), anti-Ras (RAS10) mouse mAb (1:4000, Upstate), anti-HA (HA-7) mouse mAb (1:2000, Sigma), anti-GFP (JL-8) mouse mAb (1:1000, Clontech), rabbit anti-histone H3 (1/2,000, 06-755, Millipore), rabbit anti-calnexin (1/1,500, ab22595, Abcam) or rabbit anti-GAPDH (1/5,000, ab70699, Abcam) for 1 hour at room temperature in PBST. The membrane was washed thrice with PBST,

incubated with one of the following secondary antibodies: anti-mouse (H+L) donkey HRP-conjugated antibody (Jackson IR, 1:15000) or HRP-conjugated goat anti-rabbit (1/15,000, 12-348, Millipore) for 1 hour at room temperature in 5% non-fat dried milk and 1% BSA in PBST, washed thrice with PBST, and subsequently developed with ECL Western blotting detection reagents (Thermo Scientific). For Staudinger ligation, the membrane was blocked, incubated with streptavidin-horseradish peroxidase (1 mg/mL diluted 1:25,000 in PBST, Pierce), and subsequently developed with ECL Western blotting detection reagents (Amersham).

5.8 Prenylome profiling

5.8.1 Enrichment of alk-FOH labeled proteins

RAW264.7 macrophages were pre-treated with lovastatin (10 μM, 12 hrs), then alk-FOH was added (50 μM, 12 hrs), cells were harvested, lysed in 1 mL ice-cold hypotonic buffer (5 mM triethanolamine pH 7.4, 5 mM $MgCl_2$, EDTA-free Roche protease inhibitor cocktail, 1 mM PMSF) and solubilized by dilution with 1 mL of 2X-SDS buffer (8% SDS, 100 mM triethanolamine pH 7.4, 300 mM NaCl) + 2 μL Benzonase nuclease (E1014, Sigma). Cell lysates (20 mg) were then reacted with az-azo-biotin[94] in 20 mL with CuAAC reactants (same as above) for 2 hours at room temperature. Methanol-precipitated and washed protein pellets were resuspended in 2 mL 1X-SDS buffer + 10 mM EDTA. 15 mg of proteins were diluted with 8 mL Brij buffer (1% Brij 97, 50 mM triethanolamine pH 7.4, 150 mM NaCl) and incubated with 300 μL prewashed streptavidin-agarose beads (20357, Thermo Scientific) for 1 h at room temperature. The beads were washed once with PBS + 1% SDS, thrice with PBS, and twice with ABC buffer (50 mM ammonium bicarbonate). The beads were incubated in

500 μL ABC buffer + 8 M urea + 10 mM TCEP + 20 mM iodoacetamide for 0.5 h at room temperature, and then washed twice with ABC buffer. Proteins were eluted by incubating the beads twice in 250 μL ABC buffer + 1% SDS + 25 mM $Na_2S_2O_4$ for 1 h at room temperature. Proteins from the pooled supernatants were concentrated using an Amicon Ultracel-10K (UFC501096, Millipore). Samples were then subjected to SDS-PAGE and staining with Coomassie blue. DMSO and alk-FOH lanes of the gel were then cut for trypsin digestion and peptide extraction. Extracted peptides were dried and resuspended in H_2O + 0.1% trifluoroacetic acid for mass spectrometry.

5.8.2 LC-MS/MS analysis

LC-MS/MS analysis was performed with a Dionex 3000 nano-HPLC coupled to an LTQ-Orbitrap ion trap mass spectrometer (ThermoFisher). Peptides were pressure-loaded onto a custom-made 75 μm diameter, 15 cm C18 reverse-phase column and separated with a gradient running from 95% buffer A (H_2O + 0.1% formic acid) and 5% buffer B (CH_3CN + 0.1% formic acid) to 55% buffer B over 30 min, next ramping to 95% buffer B over 10 min and holding at 95% buffer B for 10 min. One full MS scan (300-2,000 MW) was followed by three data-dependent scans of the *n*th most intense ions with dynamic exclusion enabled.

5.8.3 Database searching

Tandem mass spectra from three independent experiments were extracted by BioWorks (Thermo Scientific, version 3.3.1 SP1). All MS/MS samples were analyzed using Sequest (Thermo Scientific, SRF v. 5) and X! Tandem (TORNADO, 2010.01.01.5). Sequest and X! Tandem were set up to search the mouse International Protein Index (IPI) protein sequence database (version 3.83, 60010 entries) assuming the

digestion enzyme trypsin and allowing 2 missed cleavage sites per peptide. Sequest and X! Tandem were searched with a fragment ion mass tolerance of 1.00 Da and a parent ion tolerance of 10.0 PPM. Deamidation of asparagine and glutamine, oxidation of methionine and tryptophan, acetylation of the n-terminus and iodoacetamide derivative of cysteine were specified as variable modifications, allowing 3 modifications per peptide.

5.8.4 Criteria for protein identification

Scaffold (Proteome Software, version 3.00.04) was used to validate MS/MS based peptide and protein identifications. Peptide identifications were accepted if they could be established at greater than 95.0% probability as specified by the Peptide Prophet algorithm[129]. Peptide identifications were also required to exceed specific database search engine thresholds. Sequest identifications required at least ΔCn scores of greater than 0.10 and XCorr scores of greater than 1.8, 2.5, 3.5 and 3.5 for singly, doubly, triply and quadruply charged peptides. X! Tandem identifications required at least -Log(Expect Scores) scores of greater than 2.0. Protein identifications were accepted if they could be established at greater than 99.9% probability and contained at least 2 identified peptides. Protein probabilities were assigned by the Protein Prophet algorithm[130]. Proteins that contained similar peptides and could not be differentiated based on MS/MS analysis alone were grouped to satisfy the principles of parsimony. Proteins were considered high- or medium-confidence hits based on their number of assigned spectra.

5.9 Microscopy

For determination of ZAP localization, transfected HEK293T or MEF cells were fixed with PBS + 3.7% paraformaldehyde, permeabilized with PBS + 0.1% Triton X-100

and blocked with PBS + 2% FBS. Cells were then incubated with anti-HA antibody (1/1,000, H3663, Sigma), washed thrice, and stained with goat anti-mouse antibody conjugated to Rhodamine Red-X (1/1,000, R6393, Invitrogen). Cells were incubated with TOPRO-3 (1/1,000, Invitrogen) as a final step. Confocal images were collected using a Zeiss LSM 510 laser scanning confocal microscope equipped with a Plan-Apochromat 100X/1.40 oil objective.

5.10 Virus infections and flow cytometry

293T or Stat1 -/- MEF cells expressing ZAP constructs were infected for 24 hours with Sindbis virus encoding the enhanced green fluorescent protein (EGFP) from a duplicated subgenomic promoter (TE/5′2J/GFP)[115]. Stocks were prepared and titers determined on BHK-J cells with 10-fold serial dilutions of sample, and then plaques were visually enumerated after crystal violet staining, as previously described[99]. Multiplicities of infection (MOI) were calculated based on BHK-J-derived titers, and approximately 10-fold virus titers were necessary for equivalent levels of MEF infections. For flow cytometry, cells were fixed with PBS + 3.7% paraformaldehyde, then permeabilized and blocked with PBS + 0.1% Triton X-100 + 2% FBS. Cells were then incubated with mouse anti-HA antibody (1/1,000, H3663, Sigma), washed thrice, and stained with goat anti-mouse antibody conjugated to Rhodamine Red-X (1/1,000, R6393, Invitrogen). Results were analyzed with FlowJo software.

5.11 Synthesis of chemical reporters and secondary tags

5.11.1 General procedures

All chemicals were obtained either from Sigma-Aldrich, MP Biomedicals, Alfa Aesar, TCI, Fluka or Acros and were used as received unless otherwise noted. The silica gel used in flash column chromatography was Fisher S704 (60-200 Mesh, Chromatographic Grade). Analytical thin layer chromatography (TLC) was conducted on Merck silica gel plates with fluorescent indicator on glass (5-20 μm, 60 Å) with detection by ceric ammonium molybdate, basic $KMnO_4$ or UV light. The ^1H and ^{13}C NMR spectra were obtained on a Bruker DPX-400 spectrometer or a Bruker AVANCE-600 spectrometer equipped with a cryoprobe. Chemical shifts are reported in δ ppm values downfield from tetramethylsilane and *J* values are reported in Hz. MALDI-TOF mass spectra were obtained on an Applied Biosystems Voyager-DE. LC/MS were obtained on a Waters 500E pump and controller equipped with a Waters XBridge C18 5 μm 4.6 x 150 mm column, Waters 996 photodiode array detector and Waters Micromass ZQ mass spectrometer and the samples were single peak purity.

5.11.2 Alkynyl-fatty acids synthesis

Alkynyl-fatty acids were synthesized according to reported procedures[131-132] and were identical by ^1H NMR analysis.

Tetradec-13-ynoic acid (alk-12): ^1H NMR (400 MHz, $CDCl_3$): δ 1.22-1.30 (s, 14H), 1.29-1.70 (m, 4H), 1.96 (t, 1H, *J* = 4), 2.22 (dt, 2H, *J* = 4, 7), 2.36 (t, 2H, *J* = 7).

Hexadec-15-ynoic acid (alk-14): ^1H NMR (400 MHz, $CDCl_3$): δ 1.22-1.30 (s, 18H), 1.29-1.70 (m, 4H), 1.96 (t, 1H, *J* = 4), 2.22 (dt, 2H, *J* = 4, 7), 2.36 (t, 2H, *J* = 7).

Octadec-17-ynoic acid (alk-16): ^{1}H NMR (600 MHz, $CDCl_3$): δ 1.22-1.30 (m, 18H), 1.29-1.35 (m, 2H), 1.35-1.42 (m, 2H), 1.52 (qu, 2H, *J* = 7.1), 1.63 (qu, 2H, *J* = 7.5), 1.93 (t, 1H, *J* = 2.6), 2.18 (dt, 2H, *J* = 2.6, 7.1), 2.35 (t, 2H, *J* = 7.5).

5.11.3 Alkynyl/azido-isoprenoids synthesis

(2*E*,6*E*,10*E*)-2,6,10-trimethyl-12-((tetrahydro-2*H*-pyran-2-yl)oxy)dodeca-2,6,10-trien-1-ol (**4**) was produced according to published literature protocols and was identical to previously reported ^{1}H, ^{13}C NMR and MS analyses[71]. ^{1}H NMR (600 MHz, $CDCl_3$): δ 1.47-1.88 (m, 6H), 1.59 (s, 3H), 1.65 (s, 3H), 1.67 (s, 3H), 1.98-2.15 (m, 8H), 3.46 (ddd, 1H, *J* = 5.3, 5.3, 10.6), 3.83 (ddd, 1H, *J* = 2.9, 8.2, 11.1), 3.91 (s, 2H), 3.97 (dd, 1H, *J* = 7.6, 11.9), 4.17 (dd, 1H, *J* = 6.4, 11.9), 4.58 (t, 1H, *J* = 3.6), 5.06 (t, 1H, *J* = 6.8), 5.30 (t, 1H, *J* = 6.9), 5.32 (t, 1H, *J* = 6.9). ^{13}C NMR (150 MHz, $CDCl_3$): δ 13.8, 16.1, 16.5, 19.7, 25.6, 26.2, 26.3, 30.8, 39.4, 39.7, 62.4, 63.8, 69.1, 97.9, 120.8, 124.4, 126.0, 134.7, 135.0, 140.2. MS: calculated 322.25, found 345.33 $[M+Na]^{+}$.

2-(((2*E*,6*E*,10*E*)-3,7,11-trimethyl-12-(prop-2-yn-1-yloxy)dodeca-2,6,10-trien-1-yl)oxy)tetrahydro-2*H*-pyran (**5**) was produced according to published literature protocols and was identical to previously reported ^{1}H and ^{13}C NMR analyses[133]. ^{1}H NMR (600 MHz, $CDCl_3$): δ 1.47-1.88 (m, 6H), 1.59 (s, 3H), 1.63 (s, 3H), 1.66 (s, 3H), 1.98-2.15 (m, 8H), 2.39 (t, 1H, *J* = 2.4), 3.50 (ddd, 1H, *J* = 5.2, 5.2, 10.4), 3.88 (ddd, 1H, *J* = 3.0, 8.0, 11.1), 3.92 (s, 2H), 4.01 (dd, 1H, *J* = 7.4, 11.9), 4.06 (d, 2H, *J* = 2.4), 4.22 (dd, 1H, *J* = 6.4, 11.9), 4.61 (t, 1H, *J* = 3.6), 5.10 (t, 1H, *J* = 6.7), 5.35 (t, 1H, *J* = 6.9), 5.41 (t, 1H, *J* = 6.9). ^{13}C NMR (150 MHz, $CDCl_3$): δ 14.0, 16.0, 16.5, 19.7, 25.6, 26.3,

26.4, 30.8, 39.3, 39.7, 56.3, 62.4, 63.7, 74.2, 75.9, 80.1, 97.9, 120.7, 124.4, 129.5, 131.2, 134.9, 140.3. MS: calculated 360.27, found 383.42 $[M+Na]^+$.

(2*E*,6*E*,10*E*)-3,7,11-trimethyl-12-(prop-2-yn-1-yloxy)dodeca-2,6,10-trien-1-ol (**alk-FOH**) was produced according to published literature protocols and was identical to previously reported ^1H, ^{13}C NMR and MS analyses[133]. ^1H NMR (600 MHz, $CDCl_3$): δ 1.60 (s, 3H), 1.65 (s, 3H), 1.68 (s, 3H), 2.00-2.17 (m, 8H), 2.40 (t, 1H, *J* = 2.4), 3.93 (s, 2H), 4.07 (d, 2H, *J* = 2.4), 4.15 (d, 2H, *J* = 6.9), 5.11 (ddd, 1H, *J* = 1.2, 6.8, 6.8), 5.39-5.44 (m, 2H). ^{13}C NMR (150 MHz, $CDCl_3$): δ 14.1, 16.1, 16.4, 26.4, 26.5, 39.3, 39.6, 56.4, 59.5, 74.2, 76.0, 80.2, 123.5, 124.3, 129.5, 131.3, 135.1, 139.8. MS: calculated 276.21, found 299.33 $[M+Na]^+$.

2-(((2*E*,6*E*,10*E*)-12-bromo-3,7,11-trimethyldodeca-2,6,10-trien-1-yl)oxy)tetrahydro-2*H*-pyran (**6**): In a previously flame-dried round-bottom flask under argon atmosphere was dissolved *N*-bromosuccinimide (498 mg, 2.80 mmol) in anhydrous dichloromethane (8 mL) cooled to 0 °C. Dimethyl sulfide (247 μL, 3.36 mmol) was added dropwise over 3 minutes, and the resulting reaction mixture was cooled to -20 °C. (**4**) (603 mg, 1.87 mmol) dissolved in anhydrous dichloromethane (4 mL) was then added dropwise over 3 minutes, and the reaction mixture was stirred at 0 °C for 3 hours and then overnight at room temperature. The reaction was quenched with a saturated brine aqueous solution and extracted with dichloromethane (3 x 50 mL). The combined organic layers were dried over Na_2SO_4, filtered and concentrated under reduced pressure. The crude material was purified by silica gel flash chromatography (5% EtOAc / 95% hexanes) to yield (**6**) (317 mg, 44%) as a yellow oil. ^1H NMR (600 MHz, $CDCl_3$): δ

1.45-1.87 (m, 6H), 1.58 (s, 3H), 1.66 (s, 3H), 1.73 (s, 3H), 1.97-2.14 (m, 8H), 3.49 (ddd, 1H, *J* = 5.3, 5.3, 10.6), 3.88 (ddd, 1H, *J* = 3.0, 7.9, 11.1), 3.95 (s, 2H), 4.01 (dd, 1H, *J* = 7.4, 11.9), 4.22 (dd, 1H, *J* = 6.4, 11.9), 4.61 (t, 1H, *J* = 3.7), 5.09 (t, 1H, *J* = 6.8), 5.34 (t, 1H, *J* = 6.3), 5.56 (t, 1H, *J* = 6.8). ^{13}C NMR (150 MHz, $CDCl_3$): δ 14.7, 16.0, 16.5, 19.7, 25.6, 26.3, 26.9, 30.8, 38.8, 39.6, 41.9, 62.3, 63.7, 97.9, 120.8, 124.6, 131.3, 132.0, 134.5, 140.1. MS: calculated 384.17, found 407.33 $[M+Na]^+$.

Trimethyl((4*E*,8*E*,12*E*)-4,8,12-trimethyl-14-((tetrahydro-2*H*-pyran-2-yl)oxy)tetradeca-4,8,12-trien-1-yn-1-yl)silane (**7**): In a previously flame-dried round-bottom flask under argon atmosphere was dissolved trimethylsilylacetylene (46 μL, 0.332 mmol) in anhydrous DMF (1 mL) at room temperature. Potassium carbonate (46 mg, 0.332 mmol), sodium sulfite (21 mg, 0.166 mmol), (**6**) (85 mg, 0.221 mmol) and copper(I) iodide (2 mg, 0.011 mmol) were added sequentially and the reaction mixture was stirred for 4 hours. The reaction was quenched with a saturated ammonium chloride aqueous solution and extracted with dichloromethane (3 x 50 mL). The combined organic layers were dried over Na_2SO_4, filtered and concentrated under reduced pressure. The crude material was purified by silica gel flash chromatography (5% EtOAc / 95% hexanes) to yield (**7**) (39 mg, 44%) as a colorless oil. ^{1}H NMR (600 MHz, $CDCl_3$): δ 0.15 (s, 9H), 1.48-1.87 (m, 6H), 1.60 (s, 3H), 1.66 (s, 3H), 1.67 (s, 3H), 1.96-2.16 (m, 8H), 2.90 (s, 2H), 3.51 (ddd, 1H, 4.9, 4.9, 10.5), 3.89 (ddd, 1H, *J* = 2.9, 8.0, 11.0), 4.02 (dd, 1H, *J* = 7.4, 11.8), 4.23 (dd, 1H, *J* = 6.4, 11.9), 4.62 (t, 1H, *J* = 3.7), 4.79-4.94 (m, 1H), 5.11 (t, 1H, *J* = 5.8), 5.35 (t, 1H, *J* = 6.4). ^{13}C NMR (150 MHz, $CDCl_3$): δ 0.3, 16.1, 16.6, 19.8, 25.6, 26.5, 26.9, 30.1, 30.9, 32.3, 39.5, 39.8, 62.4, 63.8, 97.9, 104.9, 112.2, 120.8, 124.2, 126.0, 129.7, 135.2, 140.4. MS: calculated 402.30, found 403.33 $[M+H]^+$.

(2*E*,6*E*,10*E*)-3,7,11-trimethyltetradeca-2,6,10-trien-13-yn-1-ol (**alk-FOH-2**): In a round-bottom flask equipped with a condenser, (**7**) (29 mg, 0.072 mmol) was dissolved in EtOH (2 mL). Pyridinium *p*-toluenesulfonate (1.8 mg, 0.007 mmol) was added and the reaction mixture was stirred overnight at 60 °C. The solvent was removed under reduced pressure and the crude material obtained was dissolved in THF (2 mL). Tetra-n-butylammonium fluoride (317 μL of 1 M solution in THF, 0.317 mmol) was added and the reaction mixture stirred overnight at room temperature. The solvent was removed under reduced pressure and the crude material obtained was purified by silica gel flash chromatography (20% EtOAc / 80% hexanes) to yield (**alk-FOH-2**) (13 mg, 73%) as a colorless oil. ^{1}H NMR (400 MHz, $CDCl_3$): δ 1.60 (s, 3H), 1.68 (s, 6H), 1.86 (s, 1H), 1.97-2.23 (m, 8H), 2.92 (m, 2H), 4.15 (d, 2H, *J* = 6.9), 5.12 (m, 1H), 5.41 (m, 2H). ^{13}C NMR (150 MHz, $CDCl_3$): δ 13.6, 16.1, 16.4, 26.4, 27.2, 27.7, 39.4, 39.6, 59.6, 78.0, 98.9, 110.3, 123.5, 124.3, 128.8, 135.1, 139.9. MS: calculated 246.20, found 247.25 $[M+H]^+$.

Trimethyl((5*E*,9*E*,13*E*)-5,9,13-trimethyl-15-((tetrahydro-2*H*-pyran-2-yl)oxy)pentadeca-5,9,13-trien-1-yn-1-yl)silane (**8**): In a previously flame-dried round-bottom flask under argon atmosphere was dissolved 1-(trimethylsilyl)propyne (88 mg, 0.781 mmol) in anhydrous THF (1 mL) at -20 °C, and n-butyl lithium (488 μL of 1.6 M solution in hexanes, 0.781 mmol) was added dropwise. After 30 minutes, (**6**) (75 mg, 0.195 mmol) dissolved in anhydrous THF (1 mL) was added dropwise, and the reaction mixture was allowed to slowly warm to 0 °C. After stirring 12 hours at 0 °C, the reaction was quenched with ice-cold water (50 mL) and extracted with ether (3 x 50 mL). The combined organic layers were washed with a saturated $NaHCO_3$ aqueous solution (3 x 50

mL) and a saturated brine aqueous solution (150 mL), dried over Na_2SO_4, filtered and concentrated under reduced pressure. The crude material was purified by silica gel flash chromatography (5% EtOAc / 95% hexanes) to yield (**8**) (77 mg, 94%) as a yellow oil. ^{1}H NMR (600 MHz, $CDCl_3$): δ 0.13 (s, 9H), 1.46-1.76 (m, 6H), 1.56 (s, 3H), 1.60 (s, 3H), 1.68 (s, 3H), 1.98 (t, 2H, *J* = 7.0), 2.00-2.14 (m, 6H), 2.18 (t, 2H, *J* = 7.6), 2.28 (q, 2H, *J* = 6.9), 3.51 (ddd, 1H, *J* = 5.4, 5.4, 10.8), 3.89 (ddd, 1H, *J* = 2.5, 7.9, 10.9), 4.02 (dd, 1H, *J* = 7.5, 11.6), 4.23 (dd, 1H, *J* = 6.4, 12.1), 4.62 (s, 1H), 5.10 (t, 1H, *J* = 5.6), 5.15 (t, 1H, *J* = 6.6), 5.36 (t, 1H, *J* = 6.3). ^{13}C NMR (150 MHz, $CDCl_3$): δ 0.3, 16.0, 16.2, 16.6, 19.4, 19.8, 25.7, 26.5, 26.8, 30.9, 38.8, 39.7, 39.8, 62.4, 63.8, 84.7, 98.0, 107.6, 120.7, 124.1, 125.7, 133.5, 135.3, 140.4. MS: calculated 416.31, found 439.42 $[M+Na]^+$.

(2*E*,6*E*,10*E*)-3,7,11-trimethylpentadeca-2,6,10-trien-14-yn-1-ol (**alk-FOH-3**): In a round-bottom flask equipped with a condenser, (**8**) (63 mg, 0.151 mmol) was dissolved in EtOH (1.5 mL). Pyridinium *p*-toluenesulfonate (3.8 mg, 0.015 mmol) was added and the reaction mixture was stirred overnight at 60 °C. The solvent was removed under reduced pressure and the crude material obtained was dissolved in THF (1.5 mL). Tetra-n-butylammonium fluoride (332 μL of 1 M solution in THF, 0.332 mmol) was added and the reaction mixture stirred overnight at room temperature. The solvent was removed under reduced pressure and the crude material obtained was purified by silica gel flash chromatography (20% EtOAc / 80% hexanes) to yield (**alk-FOH-3**) (26 mg, 67%) as a colorless oil, and was identical to previously reported ^{1}H, ^{13}C NMR and MS analyses[134]. ^{1}H NMR (600 MHz, $CDCl_3$): δ 1.60 (s, 6H), 1.68 (s, 3H), 1.92-2.15 (m, 9H), 2.17-2.29 (m, 4H), 4.15 (d, 2H, *J* = 6.9), 5.11 (t, 1H, *J* = 6.1), 5.17 (t, 1H, *J* = 6.9),

5.41 (t, 1H, *J* = 6.6). ^{13}C NMR (150 MHz, $CDCl_3$): δ 15.9, 16.1, 16.4, 17.8, 26.4, 26.7, 38.5, 39.6, 39.7, 59.5, 68.5, 84.6, 123.5, 124.1, 125.7, 133.3, 135.3, 139.9. MS: calculated 260.21, found 283.33 $[M+Na]^+$.

2-(((2*E*,6*E*,10*E*)-12-azido-3,7,11-trimethyldodeca-2,6,10-trien-1-yl)oxy)tetrahydro-2*H*-pyran (**9**): In a round-bottom flask, (**6**) (75 mg, 0.195 mmol) was dissolved in DMSO (1 mL). Sodium azide (19 mg, 0.293 mmol) was added and the reaction mixture was stirred overnight at room temperature. The reaction was diluted with ice-cold water (50 mL) and extracted with ether (3 x 50 mL). The combined organic layers were washed with a saturated brine aqueous solution (150 mL), dried over Na_2SO_4, filtered and concentrated under reduced pressure. The crude material was purified by silica gel flash chromatography (5% EtOAc / 95% hexanes) to yield (**9**) (55 mg, 81%) as a yellow oil isomeric mixture, which was identical to previously reported ^{1}H, ^{13}C NMR and MS analyses. ^{1}H NMR (600 MHz, $CDCl_3$): δ 1.47-1.87 (m, 6H), 1.58 (s, 3H), 1.67 (s, 3H), 1.72 (s, 3H), 1.91-2.21 (m, 8H), 3.50 (m, 1H), 3.63 (s, 1H), 3.79 (t, 1H, *J* = 7.0), 3.88 (t, 1H, *J* = 9.4), 4.01 (t, 1H, *J* = 8.8), 4.23 (dd, 1H, *J* = 6.6, 11.8), 4.62 (s, 1H), 4.95 (d, 1H, *J* = 23.5), 5.12 (m, 1H), 5.37 (m, 1H). ^{13}C NMR (150 MHz, $CDCl_3$): δ 14.8, (16.1), 16.6, 17.8, 19.8, 25.7, 26.4, (26.5), (30.8), 30.9, 36.1, 39.4, 39.7, 59.6, 62.4, 63.8, (68.2), 98.0, (114.7), 120.8, 120.9, (124.6), 125.1, 130.4, 134.0, 140.2, (140.3), (142.5). MS: calculated 347.26, found 370.42 $[M+Na]^+$.

(2*E*,6*E*,10*E*)-12-azido-3,7,11-trimethyldodeca-2,6,10-trien-1-ol (**az-FOH**) was produced according to published literature protocols and yielded an isomeric mixture of **az-FOH**, which was identical to previously reported ^{1}H, ^{13}C NMR and MS analyses. ^{1}H NMR (400 MHz, $CDCl_3$): δ 1.60 (s, 3H), 1.68 (s, 3H), 1.73 (s, 3H), 1.92-2.22 (m, 8H),

3.64 (s, 1H), 3.80 (t, 1H, *J* = 7.1), 4.15 (d, 2H, *J* = 6.8), 4.96 (d, 1H, *J* = 15.5), 5.13 (m, 1H), 5.41 (t, 1H, *J* = 6.7). ^{13}C NMR (150 MHz, $CDCl_3$): δ 14.8, 16.1, 16.4, (17.8), 26.3, 26.4, (26.5), (30.7), (36.1), (39.3), 39.5, 39.6, 59.5, 68.1, (114.7), 123.5, 123.6, (124.5), 125.0, 130.4, 134.1, (134.8), 139.6, (139.8), (142.5). MS: calculated 263.20, found 264.25 $[M+H]^+$.

5.11.4 Biotin detection tag synthesis

5-azido-*N*-(15-oxo-19-((3a*S*,4*S*,6a*R*)-2-oxohexahydro-1*H*-thieno[3,4-d]imidazol-4-yl)-4,7,10-trioxa-14-azanonadecyl)pentanamide (az-biotin): In a round-bottom flask equipped with a magnetic stir bar was dissolved 5-azidopentanoic acid (140 mg, 1 mmol) in CH_2Cl_2 (10mL). *N*-methylmorpholine (121 mg, 1.2 mmol) and isobutyl-chloroformate (163.8 mg, 1.2 mmol) were added, and this reaction mixture was stirred for 30 min at 0 °C. Then, this solution of activated acid was transferred via a syringe to a solution of **biotin-PEG-amine**[54] (150 mg, 0.3 mmol) in DMF (10 mL) in another round-bottom flask equipped with a magnetic stir bar and stirred at room temperature for 3 h. The solvent was evaporated under reduced pressure and the crude mixture was purified by flash chromatography on silica gel (70% EtOAc / 20% MeOH / 10% H_2O) to afford 76 mg of **az-biotin** as a white solid (45%). ^{1}H NMR (400 MHz, CD_3OD): δ 1.5 (m, 2H), 1.6-1.8 (m, 12H), 2.2 (m, 4H), 2.7 (d, 1H, *J* = 12.7), 2.9 (dd, 1H, *J* = 4.8, 12.7), 3.2 (ddd, 1H, *J* = 4.8, 7.4, 7.4), 3.3-3.4 (m, 6H), 3.5-3.7 (m, 12H), 4.3 (m, 1H), 4.5 (m, 1H), 5.2 (br, 1H), 5.8 (br, 1H), 6.4 (br, 1H), 6.6 (br, 1H). ^{13}C NMR (100 MHz, CD_3OD): δ 19.5, 22.9, 23.2, 26.4, 26.6, 28.4, 28.7, 28.9, 36.2, 37.9, 51.5, 66.2, 68.5, 70.1, 168.03, 168.04, 173.1. MALDI-TOF: 572.5 $[M+H]^+$.

5.11.5 Rhodamine detection tags synthesis

***N*-(6-(diethylamino)-9-(2-(4-hept-6-ynoylpiperazine-1-carbonyl)phenyl)-3*H*-xanthen-3-ylidene)-*N*-ethylethanaminium (alk-rho):** In a previously flame-dried under an argon atmosphere round-bottom flask equipped with a magnetic stir bar, was dissolved 6-heptynoic acid (6 mL, 0.050 mmol) in dry DMF (0.5mL). 1-1'-Carbonyl diimidazole (8 mg, 0.050 mmol) was added in one portion, and the reaction mixture was stirred at room temperature for one hour. **Rhodamine B piperazine amide**[55] (24 mg, 0.044 mmol) was then added in one portion and the reaction mixture was stirred at room temperature overnight. The solvent was evaporated under reduced pressure and the crude mixture was purified by flash chromatography on silica gel (80% EtOAc / 13% MeOH / 7% H_2O) to afford 22 mg of **alk-rho** as a purple solid (76%). ^{1}H NMR (600 MHz, CD_3OD): δ 1.31 (t, 12H, *J* = 7.1), 1.46-1.57 (m, 2H), 1.61-1.71 (m, 2H), 2.15-2.25 (m, 3H), 2.38 (t, 2H, *J* = 7.3), 3.4 (br, 8H), 3.70 (quartet, 8H, *J* = 7.1), 6.98 (d, 2H, *J* = 2.4), 7.08 (dd, 2H, *J* = 2.4, 9.5), 7.29 (d, 2H, *J* = 9.5), 7.50-7.55 (m, 1H), 7.68-7.73 (m, 1H), 7.76-7.80 (m, 2H). ^{13}C NMR (100 MHz, CD_3OD): δ 12.8, 18.7, 25.3, 29.1, 33.4, 42.7, 46.0, 46.9, 69.9, 84.7, 97.4, 114.9, 115.4, 128.9, 131.2, 131.3, 131.8, 132.3, 133.2, 136.5, 157.0, 157.2, 159.3, 169.6, 174.0. LCMS: 619.55 $[M]^+$.

***N*-(9-(2-(4-(6-azidohexanoyl)piperazine-1-carbonyl)phenyl)-6-(diethylamino)-3*H*-xanthen-3-ylidene)-*N*-ethylethanaminium (az-rho):** In a previously flame-dried under an argon atmosphere round-bottom flask equipped with a magnetic stir bar, was dissolved 6-azidohexanoic acid (8 mg, 0.050 mmol) in dry DMF (0.5mL). 1-1'-Carbonyl diimidazole (8 mg, 0.050 mmol) was added in one portion, and the reaction mixture was stirred at room temperature for one hour. **Rhodamine B piperazine amide**[55] (25 mg,

0.046 mmol) was then added in one portion and the reaction mixture was stirred at room temperature overnight. The solvent was evaporated under reduced pressure and the crude mixture was purified by flash chromatography on silica gel (80% EtOAc / 13% MeOH / 7% H_2O) to afford 22 mg of **az-rho** as a purple solid (70%). ^{1}H NMR (600 MHz, CD_3OD): δ 1.31 (t, 12H, *J* = 7.1), 1.34-1.48 (m, 2H), 1.53-1.68 (m, 4H), 2.36 (t, 2H, *J* = 7.4), 3.3 (m, 2H), 3.40 (br, 8H), 3.69 (quartet, 8H, *J* = 7.1), 6.97 (d, 2H, *J* = 2.4), 7.08 (dd, 2H, *J* = 2.4, 9.5), 7.28 (d, 2H, *J* = 9.5), 7.50-7.54 (m, 1H), 7.68-7.72 (m, 1H), 7.75-7.80 (m, 2H). ^{13}C NMR (150 MHz, CD_3OD): δ 12.8, 25.8, 27.4, 29.7, 33.6, 42.7, 46.0, 46.9, 52.3, 97.4, 114.9, 115.4, 128.9, 131.2, 131.3, 131.8, 132.3, 133.2, 136.5, 157.0, 157.2, 159.3, 170.6, 174.0. LCMS: 650.57 $[M]^+$.

5.11.6 Azido-azo-biotin cleavable tag for proteomics synthesis

4-(2-azidoethyl)phenol (**11**). To an ice-cooled suspension of NaN_3 (546 mg, 8.40 mmol) in CH_3CN (10 mL) was slowly added Tf_2O (1.17 mL, 7.00 mmol). The mixture was stirred at 0 ºC for 2 h. A solution of tyramine (**10**) (800 mg, 5.83 mmol) and $ZnCl_2$ (79.3 mg, 0.58 mmol) in H_2O:CH_3CN (3:7) was added to the reaction mixture, followed by Et_3N (2.40 mL, 17.5 mmol) and freshly prepared N_3Tf. The reaction was kept stirring at rt for 8 h. The reaction mixture was then concentrated under vacuum, dissolved in EtOAc, and washed with H_2O twice. The organic layers were collected, dried over $MgSO_4$ and concentrated. The crude product was purified by flash column chromatography (25% EtOAc in hexane) to give colorless 4-(2-azidoethyl)phenol (**11**) (915 mg, 5.61 mmol, 96%). ^{1}H-NMR ($CDCl_3$, 400 MHz): δ 7.08 (d, 2H, J = 8.4 Hz), 6.78 (d, 2H, J = 8.4 Hz), 3.45 (t, 2H, J = 7.2 Hz), 2.82 (t, 2H, J = 7.2 Hz); ^{13}C-NMR (CDCl3,100 MHz): δ 154.3, 130.1, 129.9, 115.4, 52.6, 34.4.

(*E*)-4-((5-(2-azidoethyl)-2-hydroxyphenyl)diazenyl)benzoic acid (**12**). Solid $NaNO_2$ (3.30 g, 6.55 mmol) was added to an ice-cooled suspension of 4-aminobenzoic acid in 6M HCl (40 mL). The resulting mixture was stirred at 0 ºC and turned into a yellow-colored solution. In the meantime, dissolving 4-(2-azidoethyl)phenol (**11**) (1.19 g, 7.30 mmol) in cooled THF (15 mL) at 0 ºC, and subsequently added K_2CO_3 to this solution to adjust pH to 8. After 40 min, the diazonium salt solution was slowly added to compound 2 at 0 ºC, while the pH was kept around 8 by adding more K_2CO_3. Once the reaction was complete, removed all the solvents under vacuum. The concentrated residue was then re-dissolved in ethyl acetate, and washed with acidified H_2O (pH 2~3) for three times. The organic layers were collected, dried over $MgSO_4$ and concentrated. The crude product was purified by silica gel flash column chromatography (33% EtOAc in hexane and then 10% MeOH in CH_2Cl_2) to give yellow-colored compound **12** (1.27 g, 4.08 mmol, 56%). ^{1}H-NMR (CD_3OD, 600 MHz) δ: 8.24 (d, 2H, J = 8.5 Hz), 8.05 (d, 2H, J = 8.5 Hz), 7.89 (d, 1H, J = 1.9 Hz), 7.40 (dd, 1H, J = 8.3, 2.0 Hz), 7.04 (d, 1H, J = 8.4 Hz), 3.61 (t, 2H, J = 7.0 Hz), 2.97 (t, 2H, J = 7.0 Hz); ^{13}C-NMR (CD_3OD, 150 MHz) δ:176.6, 163.9, 163.8, 148.3, 144.9, 140.4, 139.6, 132.5, 131.3, 128.2, 61.4, 43.3. ESI-MS calcd. for $C_{15}H_{13}N_5O_3$ $[M-H]^-$: 310.0940, found 310.2.

(*E*)-2,5-dioxopyrrolidin-1-yl 4-((5-(2-azidoethyl)-2-hydroxyphenyl)diazenyl) benzoate (**13**): To compound **12** (164 mg, 0.53 mmol) dissolved in anhydrous THF (20 mL) was added DCC (119 mg, 0.58 mmol) and *N*-hydroxy-succinimide (66.7 mg, 0.58 mmol) under Ar. After the reaction was stirred at room temperature for 4 h and concentrated in vacuo. The crude solid residue was then dissolved in chilled ethyl acetate and the urea was filtered off. The filtrate was then concentrated and purified by silica gel

flash column chromatography (33% EtOAc in hexane) to give yellow-colored compound **13** (170 mg, 79%). ^{1}H-NMR ($CDCl_3$, 600 MHz): δ 8.31 (d, 2H, J = 8.3 Hz), 8.00 (d, 2H, J = 8.3 Hz), 7.87 (d, 1H, J = 1.9 Hz), 7.31 (dd, 1H, J = 8.5, 2.0 Hz), 7.05 (d, 1H, J = 8.5 Hz), 3.60 (t, 2H, J = 7.0 Hz), 2.95-2.98 (m, 6H); ^{13}C-NMR ($CDCl_3$,150 MHz): δ 169.1, 161.2, 154.3, 151.7, 137.4, 135.3, 133.6, 131.9, 130.0, 126.6, 122.4, 118.7, 52.4, 34.2, 25.7. ESI-MS calcd. for $C_{19}H_{16}N_6O_5$ $[M+H]^+$: 409.1260, found 409.3.

(*E*)-4-((5-(2-azidoethyl)-2-hydroxyphenyl)diazenyl)-*N*-(15-oxo-19-(2-oxohexahydro-1*H*-thieno[3,4-d]imidazol-4-yl)-4,7,10-trioxa-14-azanonadecyl)benzamide (**az-azo-biotin**): To compound **13** (13 mg, 0.03 mmol) dissolved in anhydrous DMF (3 mL) was added **biotin-PEG-amine**[54] (27.0 mg, 0.06 mmol). The reaction was complete after stirring at room temperature for 10 h and concentrated. The crude product was dissolved in CH_3CN:H_2O (1:1) and purified by reversed preparative HPLC column (CH_3CN: 5% to 40% in 10 min, then 40% to 100% in 40 min, **az-azo-biotin** was eluted at 33 min) to give yellow-colored product (18.0 mg, 80%). ^{1}H-NMR (CD_3OD, 400 MHz): δ 8.44 (brs, 1H), 8.00 (brs, 4H), 7.83 (d, 1H, J = 2.0 Hz), 7.33 (dd, 1H, J = 8.5, 2.0 Hz), 6.99 (d, 1H, J = 8.4 Hz), 4.46 (dd, 1H, J = 7.7, 5.0 Hz), 4.27 (dd, 1H, J = 7.8, 4.4 Hz), 3.66-3.47 (m, 18H), 3.23 (t, 2H, J = 6.7 Hz), 3.16 (td, 1H, J = 4.6, 9.2 Hz), 2.92 (t, 2H, J = 7.0 Hz), 2.68 (d, 1H, J = 12.7 Hz), 2.16 (t, 2H, J = 7.3 Hz), 1.93 (t, 1H, J = 6.3 Hz), 1.89 (t, 1H, J = 6.3 Hz), 1.76-1.52 (m, 6H), 1.42 (t, 1H, J = 7.6 Hz), 1.38 (t, 1H, J = 7.7 Hz), 1.28 (brs, 2H), 0.89 (m, 1H); ^{13}C-NMR (CD_3OD, 100 MHz): δ 175.9, 169.1, 166.1, 154.3, 153.3, 139.0, 137.8, 135.8, 131.8, 131.3, 129.6, 123.4, 119.3, 71.5, 71.3, 71.2, 70.3, 63.3, 61.6, 57.0, 53.5, 41.0, 38.9, 37.8, 36.8, 35.1,

30.7, 30.4, 29.8, 29.4, 26.8. MALDI-TOF calcd. for $C_{35}H_{49}N_9O_7S$ $[M+Na]^+$: 762.8744, found: 762.26.

5.12 ^{1}H and ^{13}C NMR spectra

SpinWorks 2.5: Standard One-dimensional 1H Experiment: alk-12

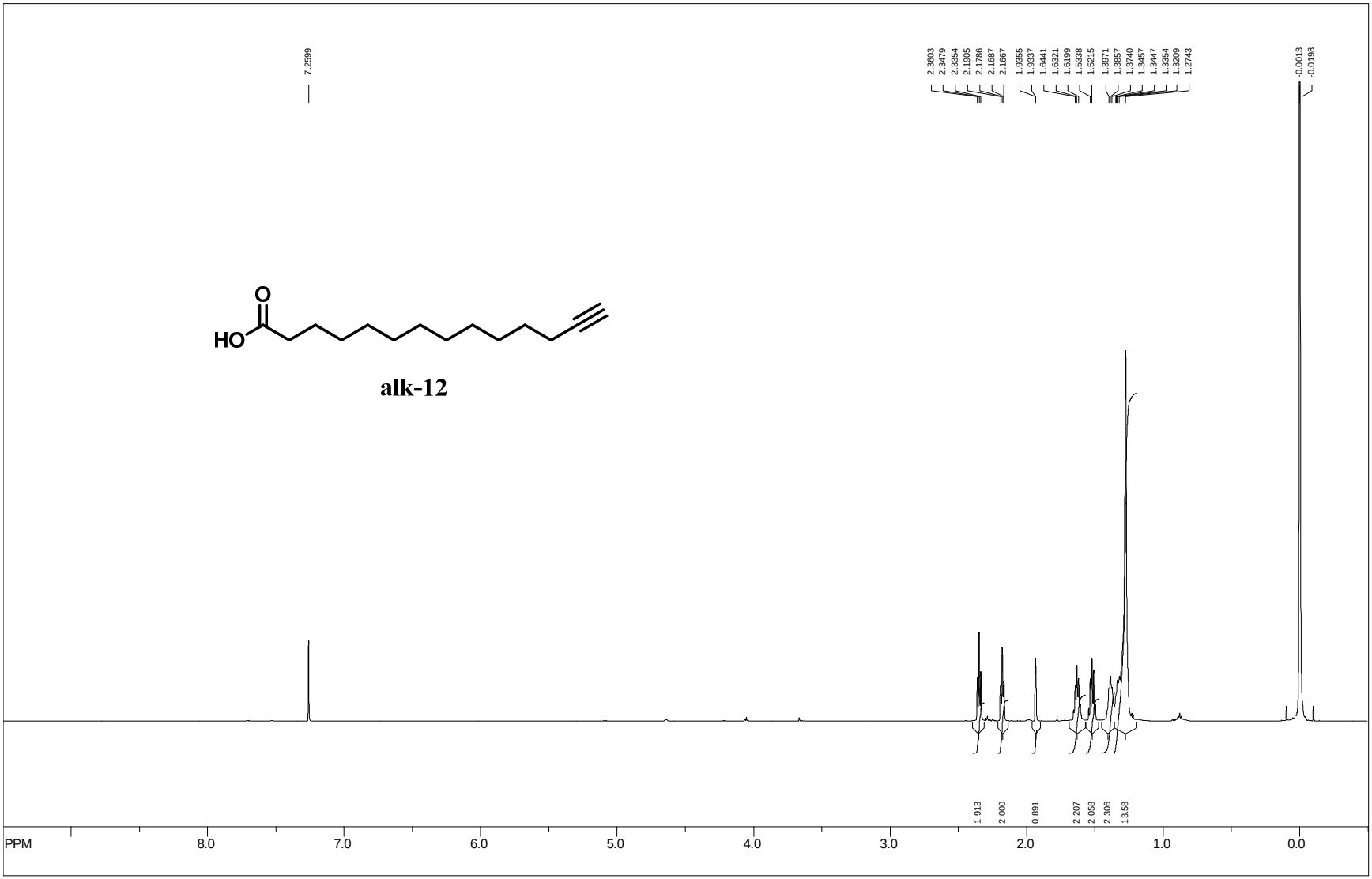

alk-12

file: C:\Users\guill_2\Documents\Backup\Chemistry\NMR\600\alk-12\1\fid expt: <zg30>
transmitter freq.: 600.112850 MHz
time domain size: 32768 points
width: 8389.26 Hz = 13.979474 ppm = 0.256020 Hz/pt
number of scans: 16

freq. of 0 ppm: 600.110018 MHz
processed size: 65536 complex points
LB: 0.000 GB: 0.0000

SpinWorks 2.5: 13C Direct Detection: alk-12

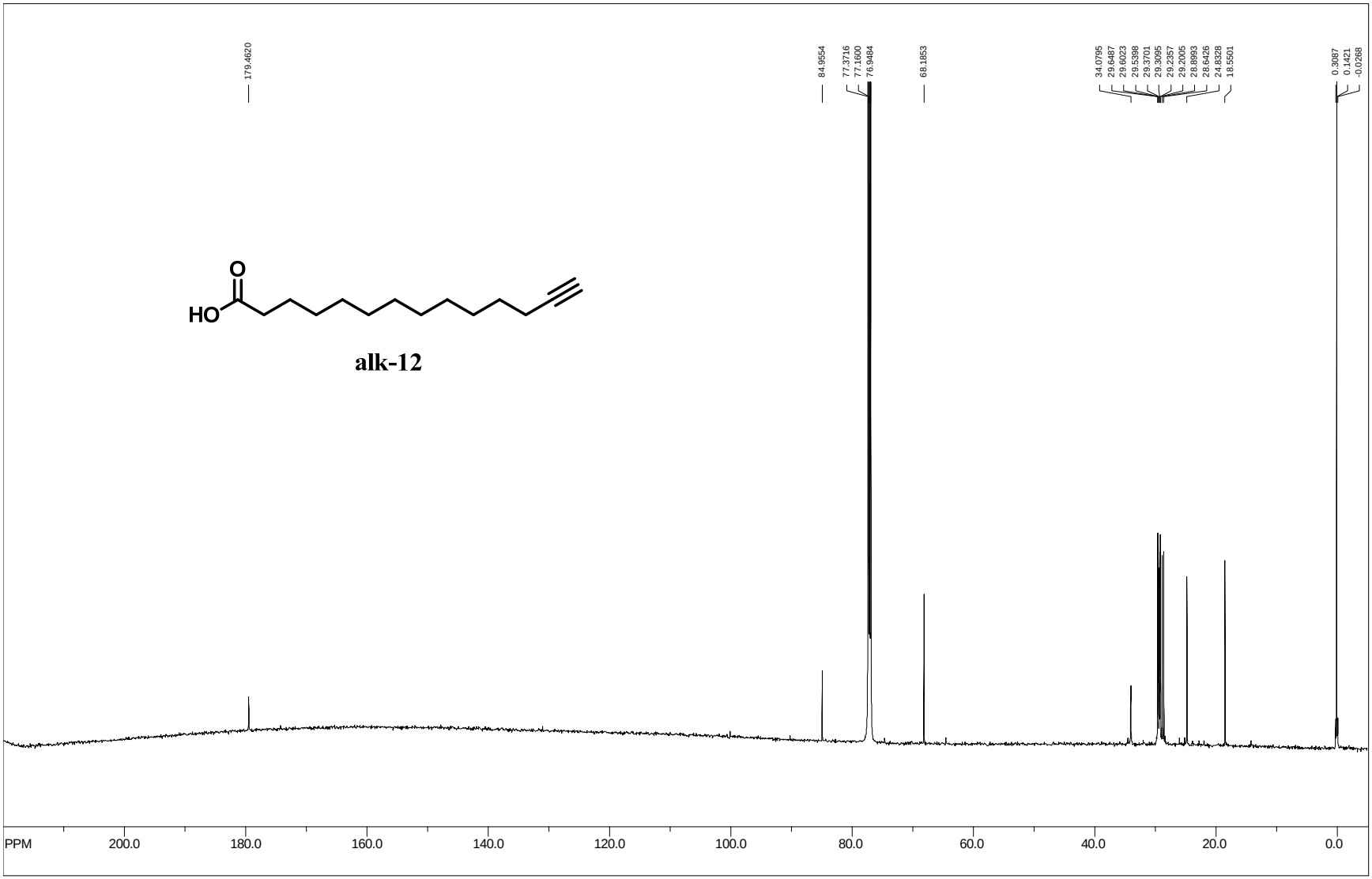

file: C:\Users\guill_2\Documents\Backup\Chemistry\NMR\600\alk-12\2\fid expt: <zgpg30>
transmitter freq.: 150.912869 MHz
time domain size: 65536 points
width: 36231.88 Hz = 240.084787 ppm = 0.552855 Hz/pt
number of scans: 794

freq. of 0 ppm: 150.897757 MHz
processed size: 32768 complex points
LB: 3.000 GB: 0.0000

SpinWorks 2.5: Standard One-dimensional 1H Experiment: alk-14

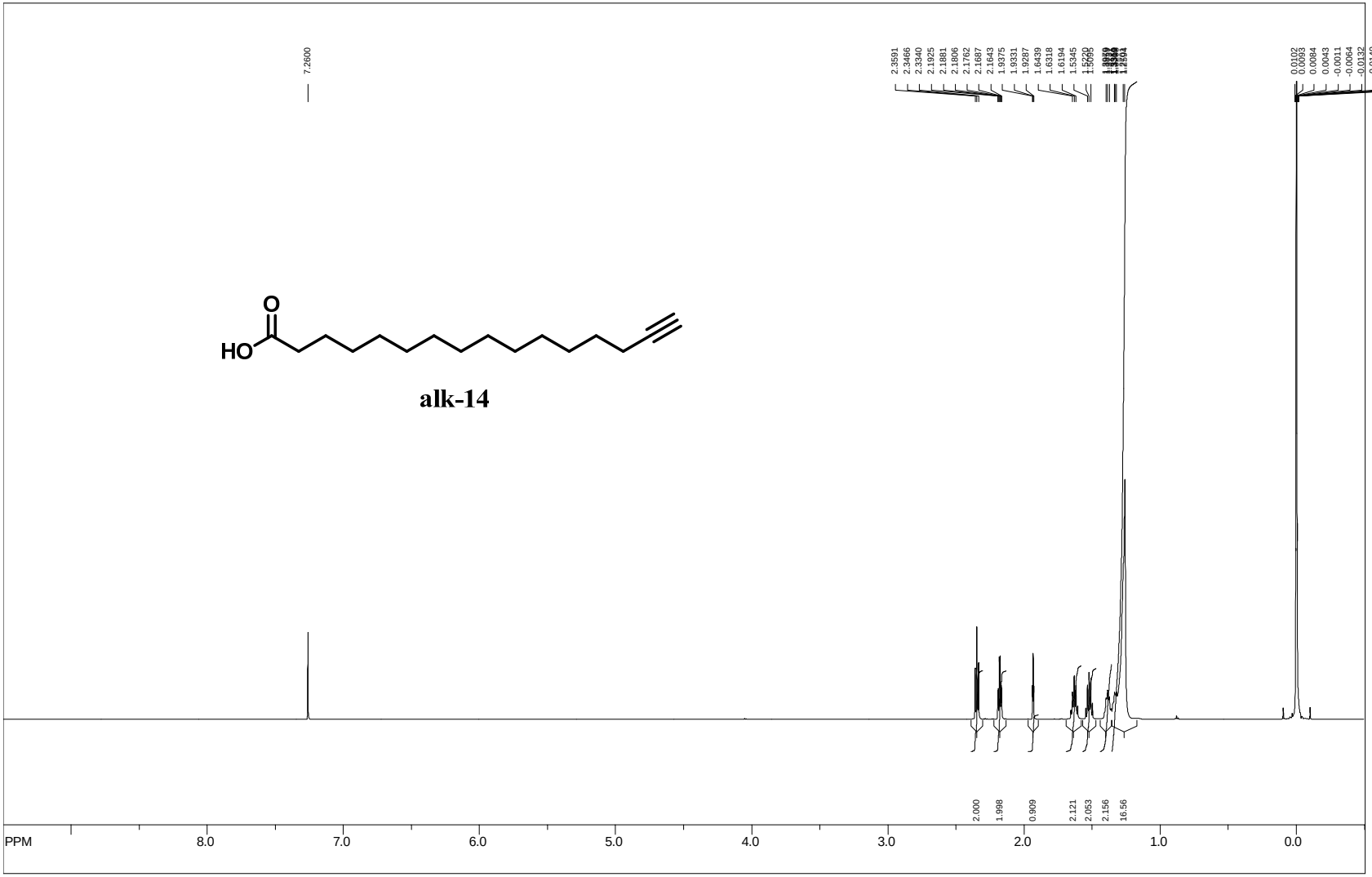

file: C:\Users\guill_2\Documents\Backup\Chemistry\NMR\600\alk-14\1\fid expt: <zg30>
transmitter freq.: 600.112850 MHz
time domain size: 32768 points
width: 8389.26 Hz = 13.979474 ppm = 0.256020 Hz/pt
number of scans: 15

freq. of 0 ppm: 600.110018 MHz
processed size: 65536 complex points
LB: 0.000 GB: 0.0000

SpinWorks 2.5: 13C Direct Detection: alk-14

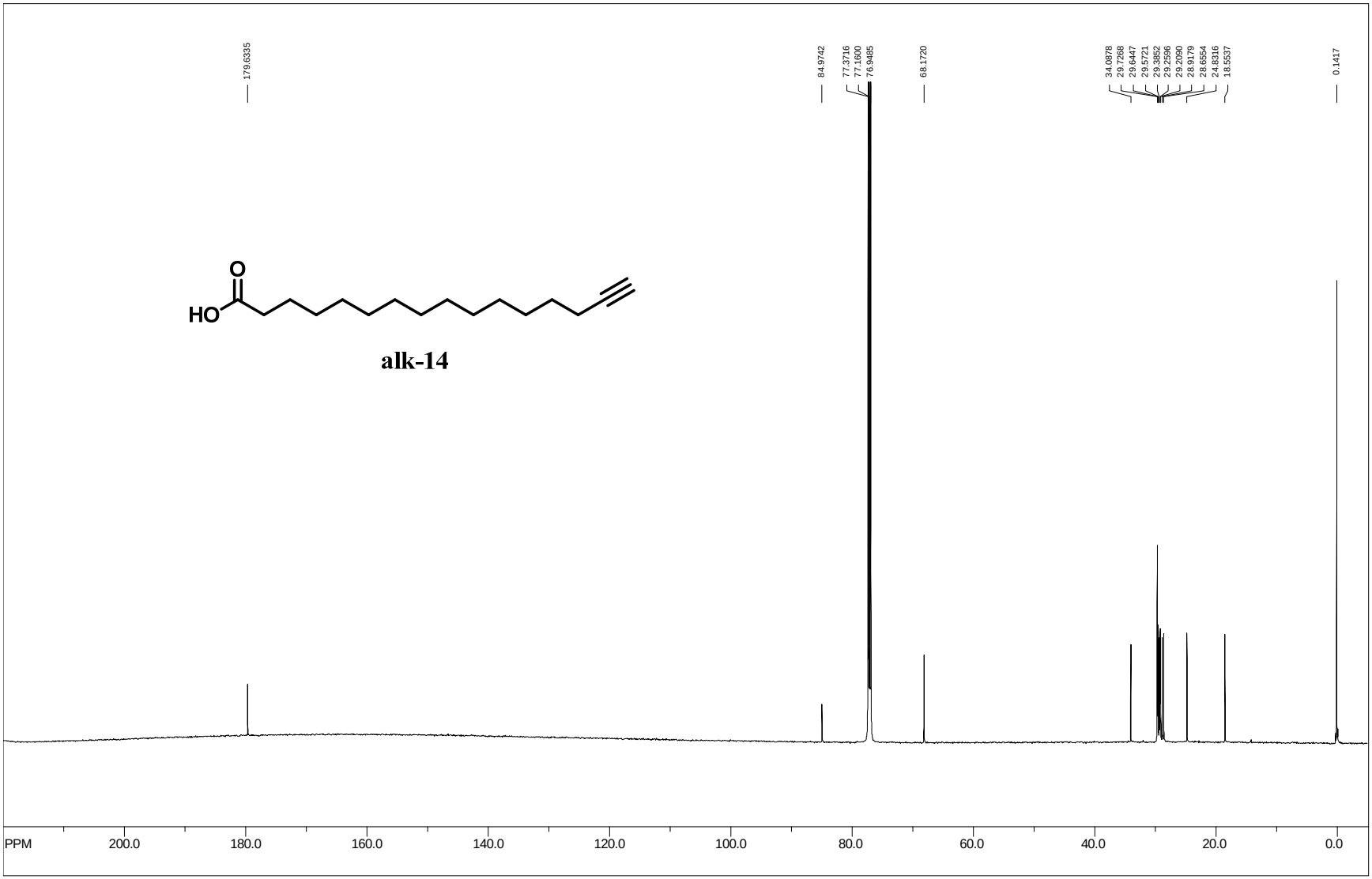

file: C:\Users\guill_2\Documents\Backup\Chemistry\NMR\600\alk-14\2\fid expt: <zgpg30>
transmitter freq.: 150.912869 MHz
time domain size: 65536 points
width: 36231.88 Hz = 240.084787 ppm = 0.552855 Hz/pt
number of scans: 828

freq. of 0 ppm: 150.897757 MHz
processed size: 32768 complex points
LB: 3.000 GB: 0.0000

SpinWorks 2.5: Standard One-dimensional 1H Experiment: alk-16

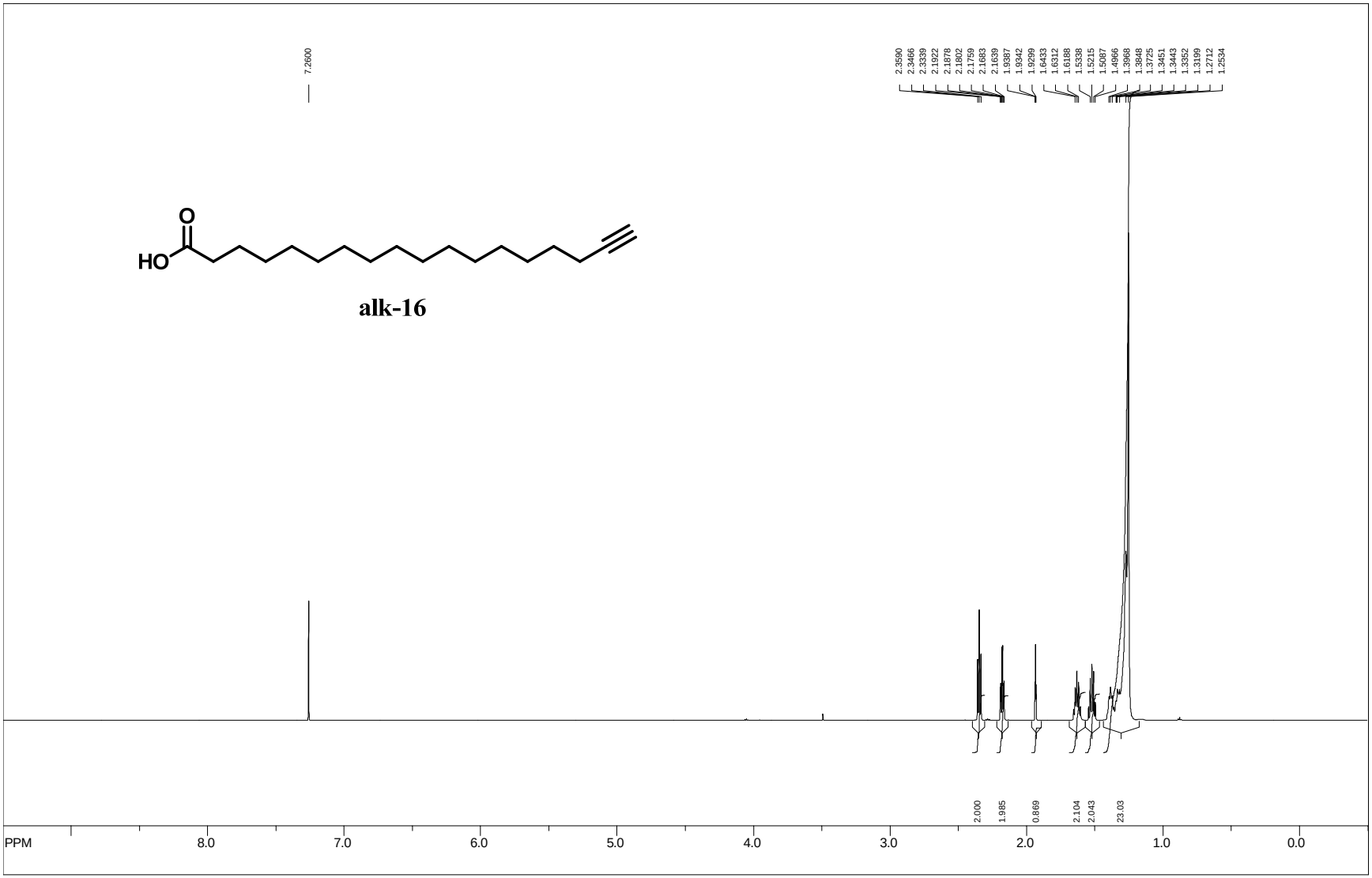

alk-16

file: C:\Users\guill_2\Documents\Backup\Chemistry\NMR\600\GCII-39\1\fid expt: <zg30>
transmitter freq.: 600.127850 MHz
time domain size: 32768 points
width: 8389.26 Hz = 13.979124 ppm = 0.256020 Hz/pt
number of scans: 32

freq. of 0 ppm: 600.125014 MHz
processed size: 65536 complex points
LB: 0.000 GB: 0.0000

SpinWorks 2.5: 13C Direct Detection: alk-16

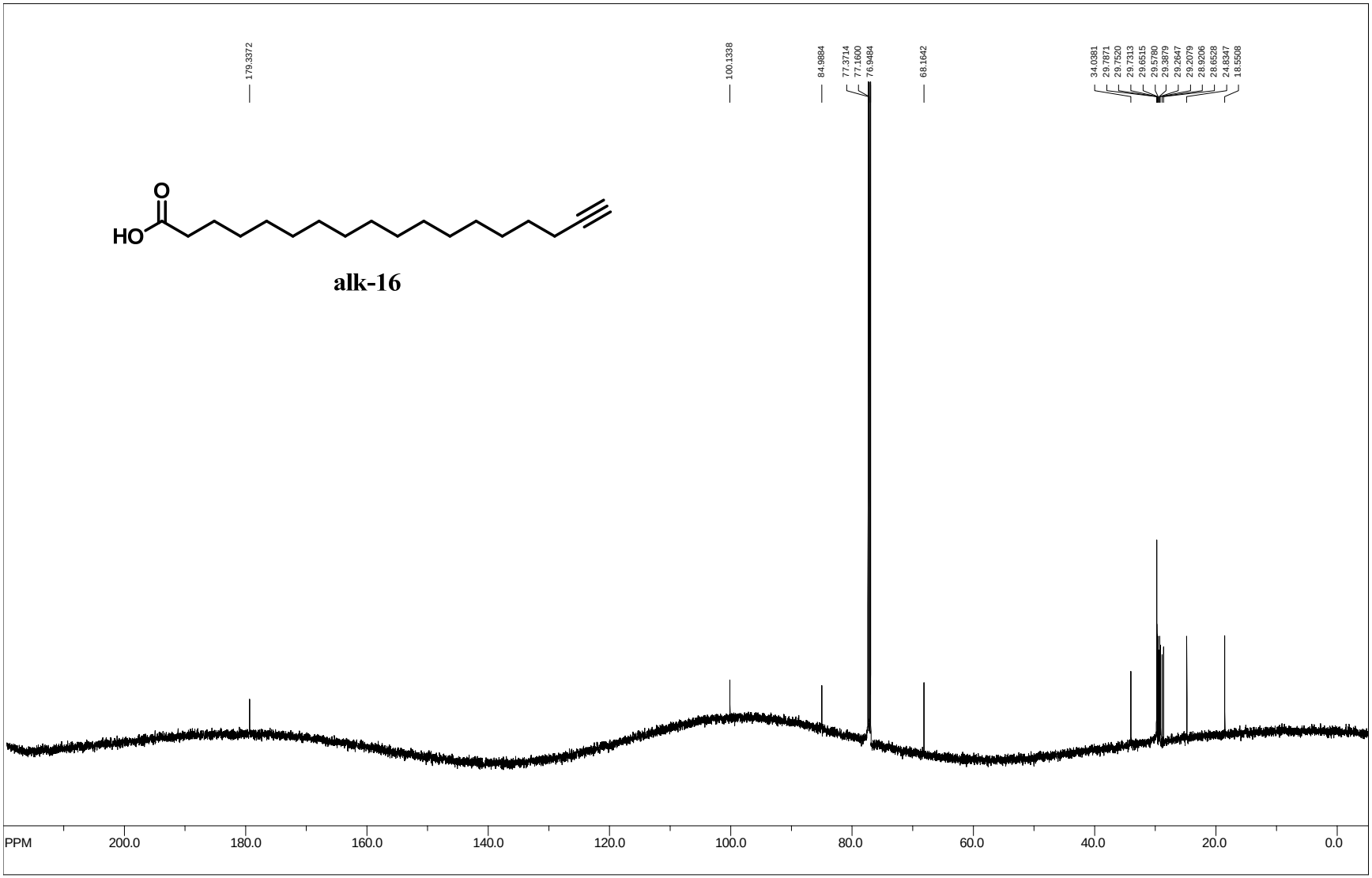

file: C:\Users\guill_2\Documents\Backup\Chemistry\NMR\600\GCII-39\2\fid expt: <zgpg30>
transmitter freq.: 150.916641 MHz
time domain size: 65536 points
width: 35971.22 Hz = 238.351601 ppm = 0.548877 Hz/pt
number of scans: 459

freq. of 0 ppm: 150.901529 MHz
processed size: 32768 complex points
LB: 0.000 GB: 0.0000

SpinWorks 2.5: Standard One-dimensional 1H Experiment: 4

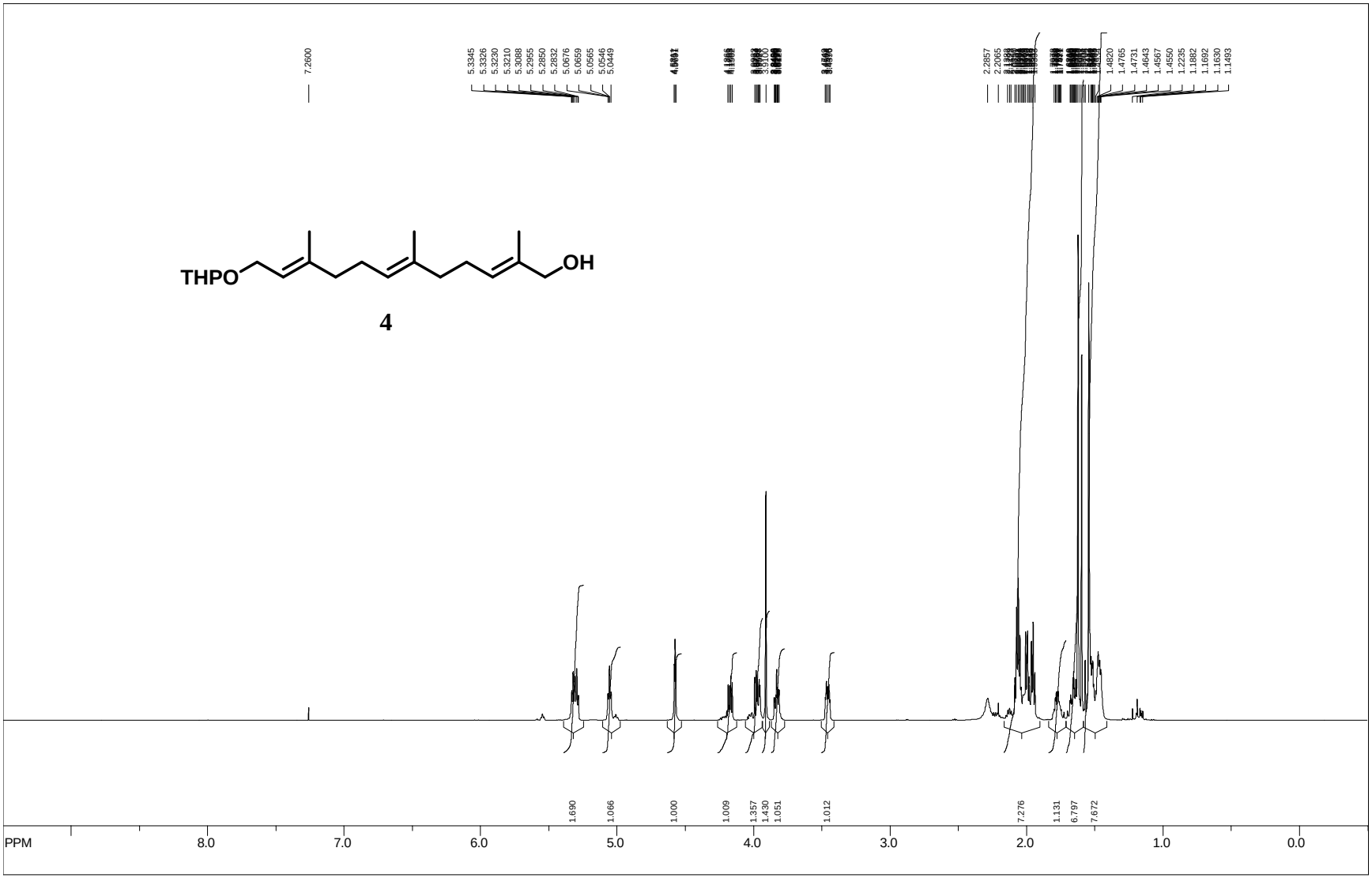

file: C:\Users\guill_2\Documents\Backup\Chemistry\NMR\600\GCIII-19\1\fid expt: <zg30>
transmitter freq.: 600.127850 MHz
time domain size: 32768 points
width: 8389.26 Hz = 13.979124 ppm = 0.256020 Hz/pt
number of scans: 15

freq. of 0 ppm: 600.125013 MHz
processed size: 65536 complex points
LB: 0.000 GB: 0.0000

SpinWorks 2.5: 13C Direct Detection: 4

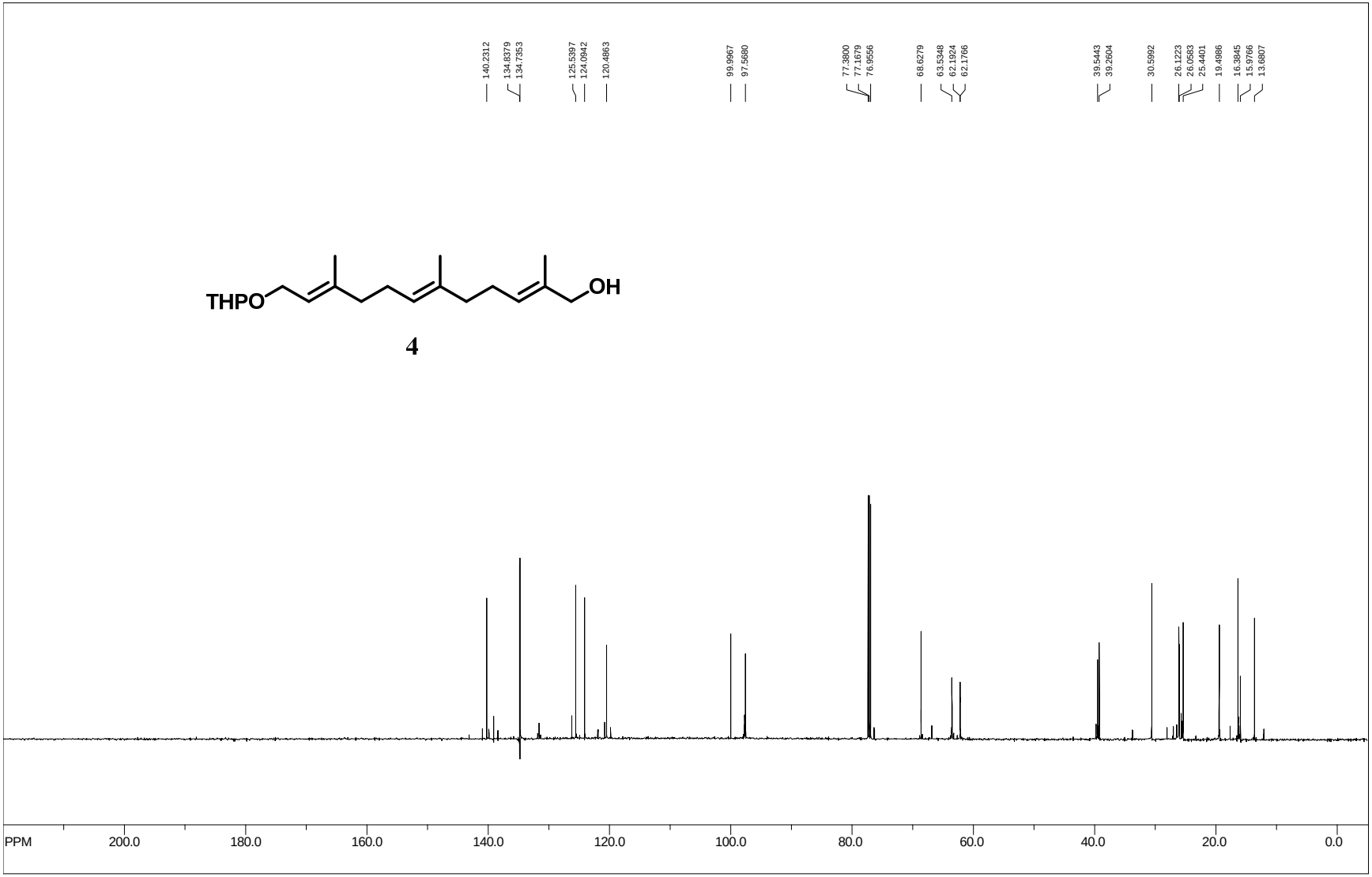

file: C:\Users\guill_2\Documents\Backup\Chemistry\NMR\600\GCIII-19\2\fid expt: <zgpg30>
transmitter freq.: 150.916642 MHz
time domain size: 65536 points
width: 36231.88 Hz = 240.078785 ppm = 0.552855 Hz/pt
number of scans: 27

freq. of 0 ppm: 150.901552 MHz
processed size: 32768 complex points
LB: 0.000 GB: 0.0000

SpinWorks 2.5: Standard One-dimensional 1H Experiment: 5

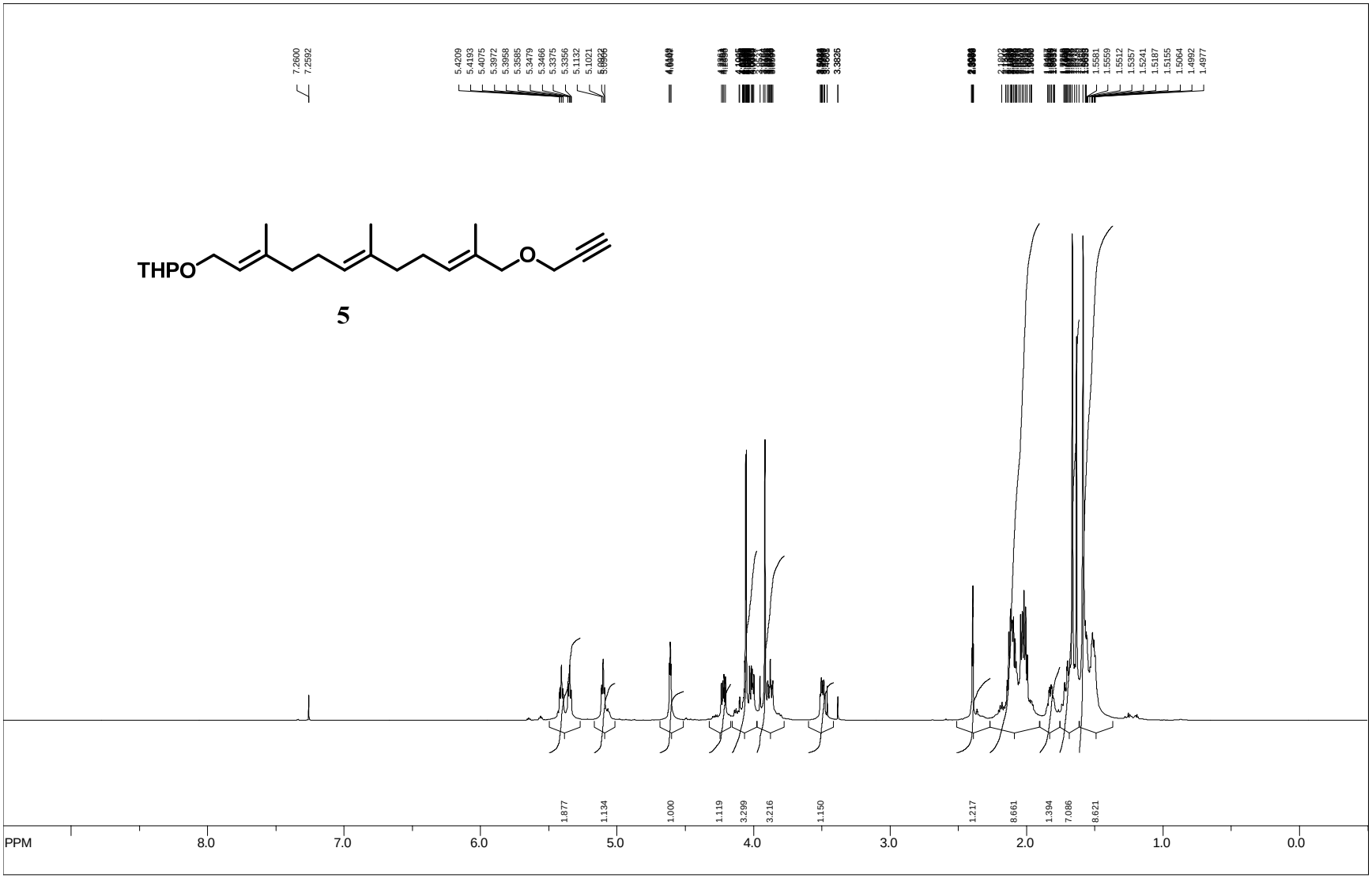

5

file: C:\Users\guill_2\Documents\Backup\Chemistry\NMR\600\GCII-63\1\fid expt: <zg30>
transmitter freq.: 600.112850 MHz
time domain size: 32768 points
width: 8389.26 Hz = 13.979474 ppm = 0.256020 Hz/pt
number of scans: 14

freq. of 0 ppm: 600.110017 MHz
processed size: 65536 complex points
LB: 0.000 GB: 0.0000

SpinWorks 2.5: 13C Direct Detection: 5

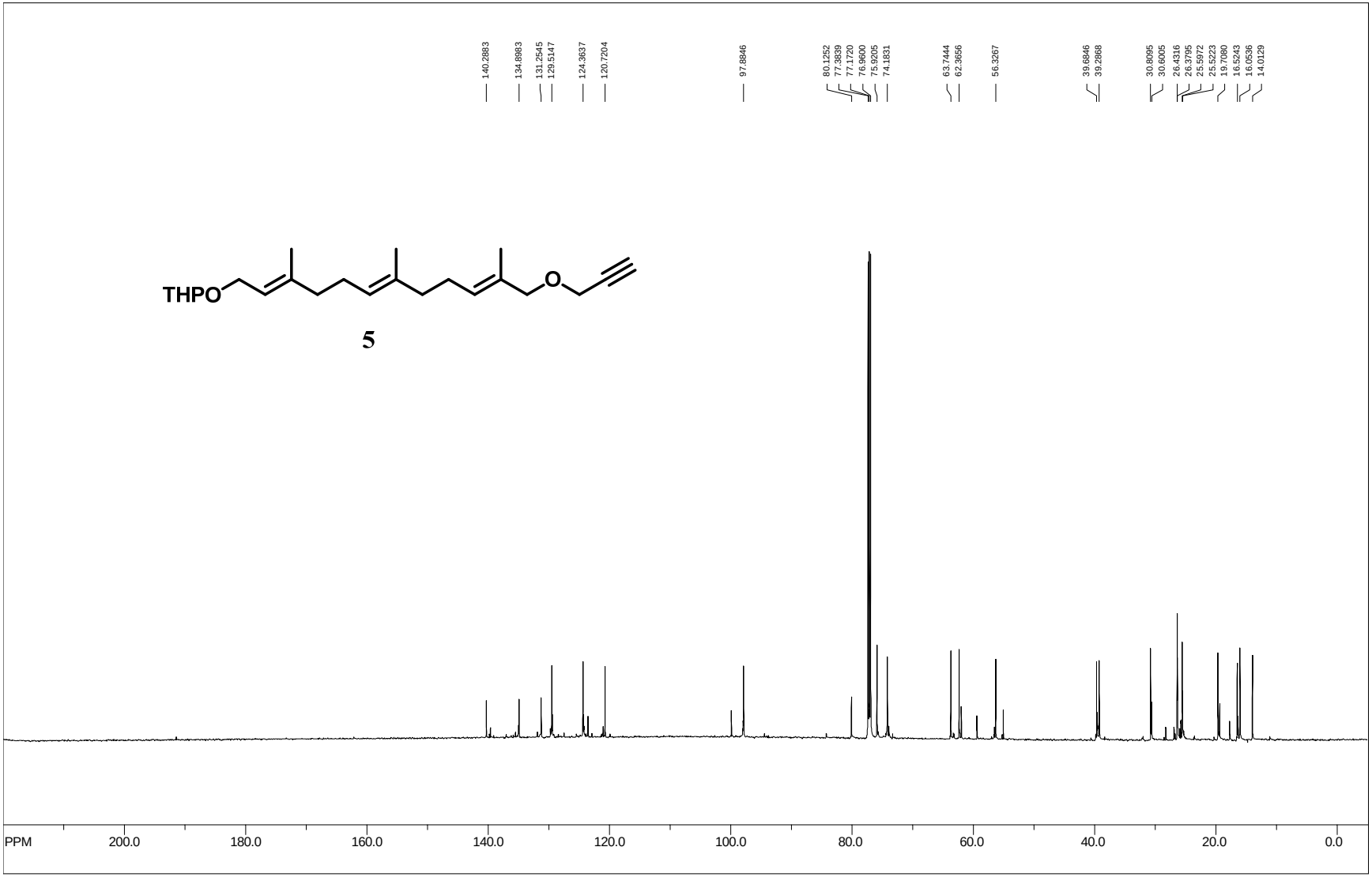

file: C:\Users\guill_2\Documents\Backup\Chemistry\NMR\600\GCII-63\3\fid expt: <zgpg30>
transmitter freq.: 150.912869 MHz
time domain size: 65536 points
width: 36231.88 Hz = 240.084787 ppm = 0.552855 Hz/pt
number of scans: 136

freq. of 0 ppm: 150.897764 MHz
processed size: 32768 complex points
LB: 0.000 GB: 0.0000

SpinWorks 2.5: Standard One-dimensional 1H Experiment: alk-FOH

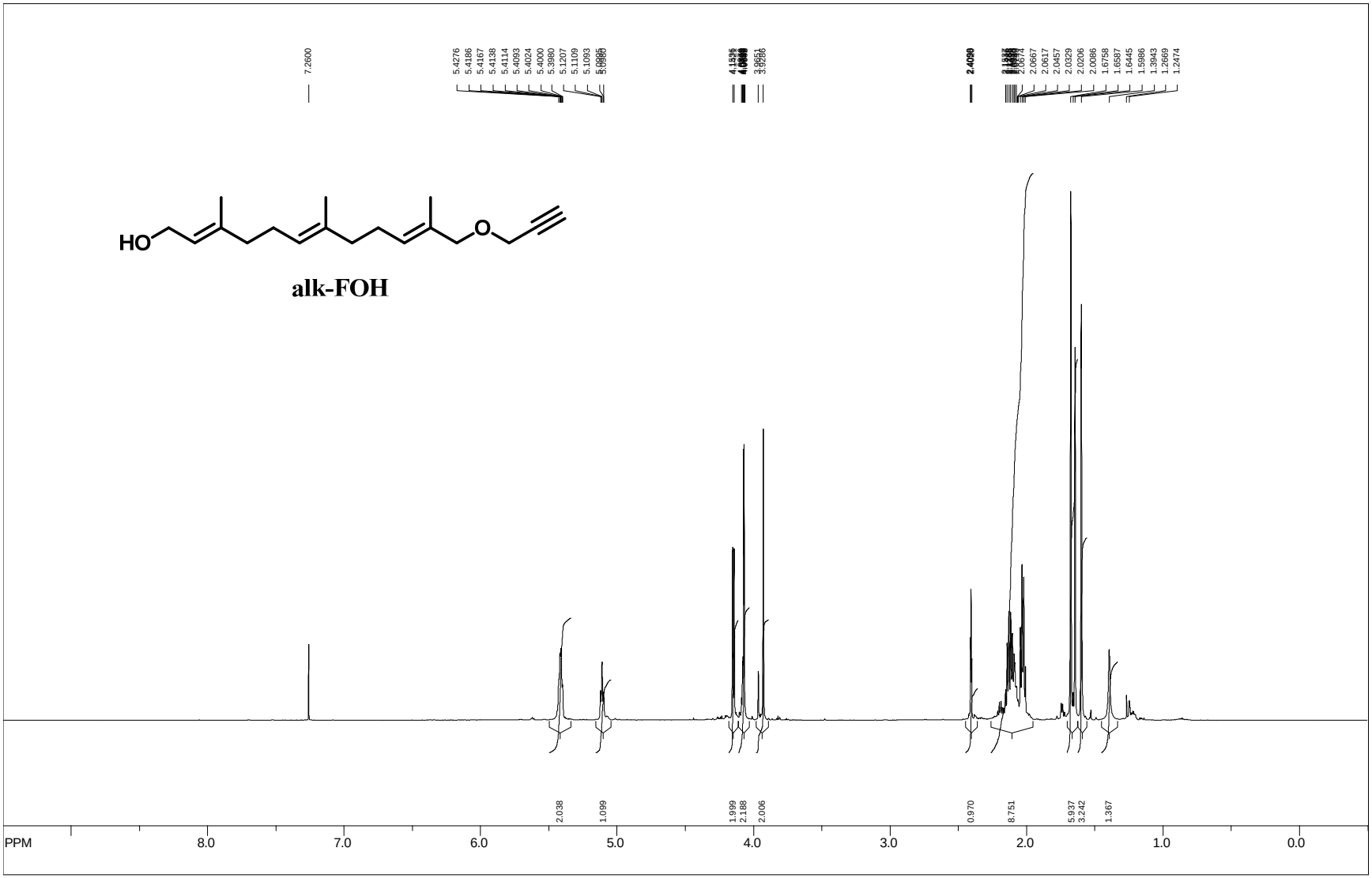

file: C:\Users\guill_2\Documents\Backup\Chemistry\NMR\600\WMI-18\1\fid expt: <zg30>
transmitter freq.: 600.127850 MHz
time domain size: 32768 points
width: 8389.26 Hz = 13.979124 ppm = 0.256020 Hz/pt
number of scans: 32

freq. of 0 ppm: 600.125013 MHz
processed size: 65536 complex points
LB: 0.000 GB: 0.0000

SpinWorks 2.5: 13C Direct Detection: alk-FOH

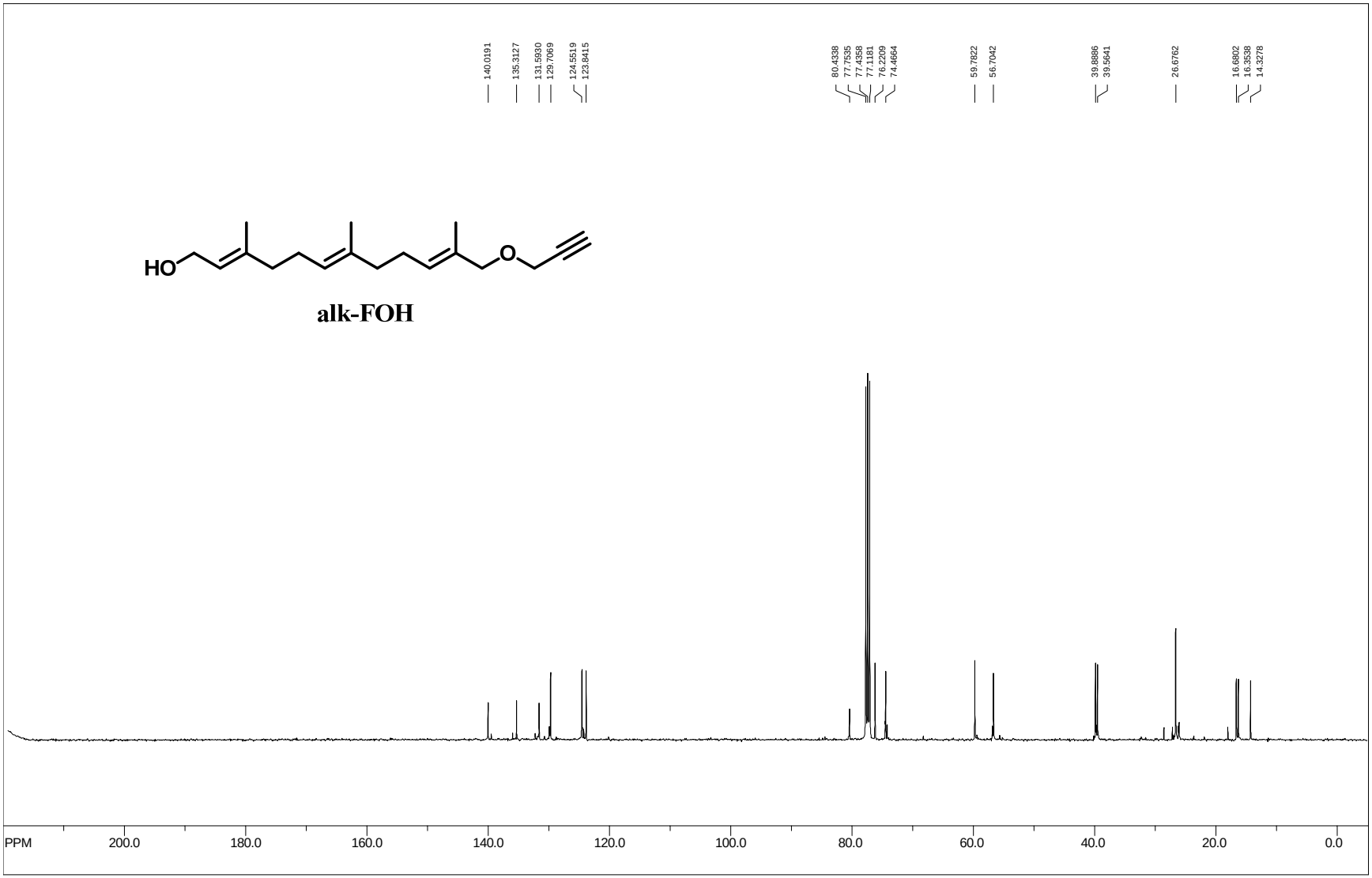

file: C:\Users\guill_2\Documents\Backup\Chemistry\NMR\400\WMI-18\2\fid expt: <zgpg30>
transmitter freq.: 100.622790 MHz
time domain size: 65536 points
width: 23980.82 Hz = 238.323897 ppm = 0.365918 Hz/pt
number of scans: 6103

freq. of 0 ppm: 100.612729 MHz
processed size: 32768 complex points
LB: 3.000 GB: 0.0000

SpinWorks 2.5: Standard One-dimensional 1H Experiment: 6

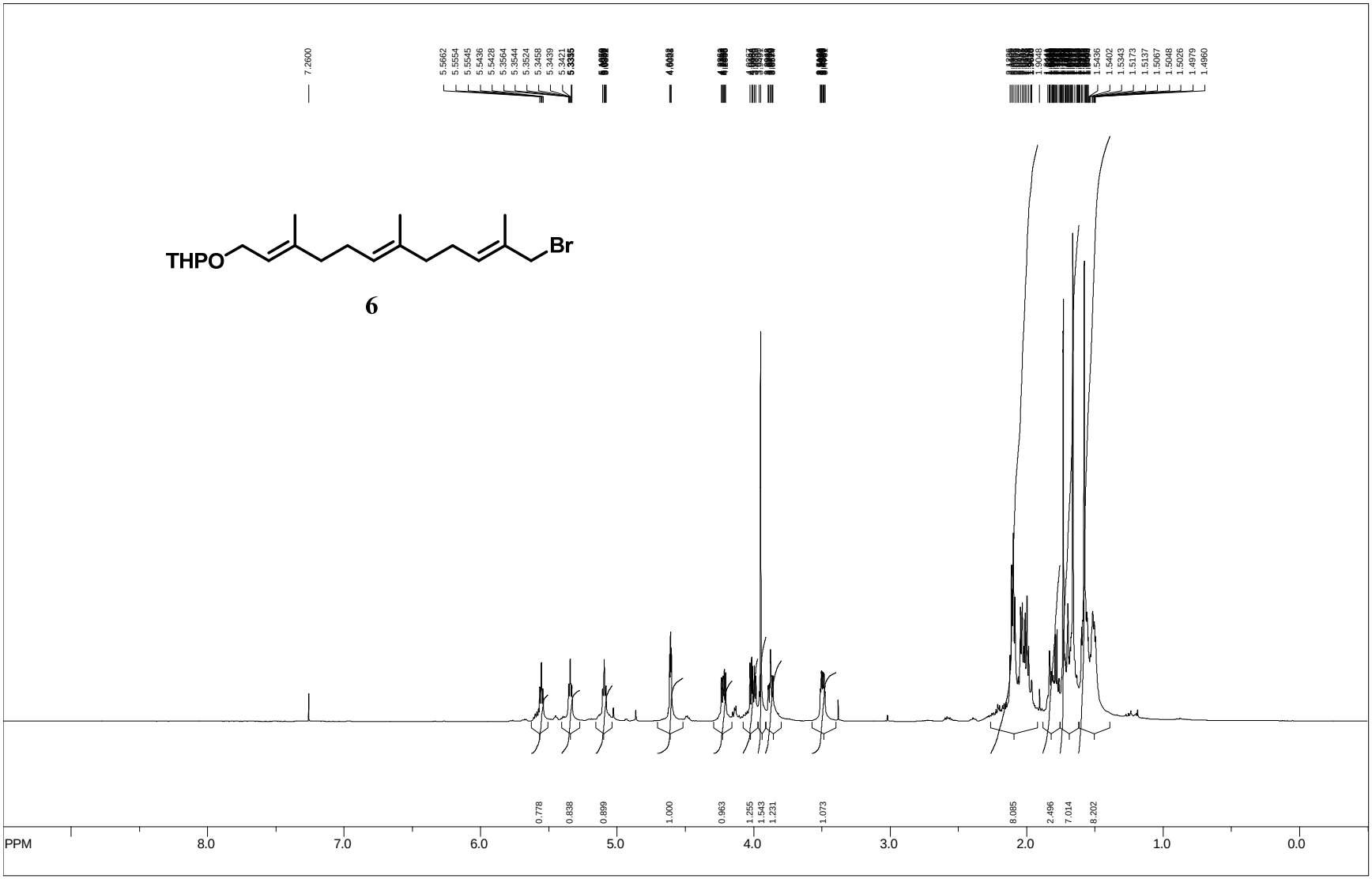

file: C:\Users\guill_2\Documents\Backup\Chemistry\NMR\600\GCIII-65\1\fid expt: <zg30>
transmitter freq.: 600.112850 MHz
time domain size: 32768 points
width: 8389.26 Hz = 13.979474 ppm = 0.256020 Hz/pt
number of scans: 12

freq. of 0 ppm: 600.110017 MHz
processed size: 65536 complex points
LB: 0.500 GB: 0.0000

SpinWorks 2.5: 13C Direct Detection: 6

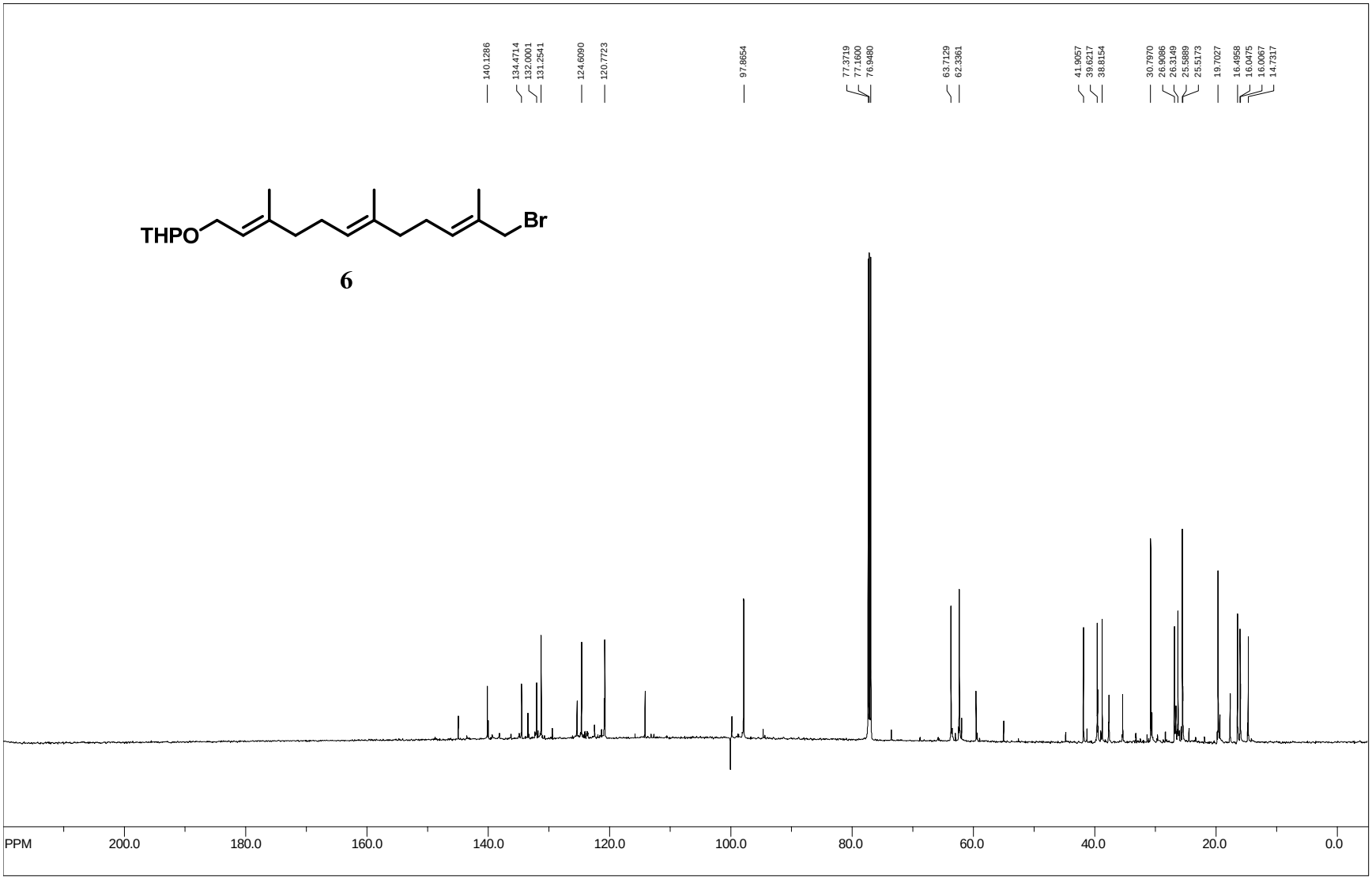

file: C:\Users\guill_2\Documents\Backup\Chemistry\NMR\600\GCIII-65\3\fid expt: <zgpg30>
transmitter freq.: 150.912869 MHz
time domain size: 65536 points
width: 36231.88 Hz = 240.084787 ppm = 0.552855 Hz/pt
number of scans: 89

freq. of 0 ppm: 150.897767 MHz
processed size: 32768 complex points
LB: 0.500 GB: 0.0000

SpinWorks 2.5: Standard One-dimensional 1H Experiment: 7

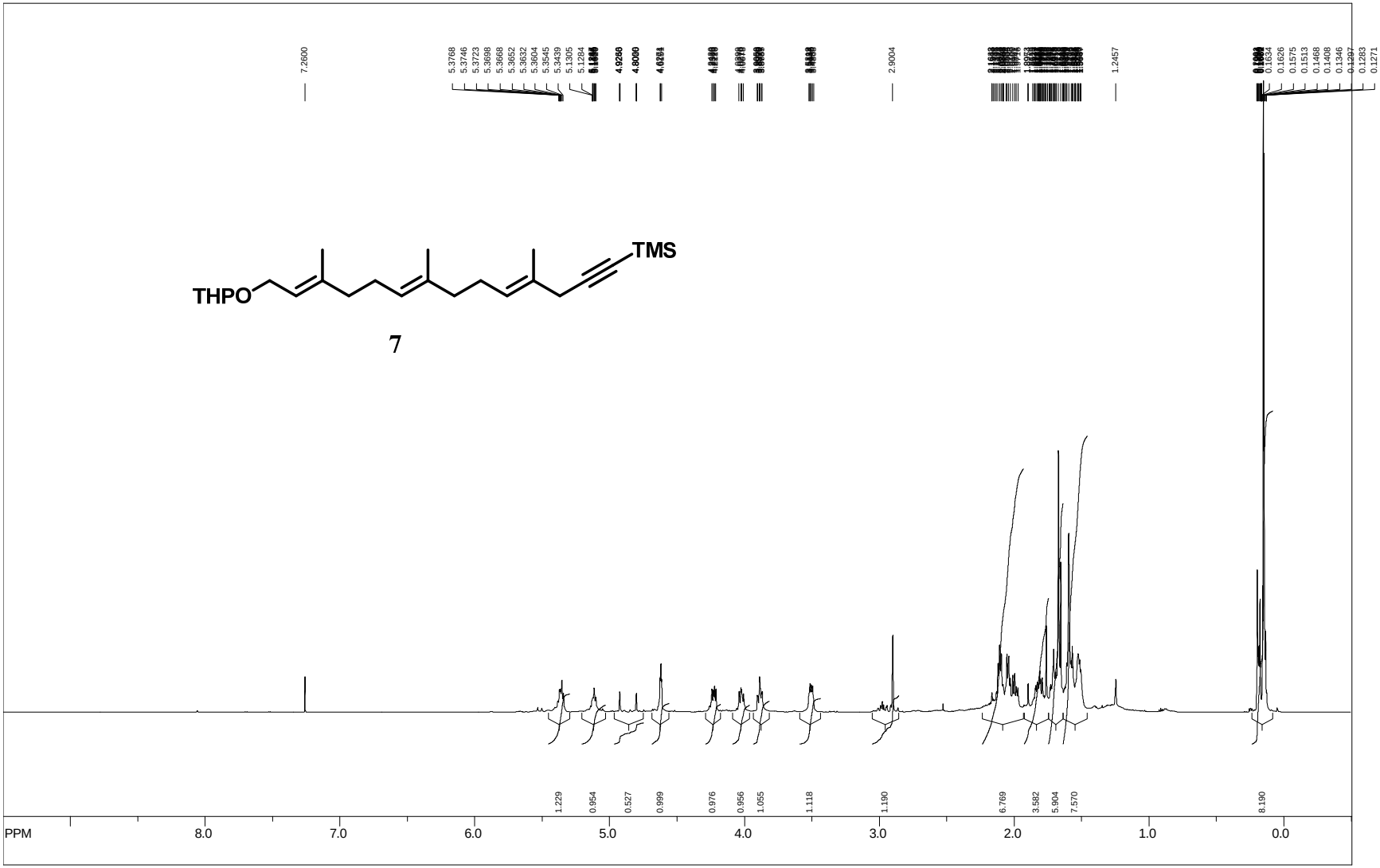

file: C:\Users\guill_2\Documents\Backup\Chemistry\NMR\600\GCIII-81\1\fid expt: <zg30>
transmitter freq.: 600.112850 MHz
time domain size: 32768 points
width: 8389.26 Hz = 13.979474 ppm = 0.256020 Hz/pt
number of scans: 15

freq. of 0 ppm: 600.110017 MHz
processed size: 65536 complex points
LB: 0.500 GB: 0.0000

SpinWorks 2.5: 13C Direct Detection: 7

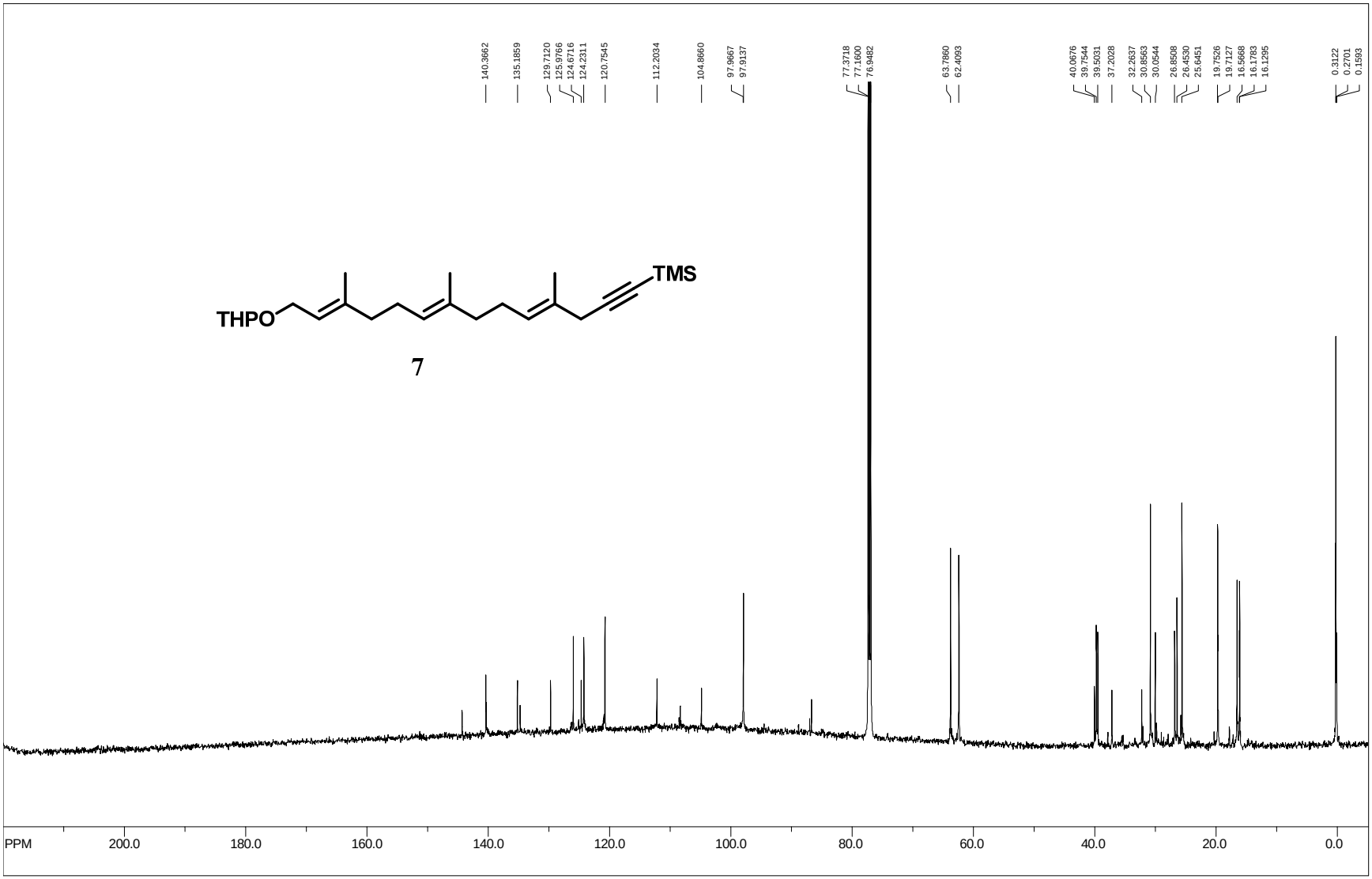

file: C:\Users\guill_2\Documents\Backup\Chemistry\NMR\600\GCIII-81\2\fid expt: <zgpg30>
transmitter freq.: 150.912869 MHz
time domain size: 65536 points
width: 36231.88 Hz = 240.084787 ppm = 0.552855 Hz/pt
number of scans: 242

freq. of 0 ppm: 150.897758 MHz
processed size: 32768 complex points
LB: 0.500 GB: 0.0000

SpinWorks 2.5: Standard one-dimentional 1H: alk-FOH-2

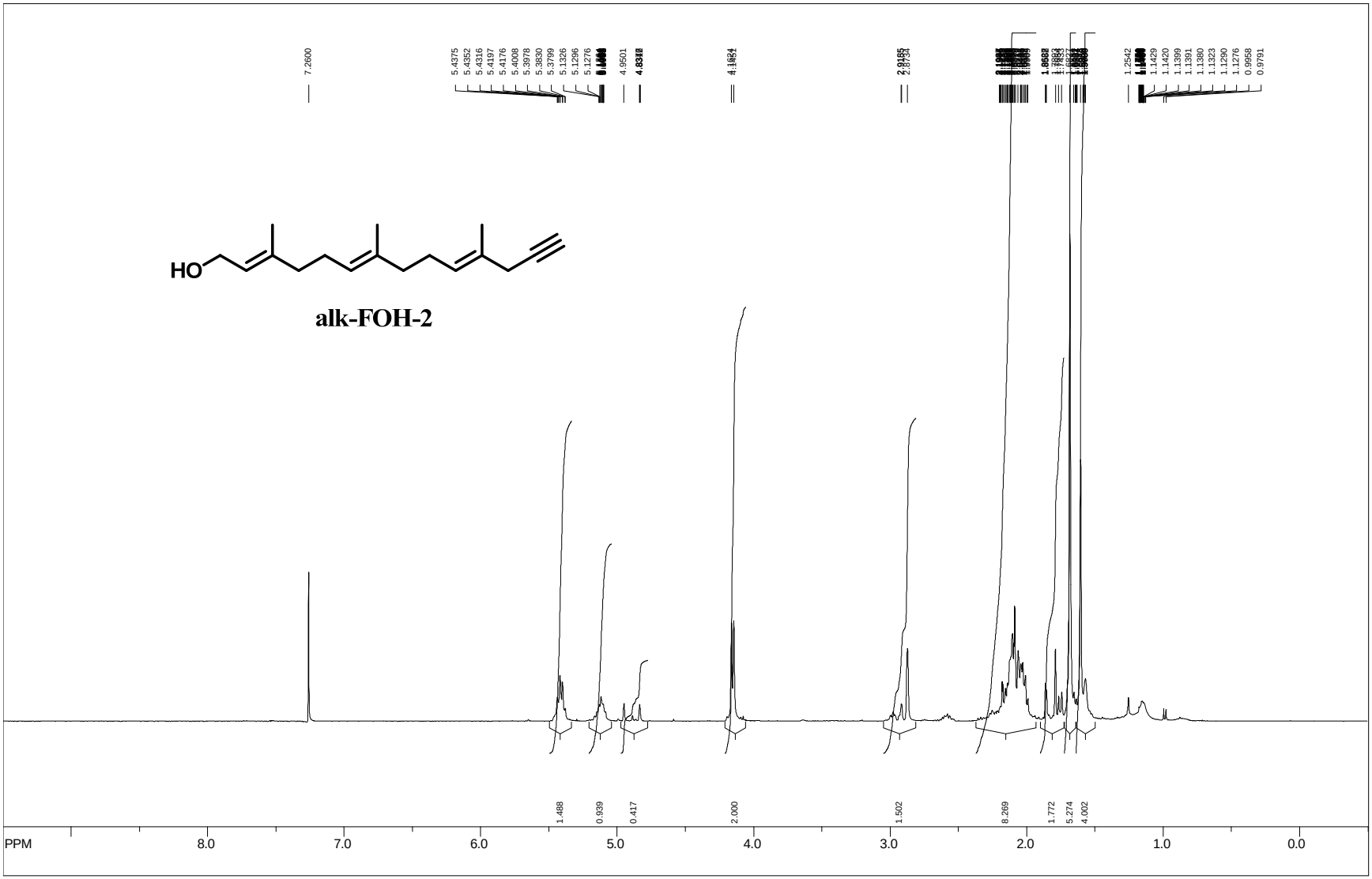

file: C:\Users\guill_2\Documents\Backup\Chemistry\NMR\400\WFM01-27Proton1\1\fid expt: <zg30>
transmitter freq.: 400.131881 MHz
time domain size: 32768 points
width: 5995.20 Hz = 14.983070 ppm = 0.182959 Hz/pt
number of scans: 64

freq. of 0 ppm: 400.130009 MHz
processed size: 32768 complex points
LB: 0.500 GB: 0.0000

SpinWorks 2.5: 13C Direct Detection: alk-FOH-2

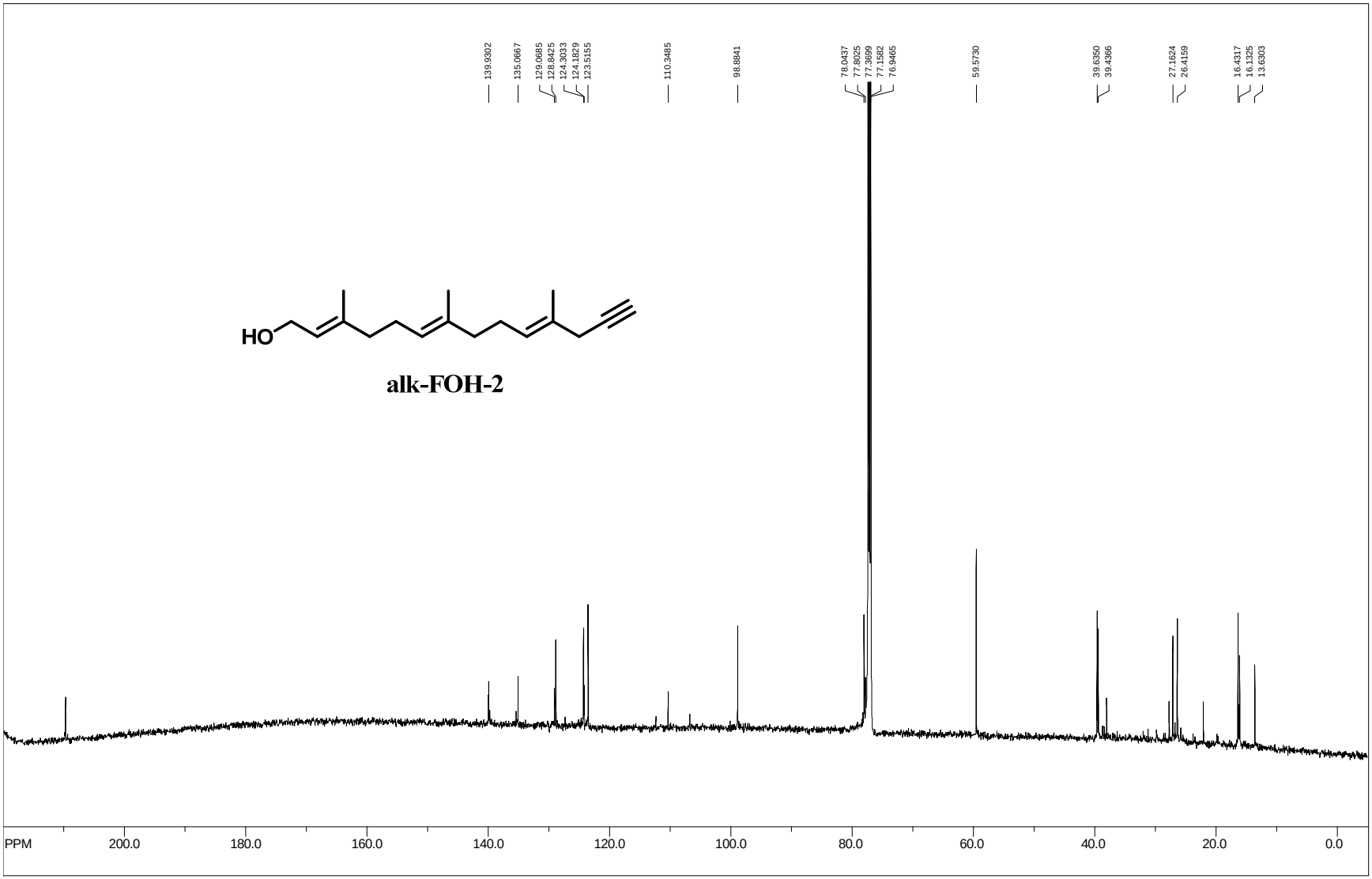

file: C:\Users\guill_2\Documents\Backup\Chemistry\NMR\600\GCIII-87\2\fid expt: <zgpg30>
transmitter freq.: 150.912869 MHz
time domain size: 65536 points
width: 36231.88 Hz = 240.084787 ppm = 0.552855 Hz/pt
number of scans: 910

freq. of 0 ppm: 150.897758 MHz
processed size: 32768 complex points
LB: 0.500 GB: 0.0000

SpinWorks 2.5: Standard One-dimensional 1H Experiment: 8

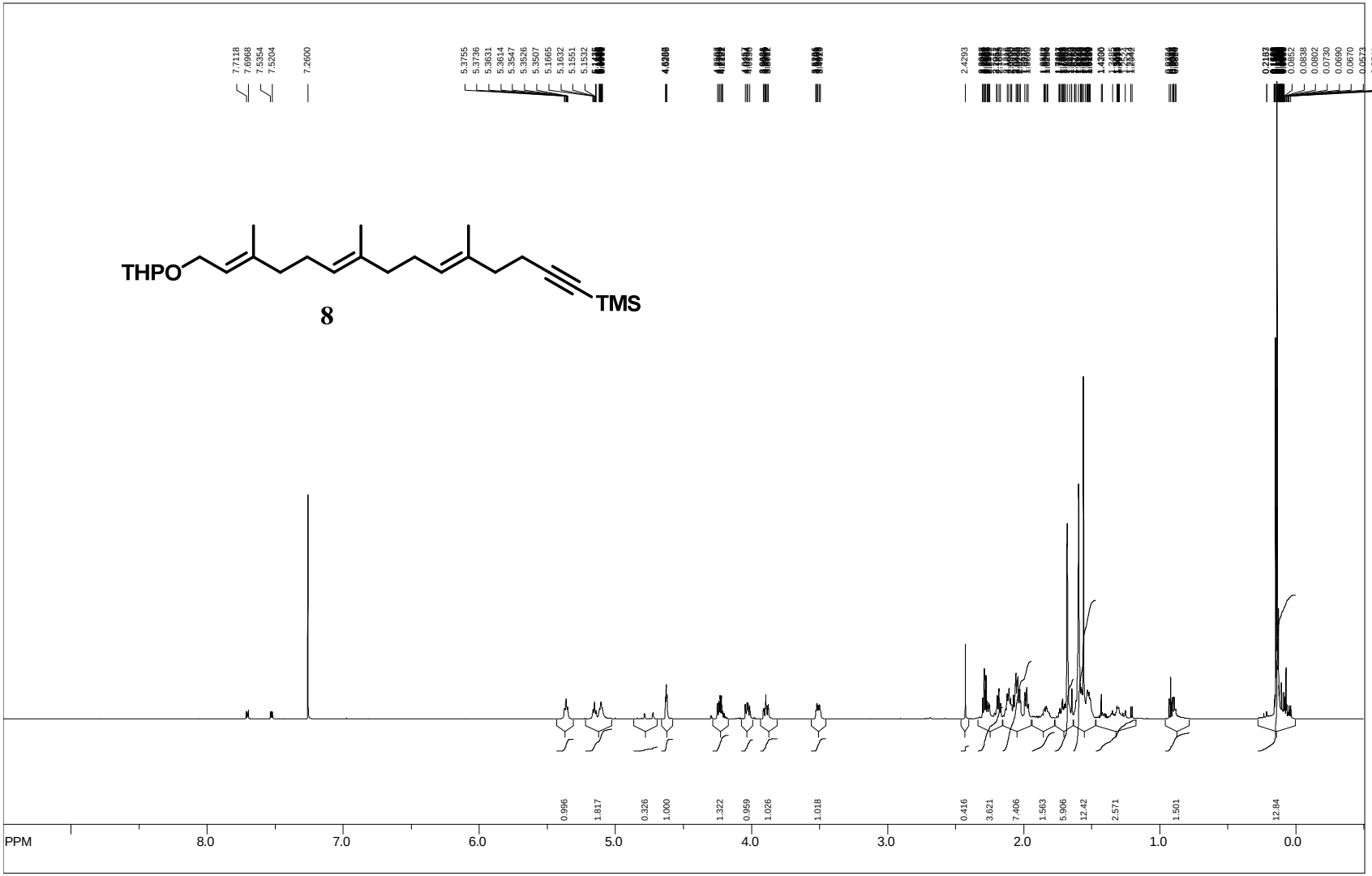

file: C:\Users\guill_2\Documents\Backup\Chemistry\NMR\600\WMI-26\1\fid expt: <zg30>
transmitter freq.: 600.112850 MHz
time domain size: 32768 points
width: 8389.26 Hz = 13.979474 ppm = 0.256020 Hz/pt
number of scans: 17

freq. of 0 ppm: 600.110017 MHz
processed size: 65536 complex points
LB: 0.500 GB: 0.0000

SpinWorks 2.5: 13C Direct Detection: 8

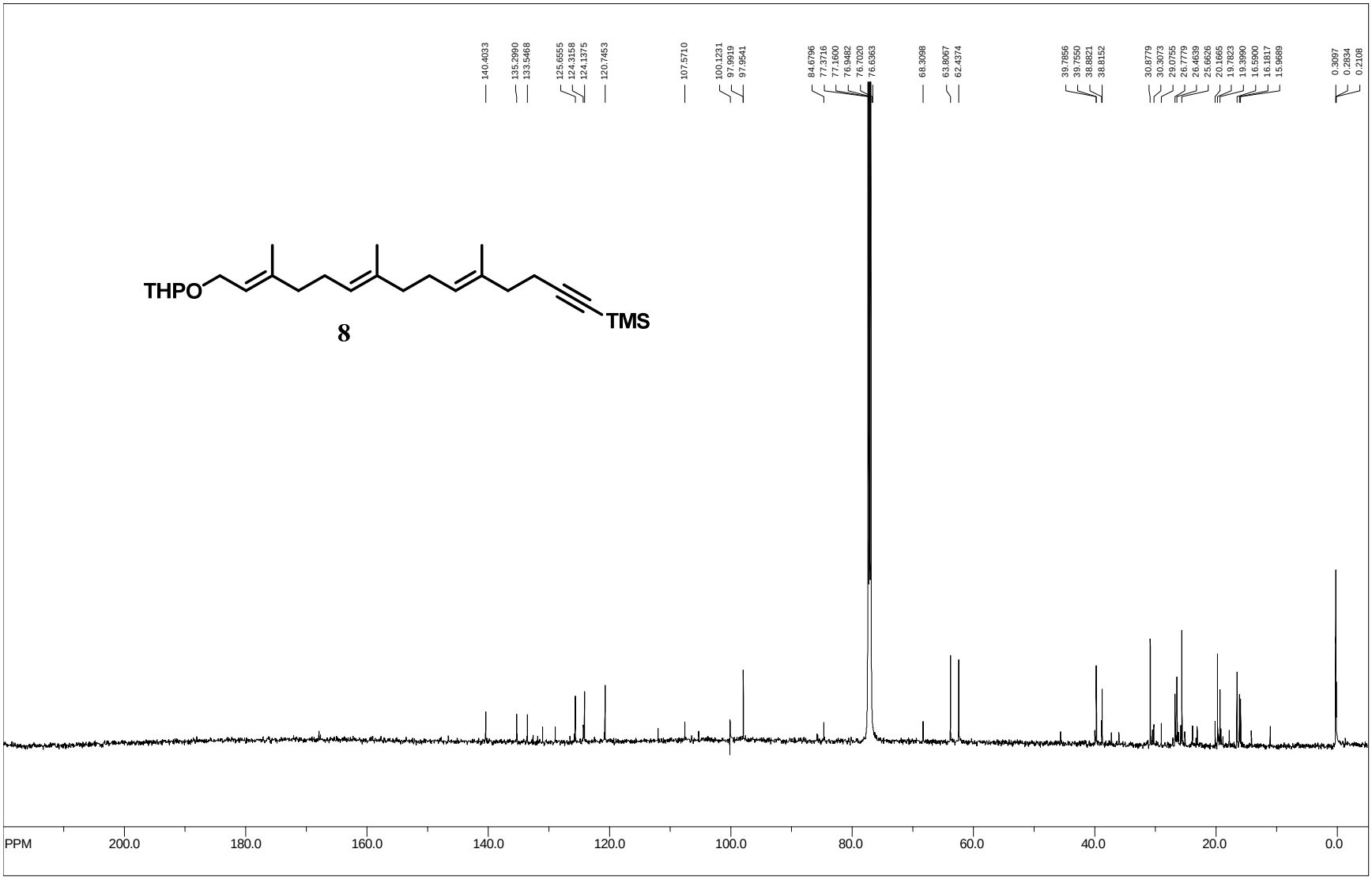

file: C:\Users\guill_2\Documents\Backup\Chemistry\NMR\600\WMI-262\fid expt: <zgpg30>
transmitter freq.: 150.912869 MHz
time domain size: 65536 points
width: 36231.88 Hz = 240.084787 ppm = 0.552855 Hz/pt
number of scans: 669

freq. of 0 ppm: 150.897757 MHz
processed size: 32768 complex points
LB: 0.500 GB: 0.0000

SpinWorks 2.5: Standard One-dimensional 1H Experiment: Alk-FOH-3

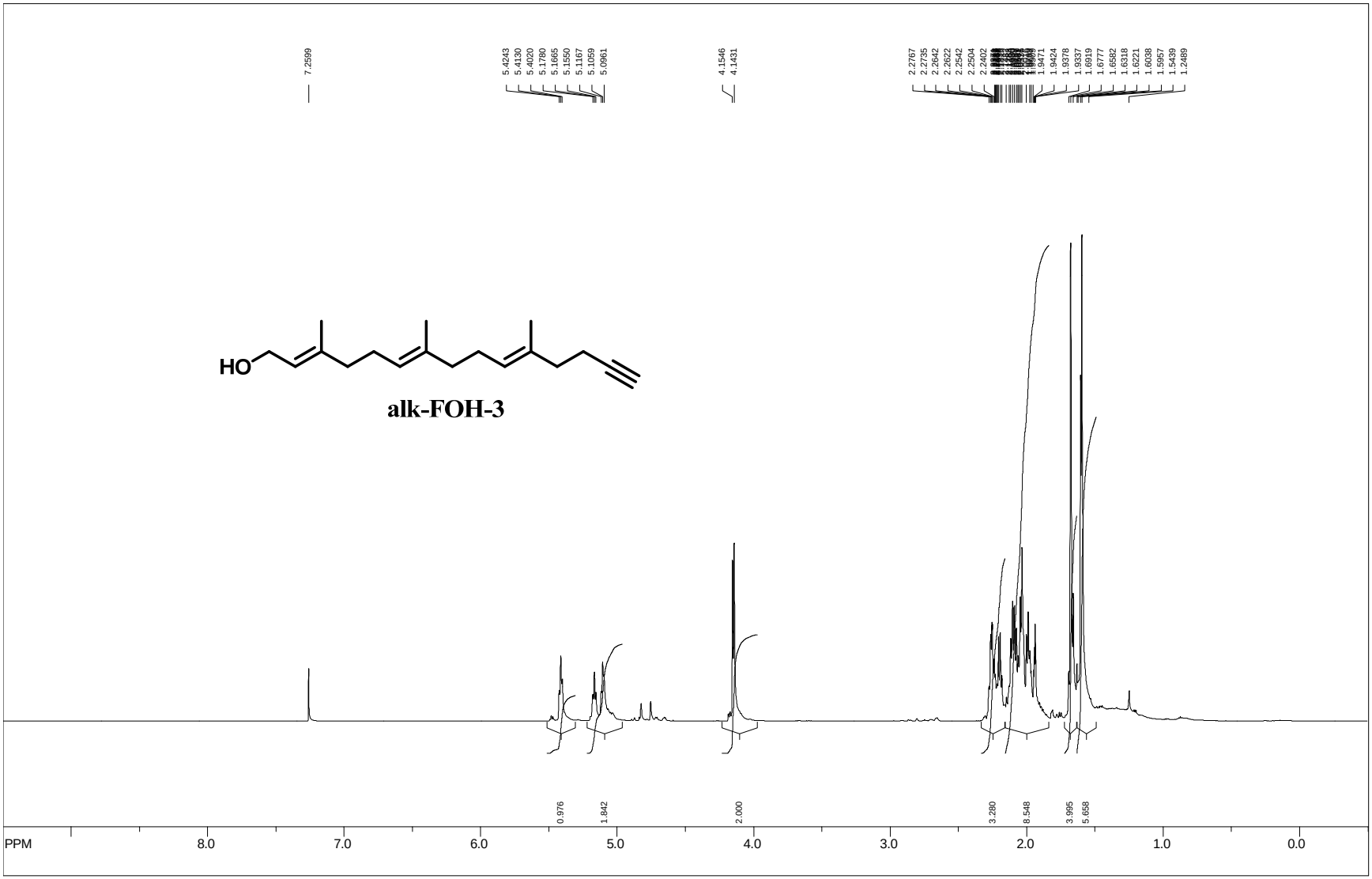

file: C:\Users\guill_2\Documents\Backup\Chemistry\NMR\600\WMI-29\1\fid expt: <zg30>
transmitter freq.: 600.112850 MHz
time domain size: 32768 points
width: 8389.26 Hz = 13.979474 ppm = 0.256020 Hz/pt
number of scans: 15

freq. of 0 ppm: 600.110017 MHz
processed size: 65536 complex points
LB: 0.000 GB: 0.0000

SpinWorks 2.5: 13C Direct Detection: Alk-FOH-3

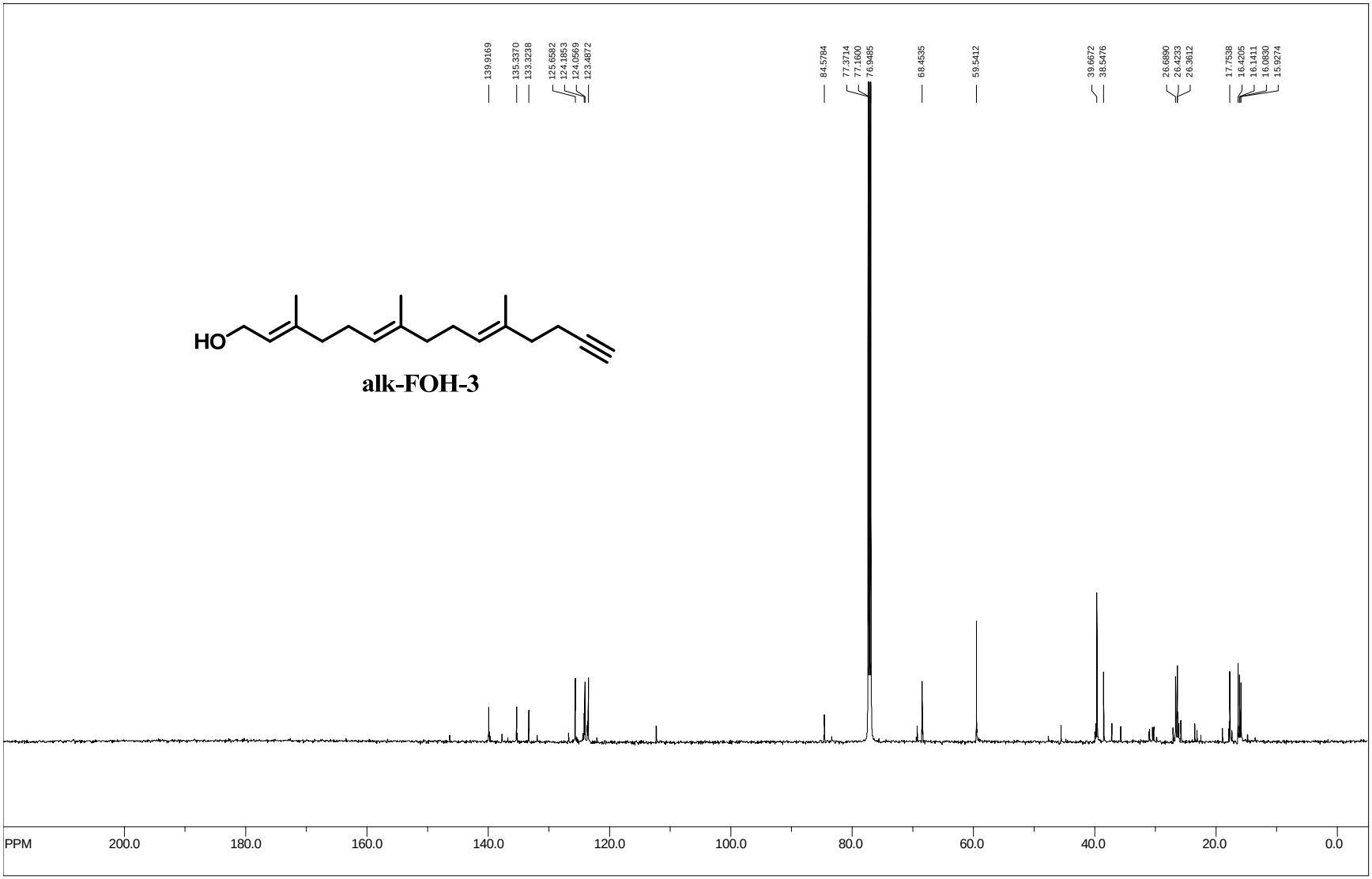

file: C:\Users\guill_2\Documents\Backup\Chemistry\NMR\600\WMI-29\2\fid expt: <zgpg30>
transmitter freq.: 150.912869 MHz
time domain size: 65536 points
width: 36231.88 Hz = 240.084787 ppm = 0.552855 Hz/pt
number of scans: 114

freq. of 0 ppm: 150.897759 MHz
processed size: 32768 complex points
LB: 0.000 GB: 0.0000

SpinWorks 2.5: Standard One-dimensional 1H Experiment: 9

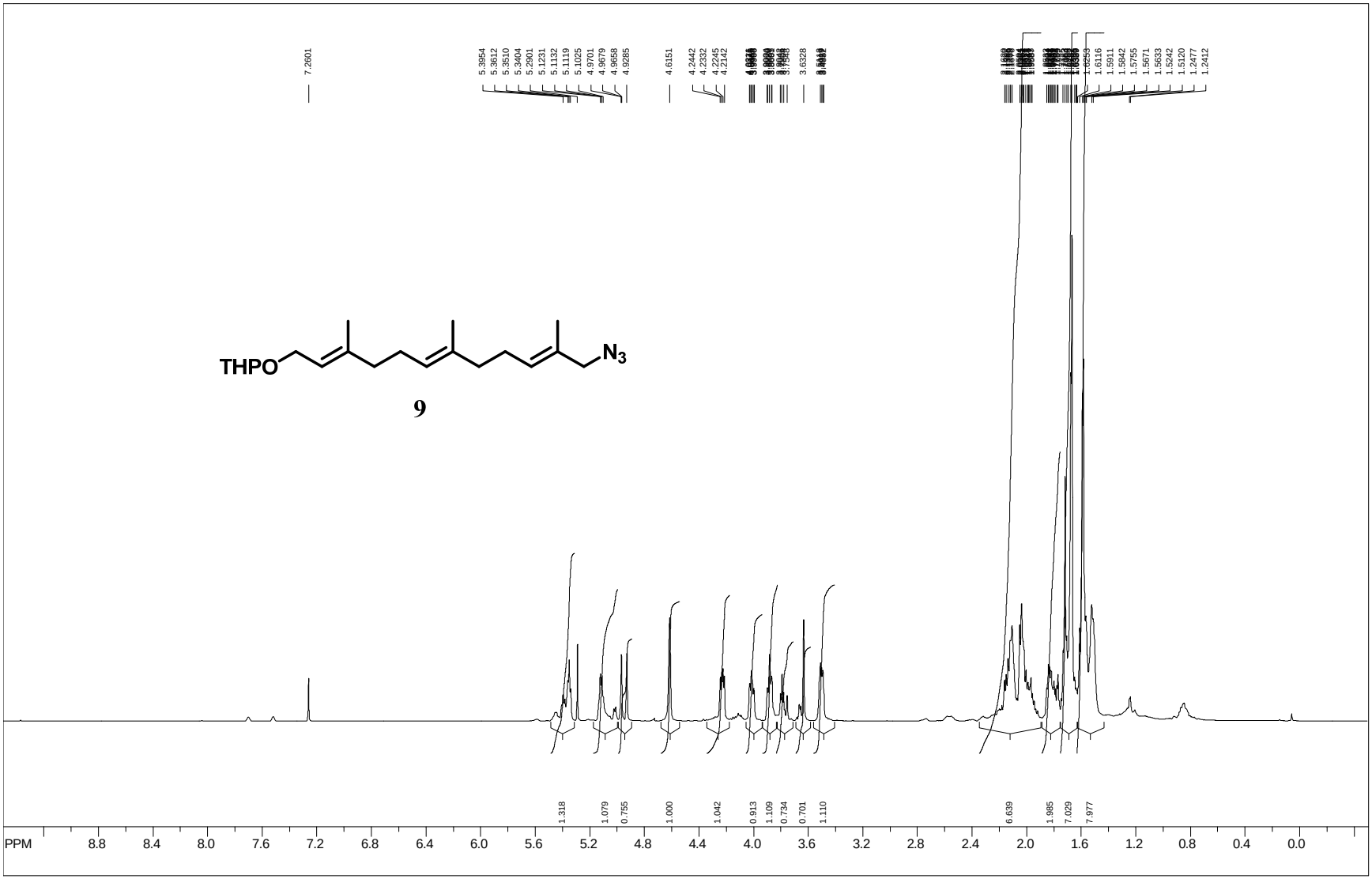

file: C:\Users\guill_2\Documents\Backup\Chemistry\NMR\600\WFM01-25Proton\3\fid expt: <zg30>
transmitter freq.: 600.127850 MHz
time domain size: 32768 points
width: 8389.26 Hz = 13.979124 ppm = 0.256020 Hz/pt
number of scans: 32

freq. of 0 ppm: 600.125015 MHz
processed size: 65536 complex points
LB: 0.000 GB: 0.0000

SpinWorks 2.5: 13C Direct Detection: 9

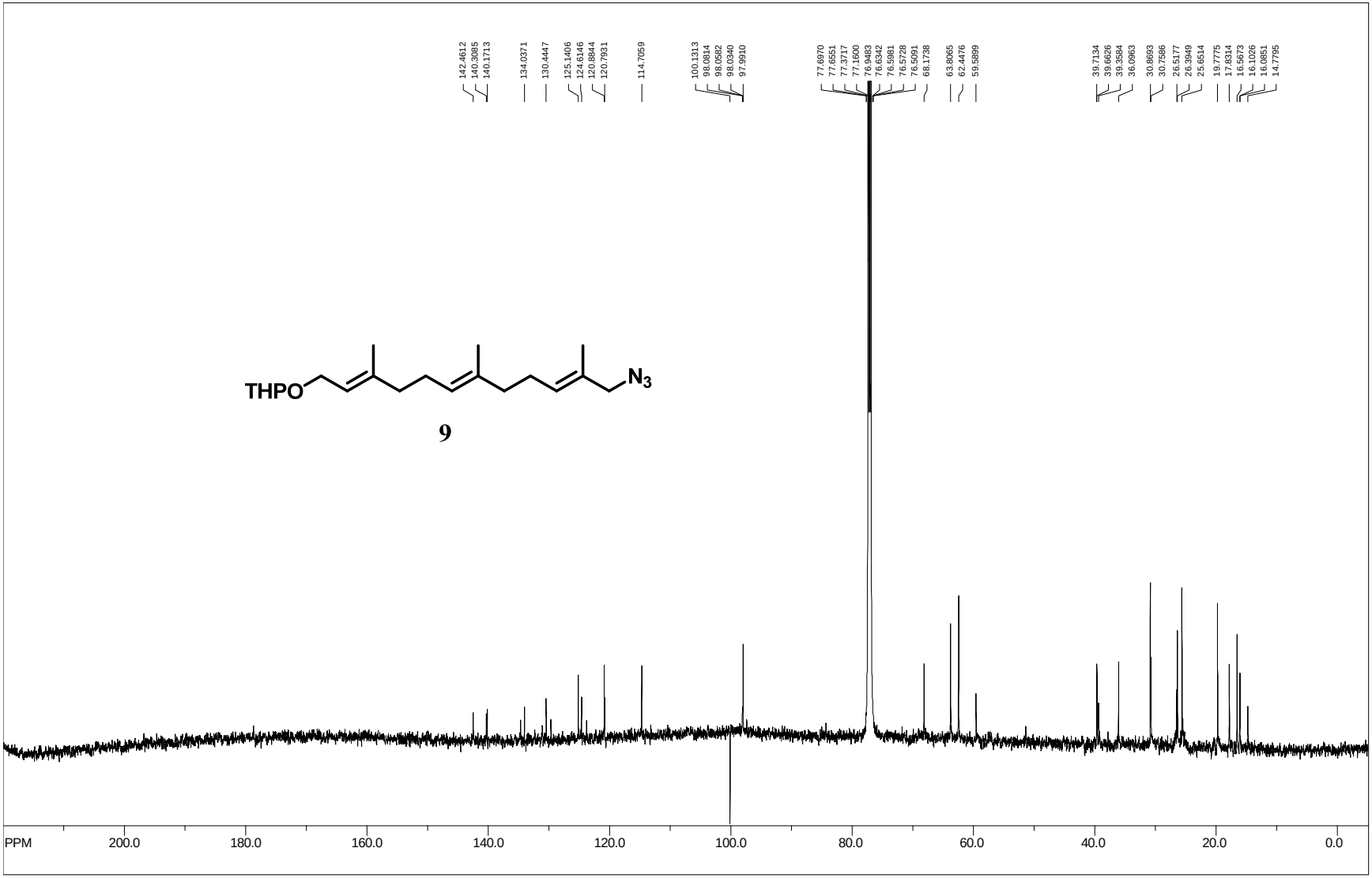

file: C:\Users\guill_2\Documents\Backup\Chemistry\NMR\600\WMI-252\fid expt: <zgpg30>
transmitter freq.: 150.912869 MHz
time domain size: 65536 points
width: 36231.88 Hz = 240.084787 ppm = 0.552855 Hz/pt
number of scans: 441

freq. of 0 ppm: 150.897758 MHz
processed size: 32768 complex points
LB: 0.000 GB: 0.0000

SpinWorks 2.5: Standard One-dimensional 1H Experiment: az-FOH

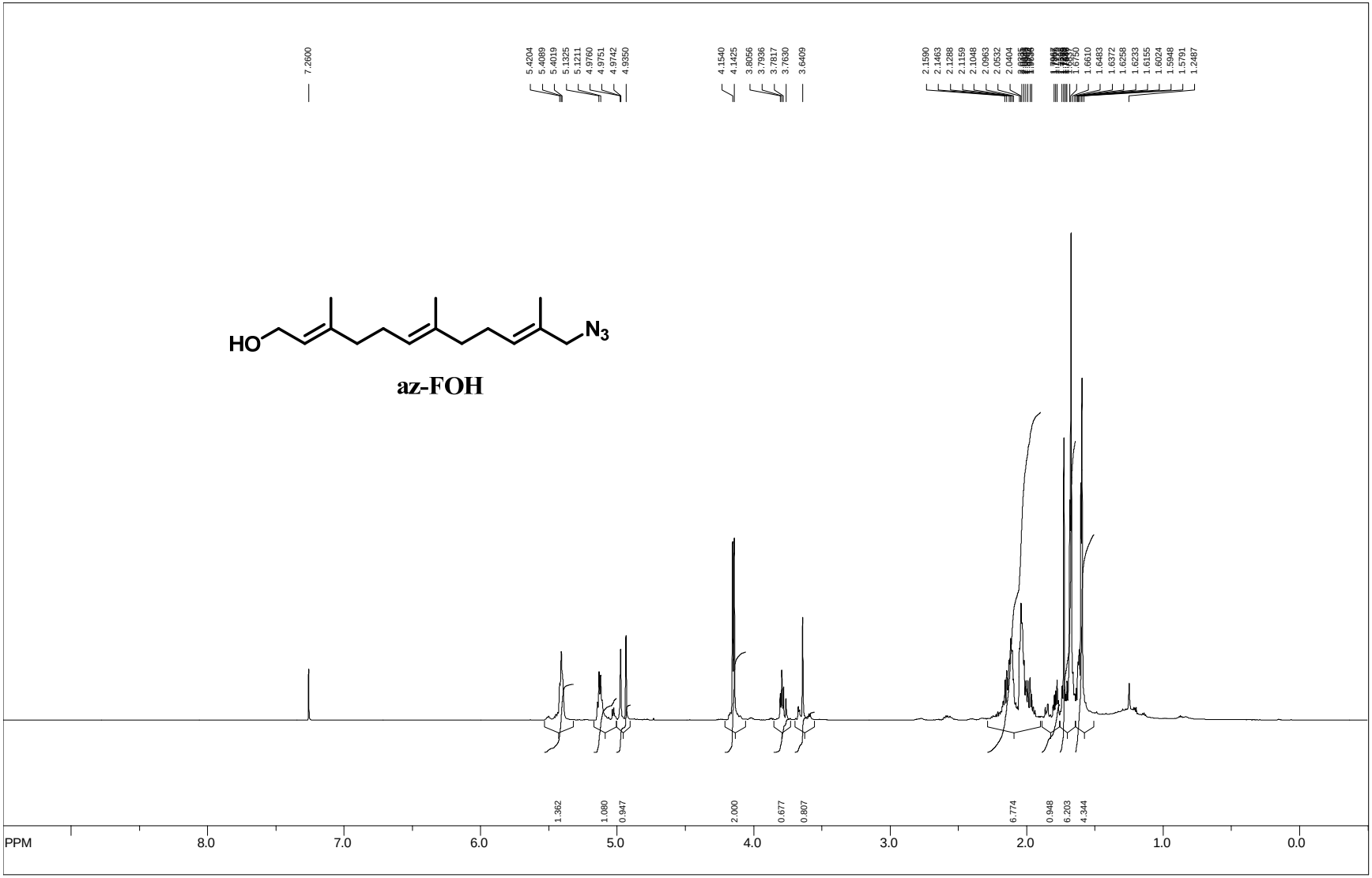

file: C:\Users\guill_2\Documents\Backup\Chemistry\NMR\600\WMI-28\1\fid expt: <zg30>
transmitter freq.: 600.112850 MHz
time domain size: 32768 points
width: 8389.26 Hz = 13.979474 ppm = 0.256020 Hz/pt
number of scans: 9

freq. of 0 ppm: 600.110017 MHz
processed size: 65536 complex points
LB: 0.000 GB: 0.0000

SpinWorks 2.5: 13C Direct Detection: az-FOH

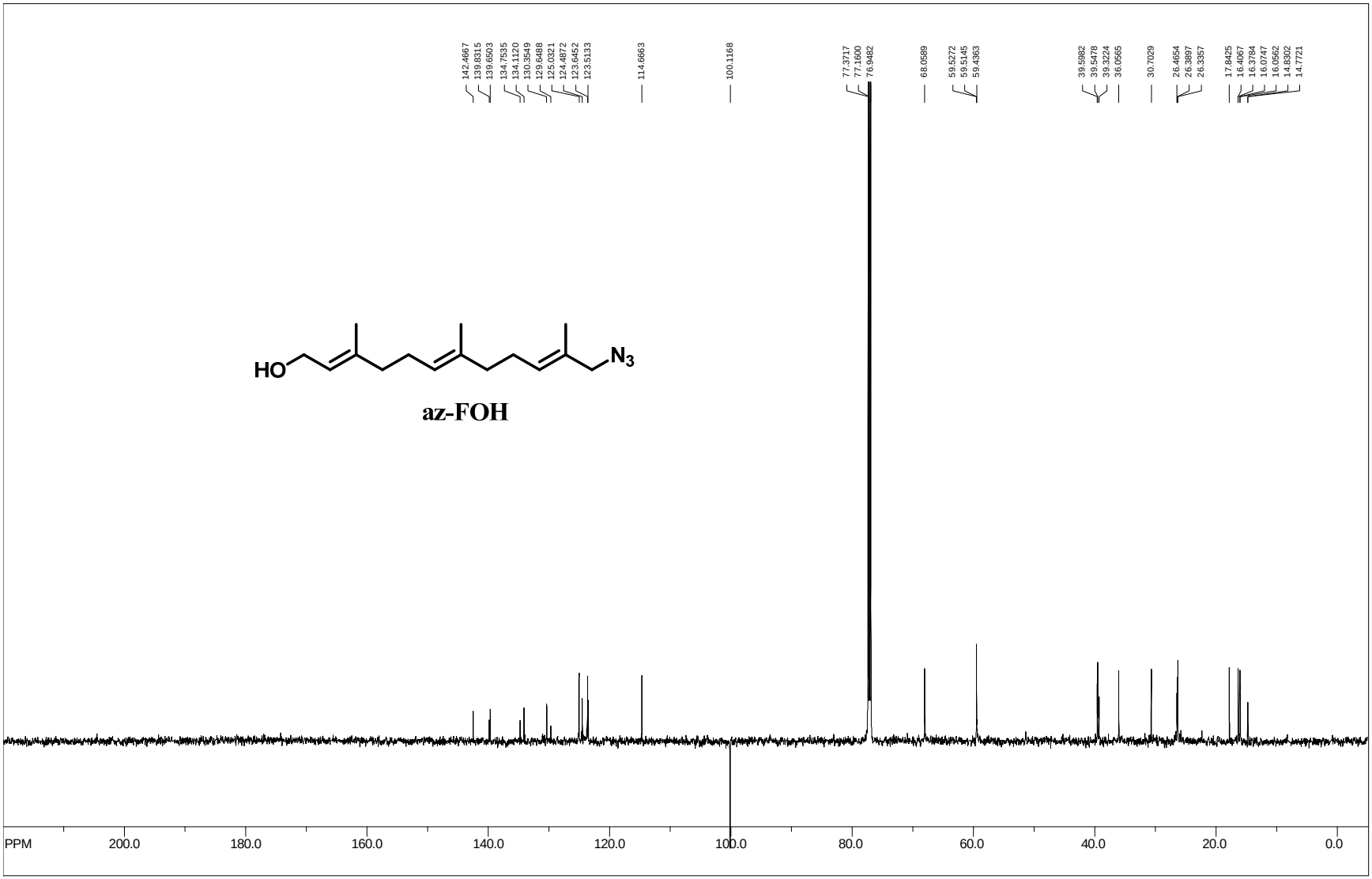

file: C:\Users\guill_2\Documents\Backup\Chemistry\NMR\600\WMI-28\2\fid expt: <zgpg30>
transmitter freq.: 150.912869 MHz
time domain size: 65536 points
width: 36231.88 Hz = 240.084787 ppm = 0.552855 Hz/pt
number of scans: 17

freq. of 0 ppm: 150.897760 MHz
processed size: 32768 complex points
LB: 0.000 GB: 0.0000

SpinWorks 2.5: Standard one-dimentional 1H: az-biotin

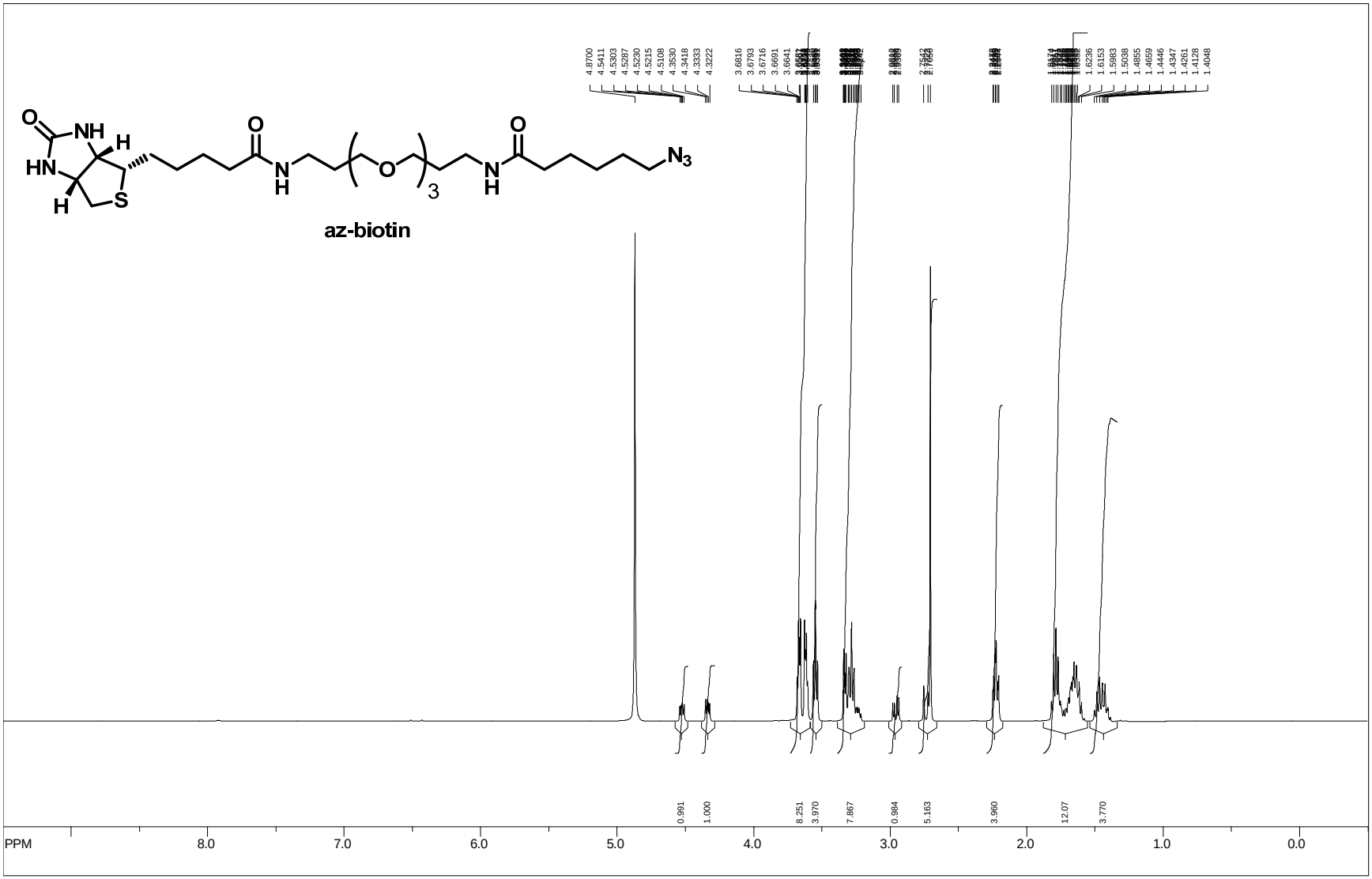

file: C:\Users\guill_2\Documents\Backup\Chemistry\NMR\400\GCI-83\1\fid expt: <zg30>
transmitter freq.: 400.131881 MHz
time domain size: 32768 points
width: 5995.20 Hz = 14.983070 ppm = 0.182959 Hz/pt
number of scans: 32

freq. of 0 ppm: 400.129997 MHz
processed size: 32768 complex points
LB: 0.000 GB: 0.0000

SpinWorks 2.5: 13C Direct Detection: az-biotin

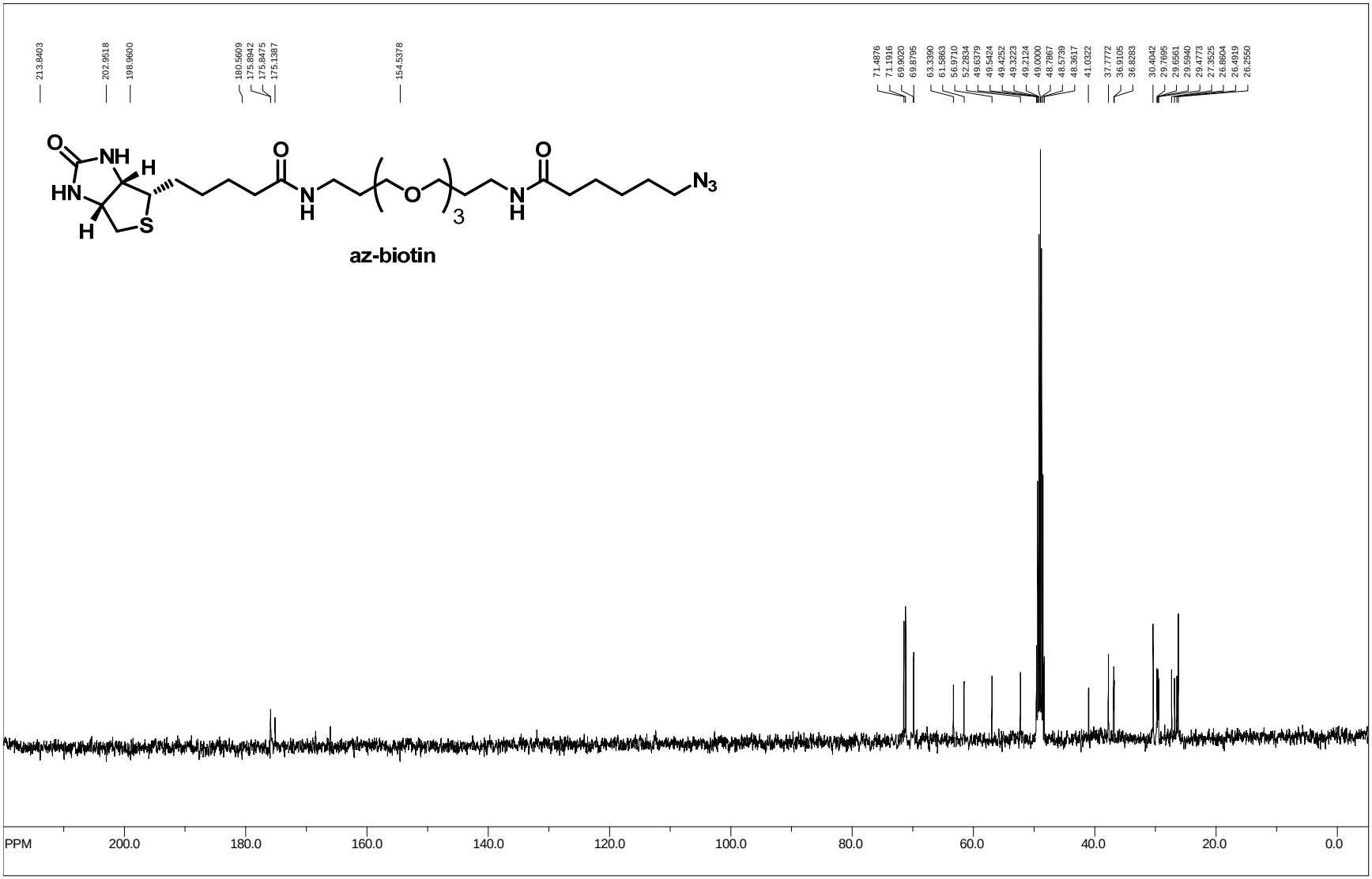

file: C:\Users\guill_2\Documents\Backup\Chemistry\NMR\400\GCI-83\2\fid expt: <zgpg30>
transmitter freq.: 100.622790 MHz
time domain size: 65536 points
width: 23980.82 Hz = 238.323897 ppm = 0.365918 Hz/pt
number of scans: 78

freq. of 0 ppm: 100.612632 MHz
processed size: 32768 complex points
LB: 3.000 GB: 0.0000

SpinWorks 2.5: Standard One-dimensional 1H Experiment: alk-rho

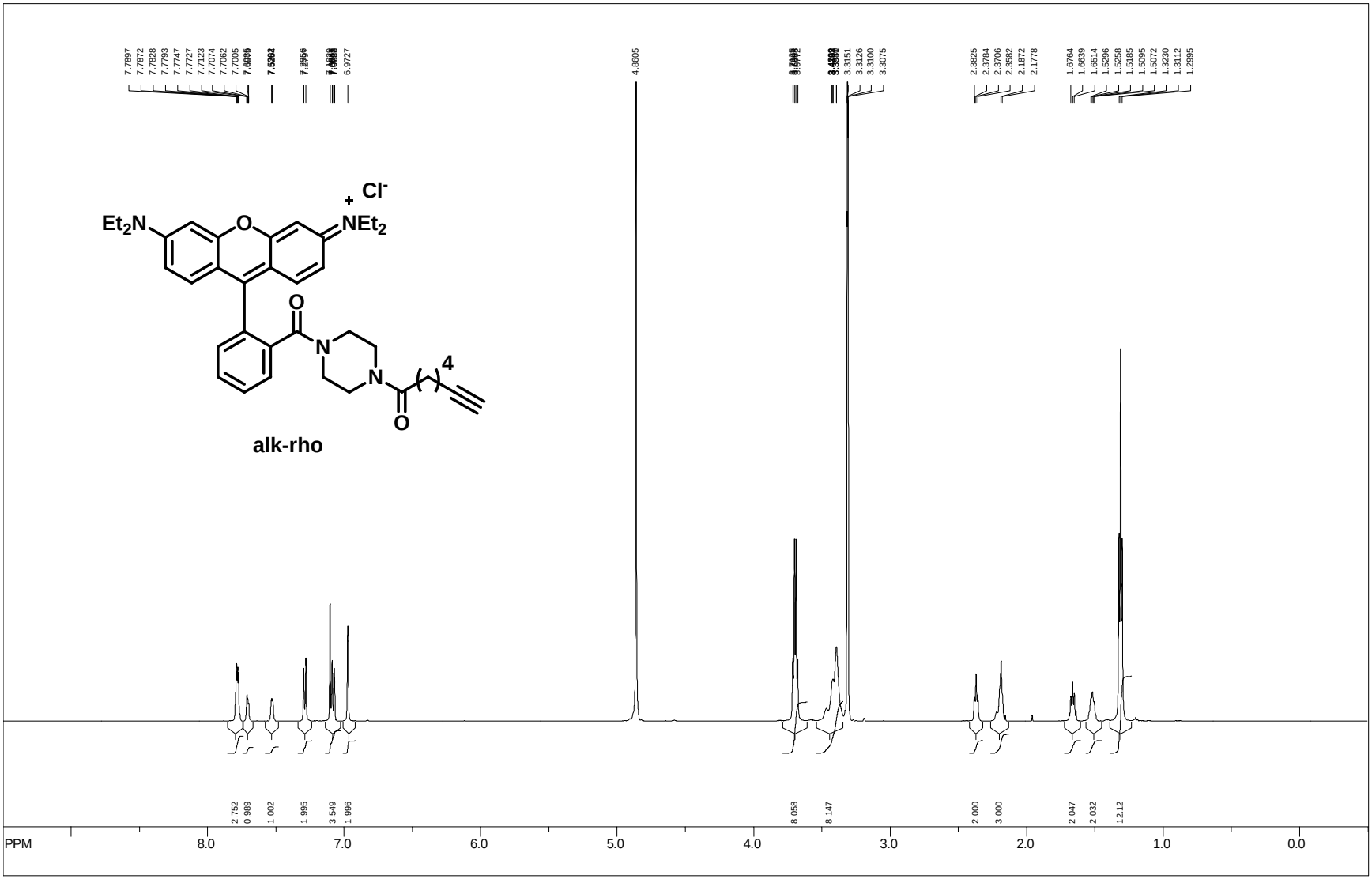

file: C:\Users\guill_2\Documents\Backup\Chemistry\NMR\600\alk-rho\1\fid expt: <zg30>
transmitter freq.: 600.127850 MHz
time domain size: 32768 points
width: 8389.26 Hz = 13.979124 ppm = 0.256020 Hz/pt
number of scans: 32

freq. of 0 ppm: 600.124094 MHz
processed size: 65536 complex points
LB: 3.000 GB: 0.0000

SpinWorks 2.5: 13C Direct Detection: alk-rho

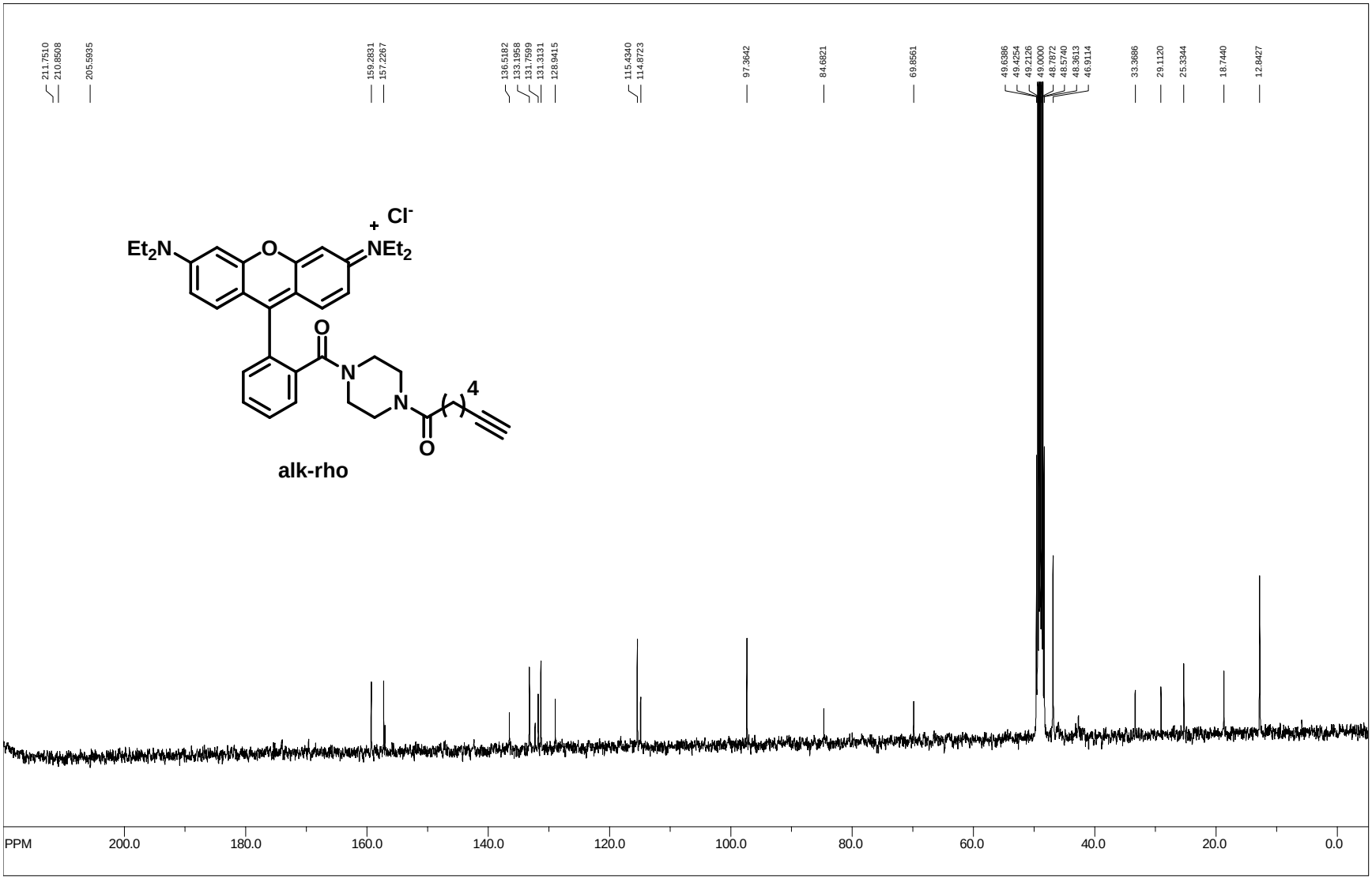

file: C:\Users\guill_2\Documents\Backup\Chemistry\NMR\400\GCII-07\2\fid expt: <zgpg30>
transmitter freq.: 100.622790 MHz
time domain size: 65536 points
width: 23980.82 Hz = 238.323897 ppm = 0.365918 Hz/pt
number of scans: 978

freq. of 0 ppm: 100.612628 MHz
processed size: 32768 complex points
LB: 3.000 GB: 0.0000

SpinWorks 2.5: Standard One-dimensional 1H Experiment: az-rho

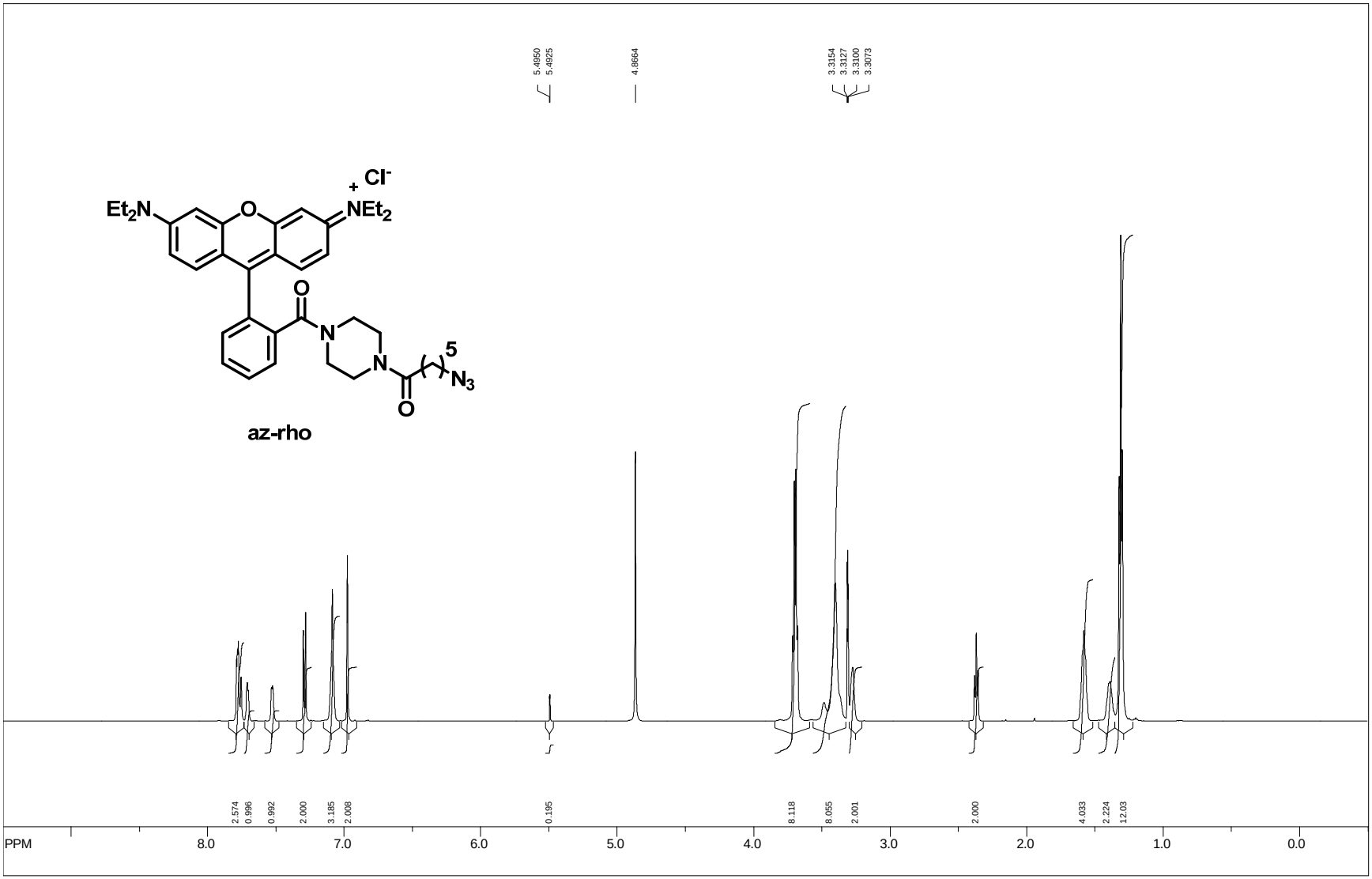

file: C:\Users\guill_2\Documents\Backup\Chemistry\NMR\600\az-rho\2\fid expt: <zg30>
transmitter freq.: 600.127850 MHz
time domain size: 32768 points
width: 8389.26 Hz = 13.979124 ppm = 0.256020 Hz/pt
number of scans: 32

freq. of 0 ppm: 600.124092 MHz
processed size: 65536 complex points
LB: 3.000 GB: 0.0000

SpinWorks 2.5: 13C Direct Detection: az-rho

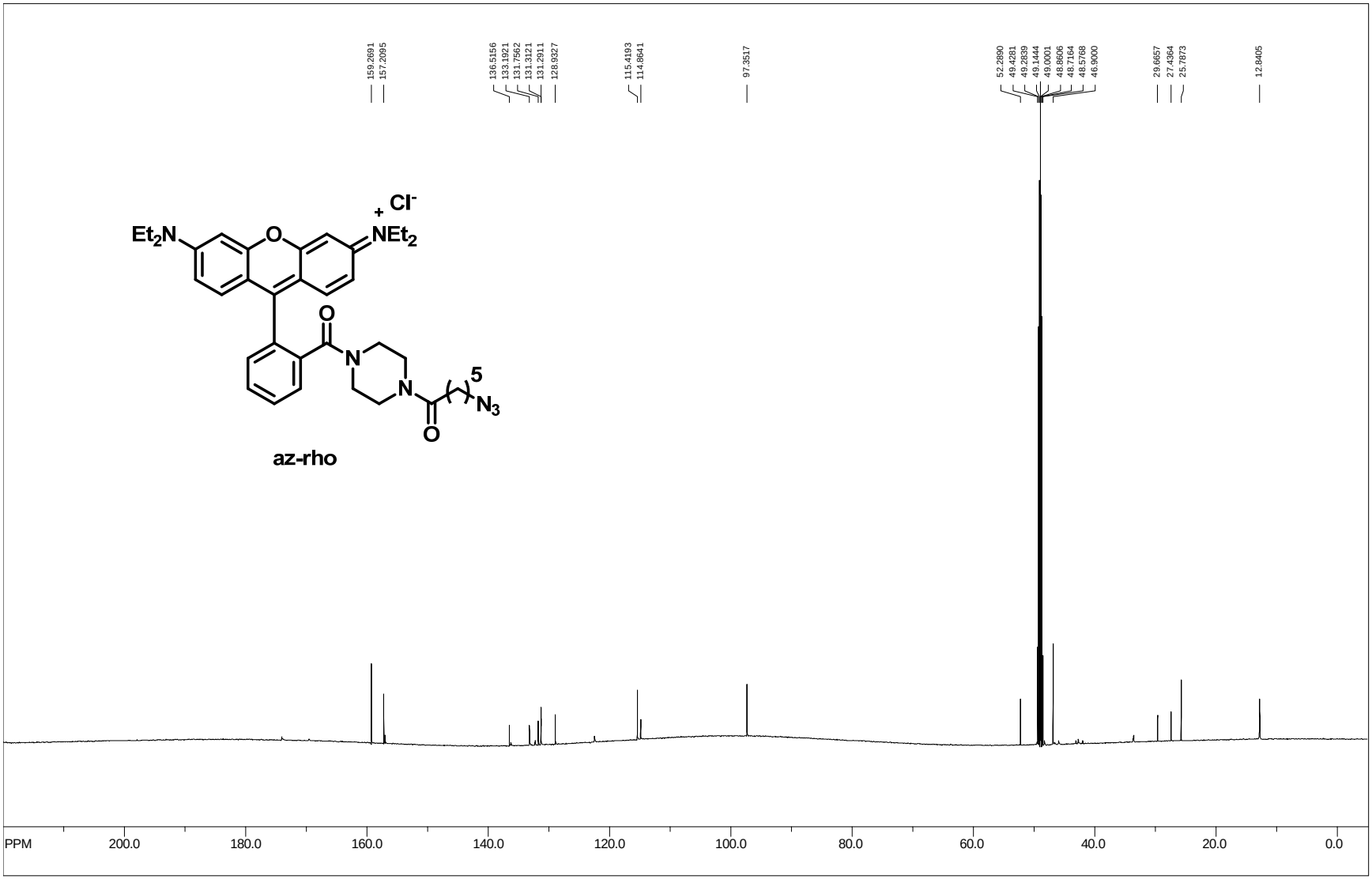

file: C:\Users\guill_2\Documents\Backup\Chemistry\NMR\600\az-rho\1\fid expt: <zgpg30>
transmitter freq.: 150.916641 MHz
time domain size: 65536 points
width: 35971.22 Hz = 238.351601 ppm = 0.548877 Hz/pt
number of scans: 10000

freq. of 0 ppm: 150.901113 MHz
processed size: 32768 complex points
LB: 3.000 GB: 0.0000

SpinWorks 2.5: Standard One-dimensional 1H Experiment: 11

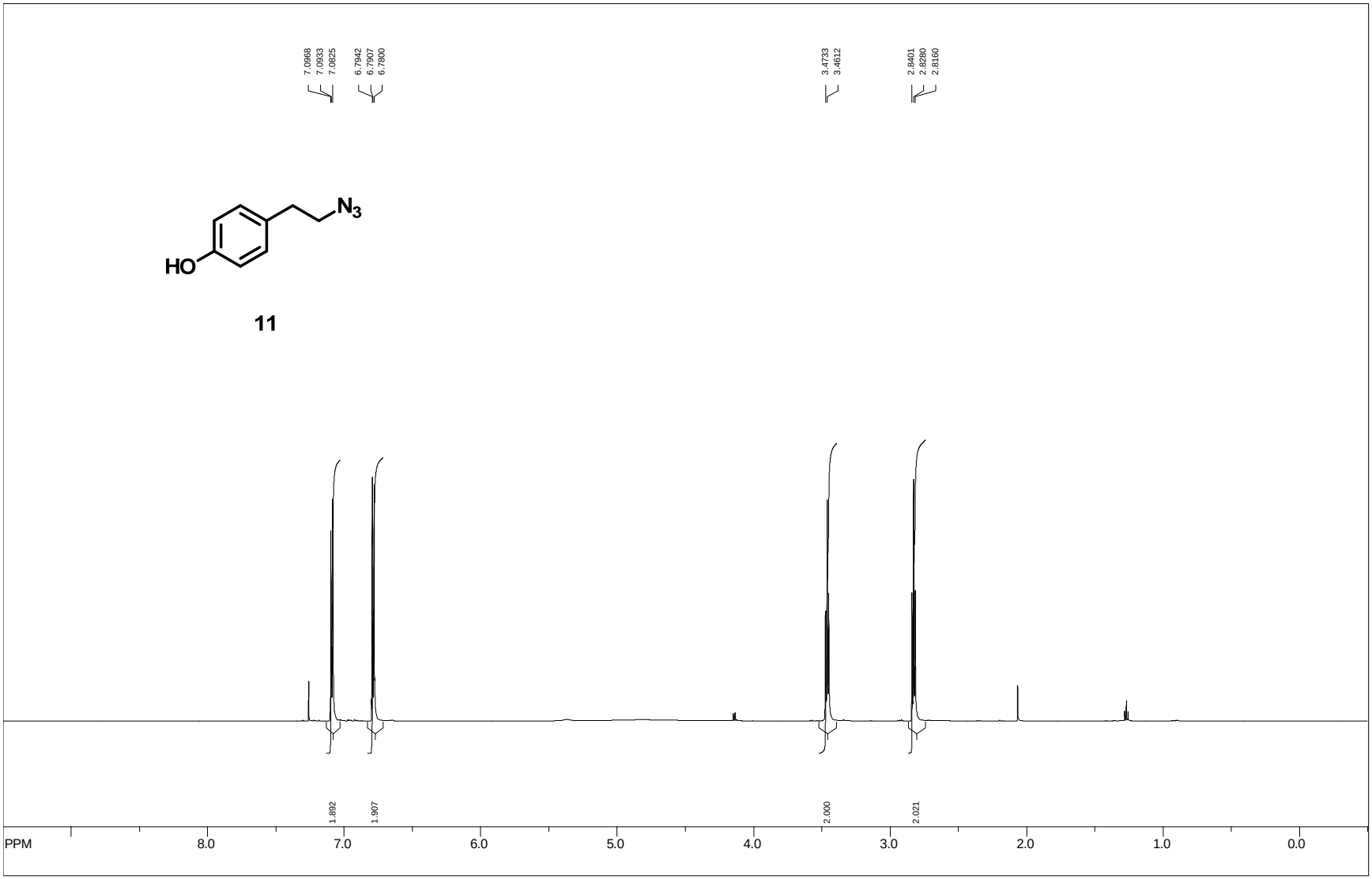

file: C:\Users\guill_2\Documents\Backup\Chemistry\NMR\600\GCIII-51\2\fid expt: <zg30>
transmitter freq.: 600.112850 MHz
time domain size: 32768 points
width: 8389.26 Hz = 13.979474 ppm = 0.256020 Hz/pt
number of scans: 12

freq. of 0 ppm: 600.110017 MHz
processed size: 65536 complex points
LB: 3.000 GB: 0.0000

SpinWorks 2.5: 13C Direct Detection: 11

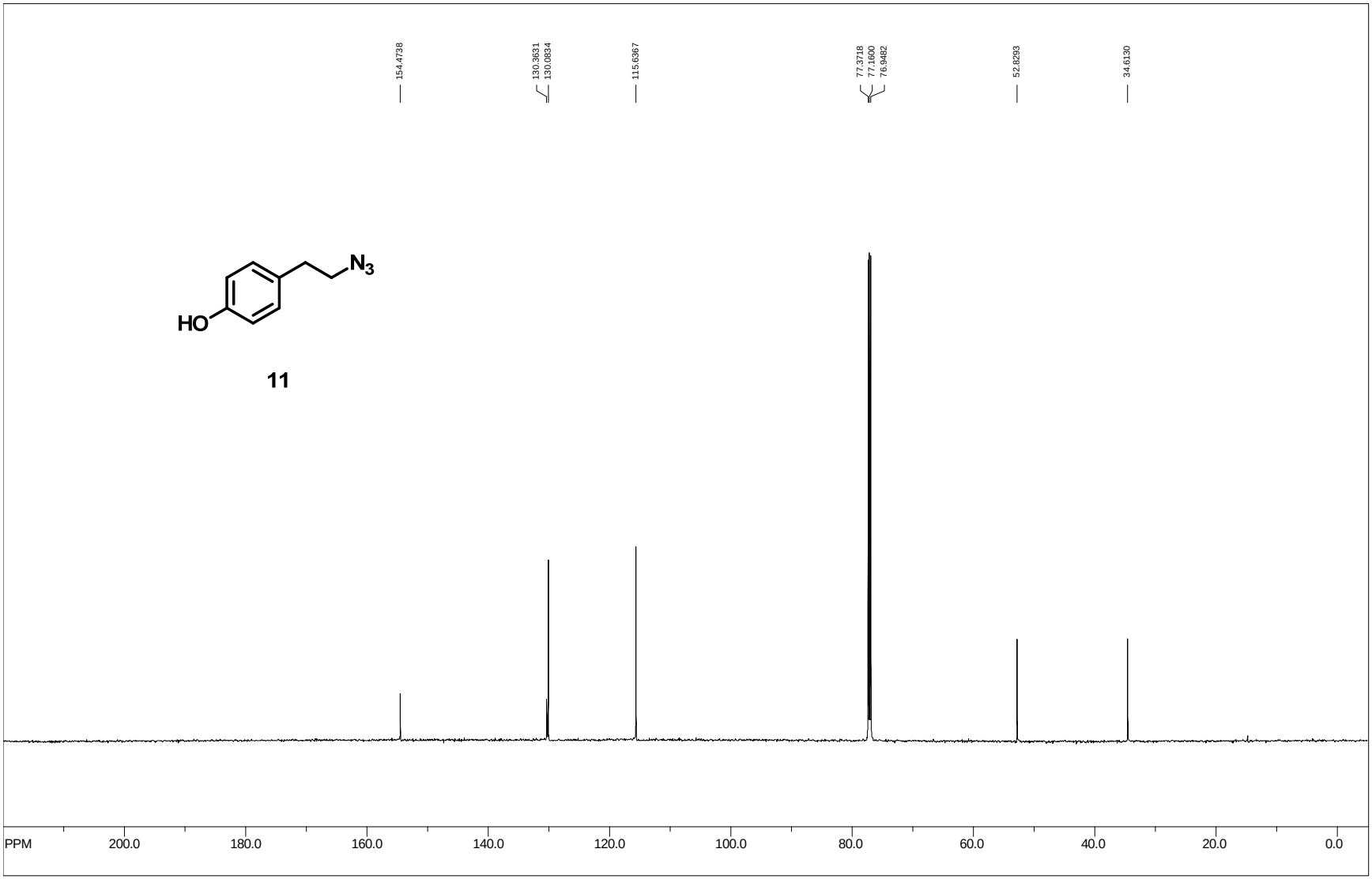

file: C:\Users\guill_2\Documents\Backup\Chemistry\NMR\600\GCIII-51\3\fid expt: <zgpg30>
transmitter freq.: 150.912869 MHz
time domain size: 65536 points
width: 36231.88 Hz = 240.084787 ppm = 0.552855 Hz/pt
number of scans: 32

freq. of 0 ppm: 150.897762 MHz
processed size: 32768 complex points
LB: 3.000 GB: 0.0000

SpinWorks 2.5: Standard One-dimensional 1H Experiment: 12

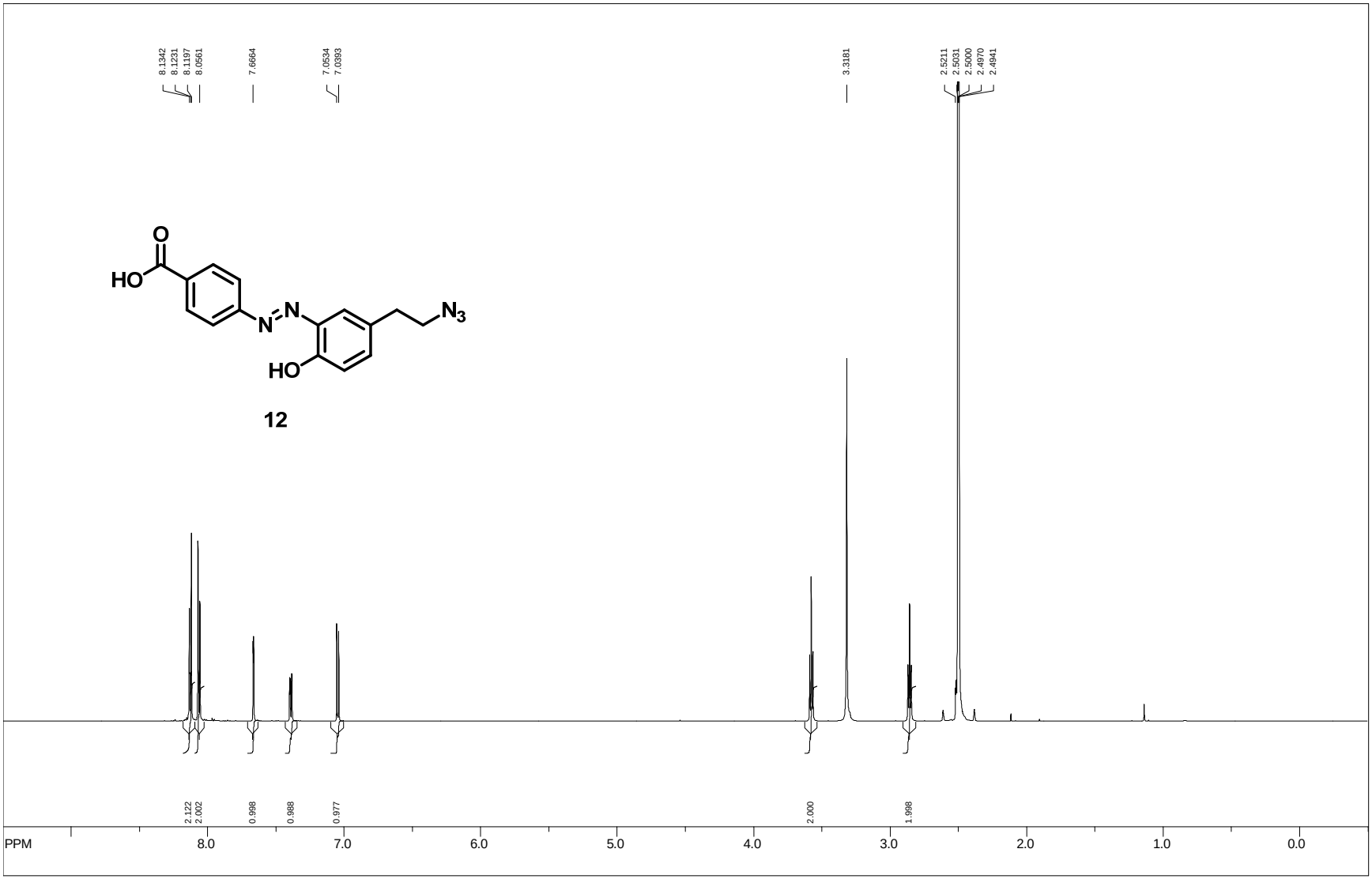

file: C:\Users\guill_2\Documents\Backup\Chemistry\NMR\600\GCII-69B\1\fid expt: <zg30>
transmitter freq.: 600.112850 MHz
time domain size: 32768 points
width: 8389.26 Hz = 13.979474 ppm = 0.256020 Hz/pt
number of scans: 24

freq. of 0 ppm: 600.110007 MHz
processed size: 65536 complex points
LB: 3.000 GB: 0.0000

SpinWorks 2.5: 13C Direct Detection: 12

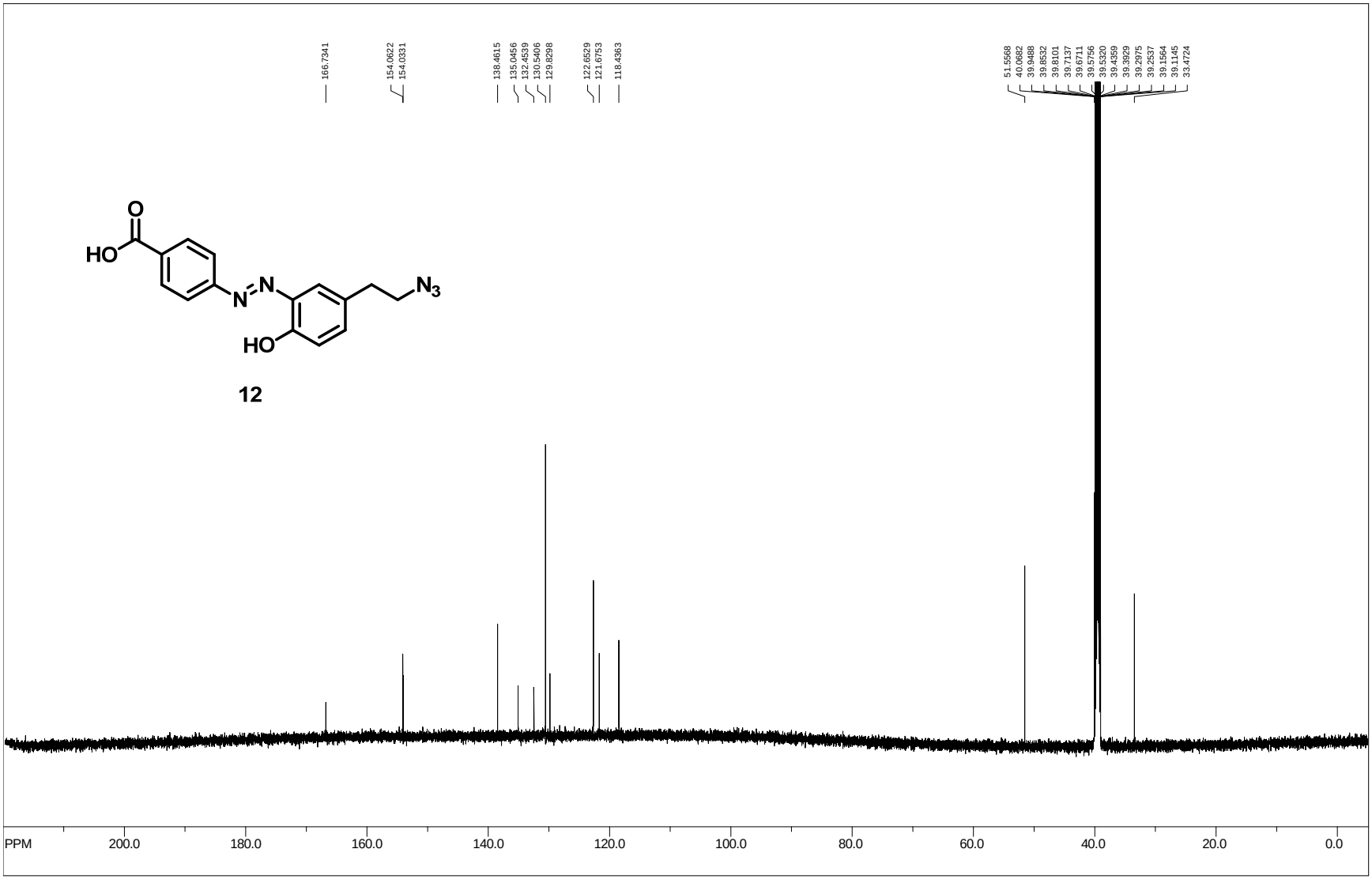

file: C:\Users\guill_2\Documents\Backup\Chemistry\NMR\600\GCIII-69B\2\fid expt: <zgpg30>
transmitter freq.: 150.912869 MHz
time domain size: 65536 points
width: 36231.88 Hz = 240.084787 ppm = 0.552855 Hz/pt
number of scans: 1000

freq. of 0 ppm: 150.897851 MHz
processed size: 32768 complex points
LB: 3.000 GB: 0.0000

SpinWorks 2.5: Standard One-dimensional 1H Experiment: 13

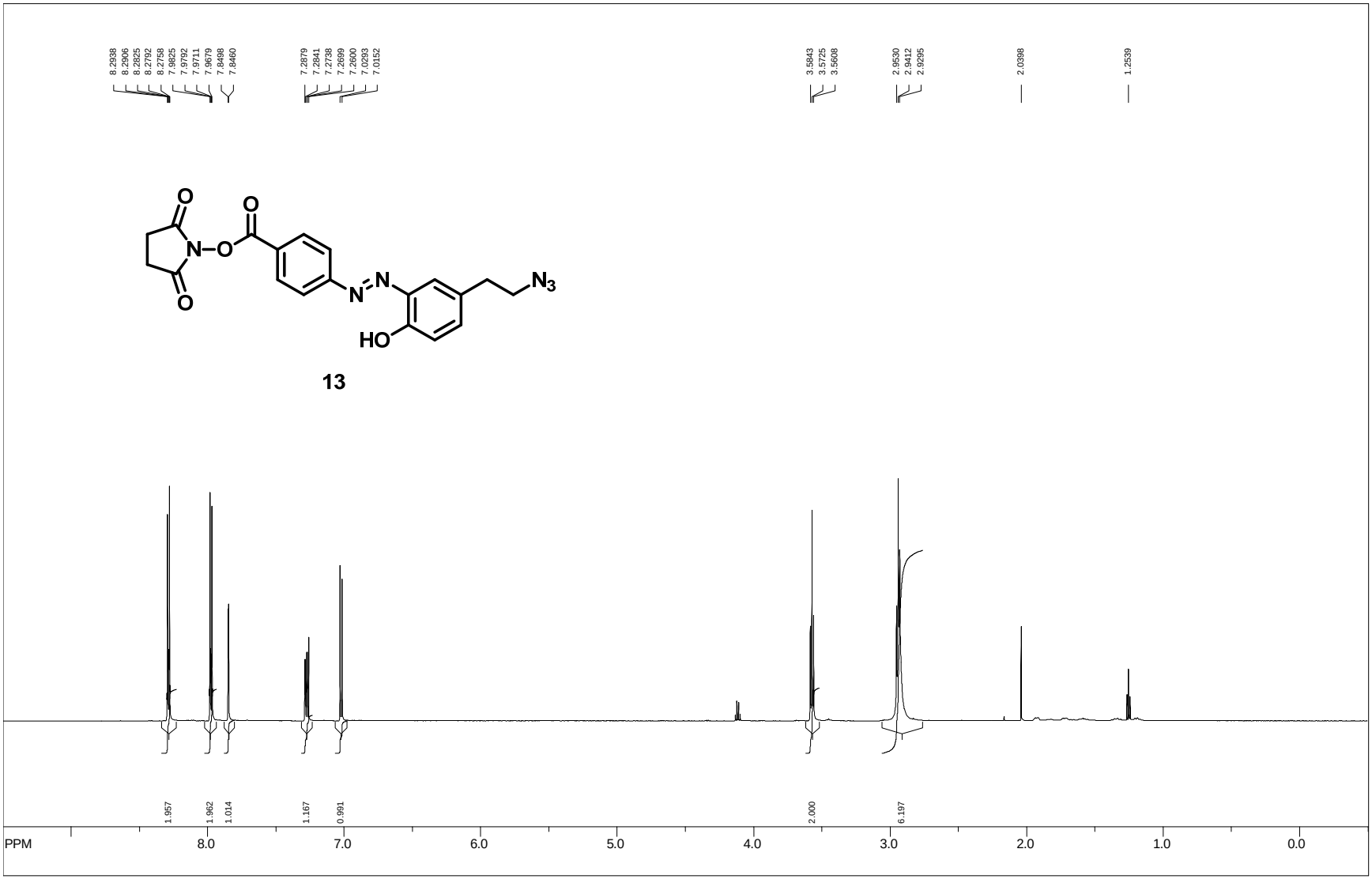

file: C:\Users\guill_2\Documents\Backup\Chemistry\NMR\600\GCIII-79\1\1\fid expt: <zg30>
transmitter freq.: 600.112850 MHz
time domain size: 32768 points
width: 8389.26 Hz = 13.979474 ppm = 0.256020 Hz/pt
number of scans: 12

freq. of 0 ppm: 600.110017 MHz
processed size: 65536 complex points
LB: 3.000 GB: 0.0000

SpinWorks 2.5: 13C Direct Detection: 13

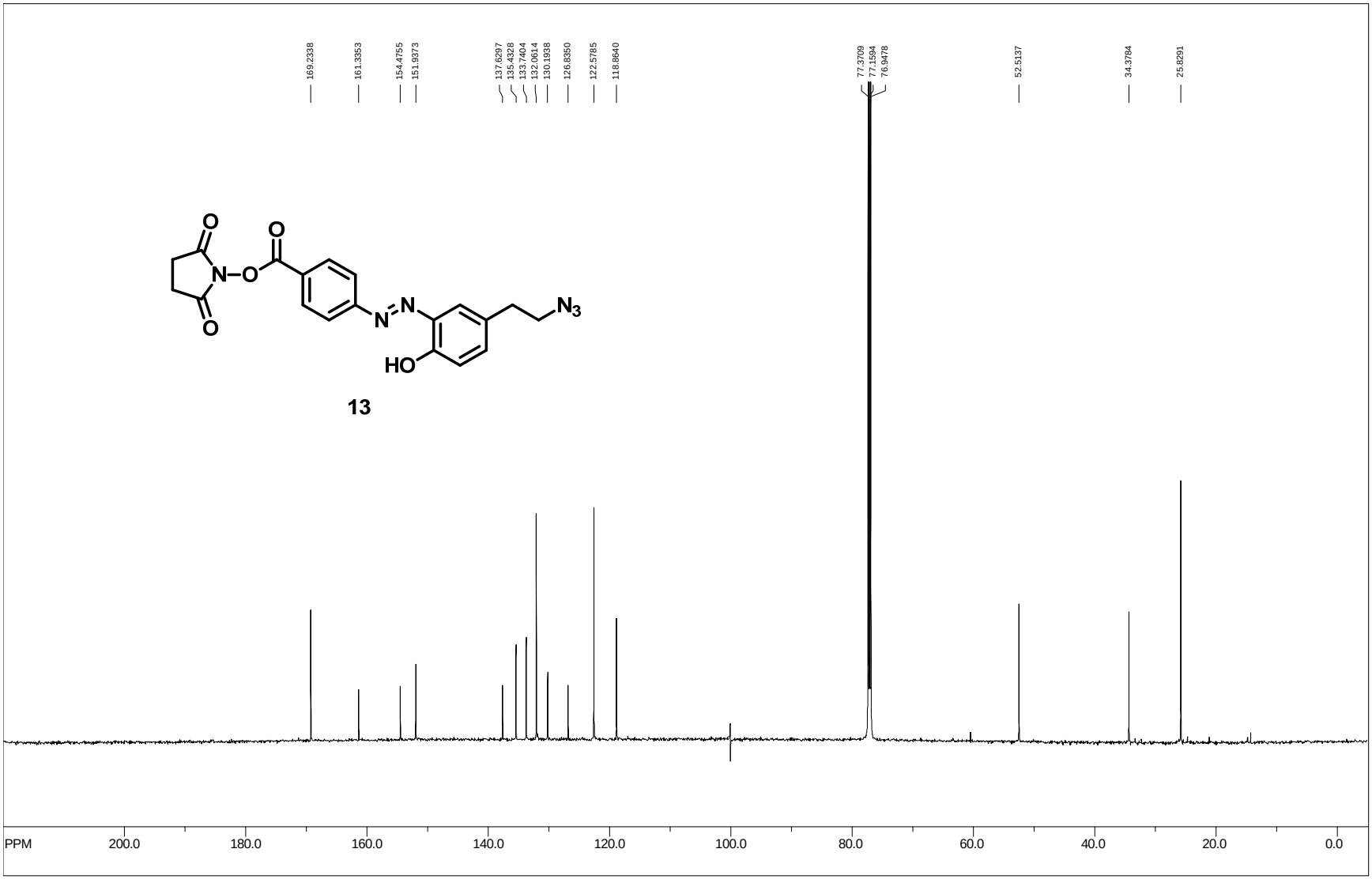

file: C:\Users\guill_2\Documents\Backup\Chemistry\NMR\600\GCIII-79\2\fid expt: <zgpg30>
transmitter freq.: 150.912869 MHz
time domain size: 65536 points
width: 36231.88 Hz = 240.084787 ppm = 0.552855 Hz/pt
number of scans: 159

freq. of 0 ppm: 150.897761 MHz
processed size: 32768 complex points
LB: 3.000 GB: 0.0000

SpinWorks 2.5: Standard One-dimensional 1H Experiment: az-azo-biotin

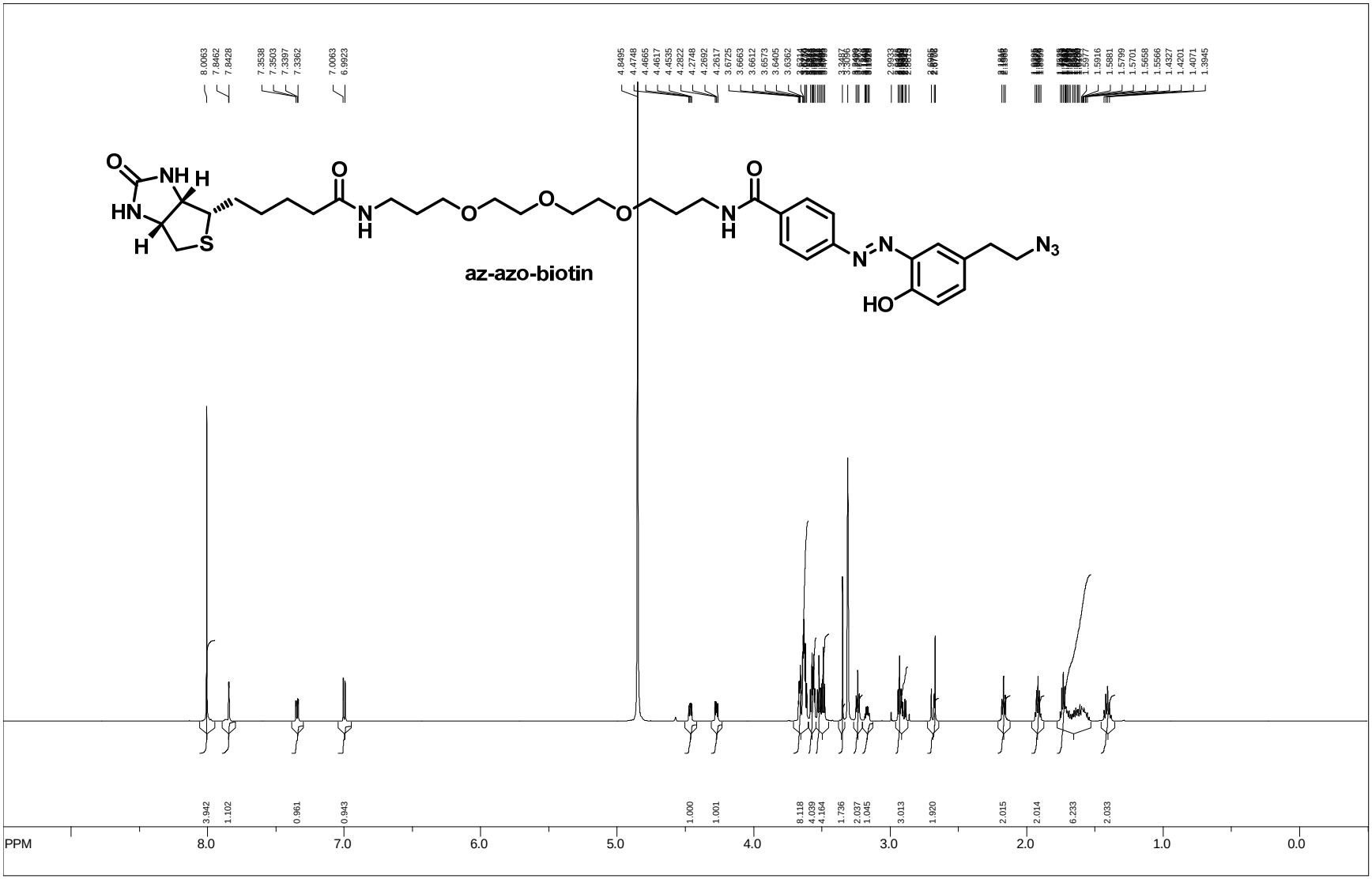

file: C:\Users\guill_2\Documents\Backup\Chemistry\NMR\600\az-diazo-biotin\1\fid expt: <zg30>
transmitter freq.: 600.112850 MHz
time domain size: 32768 points
width: 8389.26 Hz = 13.979474 ppm = 0.256020 Hz/pt
number of scans: 25

freq. of 0 ppm: 600.110014 MHz
processed size: 65536 complex points
LB: 0.000 GB: 0.0000

SpinWorks 2.5: 13C Direct Detection: az-azo-biotin

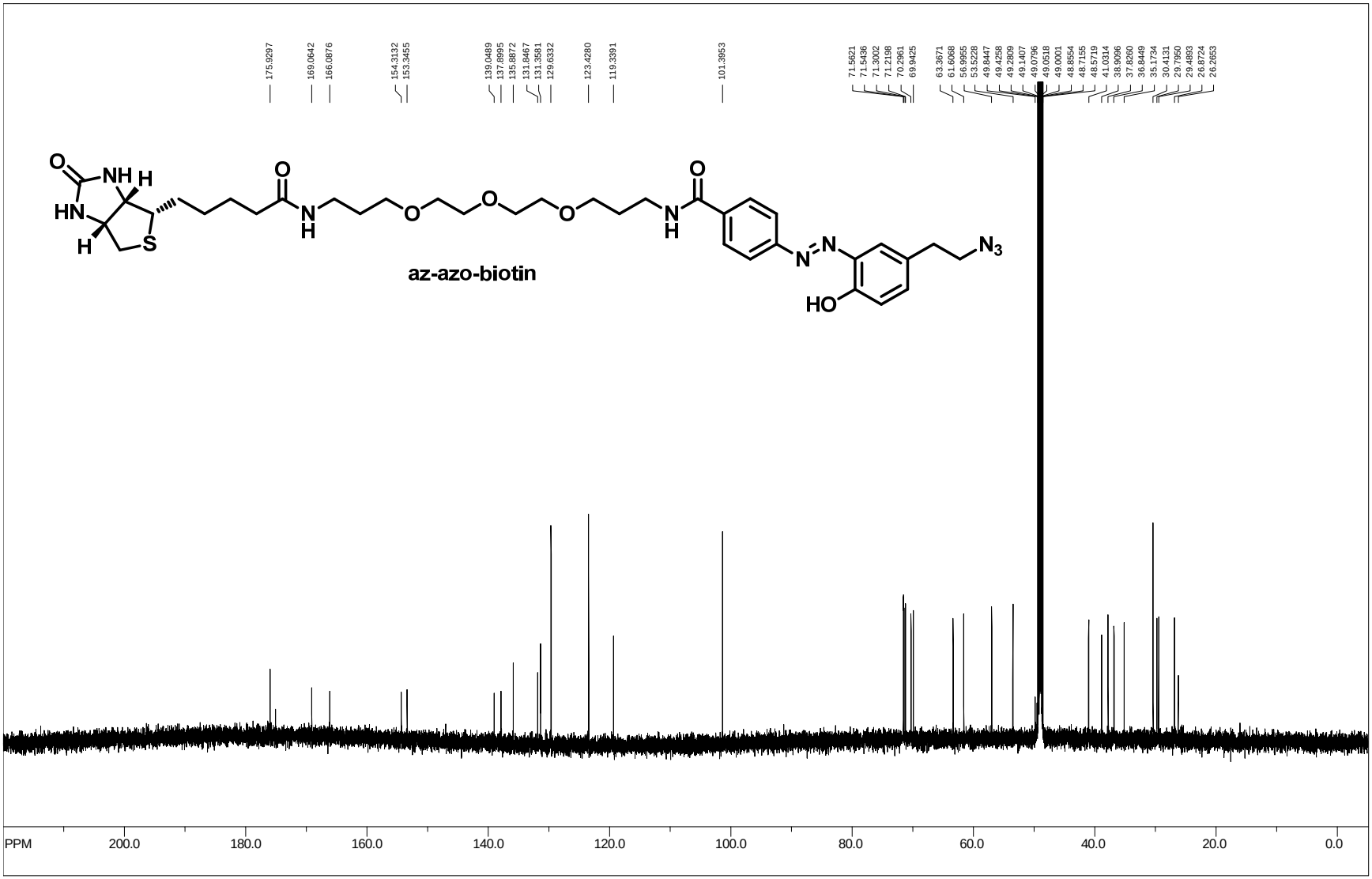

file: C:\Users\guill_2\Documents\Backup\Chemistry\NMR\600\az-diazo-biotin\2\fid expt: <zgpg30>
transmitter freq.: 150.912869 MHz
time domain size: 65536 points
width: 36231.88 Hz = 240.084787 ppm = 0.552855 Hz/pt
number of scans: 875

freq. of 0 ppm: 150.897567 MHz
processed size: 32768 complex points
LB: 3.000 GB: 0.0000

CHAPTER VI. Bibliography

1. **Resh, M.D.,** ***Trafficking and signaling by fatty-acylated and prenylated proteins.*** **Nat Chem Biol, 2006. 2(11): p. 584-90.**

2. **Konstantinopoulos, P.A., M.V. Karamouzis, and A.G. Papavassiliou,** ***Post-translational modifications and regulation of the RAS superfamily of GTPases as anticancer targets.*** **Nat Rev Drug Discov, 2007. 6(7): p. 541-55.**

3. **Fukata, Y. and M. Fukata,** ***Protein palmitoylation in neuronal development and synaptic plasticity.*** **Nat Rev Neurosci, 2010. 11(3): p. 161-75.**

4. **Charron, G., J. Wilson, and H.C. Hang,** ***Chemical tools for understanding protein lipidation in eukaryotes.*** **Curr Opin Chem Biol, 2009. 13(4): p. 382-91.**

5. **Hang, H.C., J.P. Wilson, and G. Charron,** ***Bioorthogonal chemical reporters for analyzing protein lipidation and lipid trafficking.*** **Acc Chem Res, 2011. 44(9): p. 699-708.**

6. **Hannoush, R.N. and J. Sun,** ***The chemical toolbox for monitoring protein fatty acylation and prenylation.*** **Nat Chem Biol, 2010. 6(7): p. 498-506.**

7. **Charron, G., et al.,** ***Robust fluorescent detection of protein fatty-acylation with chemical reporters.*** **J Am Chem Soc, 2009. 131(13): p. 4967-75.**

8. **Charron, G., et al.,** ***Alkynyl-farnesol reporters for detection of protein S-prenylation in cells.*** **Mol Biosyst, 2011. 7(1): p. 67-73.**

9. **Rangan, K.J., et al.,** ***Rapid visualization and large-scale profiling of bacterial lipoproteins with chemical reporters.*** **J Am Chem Soc, 2010. 132(31): p. 10628-9.**

10. **Yount, J.S., et al.,** ***Palmitoylome profiling reveals S-palmitoylation-dependent antiviral activity of IFITM3.*** **Nat Chem Biol, 2010. 6(8): p. 610-4.**

11. **Ivanov, S.S., et al., *Lipidation by the host prenyltransferase machinery facilitates membrane localization of Legionella pneumophila effector proteins.* J Biol Chem, 2010. 285(45): p. 34686-98.**

12. **Hicks, S.W., et al., *Subcellular targeting of Salmonella virulence proteins by host-mediated S-palmitoylation.* Cell Host Microbe, 2011. 10(1): p. 9-20.**

13. **van Meer, G., D.R. Voelker, and G.W. Feigenson, *Membrane lipids: where they are and how they behave.* Nat Rev Mol Cell Biol, 2008. 9(2): p. 112-24.**

14. **Sud, M., et al., *LMSD: LIPID MAPS structure database.* Nucleic Acids Res, 2007. 35(Database issue): p. D527-32.**

15. **Feigenson, G.W., *Phase behavior of lipid mixtures.* Nat Chem Biol, 2006. 2(11): p. 560-3.**

16. **Ikonen, E., *Cellular cholesterol trafficking and compartmentalization.* Nat Rev Mol Cell Biol, 2008. 9(2): p. 125-38.**

17. **Recktenwald, D.J. and H.M. McConnell, *Phase equilibria in binary mixtures of phosphatidylcholine and cholesterol.* Biochemistry, 1981. 20(15): p. 4505-10.**

18. **Feigenson, G.W., *Phase boundaries and biological membranes.* Annu Rev Biophys Biomol Struct, 2007. 36: p. 63-77.**

19. **Sprong, H., P. van der Sluijs, and G. van Meer, *How proteins move lipids and lipids move proteins.* Nat Rev Mol Cell Biol, 2001. 2(7): p. 504-13.**

20. **Levental, I., M. Grzybek, and K. Simons, *Greasing their way: lipid modifications determine protein association with membrane rafts.* Biochemistry, 2010. 49(30): p. 6305-16.**

21. **Farazi, T.A., G. Waksman, and J.I. Gordon, *The biology and enzymology of protein N-myristoylation.* J Biol Chem, 2001. 276(43): p. 39501-4.**

22. **Linder, M.E. and R.J. Deschenes, *Palmitoylation: policing protein stability and traffic.* Nat Rev Mol Cell Biol, 2007. 8(1): p. 74-84.**

23. Mann, R.K. and P.A. Beachy, *Novel lipid modifications of secreted protein signals.* Annu Rev Biochem, 2004. 73: p. 891-923.

24. Takada, R., et al., *Monounsaturated fatty acid modification of Wnt protein: its role in Wnt secretion.* Dev Cell, 2006. 11(6): p. 791-801.

25. Gelb, M.H., et al., *Therapeutic intervention based on protein prenylation and associated modifications.* Nat Chem Biol, 2006. 2(10): p. 518-28.

26. Lobell, R.B., *Prenylation of Ras GTPase superfamily proteins and their function in immunobiology.* Adv Immunol, 1998. 68: p. 145-89.

27. Finlay, B.B. and G. McFadden, *Anti-immunology: evasion of the host immune system by bacterial and viral pathogens.* Cell, 2006. 124(4): p. 767-82.

28. Ewers, H. and A. Helenius, *Lipid-mediated endocytosis.* Cold Spring Harb Perspect Biol, 2011. 3(8): p. a004721.

29. Li, H., et al., *Myristoylation is required for human immunodeficiency virus type 1 Gag-Gag multimerization in mammalian cells.* J Virol, 2007. 81(23): p. 12899-910.

30. Thaa, B., et al., *Intrinsic membrane association of the cytoplasmic tail of influenza virus M2 protein and lateral membrane sorting regulated by cholesterol binding and palmitoylation.* Biochem J, 2011. 437(3): p. 389-97.

31. Lee, C.Z., et al., *Isoprenylation of large hepatitis delta antigen is necessary but not sufficient for hepatitis delta virus assembly.* Virology, 1994. 199(1): p. 169-75.

32. Srikanth, C.V., et al., *Salmonella effector proteins and host-cell responses.* Cell Mol Life Sci, 2011. 68(22): p. 3687-97.

33. Alix, E., S. Mukherjee, and C.R. Roy, *Subversion of membrane transport pathways by vacuolar pathogens.* J Cell Biol, 2011. 195(6): p. 943-52.

34. Ham, H., A. Sreelatha, and K. Orth, *Manipulation of host membranes by bacterial effectors.* Nat Rev Microbiol, 2011. 9(9): p. 635-46.

35. **Nimchuk, Z., et al.,** ***Eukaryotic fatty acylation drives plasma membrane targeting and enhances function of several type III effector proteins from Pseudomonas syringae.*** **Cell, 2000. 101(4): p. 353-63.**

36. **Reinicke, A.T., et al.,** ***A Salmonella typhimurium effector protein SifA is modified by host cell prenylation and S-acylation machinery.*** **J Biol Chem, 2005. 280(15): p. 14620-7.**

37. **Price, C.T., et al.,** ***Exploitation of conserved eukaryotic host cell farnesylation machinery by an F-box effector of Legionella pneumophila.*** **J Exp Med, 2010. 207(8): p. 1713-26.**

38. **Price, C.T., et al.,** ***Host-mediated post-translational prenylation of novel dot/icm-translocated effectors of legionella pneumophila.*** **Front Microbiol, 2010. 1: p. 131.**

39. **Andriotis, V.M. and J.P. Rathjen,** ***The Pto kinase of tomato, which regulates plant immunity, is repressed by its myristoylated N terminus.*** **J Biol Chem, 2006. 281(36): p. 26578-86.**

40. **Bijlmakers, M.J.,** ***Protein acylation and localization in T cell signaling (Review).*** **Mol Membr Biol, 2009. 26(1): p. 93-103.**

41. **Resh, M.D.,** ***Use of analogs and inhibitors to study the functional significance of protein palmitoylation.*** **Methods, 2006. 40(2): p. 191-7.**

42. **Buglino, J.A. and M.D. Resh,** ***Hhat is a palmitoylacyltransferase with specificity for N-palmitoylation of Sonic Hedgehog.*** **J Biol Chem, 2008. 283(32): p. 22076-88.**

43. **Prescher, J.A. and C.R. Bertozzi,** ***Chemistry in living systems.*** **Nat Chem Biol, 2005. 1(1): p. 13-21.**

44. **Kho, Y., et al.,** ***A tagging-via-substrate technology for detection and proteomics of farnesylated proteins.*** **Proc Natl Acad Sci U S A, 2004. 101(34): p. 12479-84.**

45. **Hang, H.C., et al.,** ***Chemical probes for the rapid detection of Fatty-acylated proteins in Mammalian cells.*** **J Am Chem Soc, 2007. 129(10): p. 2744-5.**

46. **Kostiuk, M.A., et al.,** ***Identification of palmitoylated mitochondrial proteins using a bio-orthogonal azido-palmitate analogue.*** **FASEB J, 2008. 22(3): p. 721-32.**

47. **Martin, D.D., et al.,** ***Rapid detection, discovery, and identification of post-translationally myristoylated proteins during apoptosis using a bio-orthogonal azidomyristate analog.*** **FASEB J, 2008. 22(3): p. 797-806.**

48. **Ching, W., H.C. Hang, and R. Nusse,** ***Lipid-independent secretion of a Drosophila Wnt protein.*** **J Biol Chem, 2008. 283(25): p. 17092-8.**

49. **Wang, Q., et al.,** ***Bioconjugation by copper(I)-catalyzed azide-alkyne [3 + 2] cycloaddition.*** **J Am Chem Soc, 2003. 125(11): p. 3192-3.**

50. **Rostovtsev, V.V., et al.,** ***A stepwise huisgen cycloaddition process: copper(I)-catalyzed regioselective "ligation" of azides and terminal alkynes.*** **Angew Chem Int Ed Engl, 2002. 41(14): p. 2596-9.**

51. **Tornoe, C.W., C. Christensen, and M. Meldal,** ***Peptidotriazoles on solid phase: [1,2,3]-triazoles by regiospecific copper(i)-catalyzed 1,3-dipolar cycloadditions of terminal alkynes to azides.*** **J Org Chem, 2002. 67(9): p. 3057-64.**

52. **Speers, A.E. and B.F. Cravatt,** ***Profiling enzyme activities in vivo using click chemistry methods.*** **Chem Biol, 2004. 11(4): p. 535-46.**

53. **Abrams, S.R. and A.C. Shaw,** ***Triple Bond Isomerizations - 2-Decyn-1-Ol to 9-Decyn-1-Ol.*** **Organic Syntheses, 1988. 66: p. 127-131.**

54. **Wilbur, D.S., et al.,** ***Antibody fragments in tumor pretargeting. Evaluation of biotinylated Fab' colocalization with recombinant streptavidin and avidin.*** **Bioconjug Chem, 1996. 7(6): p. 689-702.**

55. **Nguyen, T. and M.B. Francis,** ***Practical synthetic route to functionalized rhodamine dyes.*** **Org Lett, 2003. 5(18): p. 3245-8.**

56. **Agard, N.J., et al.,** ***A comparative study of bioorthogonal reactions with azides.*** **ACS Chem Biol, 2006. 1(10): p. 644-8.**

57. **Paige, L.A., et al.,** ***Metabolic activation of 2-substituted derivatives of myristic acid to form potent inhibitors of myristoyl CoA:protein N-myristoyltransferase.*** **Biochemistry, 1990. 29(46): p. 10566-73.**

58. **Webb, Y., L. Hermida-Matsumoto, and M.D. Resh,** ***Inhibition of protein palmitoylation, raft localization, and T cell signaling by 2-bromopalmitate and polyunsaturated fatty acids.*** **J Biol Chem, 2000. 275(1): p. 261-70.**

59. **Drisdel, R.C. and W.N. Green,** ***Labeling and quantifying sites of protein palmitoylation.*** **Biotechniques, 2004. 36(2): p. 276-85.**

60. **Paige, L.A., et al.,** ***Reversible palmitoylation of the protein-tyrosine kinase p56lck.*** **J Biol Chem, 1993. 268(12): p. 8669-74.**

61. **Alland, L., et al.,** ***Dual myristylation and palmitylation of Src family member p59fyn affects subcellular localization.*** **J Biol Chem, 1994. 269(24): p. 16701-5.**

62. **Zhang, W., R.P. Trible, and L.E. Samelson,** ***LAT palmitoylation: its essential role in membrane microdomain targeting and tyrosine phosphorylation during T cell activation.*** **Immunity, 1998. 9(2): p. 239-46.**

63. **Hancock, J.F., et al.,** ***All ras proteins are polyisoprenylated but only some are palmitoylated.*** **Cell, 1989. 57(7): p. 1167-77.**

64. **Liang, X., et al.,** ***The N-terminal SH4 region of the Src family kinase Fyn is modified by methylation and heterogeneous fatty acylation: role in membrane targeting, cell adhesion, and spreading.*** **J Biol Chem, 2004. 279(9): p. 8133-9.**

65. **Liang, X., et al.,** ***Heterogeneous fatty acylation of Src family kinases with polyunsaturated fatty acids regulates raft localization and signal transduction.*** **J Biol Chem, 2001. 276(33): p. 30987-94.**

66. **Tang, Y., et al.,** ***Acetylation is indispensable for p53 activation.*** **Cell, 2008. 133(4): p. 612-26.**

67. **Wilson, J.P., et al.,** ***Proteomic analysis of fatty-acylated proteins in mammalian cells with chemical reporters reveals S-acylation of histone H3 variants.*** **Mol Cell Proteomics, 2011. 10(3): p. M110 001198.**

68. Zhang, M.M., et al., *Tandem fluorescence imaging of dynamic S-acylation and protein turnover.* Proc Natl Acad Sci U S A, 2010. 107(19): p. 8627-32.

69. Zuckerman, D.M., et al., *Differential regulation of two palmitoylation sites in the cytoplasmic tail of the beta1-adrenergic receptor.* J Biol Chem, 2011. 286(21): p. 19014-23.

70. Hosokawa, A., et al., *Evaluation of an alkyne-containing analogue of farnesyl diphosphate as a dual substrate for protein-prenyltransferases.* Int. J. Pept. Res. Ther., 2007. 13(1-2): p. 345-354.

71. Rose, M.W., et al., *Evaluation of geranylazide and farnesylazide diphosphate for incorporation of prenylazides into a CAAX box-containing peptide using protein farnesyltransferase.* J Pept Res, 2005. 65(6): p. 529-37.

72. Davisson, V.J., et al., *Phosphorylation of isoprenoid alcohols.* J. Org. Chem., 1986. 51(25): p. 4768-79.

73. Chan, L.N., et al., *A novel approach to tag and identify geranylgeranylated proteins.* Electrophoresis, 2009. 30(20): p. 3598-606.

74. Stein, M.A., et al., *Identification of a Salmonella virulence gene required for formation of filamentous structures containing lysosomal membrane glycoproteins within epithelial cells.* Mol Microbiol, 1996. 20(1): p. 151-64.

75. Beuzon, C.R., et al., *Salmonella maintains the integrity of its intracellular vacuole through the action of SifA.* EMBO J, 2000. 19(13): p. 3235-49.

76. Boucrot, E., et al., *Salmonella typhimurium SifA effector protein requires its membrane-anchoring C-terminal hexapeptide for its biological function.* J Biol Chem, 2003. 278(16): p. 14196-202.

77. Maurer-Stroh, S. and F. Eisenhaber, *Refinement and prediction of protein prenylation motifs.* Genome Biol, 2005. 6(6): p. R55.

78. Horwitz, M.A., *Formation of a novel phagosome by the Legionnaires' disease bacterium (Legionella pneumophila) in human monocytes.* J Exp Med, 1983. 158(4): p. 1319-31.

79. **Horwitz, M.A., *The Legionnaires' disease bacterium (Legionella pneumophila) inhibits phagosome-lysosome fusion in human monocytes.* J Exp Med, 1983. 158(6): p. 2108-26.**

80. **Kagan, J.C., et al., *Legionella subvert the functions of Rab1 and Sec22b to create a replicative organelle.* J Exp Med, 2004. 199(9): p. 1201-11.**

81. **Kagan, J.C. and C.R. Roy, *Legionella phagosomes intercept vesicular traffic from endoplasmic reticulum exit sites.* Nat Cell Biol, 2002. 4(12): p. 945-54.**

82. **Tilney, L.G., et al., *How the parasitic bacterium Legionella pneumophila modifies its phagosome and transforms it into rough ER: implications for conversion of plasma membrane to the ER membrane.* J Cell Sci, 2001. 114(Pt 24): p. 4637-50.**

83. **Ninio, S. and C.R. Roy, *Effector proteins translocated by Legionella pneumophila: strength in numbers.* Trends Microbiol, 2007. 15(8): p. 372-80.**

84. **Burstein, D., et al., *Genome-scale identification of Legionella pneumophila effectors using a machine learning approach.* PLoS Pathog, 2009. 5(7): p. e1000508.**

85. **Franco, I.S., H.A. Shuman, and X. Charpentier, *The perplexing functions and surprising origins of Legionella pneumophila type IV secretion effectors.* Cell Microbiol, 2009. 11(10): p. 1435-43.**

86. **Vogel, J.P., et al., *Conjugative transfer by the virulence system of Legionella pneumophila.* Science, 1998. 279(5352): p. 873-6.**

87. **Segal, G., M. Purcell, and H.A. Shuman, *Host cell killing and bacterial conjugation require overlapping sets of genes within a 22-kb region of the Legionella pneumophila genome.* Proc Natl Acad Sci U S A, 1998. 95(4): p. 1669-74.**

88. **Ensminger, A.W. and R.R. Isberg, *Legionella pneumophila Dot/Icm translocated substrates: a sum of parts.* Curr Opin Microbiol, 2009. 12(1): p. 67-73.**

89. **Nagai, H., et al.,** ***A bacterial guanine nucleotide exchange factor activates ARF on Legionella phagosomes.*** **Science, 2002. 295(5555): p. 679-82.**

90. **Machner, M.P. and R.R. Isberg,** ***Targeting of host Rab GTPase function by the intravacuolar pathogen Legionella pneumophila.*** **Dev Cell, 2006. 11(1): p. 47-56.**

91. **Murata, T., et al.,** ***The Legionella pneumophila effector protein DrrA is a Rab1 guanine nucleotide-exchange factor.*** **Nat Cell Biol, 2006. 8(9): p. 971-7.**

92. **Nguyen, U.T., et al.,** ***Analysis of the eukaryotic prenylome by isoprenoid affinity tagging.*** **Nat Chem Biol, 2009. 5(4): p. 227-35.**

93. **DeGraw, A.J., et al.,** ***Evaluation of alkyne-modified isoprenoids as chemical reporters of protein prenylation.*** **Chem Biol Drug Des, 2010. 76(6): p. 460-71.**

94. **Yang, Y.Y., J.M. Ascano, and H.C. Hang,** ***Bioorthogonal chemical reporters for monitoring protein acetylation.*** **J Am Chem Soc, 2010. 132(11): p. 3640-1.**

95. **Yang, Y.Y., et al.,** ***Comparative analysis of cleavable azobenzene-based affinity tags for bioorthogonal chemical proteomics.*** **Chem Biol, 2010. 17(11): p. 1212-22.**

96. **Cavender, C.J. and V.J. Shiner,** ***Trifluoromethanesulfonyl Azide - Its Reaction with Alkyl Amines to Form Alkyl Azides.*** **Journal of Organic Chemistry, 1972. 37(22): p. 3567-&.**

97. **Raschke, W.C., et al.,** ***Functional macrophage cell lines transformed by Abelson leukemia virus.*** **Cell, 1978. 15(1): p. 261-7.**

98. **Gao, G., X. Guo, and S.P. Goff,** ***Inhibition of retroviral RNA production by ZAP, a CCCH-type zinc finger protein.*** **Science, 2002. 297(5587): p. 1703-6.**

99. **Bick, M.J., et al.,** ***Expression of the zinc-finger antiviral protein inhibits alphavirus replication.*** **J Virol, 2003. 77(21): p. 11555-62.**

100. **Muller, S., et al.,** ***Inhibition of filovirus replication by the zinc finger antiviral protein.*** **J Virol, 2007. 81(5): p. 2391-400.**

101. Zhu, Y., et al., *Zinc-finger antiviral protein inhibits HIV-1 infection by selectively targeting multiply spliced viral mRNAs for degradation.* Proc Natl Acad Sci U S A, 2011. 108(38): p. 15834-9.

102. Liu, L., et al., *ZAP is a CRM1-dependent nucleocytoplasmic shuttling protein.* Biochem Biophys Res Commun, 2004. 321(3): p. 517-23.

103. Guo, X., et al., *The zinc finger antiviral protein directly binds to specific viral mRNAs through the CCCH zinc finger motifs.* J Virol, 2004. 78(23): p. 12781-7.

104. Chen, S., et al., *Structure of N-terminal domain of ZAP indicates how a zinc-finger protein recognizes complex RNA.* Nat Struct Mol Biol, 2012. 19(4): p. 430-5.

105. Chen, G., et al., *p72 DEAD box RNA helicase is required for optimal function of the zinc-finger antiviral protein.* Proc Natl Acad Sci U S A, 2008. 105(11): p. 4352-7.

106. Ye, P., et al., *DEXH-Box protein DHX30 is required for optimal function of the zinc-finger antiviral protein.* Protein Cell, 2010. 1(10): p. 956-64.

107. Guo, X., et al., *The zinc-finger antiviral protein recruits the RNA processing exosome to degrade the target mRNA.* Proc Natl Acad Sci U S A, 2007. 104(1): p. 151-6.

108. Aravind, L., *The WWE domain: a common interaction module in protein ubiquitination and ADP ribosylation.* Trends Biochem Sci, 2001. 26(5): p. 273-5.

109. Kerns, J.A., M. Emerman, and H.S. Malik, *Positive selection and increased antiviral activity associated with the PARP-containing isoform of human zinc-finger antiviral protein.* PLoS Genet, 2008. 4(1): p. e21.

110. Hayakawa, S., et al., *ZAPS is a potent stimulator of signaling mediated by the RNA helicase RIG-I during antiviral responses.* Nat Immunol, 2011. 12(1): p. 37-44.

111. **Leung, A.K., et al.,** ***Poly(ADP-ribose) regulates stress responses and microRNA activity in the cytoplasm.*** **Mol Cell, 2011. 42(4): p. 489-99.**

112. **Ryman, K.D., et al.,** ***Sindbis virus translation is inhibited by a PKR/RNase L-independent effector induced by alpha/beta interferon priming of dendritic cells.*** **J Virol, 2005. 79(3): p. 1487-99.**

113. **Law, L.M., et al.,** ***Identification of a dominant negative inhibitor of human zinc finger antiviral protein reveals a functional endogenous pool and critical homotypic interactions.*** **J Virol, 2010. 84(9): p. 4504-12.**

114. **Durbin, J.E., et al.,** ***Targeted disruption of the mouse Stat1 gene results in compromised innate immunity to viral disease.*** **Cell, 1996. 84(3): p. 443-50.**

115. **Frolova, E.I., et al.,** ***Roles of nonstructural protein nsP2 and Alpha/Beta interferons in determining the outcome of Sindbis virus infection.*** **J Virol, 2002. 76(22): p. 11254-64.**

116. **Yount, J.S., G. Charron, and H.C. Hang,** ***Bioorthogonal proteomics of 15-hexadecynyloxyacetic acid chemical reporter reveals preferential targeting of fatty acid modified proteins and biosynthetic enzymes.*** **Bioorg Med Chem, 2012. 20(2): p. 650-4.**

117. **Kinsella, B.T. and W.A. Maltese,** ***rab GTP-binding proteins with three different carboxyl-terminal cysteine motifs are modified in vivo by 20-carbon isoprenoids.*** **J Biol Chem, 1992. 267(6): p. 3940-5.**

118. **Farnsworth, C.C., et al.,** ***Rab geranylgeranyl transferase catalyzes the geranylgeranylation of adjacent cysteines in the small GTPases Rab1A, Rab3A, and Rab5A.*** **Proc Natl Acad Sci U S A, 1994. 91(25): p. 11963-7.**

119. **Kinsella, B.T., R.A. Erdman, and W.A. Maltese,** ***Carboxyl-terminal isoprenylation of ras-related GTP-binding proteins encoded by rac1, rac2, and ralA.*** **J Biol Chem, 1991. 266(15): p. 9786-94.**

120. **Falsetti, S.C., et al.,** ***Geranylgeranyltransferase I inhibitors target RalB to inhibit anchorage-dependent growth and induce apoptosis and RalA to inhibit anchorage-independent growth.*** **Mol Cell Biol, 2007. 27(22): p. 8003-14.**

121. Berzat, A.C., et al., ***Transforming activity of the Rho family GTPase, Wrch-1, a Wnt-regulated Cdc42 homolog, is dependent on a novel carboxyl-terminal palmitoylation motif.*** **J Biol Chem, 2005. 280(38): p. 33055-65.**

122. Kang, R., et al., ***Neural palmitoyl-proteomics reveals dynamic synaptic palmitoylation.*** **Nature, 2008. 456(7224): p. 904-9.**

123. Melkonian, K.A., et al., ***Role of lipid modifications in targeting proteins to detergent-resistant membrane rafts. Many raft proteins are acylated, while few are prenylated.*** **J Biol Chem, 1999. 274(6): p. 3910-7.**

124. van Meer, G. and A.I. de Kroon, ***Lipid map of the mammalian cell.*** **J Cell Sci, 2011. 124(Pt 1): p. 5-8.**

125. Kobayashi, T., et al., ***Separation and characterization of late endosomal membrane domains.*** **J Biol Chem, 2002. 277(35): p. 32157-64.**

126. Frolova, E.I., et al., ***Functional Sindbis virus replicative complexes are formed at the plasma membrane.*** **J Virol, 2010. 84(22): p. 11679-95.**

127. den Boon, J.A. and P. Ahlquist, ***Organelle-like membrane compartmentalization of positive-strand RNA virus replication factories.*** **Annu Rev Microbiol, 2010. 64: p. 241-56.**

128. Vocadlo, D.J., et al., ***A chemical approach for identifying O-GlcNAc-modified proteins in cells.*** **Proc Natl Acad Sci U S A, 2003. 100(16): p. 9116-21.**

129. Keller, A., et al., ***Empirical statistical model to estimate the accuracy of peptide identifications made by MS/MS and database search.*** **Anal Chem, 2002. 74(20): p. 5383-92.**

130. Nesvizhskii, A.I., et al., ***A statistical model for identifying proteins by tandem mass spectrometry.*** **Anal Chem, 2003. 75(17): p. 4646-58.**

131. Hébert, N., et al., ***A new reagent for the removal of the 4-methoxybenzyl ether: application to the synthesis of unusual macrocyclic and bolaform phosphatidylcholines.*** **J Org Chem, 1992. 57(6).**

132. Augustin, K.E. and H. Schafer, *Conversion of oleic acid to 17- and 18-substituted stearic acid derivatives by way of the "acetylene zipper"*. Liebigs Ann Chem, 1991. 1991(10).

133. Hosokawa, A., et al., *Evaluation of an alkyne-containing analogue of farnesyl diphosphate as a dual substrate for protein-prenyltransferases.* Int J Pept Res Ther, 2007. 13(1-2): p. 345.

134. Cox, N.J.G., S.D. Mills, and G. Pattenden, *Macrocyclizations using allylic radical intermediates. A new synthetic approach to natural 14-membered cembranoids.* J Chem Soc Perkins Trans 1, 1992(11).